Theoretical Study on Toughening and Design against Fracture of Functionally Graded Thermal Barrier Coatings

Hideaki Tsukamoto, Dr

School of Mechanical Engineering
The University of Adelaide

In accordance with the requirement of the University of Adelaide for the degree of Doctor of Philosophy

January 2008

Declaration

This contains no material which has been accepted for the award of any other degree or diploma in any university or other tertiary institution and, to the best of my knowledge and belief, contains no material previously published or written by another person, except where due reference has been made in the text.

I give consent to this copy of my thesis being made available in the University Library.

The author acknowledges that copyright of published works contained within this thesis resides with the copyright holders of those works.

Signed

Date

Acknowledgements

I would like to thank Dr Andrei Kotousov and Dr Sook-Ying Ho for their guidance and suggestions throughout the course of work. I would like to thank Professor Valerie Linton for her warm suggestions and supports. I would like to thank Professor Colin Hansen for his great supports. I would like to thank Ms. Karen Adams for her assistance with language in the thesis. I would like to thank my colleagues at School of Mechanical Engineering at the University of Adelaide for their friendly assistances and collaborations. I would like to thank Professor Kyoko Sheridan at Faculty of the Professions for her warm supports. Finally, I express my deep gratitude to my wife, my parents and my wife's parents for their warm mental and physical supports.

Abstract

Functionally graded thermal barrier coatings (FG TBCs) are advanced multi-phase composites that are engineered to have a smooth spatial gradation of material constituents, which are normally ceramics and metal. The smooth gradation results in the reduction of thermal stresses, minimization or elimination of stress concentrations and singularities at interface corners, and increase in bonding strength. FG TBCs are able to survive very high temperatures and temperature gradients, which makes them very promising in many current and future applications including nuclear reactors, engines, turbines and leading edges of hypersonic vehicles.

FG TBCs inherit fatal weaknesses of ceramics, its brittleness, which often leads to fractures during temperature excursions. Despite of many studies on toughening of brittle ceramics conducted in the past three decades, there was not much work so far done on the toughening of FG TBCs.

The present project has two aims. The first aim is to develop a general micromechanical theory of the stress-induced transformation toughening of multi-phase composites and the second aim is to develop a theoretical model for FG TBCs toughened by transformable particles, which can be used in the design and fabrication of FG TBCs for applications where the high fracture resistance is mandatory.

A new theoretical model for transformation toughening in multi-phase composites is developed based on a combination of micromechanics and fracture mechanics approaches. According to the developed model, the effect of thermal residual stresses due to the mismatch in thermal expansion coefficients of constituent phases on toughening is found to be very strong.

A methodology of design of FG TBCs toughened by phase transformation of ZrO_2 is investigated by incorporating the developed micromechanics-based model for transformation toughening in multi-phase composites into the classical lamination theory (CLT). A new parameter such as an effective stress intensity factor is introduced for investigating the fracture behaviour and toughening effect in FG TBCs. As an example, Ni-ZrO_2 FG TBC systems subjected to a thermal shock conditions are analysed and general guidelines for the design of such system with improved fracture properties are developed.

Contents

List of figures

List of tables

Chapter 1

Introduction

1.1 Background of functionally graded thermal barrier coatings (FG TBCs)

Functionally graded thermal barrier coatings (FG TBCs) are promising candidates for application to structures working under high temperatures and temperature gradients. FG TBCs have been studied intensively since they were developed in Japan in the 1980's. FG TBCs are advanced multiphase composite materials that are engineered to have a smooth spatial variation of material constituents. This variation results in an inhomogeneous structure with smoothly varying thermal and mechanical properties. The advantages in using an FG TBC as an alternative to joining directly together two dissimilar materials, such as ceramics and metals, include smoothing of thermal stress distributions across the layers, minimization or elimination of stress concentrations and singularities at the interface corners, and an increase in bonding strength. These advantages are achieved by fabricating the composite material with a pre-determined gradual spatial variation of the volume fractions and microstructure of its material constituents according to functional performance requirements.

1.2 Gaps and aims

The ceramic-rich side of FG TBCs is so brittle that cracks usually initiate and propagate from the ceramic surface into the FG layers under unsteady heat-flow conditions such as thermal shock loadings [Han et al. 2006; Kokini et al. 2002]. However, little work has been done so far to overcome this problem.

In the past three decades various mechanisms have been identified and investigated for toughening of ceramics and ceramic-matrix composites. These mechanisms include bridging toughening, transformation toughening, crack deflection and branching, micro-crack toughening and others. However, there has been no attempt to apply these mechanisms to improve the overall fracture properties FG TBCs. The current project aims to fill this gap. The stress-induced

transformation toughening mechanism was selected for investigation because it is one of the strongest toughening mechanisms found in previous experimental studies on ceramics.

The present project had two specific aims. First, it aimed to develop a theoretical model for transformation toughening in multi-phase composites, based on micromechanical [Wakashima and Tsukamoto 1991] and fracture mechanics approaches [Stump and Budiansky 1988]. This new model allowed the investigation of the influence of the mismatch in material properties of constituent phases on the toughening effect. The micromechanical model was also used to elucidate some experimental tendencies, which previously have not been properly explained or investigated. The second aim of this project was to develop a methodology for design of FG TBCs with improved fracture properties by transformation toughening with ZrO_2. This was accomplished by combining the micromechanical model developed above for transformation toughening in multi-phase composites with the classical lamination theory (CLT). The guidelines for design against fracture of FG TBCs subjected to various thermo-mechanical boundary conditions were provided on the basis of micromechanics and fracture mechanics considerations. The thesis also provided recommendations for material selections, compositional gradations and dimensions in the FG TBCs, which could be applied to aerospace and automobile structures exposed to super high-temperature and temperature-gradient conditions.

1.3 Scope of thesis

This thesis consists of seven chapters. The introduction is presented earlier in this chapter. Chapter 2 includes a review of literature on the theoretical and numerical study of fracture of FG TBCs, the design of FG TBCs, and the toughening mechanisms in ceramics and ceramic-matrix composites (CMCs). It also includes a brief review of micromechanical theories.

In Chapter 3, fundamental issues of linear elastic fracture mechanics are described. Firstly, the stress intensity factor is defined via the complex variable method. Next, the singular integral equation method is described. The singular integral equation method is also applied to the analysis of the influence of T

(transverse)-stress on short-fibre bridging toughening in multi-phase composites, which was performed as an additional work of the project as shown in Chapter 7.

In Chapter 4, earlier work on the continuum model for the transformation toughening mechanisms by Stump and Budiansky [1989] is described. This model was applied only to investigate the transformation toughening effect in so called "homogeneous" composites with constituent phases that have the same material properties.

In Chapter 5, a mean-field micromechanical approach by Wakashima and Tsukamoto [1991] is described and applied to develop a new micromechanical theory for transformation toughening. This theory was developed by incorporating the mean-field micromechanical model with the continuum model [Stump and Budiansky 1988], and can investigate the effect of mismatch in material properties of constituent phases on toughening. Through numerical examinations, some of which are compared with the available experimental measures, the validity of the developed model for transformation toughening is examined. ZrO_2-enriched SiC/ Al composites were investigated, which have large potential for structural components demanding high stiffness, high strength, high resistance to wear and heat, and low weight. The obtained results indicated a large influence of the mismatch in material properties of constituents and microstructure on the toughening characteristics.

In Chapter 6, a theoretical model for FG TBCs toughened by transformation of ZrO_2 is described, which was developed by combining the developed micromechanical theory for transformation toughening in multi-phase composites with the classical lamination theory (CLT). As an example, Ni-ZrO_2 FG TBCs, which currently attract considerable attention as effective thermal shielding structures in aerospace and automotive industries, were selected for further numerical investigation. The effect of the compositional gradations on the fracture resistance under thermal shock conditions and the strength of transformation toughening were studied. The obtained simulation results can be used in the design and fabrication of advanced Ni-ZrO_2 FG TBC systems with improved fracture resistance properties. The contents of this thesis are summarized in Chapter 7.

Chapter 2

Review of literature

2.1 Introduction

Most of the early theoretical and numerical studies on FG TBCs focused on predicting the thermal stresses generated in the materials [Ravichandran 1994; Cho and Ha 2001]. However, it has been claimed by some researchers [Han et al. 2006; Kokini et al. 2002] that the ceramic coating layer is very brittle in FG TBCs and cracks usually initiate and propagate from this coating surface layer, particularly under thermal shock loading conditions. In an attempt to overcome this problem, some researchers [Jin 2004; Jin and Luo 2006; Wang et al. 2004] investigated the failure behaviour of FG TBCs based on the fracture-mechanics consideration. Many studies have been done to investigate the toughening mechanisms in ceramics and ceramic composites. These are considered to be also applied to the toughening of FG TBCs. In the following, the literature is reviewed, which is relevant to the thermo-mechanical behaviour, including thermal fracture, of FG TBCs and the toughening mechanisms of ceramics and ceramic composites.

First, the literature describing various aspects of FG TBCs is reviewed. The literature reviewed here on design and analysis of FG TBCs is classified into three categories such as (1) fracture analysis of FG TBCs, (2) analytical and numerical modellings besides fracture analysis and (3) design procedures of FG TBCs. These are followed by the review of literature on manufacturing and thermo-mechanical testing procedures of FG TBCs.

Second, the literature on toughening mechanisms in ceramics and ceramic composites is reviewed, such as transformation toughening, bridging toughening, micro-cracking toughening, crack diffraction and others. The general concept behind these mechanisms is described, and the bridging and micro-cracking toughening mechanisms are discussed in detail. The literature on the transformation toughening, which is considered to be the most suitable for toughening of FG TBCs considered in the present project, is reviewed extensively.

The third focus of the literature review is on the micromechanical theories to predict thermo-mechanical properties of inhomogeneous materials. There are various micromechanical approaches analysing effective properties of the composites, some of which are discussed. This study specifically focuses on a mean-field micromechanical approach based on Wakashima-Tsukamoto estimate [Wakashima and Tsukamoto 1991].

Finally, the key issues arising from this review are critically summarized to reveal the need for the investigation into toughening of FG TBCs based on micromechanics and fracture mechanics considerations. The direction of the research in the project is clearly given.

2.2 Functionally Graded Thermal Barrier Coatings (FG TBCs)

2.2.1 General concept

Thermal barrier coatings (TBCs) have been developed for more than 35 years for various applications and structures working under super high temperatures and temperature gradients. A thermal barrier coating represents a thin layer of a material with high insulating properties, such as ceramics, that is bonded to a substrate, which is usually metal, to protect the metal structure during temperature excursions. The application of TBCs can significantly increase the operating temperatures up to 1400-1500 ^{o}C, increase efficiency and improve the durability of the components. The TBCs are currently being developed or considered for hypersonic applications, automotive engines, nuclear fusion reactors and heavy-duty utilities (i.e. diesel trucks, electric power generators, etc [Koizumi 1997]).

The durability requirements of TBCs for these applications are increasing rapidly [Martena et al. 2006]. Examples include reusable rockets and air-breathing space vehicles. In many of TBC applications, stresses due to the difference in thermal expansion of the TBC and substrate can have a detrimental effect on the fatigue and hence service life of the high temperature component. One important way to reduce the adverse effects of thermal stresses is to use functionally graded thermal coatings, where thermal and mechanical properties vary gradually throughout the thickness. In a metal-ceramic

functionally graded thermal barrier coatings (FG TBCs), the ceramic-rich side is exposed to high temperatures, or placed in the region where there is a potentially severe temperature variation. Fig. 2-1 shows a schematic illustration of functionally graded thermal barrier coatings (FG TBCs). The concept of functionally gradation can reduce the thermal mismatch and, therefore, largely reduce the possibility of fracture caused by thermal stresses. Sintering, thermal spraying, chemical and physical vapour depositions, diffusion bonding, and combustion synthesis are all known processing technologies which may be used to fabricate such compositionally graded systems. Using such methods, pre-determined compositional gradation in FG TBCs can be achieved.

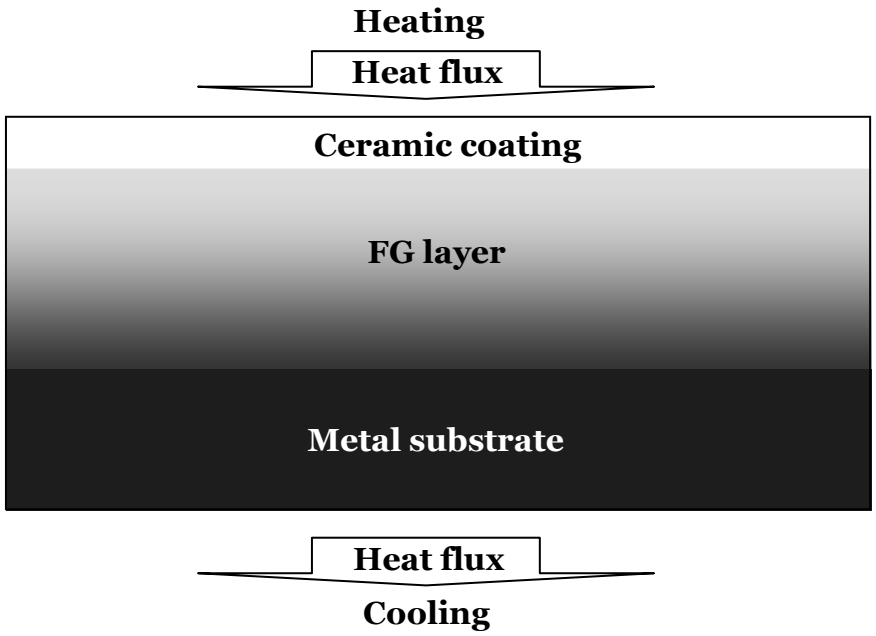

Figure 2-1: Schematic illustration of a functionally graded thermal barrier coating (FG TBC).

2.2.2 Design and analysis of FG TBCs

2.2.2.1 Fracture mechanics of FG TBCs

The gradations in functionally graded materials (FGMs) result in an inhomogeneous structure with smoothly or step-wisely varying thermal and mechanical properties. An important aspect of the problem in design of

components involving FGMs is to consider the mechanical failure, in particular, the fracture failure. Experimental observations of cracking in FGMs have been reported particularly in the ceramic rich part of the materials [Han et al. 2006; Kokini et al. 2002]. The analysis related to fatigue and fracture characterization of the FGMs requires the solution of certain standard crack problems based on the linear elastic fracture mechanics.

Jin et al. [1994; 1996] studied the crack-tip stress fields of functionally graded elastic material and found that it has the singularity as $r^{-1/2}$ and the same angular distribution structure as that of a crack in a single elastic material. For crack-tip fields, the only difference between FGMs and homogeneous elastic materials is that the continuous variation of mechanical properties of FGMs has remarkable effects on stress intensity factors (SIFs). Therefore, an important task of fracture analysis of FGMs is to study the effects of continuous gradient variations of mechanical properties on SIFs. Konda and Erdogan [1994] used the integral transform method to investigate the mixed-mode crack problem in a non-homogeneous elastic medium. Kim and Paulino [2002] used finite element method to evaluate the mixed-mode SIFs in FGMs.

In fracture analysis of FGMs, the interfacial cracks between functionally gradient coating and homogenous substrate and the functionally gradient interlayer cracks between two homogenous materials are two kinds of problems attracting the attention of many researchers. Chen and Erdogan [1996] used Fourier transform to derive the Cauchy singular integral equation for interfacial crack of a non-homogeneous coating bonded to a homogeneous substrate, and used the allocation method to obtain numerical solutions of SIFs and the strain energy release rates. Jin and Batra [1996], Qian et al. [1997], Shaw [1998], Huang et al. [2002; 2003] and Guo et al. [2004] also studied interfacial crack problems of functionally graded coatings under different conditions. Wang et al. [1997] solved the torsion problem of a penny-shaped crack at the interface between two distinctly different materials by presenting the generalized interlayer model, and obtained the SIFs by solving a singular integral equation. Li and Weng [2001], Wang et al. [2003] and Huang et al. [2004] also adopted integral transform to investigate fracture problem of functionally graded interfacial zone.

Aside from integral transform method, finite element method (FEM) is a widely used. Chi and Chung [2003] used finite element method to investigate the cracking in coating–substrate composites with multi-layered and FGM coatings. Sami et al. [2003] studied an interface crack between a functionally graded coating and a homogeneous substrate under thermo-mechanical loading by FEM.

The effects of material inhomogeneities on the crack–tip driving force in general inhomogeneous bodies have been evaluated using two-dimensional crack models [Simha et al. 2003]. Meanwhile, a few researchers have investigated three-dimensional crack problems in FGMs. Penny-shaped cracks in bonded materials with a FGM interfacial zone under torsion and normal tractions were investigated using a Fourier transform-based analytical method [Ozturk and Erdogan 1995; Ozturk and Erdogan 1996]. Mode I crack growth in ceramic/metal FGMs was studied using a three-dimensional finite element method by Jin et al. [2002]. Because of extreme difficulties in solving three-dimensional crack problems in FGMs, very limited results have been made available in relevant open literatures about three-dimensional fracture mechanics in FGMs. A boundary element method (BEM) for accurate and efficient evaluations of crack problems in multilayered solids and FGMs was employed in the studies by Yue and Xiao [2002] and Yue et al. [2003].

Under elevated temperature conditions, FGMs exhibit creep and relaxation behaviour. In the framework of linear continuum theory, such behaviour can be studied as viscoelasticity. Generally speaking, the viscoelastic response may be obtained from the elastic solution via the correspondence principle [Christensen 1969], or the analogy between the Laplace transform of the viscoelastic solution and the corresponding elastic solution. Fracture behaviour of homogeneous materials has been investigated by Broberg [1999] who has given some examples of stress intensity factors for stationary cracks in viscoelastic solids. Atkinson and Chen [1996; 1997] have investigated cracks in layered viscoelastic materials.

The material properties of FGMs are continuously graded with gradual change in microstructural details over predetermined geometrical orientations and distances, such as composition, morphology, and crystal structure. For polymer-based FGMs, their creep and relaxation behaviour may be studied by

viscoelasticity [Parameswaran and Shukla 1998; Lambros et al. 1999; Marur and Tippur 2000]. However, in general, the correspondence principle does not hold for FGMs. To avoid this problem, Paulino and Jin [2001 (a)] have shown that the correspondence principle can still be used to obtain the viscoelastic solution for a class of FGMs exhibiting relaxation (or creep) functions with separable kernels in space and time. By revisiting such correspondence principle for FGMs, they have subsequently studied crack problems of FGM strips subjected to anti-plane shear conditions [Paulino and Jin 2001 (b); Paulino and Jin 2001 (c)].

Other studies on crack problems of inhomogeneous viscoelastic materials directly solve the viscoelastic governing equations. Schovanec and co-workers have considered stationary cracks [Alex and Schovanec 1996], quasi-static crack propagation [Herrmann and Schovanec 1990] and dynamic crack propagation [Herrmann and Schovanec 1994] in inhomogeneous viscoelastic media under anti-plane shear conditions. Schovanec and Walton also considered quasi-static propagation of a plane strain mode I crack in a power-law inhomogeneous linearly viscoelastic body and calculated the corresponding energy release rate [Schovanec and Walton 1987]. A separable form for the relaxation functions was employed by Alex and Schovanec [1996], Herrmann and Schovanec [1990], Herrmann and Schovanec [1994], Schovanec and Walton [1987]. Yang [2000] performed stress analysis in FGM cylinders where steady-state creep conditions are considered only for the homogeneous material.

In recent years, criteria of the failure in FG TBCs under thermal environments have been extensively discussed [Wang et al. 2004]. There are two approaches to be roughly categorized. In the first approach, the magnitude of the maximum tensile stress in the constituent is correlated with the possibility of failure (called “maximum local tensile stress criterion”). This approach assumes that there are no pre-existing flaws inside the medium. Material properties are selected to avoid the initiation of fracture by thermal stresses. In general this requires materials with high values of tensile strength, thermal conductivity, and thermal diffusivity combined with low values of the thermal expansion coefficient, Young’s modulus and Poisson’s ratio. Material inhomogeneity can be chosen such that the thermal stress can be minimized. The second approach to the determination of thermal stress resistance of the

FGMs is concerned with the extent of crack growth (called "maximum stress intensity factor criterion"). Many theoretical models of the crack problem under thermal stress conditions have been developed for FGMs as mentioned.

The analysis for solving problems relevant to cracks existing in FG TBCs is now a hot topic. In the design of FG TBCs, it is important to choose suitable failure criteria out of the "maximum local tensile stress" and "maximum stress intensity factor". In the next section, the literature focusing on the thermal stresses in FG TBCs is reviewed, which is more relevant to "maximum local tensile stress" criterion.

2.2.2.2 Analytical and numerical modelling

In the design of FG TBCs, the methods to analyse and estimate the stress states in FG TBCs under various thermo-mechanical boundary conditions [Shabana and Noda 2001] are essential. Many kinds of micromechanics-based methods for calculating effective thermo-mechanical properties and numerical technique such as finite element method (FEM) and boundary element method (BEM) exist. They have advantages and disadvantages in each. Since micromechanics-based analytical methods will be described later, we pay attention to some other numerical techniques used for the simulation of thermal stresses in FGMs.

Firstly, we look at analysis of temperature field. Determination of transient temperature field is an important but difficult topic, due to continuously varied material properties of FGMs. Since most of FGMs show one-dimensional inhomogeneity, the temperature field can be readily obtained by composite laminated plate model, finite difference method, finite element method and others for simple one-dimensional heat conduction. Taking into account the effect of temperature dependency of material properties, Tanigawa et al. [1996] investigated a one-dimensional transient heat conduction problem of a FGM plate. Also the associate thermal stress distributions for an infinitely long FGM plate were analysed. Jin and Paulino [2002] proposed a multi-layered material model to treat the transient thermal conduction problem for an FGM strip. They gave a simple approach by means of Laplace transform technique and obtained an analytical asymptotic solution of temperature for

short times. Elperin and Rudin [2002] studied temperature field and the associated thermal stresses in a functionally graded material caused by a laser thermal shock. Abd-Alla et al. [2000] investigated the transient temperature field in an inhomogeneous orthotropic multilayered cylinder by means of Laplace transform technique. Obata and Noda [1993] obtained a perturbation solution for the one-dimensional transient temperature field in FGMs. Wang et al. [2005] used a finite element method in conjunction with the finite difference method to solve the system of time-dependent equations that govern the transient temperature distribution.

For the analysis of thermo-mechanical behaviour of FGMs, several conventional averaging methods for usual dual-phase composites have been widely employed to estimate thermo-mechanical properties, such as the rules of mixture, the mean-field micromechanics models [Mori and Tanaka 1973; Wakashima and Tsukamoto 1991] and the unit cell model [Ravichandran 1994]. Owing to the assumptions made in these models, while easily predicting the overall thermo-mechanical behaviour, they may be insufficient to predict the reliable thermo-elastic behaviour of FGMs. As is well known, the response of phase materials in reality relies on the shape and size, the orientation and dispersion structure of constituents and the loading and boundary conditions [Reiter et al 1997; Christensen 1979]. Recently, the numerical analysis approaches utilizing finite-element discretized models, for the accurate behaviour prediction, have been proposed by several investigators. Dvorak et al. [Christensen 1979] presented a discrete micromechanics model in which each inclusion is replaced with a planar hexagonal cell, and carried out the comparative numerical experiments in order for the assessment of the Mori–Tanaka method for various dispersion structures. Grujicic and Zhang [1998] proposed a numerical analysis technique for determining the accurate effective microstructure-dependent elastic properties, by utilizing the Voronoi cell finite element method. Cho and Ha [2001] numerically compared the elastic and thermo-elastic predictions by three representative averaging approaches, the linear and modified rules of mixtures and the Wakashima-Tsukamoto estimate [Wakashima and Tsukamoto 1991], with those predicted by finite-element discretized models employing rectangular cells.

In a metal–ceramic FGM, yielding in the metallic phase can greatly affect the stress distribution within the FGM, and thus a stress analysis based only on elastic material behaviour will not be accurate. In such cases, it is worth noting that plastic deformation can occur solely as a result of thermal loads. Numerical investigations have also been carried out to study the thermo-elastoplastic behaviour of metal-ceramic FGMs using both the domain-type methods, such as the finite element method (FEM) [Giannakopoulos et al. 1995; Finot and Suresh 1996; Weissenbek et al. 1997], and the boundary-type methods, such as the boundary element method (BEM) [Sladek et al. 2005]. Many analytical or semi-analytical solutions have been reported to date. However, FEA and BEA, although accurate, involve extensive and costly computations. Therefore there is also a strong need for accurate analytical formulations to predict nonlinear FGM behaviour.

The creep behaviour of the metal phase in FGMs should be considered in the stress analysis because FGMs are used at high temperatures [Yang 2000]. Due to the difference in the thermal expansion coefficients and in the elastic constants, high stresses develop after a homogeneous temperature change in such a ceramic-metal joint. For linear elastic material behaviour, there even exist stress singularities at the intersection of the interface and the free edge. To reduce this stress level and to avoid the stress singularity, a functionally graded material (FGM) is usually introduced. Stresses in FGM under thermal loading have been analysed extensively with regard to the elastic material behaviour in the past decades [Arai et al. 1990; Erdogan and Wu 1993; Fukui and Yamanaka 1993; Hirano and Teraki 1993; Obata and Noda 1994; Tanigawa 1995; Yang 1998a]. However, there has been a lack of investigation into the stress analysis that considers material creep behaviour. So far, there have been few analytical solutions for the calculation of the stresses depending on time, temperature and the transition functions of the material in FGM [Tsukamoto 2003].

Some researchers consider the thermal stresses introduced in the process of fabrication. Since the FGMs are cooled to room temperature after fabricating at high temperature, the thermal stress is induced in the FGMs due to the fabrication process. It is very important to consider the fabrication process when discussing the thermal stresses in the FGMs. However, many studies [Reddy and Chin 1998; Obata and Noda 1993; Fuchiyama et al. 1993] of FGMs

subjected to thermal loading were carried out without taking into consideration the residual stress due to the fabrication process. The first study taking the fabrication process into consideration was done by Arai et al. [1993] who treated the sintered residual stress, thermal stresses at heating and total residual stress after cooling in the FGM plate (FGP) by use of the finite element method (FEM). Noda et al. [1998] studied the thermo-elastic behaviour in a particle-reinforced FGP, taking the fabrication process into consideration by use of the thermo-elastic-plastic constitutive equation developed by Asakawa et al. [1989].

Many kinds of analytical methods have been proposed for investigating thermo-mechanical behaviour of FGMs such as transient temperature and thermal stress distributions in FGMs under various thermo-mechanical boundary conditions. Numerical techniques such as FEA and BEA were used for such analysis in many studies. The micromechanical approach is one of possible methods, which have been investigated for the analysis of inhomogeneous materials including FGMs, to estimate effective material properties. The analytical methods based on micromechanics approach considering inelastic deformations were proposed by Tsukamoto [2003].

2.2.2.3 Design of FG TBCs

FGMs permit tailoring of material composition so as to derive maximum benefits from their inhomogeneity. The performance of a FGM is not just a function of the properties and mass of its material constituents alone, but is directly related to the ability of the designer to utilize the materials in the most suitable fashion. Thus, the design of FG TBCs is a very important which requires the accurate simulation of its response to complex thermo-mechanical loads and boundary conditions.

One of the most important aspects in optimum design of FG TBCs is to choose suitable objective functions and design valuables from the material science viewpoints. In the study by Markworth and Saunders [1994], the heat flow was used for a (maximized or minimized) objective function, and compositional gradation was chosen as the design valuable. Only elastic analysis was done using the rule of mixture to estimate thermo-elastic effective properties of the composites. Nadeau and Ferrari [1999] carried out a design of

composite with graded layers consisting of continuous matrix and short fibres. The objective functions were relevant to the strain energy and curvature of the composite. For design valuables, the gradation of volume fraction, aspect ratio and orientation distribution of fibres were used. Effective properties of composites were estimated according to the constitutive equation based on the Mori-Tanaka's mean field approximation and other methods.

Knowledge of the thermal fracture resistance behaviour of FG TBCs is critical for such a material design in high temperature applications. There has been some progress in analysis of the thermal fracture of FG TBCs. The effect of compositional gradations on the edge cracking in FG TBCs bonded to a homogeneous substrate subjected to a thermal shock loading was investigated by Jin et al. [Jin 2004; Jin and Luo 2006]. Wang et al. [2004] calculated transient temperature fields and associated thermal stresses in FG TBCs using a finite element and finite difference methods. They design FG TBCs using both criteria of "maximum local tensile stress" and "maximum stress intensity factor". Han et al. [2006] carried out a multiple surface cracking analysis to investigate the thermal shock resistance behaviour of FG TBCs and design of them. They designed FG TBCs by examining the effect of compositional gradations and densities of multiple cracks generated in the surface coating on the thermal stress intensity factor based on the facture mechanics consideration.

The different objective functions and different design variables have been used in each research to their demand, although most researchers [Markworth and Saunders 1995; Nadeau and Ferrari 1999; Cho and Shin 2004] took compositional gradations as one of design variables. In the present project, the design against fracture of FG TBCs is carried out by adopting a new parameter relevant to the stress intensity factor as an objective function and using a compositional gradation as a design valuable.

2.2.3 Manufacturing and testing

The manufacturing process of a FGM can usually be divided in building the spatially inhomogeneous structure ("gradation") and transformation of this structure into a bulk material ("consolidation") [Kieback et al. 2003]. Gradation processes can be classified into three categories, which are constitutive,

homogenizing and segregating processes. Constitutive processes can be performed as a stepwise graded structure from precursor materials or powders. Gradation structure in homogenizing processes can be formed by material transport from a sharp interface between two materials. In segregating processes, a macroscopically homogeneous material is converted into a graded material by material transport caused by an external field (for example a gravitational or electric field). Homogenizing and segregating processes can produce continuous gradients not step-wise ones. However, there are some limitations in making gradational microstructure.

The gradation step was followed by sintering or solidification for a consolidation process. The consolidation process will be performed considering the characteristic of FGMs. For example, the processing conditions should be chosen in such a way that the gradation pattern which is pre-designed is not altered. Uneven shrinkage of FGMs during free sintering which results from their fundamental characteristic should be taken into consideration. The sintering behaviour is influenced by porosity, particle size and shape and composition of the powder mixture. Hot pressing [Yang et al. 2003] or hot isostatic pressing [Ito et al. 2001] is commonly used to make higher density samples. If a temperature gradient during consolidation is necessary, liquid-phase sintering [Eso et al. 2005], laser assisted sintering [Lee et al. 2001], and spark plasma sintering [Gu et al. 1997] have been proposed.

Besides the well-established powder metallurgical technique, melt processing is widespread for FGMs in which metal phase is contained. Sedimentation casting, centrifugal casting [Watanabe et al. 2001] and directional solidification [Kato et al. 2000] etc. have been used so far. There are various methods existing, but each of these methods has its merit and disadvantages.

The FGM is evaluated by using relevant performance tests and the results are fed back to the design process and stored in the database. The performance tests include the local evaluation of microstructure and material properties to show the performance of designed structure and properties distribution. They also include the evaluation of overall performance of FGM properties. Although conventional methods may be applicable, some modifications, or the development of new methods, are necessary because of difficulties in

measurement due to the continuous change of properties in the local region. Moreover, fracture behaviour in a ceramic/metal FGM may change from brittle to ductile fracture due to the gradual variation of the amount of ductile metal phase. The overall mechanical behaviour of FGM has to be evaluated, not only on the macroscopic scale, but also on a microscopic scale, such as damage growth, micro-crack initiation at interfaces and crack propagation. In many applications, FGMs may be exposed to constant or alternating thermal loading with high temperature gradient from one side to the other. Thermal shock resistance, thermal fatigue characteristics, temperature profile must be evaluated [Kawasaki and Watanabe 1997].

Thermal stresses evolving in FGMs subjected to temperature fluctuations have previously been examined by means of diffraction techniques. In the case of X-ray or neutron diffraction, the residual strains are measured directly on the basis of a shift in lattice spacing; assuming isotropic elasticity, the residual stresses are calculated from measured (or assumed) elastic constants. The estimation of residual stresses by X-rays is restricted to near-surface regions (typically several micrometers beneath the surface) of the layered specimen, while neutrons can penetrate much deeper. Finot et al. [1996] conducted direct measurements of the evolution of curvature to evaluate stress field in FG TBCs. Thermal shock test have been conducted using various heating methods by many researchers [Kokini et al. 2002; Kawasaki and Watanabe 1997].

Microhardness profiles of FG TBCs were obtained utilizing a Vickers indenter [Limarga et al. 2005; Larsson and Odén 2004]. Indentation technique was also adopted to measure the fracture toughness in many studies [Hvizdos et al. 2007; Heian et al. 2004]. Limarga et al. [2005] investigated mechanical properties of plasma-sprayed multilayered Al_2O_3/ZrO_2 thermal barrier coatings using these methods.

Some researchers [Kokini et al. 2002; Han et al. 2007; Hamatani et al. 2003] conducted experimental works to investigate the thermal shock fracture resistance of FG TBCs. Kokini et al. [2002] and Han et al. [2007] investigated generation of cracks in the ceramic surface layers in FG TBCs. Kokini et al. [2002] conducted an experimental study to investigate the thermal fracture behaviour of plasma-sprayed yttria stabilized zirconia-NiCoCrAlY bond coat alloy FG TBCs when subjected to a thermal shock loading. Han et al. [2007]

investigated the influence of gradation of the composition on thermal shock behaviour of CeO_2–Y_2O_3–ZrO_2 graded thermal barrier coatings. Hamatani et al. [2003] investigated the effects of the compositional gradation profile and coating density in FG TBCs on the thermal shock resistance. The FG TBCs consisted of ZrO_2-8wt.%Y_2O_3 (YSZ) top coating, YSZ-Ni-20 wt. %Cr (NiCr) FGM coating, NiCr under coating and copper substrate, and the thermal shock resistance test was conducted under temperature gradient conditions.

The establishment of a such thermo-mechanical performance test is gaining increasing importance, because it enables us to evaluate the structural integrity of the prepared gradient materials, in order to use FGMs in a practical way. More effort should be focused on the establishment of a standardized performance test of such kinds of advanced composites.

2.3 Toughening mechanism of ceramics and ceramic composites

2.3.1 General Concept

The intrinsic brittleness is a key problem in the widespread application of the ceramic materials in general and FGM TBCs in particular. In order to reduce the brittleness and to increase the strength and the toughness, varieties of toughening mechanisms, such as the crack deflection, crack bridging, crack branching, crack bowing, crack pinning, micro-cracking, transformation toughening and the synergism toughening, etc. have been investigated in the past four decades. As a result, the mechanical properties and performances and the reliability of the ceramics and ceramic composites have been significantly improved [Shi and Pan 2007; Jiang et al. 1999; Vashishth et al. 1997; Rose 1986b]. For example, the maximum fracture toughness achieved by long-fibre bridging is around 20 $MPam^{1/2}$ in SiC/SiC composites, that achieved by particulate bridging is around 15$MPam^{1/2}$ in Al_2O_3/ SiC composites, that achieved by transformation is around 15$MPam^{1/2}$ in PSZ/Al_2O_3 composites, that achieved by micro-cracking is around 7 $MPam^{1/2}$ in ZrO_2/ Al_2O_3 composites, and that achieved by deflection is around 2-4$MPam^{1/2}$ in Al_2O_3/ NiAl composites [Hannink 2000; Anderson 2005; Tuan 2000].

The resistance of such brittle solids as ceramics and ceramic-matrix composites to the propagation of cracks can be greatly influenced by microstructure, inhomogeneities and reinforcements. Toughening mechanisms can be categorized into three types: {1} toughening due to the presence of inhomogeneities [Meguid 1996; Budiansky, Hutchinson and Evans 1986], {2} toughening due to transformation strains [Rose 1986b; Kelly and Rose 2002] and {3} toughening due to stress induced micro-cracking [Faber and Evans 1983; Vashishth et al. 1997]. The crack deflection, crack bridging, crack branching, crack bowing, crack pinning are in the first category. In addition, some synergetic effects are achieved using combination of some of these toughening mechanisms such as bridging and transformation toughening mechanisms. In the following, micro-cracking and bridging toughening mechanisms are dicussed in detail. These toughening mechanisms have some disadvantages and limitations in application to FG TBCs. Proper reinforcement configuration using the crack bridging mechanism is difficult to form in FG TBCs, while micro-cracks and pores are also capable of generating and propagating cracks, and also large toughening effect cannot be expected. The stress-induced transformation toughening mechanism could now be considered to be the best toughening mechanism for FG TBC structures [Tsukamoto and Kotousov 2007], which is described in detail and investigated in the present project.

2.3.2 Micro-cracking Toughening

Brittle materials sometimes contain extensive micro-cracks. Such a region in which micro-cracks are generated is known as process zone, and it is developed in front of a macro-crack [Hoagland et al. 1973; Claussen 1976; Faber and Evans 1983; Hu and Wittmann 1992; Wittmann et al. 1994] as shown Fig. 2-2. This phenomenon occurs in ceramics, rocks and concrete-like materials. Micro-cracking damage tends to toughen the material at the macroscopic scale level for stationary and steadily growing cracks [Faber and Evans 1983; Ruhle et al. 1986; Ruhle and Evans 1987; Han and Suresh 1989].

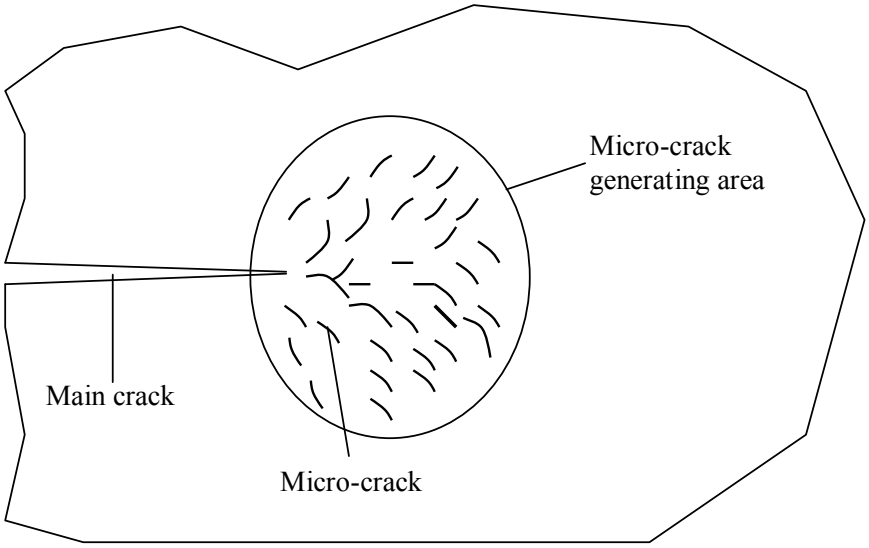

Figure 2-2:
Schematic illustration of micro-cracking toughening.

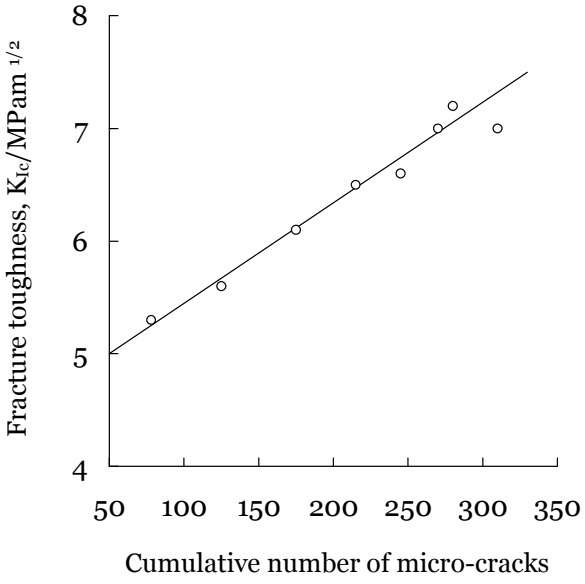

Figure 2-3: Fracture toughness plotted against the cumulative number of micro-cracks in bovine bones [Vashishth et al. 1997].

The relation between fracture toughness and cumulative number of micro-cracks in bovine bones is shown in Fig.2-3 [Vashishth et al. 1997]. We can see the proportional relation between the toughness and the cumulative number of micro-cracks.

The effects of micro-crack toughening in quasi-brittle solids have been theoretically studied with two competing approaches in the literature. The first follows the continuum damage mechanics concept and the micro-cracking zone is modelled as a damaged region with reduced effective moduli. Attention has been focused on the derivation of appropriate constitutive relations governing the micro-cracking zone and the calculation of shielding contributions resulting from the model [Evans and Faber 1984; Evans and Fu 1985; Charalambides and McMeeking 1987; Hutchinson 1987; Ortiz 1987; Ortiz and Giannakopoulos 1989]. The continuum mechanics models interpret the tip of the main crack to be situated in the effective micro-cracked material through the assumption of formation of the process zone. As a result, the shielding contribution is partially counteracted by the toughness degradation of the microcracked material, which should be taken into account to arrive at the net outcome of micro-crack toughening. Although some attempts have been made to clarify the degradation effect [Ortiz 1987; Rose 1986a], the full extent of the toughness degradation is still unknown at present.

The second approach to analysis of the micro-crack toughening effects relies upon fundamental micromechanics analysis in which the micro-cracking zone is modelled as containing multiple discrete micro-cracks in the vicinity of a main crack. This has prompted a number of researchers to investigate the interaction effects between a main crack and micro-cracks using different analytical and numerical techniques [Rose 1986a; Rubinstein 1986; Kachanov 1987; Hori and Nemat-Nasser 1987; Chudnovsky and Wu 1992; Shum and Hutchinson 1990; Gong and Horii 1989]. Exact and explicit series solution to the problem has been provided by Gong and Horii [1989], which has also been extended to treat other interacting micro-defects [Gong and Meguid 1991; Gong and Meguid 1992; Gong and Meguid 1993]. The effect of the release of residual stresses has been included by Gong and Meguid [1991], where the equivalence

between discrete and continuum approaches has been shown. The convergent series solution provides the exact results to the problem.

Furthermore, the closed-form approximate solutions can be readily obtained in a systematic manner by retaining the leading order terms of the general solution. The advantage in using the closed-form approximate solution is that it can be used for the quantitative analysis of micro-crack toughening by integrating the contribution of all the micro-cracks within the process zone. In contrast, most previous studies utilizing the interaction model have been confined to qualitative analyses by investigating some special arrays of a finite number of micro-cracks. It is worth noting that the shielding contribution in the discrete interaction model has a different physical implication from that in the continuum mechanics model. In the interaction model, the reduction of the stress intensity of the main crack is estimated in the original matrix material, thus providing a direct measure of micro-crack toughening.

Therefore it is only meaningful to compare the ultimate toughening (not shielding) effects resulting from the interaction and continuum models. In both models, it has been observed that the choice of micro-cracking criteria plays a major role in the subsequent toughening estimates [Hutchinson 1987; Gong and Meguid 1991].

There are fairly few materials where toughening by micro-cracks has been rigorously verified experimentally [Sigl 1996]. Fully validated examples of micro-crack toughening are restricted to composite materials such as zirconia-toughened alumina [Riihle et al. 1987], SiC-TiB_2 [Gu et al. 1992], and some of the liquid-phase sintered SiC ceramics [Kessler et al. 1992]. The process zone width in these materials is fairly small, i.e. an appreciable micro-crack density extends only across a few grain diameters [Gu et al. 1992]. In all cases micro-cracking is assisted by alternative energy absorbing processes such as martensitic transformation or crack bridging.

2.3.3 Bridging Toughening

Fracture toughness of ceramic materials can be improved remarkably by incorporating short or long fibres. Crack-bridging which is associated with the formation of ligaments by mechanical interlocking of grains and the presence of

whiskers and fibres is an important mechanism in ceramic and ceramic composites. Fig2-4 shows a schematic illustration of a short fiber-bridging toughening mechanism. The presence of such ligaments will increase the fracture toughness of the material. Two types of reinforcing elements that can bridge between the crack surfaces exist: ductile and brittle.

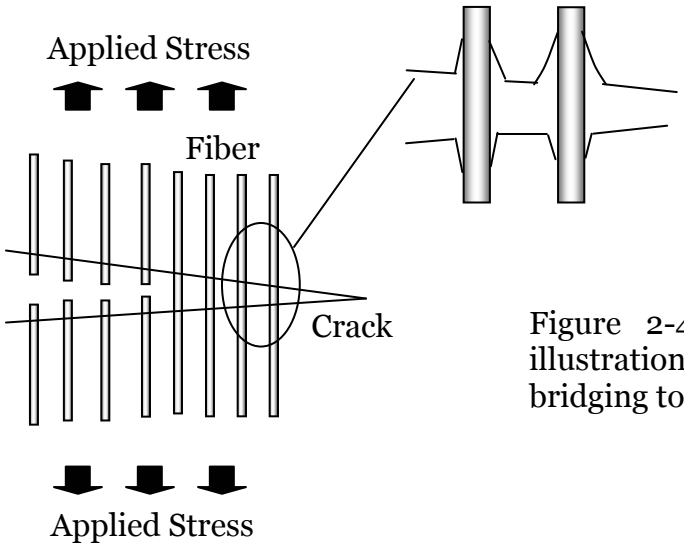

Figure 2-4: Schematic illustration of short-fibre bridging toughening.

Fig.2-5 shows the relation between the fracture toughness and volume fraction of SiC whiskers in SiC_w/AlN composites. In this composite, a main toughening mechanism is a whisker bridging [Jiang et al. 1999].

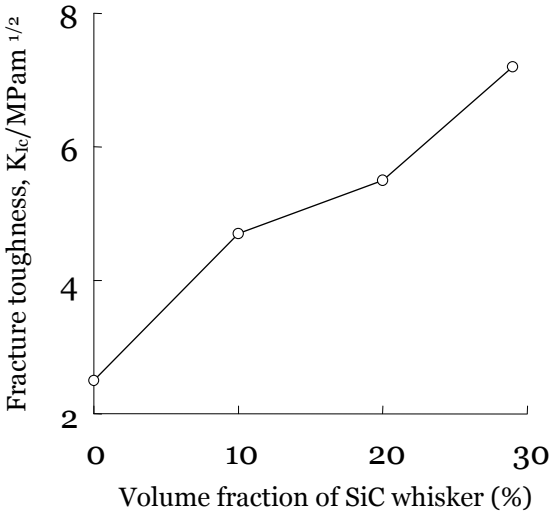

Figure 2-5: Fracture toughness plotted against volume fraction of SiC whiskers in SiC_w/ AlN composites [Jiang et al. 1999].

In the case of ductile bridging, toughness is induced by crack trapping, crack bridging and plastic dissipation. [Kotoul and Vrbka 2003] Fracture toughness enhancement of brittle matrix composites with distributed ductile particles have been discussed extensively in the literature. A phenomenological explanation of toughening can be described. An existing initial flaw in a brittle matrix propagates. The stress concentration around the particles circumvents the ductile particles which are thus left intact behind the crack tip. They act as bridges between the opposing faces of the crack. In the course of further crack opening they deform plastically to a critical elongation and fail by ductile rupture. These particles also prevent excessive crack opening. Since the crack driving force must reach a critical value for further crack extension, this requires a higher value of the applied stress because of the particles. Stretched ductile particles (ligaments) have been detected at considerable distances behind the crack tip.

This mechanism has been already experimentally confirmed with various composites. For example, the toughness of an Al reinforced Al_2O_3 is increased up to 10 $MPam^{1/2}$ compared to 2~3 $MPam^{1/2}$ for the unreinforced Al_2O_3 [Prielipp et al. 1995]. In addition, other properties like strength, reliability and thermal shock resistance are increased [Prielipp et al. 1995; Knechtel et al. 1995]. The mechanism for most of the enhanced properties and mainly for the toughening is the ability of the metal reinforcements to bridge an advancing crack and to exert crack closure stresses on the crack wake [Sigl et al. 1988; Ashby et al. 1989].

The synergistic interactions between transformation toughening and crack bridging by soft particles in a NiAl composite reinforced with 2 mol% yttria partially stabilized zirconia and molybdenum particles are investigated by Li and Soboyejo [1999]. The theoretical study on this mechanism was firstly done by Budiansky et al. [1983].

Furthermore, this mechanism has also been investigated in FG TBCs. In the study by Cai and Bao [1998], crack bridging in the FGM coating is analysed using a position-dependent crack bridging law. Considered is multiple cracking in a ceramic/metal FGM coating perfectly bonded to a homogeneous metal substrate. The coating is taken to be a composite with the local volume fraction of metal varying through the coating thickness according to a power-law type

relation. Elastic and plastic deformation of the metal phase in the coating is included in the model through the crack bridging analysis. Systematic finite element predictions are made for the fracture driving force of bridged multiple cracks in a FGM coating as determined by the crack bridging characteristics, coating gradation, the crack length and spacing, and the applied load [Cai and Bao 1998].

In the case where the bridging material is brittle, the toughness of the fibres or whiskers is similar to the matrix. The inducement of bridging is governed by interfacial properties. This interface provides the means for the transfer of loads from the matrix to the reinforcing fibres. A common problem in characterizing the interfacial behaviour of ceramic matrix composites lies in the complete identification of the various significant parameters which dictate that behaviour. Typically, they include: the critical shear stress for shear debonding, the coefficient of sliding friction, fracture between matrix and fibres and residual stresses. Fundamental information on the strength of the interfacial bond between the fibre and the matrix in ceramic matrix composites can be obtained by using the single concentric pull-out model [Song et al. 1999]. Two analytically-based approaches have been adopted in the treatment of that model. The first utilizes the stress approach to describe the process of sliding and debonding in terms of two parameters: the critical shear stress and the coefficient of sliding friction. The second approach employs micromechanics techniques to describe the conditions necessary for crack growth at the interface of two distinct phases [Meguid 1996].

As mentioned above, it can be considered that intact fibre bridging and broken fibre pullout operate simultaneously. The fracture resistance is provided by the development of fibre bridging and fibre pullout in the crack wake, so the intervening fracture resistance curve, or R curve in fibre-reinforced ceramics is of great interest. Several theoretical analyses of the fibre bridging process have been proposed [Budiansky, Hutchinson and Evans 1986; McCartney 1987; Chiang et al. 1993], and a model of fibre pullout based on weakest-link statistics is also provided by Thouless and Evans [1988]. Although these works are for a static crack, Song et al. [1999] provided a model including both fibre bridging and fibre pullout to calculate the R-curve of a propagating crack.

Considerable numbers of experimental works have been done by many researchers. It has been demonstrated in recent works that fracture toughness and flexural strength of polycrystalline Al_2O_3 can be significantly improved by addition of SiC whiskers. Becher and Wei [1984], Wei and Becher [1985], Becher et al. [1986] and Homeny et al. [1987] have achieved fracture toughness values approaching 10MPa $m^{1/2}$ and flexural strength values approaching 800MPa. As mentioned by Garnier et al. [2005], toughening mechanisms, such as crack deflection, whisker pullout and whisker bridging, depends to a large extent on the nature of the whisker/matrix interface. Several factors affect the whisker/matrix interface, including matrix chemistry, whisker surface chemistry, whisker morphology and thermal expansion mismatches. The internal stresses are also expected to affect the toughening behaviour of SiC-whiskers reinforced alumina matrix composite as shown by Predecki et al. [1988] and Li and Bradt [1989]. The composites with other ceramic matrix reinforced by SiC wiskers have been also investigated on bridging toughening by many researchers. Li et al. [2006] investigated microstructure and properties of (SiC, TiB_2)/B_4C composites, and Baldacim et al. [2003] investigated mechanical properties of Si_3N_4–SiC_w composites.

Meanwhile, it is well recognized that the mechanical properties of fibre composites are highly dependent on the integrity of the interface [Kim and Mai 1998]. Interface debonding and post-debonding friction are two important mechanisms of energy absorption during the failure of a composite interface. Either high strength or high toughness, or both, of composite materials can be achieved by modifying the interface properties. Experimental studies have been performed to understand the effect of interface on the mechanical behaviour of composites. Among these tests, the single-fibre pull-out test is one of the most powerful tools to study the fracture behaviour of a fibre-bridged crack in a fibre composite. To provide a theoretical basis for the single-fibre pull-out test, several models have been developed. Gao, Mai and Cotterell [1988] presented the first fracture mechanics analysis including the effects of interfacial friction in the debonding region, fibre Poisson contraction and initial thermal residual pressure on the stress distributions by extending the Lame solution for a 2D-axisymmetric problem to the pull-out problem,. Another relevant piece of work, also based on the Lame solution, was developed by Hutchinson and Jensen

[1990], whose solution is derived for composite systems with residual stresses in both radial and axial directions.

Accordingly, the bridging mechanism has been investigated experimentally and theoretically by many researchers from various aspects. This toughening mechanism is extremely effective for bulk ceramics and ceramic matrix composites. However, it is difficult to use it in toughening of TBCs since TBCs are usually very thin. In the following, transformation toughening, which is the most promising toughening of TBCs, is described.

2.3.4 Transformation toughening

The stress-induced transformation toughening mechanism, which has recently attracted a great deal of attention in toughening of brittle intermetallic compounds [Kelly and Rose 2002], could now be considered to be the best toughening mechanism for FG TBC structures as already described. The essence of transformation toughening can be illustrated in Fig. 2-6. Under an applied load stress-induced transformation occurs at the crack tip and produces a transformation zone. As the crack grows, a "wake" of transformed material is left behind, in which the remaining strain lead to an increase in the toughness [Kelly and Rose 2002].

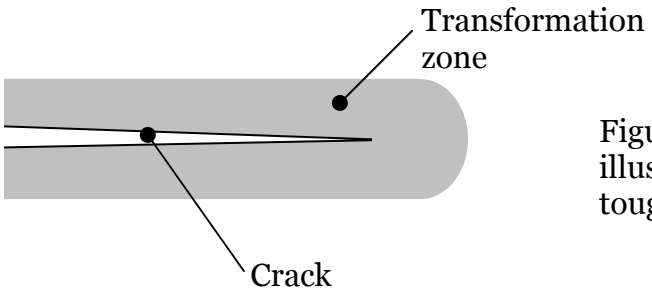

Figure 2-6: Schematic illustration of transformation toughening.

Fig. 2-7 shows the relation between fracture toughness and volume fraction of ZrO_2 particles in ZrO_2/ Ti_3SiC_2 composites [Shi and Pan 2007]. As seen here, relatively high toughening can be obtained. In the following, the

experimental and theoretical literature on transformation toughening by ZrO_2 is reviewed.

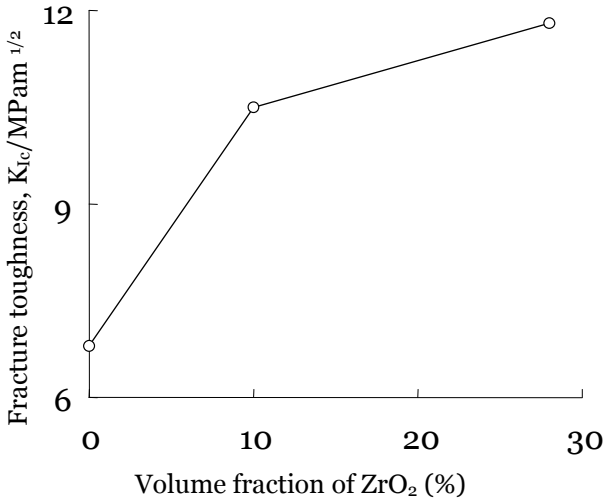

Figure 2-7: Fracture toughness plotted as a function of volume fraction of ZrO_2 particles in ZrO_2/ Ti_3SiC_2 composites [Shi and Pan 2007].

2.3.4.1 Experimental studies

The phenomenon of stress transformation in zirconia-enriched composites was first reported by Garvie et al. [1975]. Some of the early experimental investigations on zirconia composites were performed by Gupta et al. [1978], Evans and Heuer [1980], Lange [1982] and others. In accordance with these investigations, the unconstrained phase transformation of zirconia particles results in approximately 4% dilatation and 16% shear strain. However, the particles embedded into a composite transform with twin bands of an alternative character so that the overall change in shear strain is very small. Therefore, the strain changes due to stress-induced phase transformation in composites are usually assumed to be dilatant as illustrated in Fig.2-8.

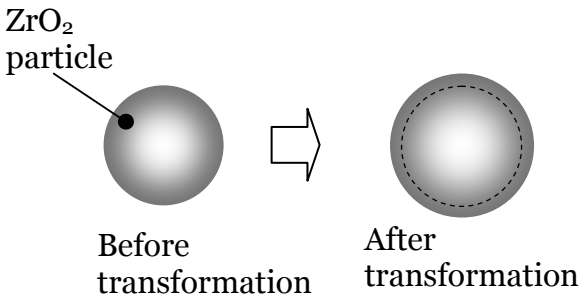

Figure 2-8: Stress-induced phase transformation with a dilatant strain.

When the particles surround a stable or a growing crack, the high stress concentration near the crack tip will trigger the transformation of zirconia particles near the crack tip [Stump and Budiansky 1989]. The typical transformation zone sizes found experimentally are of the order of 20 μm or less [Casellas et al. 2001]. The dilatant transformation will induce closure tractions on/along the crack faces. The overall stress concentration near the crack tip is, therefore, reduced; hence, the fracture toughness of the composite is enhanced, since a higher remote stress must be applied to reach the critical conditions at the crack tip.

The stress-induced transformation toughening mechanism was successfully used to increase the fracture toughness of brittle ceramics [Kelly and Rose 2002; Basu et al. 2004]. In recent years, the demand for the development of super high temperature resistant and light-weight materials applied to aero-space structures has stimulated intensive research on the transformation toughening of brittle intermetallics composites, particularly with molybdenum or nickel aluminide matrices [Sbaizero et al. 2003]. The transformation toughening mechanism is now regarded as the most effective way to enhance the fracture toughness of ceramics and ceramic matrix composites [Cesari et al. 2006; Basu et al. 2004; Kelly and Rose 2002].

2.3.4.2 Theoretical studies

The continuum models of the phenomenon were developed by Lange [1982], McMeeking and Evans [1982], Budiansky et al. [1983] and Stump and Budiansky [1989]. All these models are based on the assumption of effectively homogenous composite material, where only macroscopic aspects of the material deformation are considered. Strictly speaking, these theories are only applicable to the composite with the same material properties of all constituent phases, which have to be equal to the material properties of zirconia. However, in a real composite, the effect of the mismatch in material properties for all constituent phases on the transformation toughening mechanism can be significant.

Consider, for example, a limiting case, a two-phase composite with rigid matrix and soft transformable particles. In such composite the stress induced transformation in the particles will not affect the dilatation of the representative volume element (RVE) of the composite [Hill 1963] and, in its turn, the high stress concentration in the RVE in the vicinity of the crack tip will generate much less stress in the particles reducing the size of the transformation zone. Both mechanisms will lead to much less toughening effect in comparison with that predicted assuming the homogenous material with the effective properties of the composite (continuum models). It can be shown that the opposite situation to that described above takes place for a composite with soft matrix and rigid particles. When a multi-phase composite is enriched with zirconia particles, the final effect of the mismatch in the material properties of the constituent phases is difficult to envisage [Tsukamoto and Kotousov 2007; Chen and Tuan 2001; Chen et al. 2000].

A number of numerical studies have reported a significant influence of local stress concentration, particle size, shape and microstructure on the transformation toughening mechanism. Some of these factors were recently analysed using a hybrid finite element method [Alfano et al. 2006; Zeng et al. 2004] and micro-mechanical approach [Tsukamoto and Kotousov 2006]. For multi-phase composites, in addition to the factors discussed above, a strong influence of the non-transforming dispersed phases on the transformation toughening mechanism is also expected. This was confirmed by results of some

experimental investigations [Chen and Tuan 2001; Chen et al. 2000]. However, it seems so far there were no attempts to study theoretically the toughening effect in multi-phase composites [Zeng et al. 2004]. The details of this point are mentioned in the critical review.

2.4 Micromechanics of composite materials

Continuum mechanics deals with ideal homogeneous materials, which describe their response to external exertions using appropriate constitutive relations. It is a trivial statement that any materials are microscopically inhomogeneous, even if it appears homogeneous at some natural scale of observation. Inevitably, a description of any material in terms of continuum mechanics is an approximation. This leads us to a fundamental and widespread problem of science and technology, concerning micro-macro interconnection, i.e. a proper and reliable determination of the macroscopic behaviour of a medium which exhibits microscopic heterogeneity, on the base of the appropriate and available microstructural information [Markov 2000].

A considerable large effort has been made for estimates of the overall elastic properties of composite materials. Extensive investigations on the effective thermo-physical properties of mixers and composites were initiated more than a hundred years ago by the famous scientists J.C Maxwell, Lord Rayleigh, and Albert Einstein.

The two extreme rule-of-mixture models are the Voigt estimate (VE) and Reuss estimate (RE) that are proposed to describe the two-phase composites. The VE corresponds to the case when the applied load causes equal strains in the two phases. The overall composite stress is the sum of stresses carried by each phase. Therefore, the overall Young's modulus is the average of the moduli of the constituents weighted by the volume fraction. The RE corresponds to the case when each phase of the composite carries an equal stress. The overall strain in the composite is the sum of the net strain carried by each phase.

Many fundamental aspects of the continuum mechanics theory of inhomogeneous media have been studied by solid mechanics scientists or applied mathematicians, for example, Eshelby, Hashin, Shtrikman, Hill,

Walpole, Willis, Levin, Rosen, Shapery and others. Besides these, a large number of papers have been published, the subject therein being mostly the prediction of overall elastic constants. Hashin [1983] classifies them into three categories: (a) direct approach, (b) variational approach and (c) approximations.

The direct approach implies those calculations which yield exact closed-form solutions to the overall properties of an "ideal" composite, wherein some geometrical or other simplification is introduced for only mathematical reasons. The variational approach is an alternative method of rigorous theoretical treatment of the problem. However, since the details in phase geometry other than the phase volume fractions are usually unspecified, the results are given as the upper and lower bounds for the overall properties with substantial margins between them. Thus, from a practical point of view, theoretical rigor must often be sacrificed, i.e. some reasonable approximation is used to obtain closed-form estimates for the overall properties of various type of composite of practical importance [Wakashima and Tsukamoto 1991]. Among such approximate methods, the self-consistent model [Hill 1965], its modification and mean-field micromechanics using Mori-Tanaka concept [Mori and Tanaka 1973] are relatively popular [Wakashima and Tsukamoto 1991].

The self-consistent model and its modification replace the actual "many-body" problem by a "one-body" problem via the concept of an effective medium, i.e. among numerous existing particles there is only one that is retained as it stands while all the others are smeared out so that they become, together with their surrounding matrix, an effectively homogeneous medium having the overall properties to be sought. In the original self-consistent model, the single particle is directly embedded in the effective medium (Fig.2-9). On the other hand, its modification, called a generalized self-consistent, or three phase, model, considers a "composite particle" consisting of a particle core and a matrix shell, instead of the particle itself in the original model.

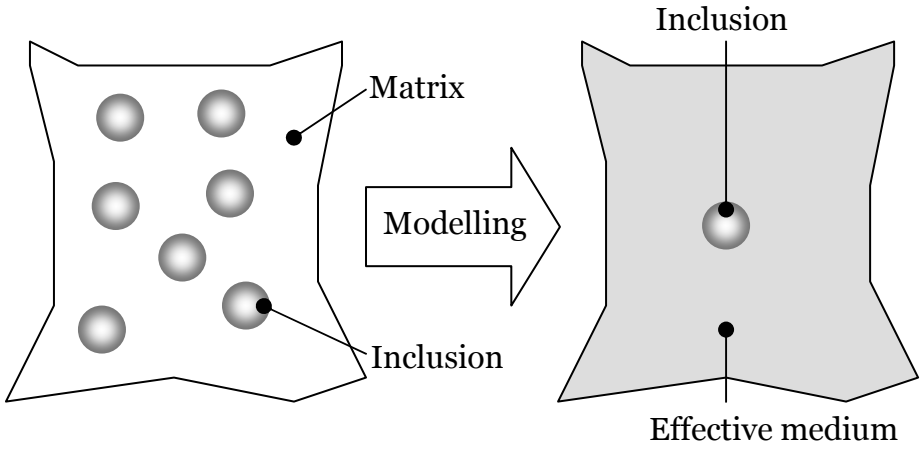

Figure2-9: Self-consistent model.

The approximate method, called the mean-field micromechanics model, started from as attempt, in predicting the overall coefficients of thermal expansion (CTEs) of composites, to exploit Eshelby's work by incorporating the Mori-Tanaka concept for the average stress over the matrix of a homogeneous material with identical misfitting aligned inclusions. Wakashima and Tsukamoto [1991] investigated a mean-field micromechanical approach based on Eshelby's equivalent methods and Mori-Tanaka's mean field concept (Wakashima-Tsukamoto estimate). In their article, thermo-mechanical effective properties such as elastic constants, thermal expansion coefficients as well as thermal conductivity of multi-phase composites were derived. Furthermore, the micro-stress in each phase is expressed in closed-form, and recently their approach has been used to analyse thermal stress states in FG TBCs by Tsukamoto and others [1990; 1992; 2003]

The upper and lower bounds, which restrict the range of overall moduli and thermal expansion coefficient for a macroscopically isotropic inhomogeneous material made up of isotropic phases with arbitrary phase geometry, were derived by Hashin and Shtrickman [1963] using variational approach. Some researcher investigated and discussed the approximation methods mentioned here through the comparison with the Hashin-Shtrikman bounds.

Wakashima-Tsukamoto estimate, which is employed in this study, seems useful and easy to predict effective thermo-mechanical properties of multi-phase composites. The effective thermo-mechanical properties obtained from this estimate are inside the Hashin-Shtrikman bounds for two phase composites. This approach was already adopted to the design and analysis of FG TBCs by Tsukamoto [2003]

2.5 Critical review

2.5.1 Transformation toughening

The stress-induced transformation toughening mechanism has been successfully used to increase the fracture toughness in structural ceramics. The continuum models of the stress-induced transformation toughening phenomenon were developed by Lange [1982], McMeeking and Evans [1982], Budiansky et al. [1983] and Stump and Budiansky [1989]. A special tribute should be given to a very important contribution into the area by an Australian scientist, Dr Francis Rose [1986b] who discovered the so called lock-up effect, or phenomenon of infinite toughness in zirconia enriched composites. Continuum models of stress-induced transformation toughening significantly enhanced the understanding of the toughening mechanism. They also showed that the size of the transformation zone was important in determining the overall levels of toughening for steady state and growing cracks. **However, all these models are based on the assumption of an effectively homogenous composite material, where only macroscopic aspects of the material deformation are considered.** As such, the continuum models ignore the mismatch effect in material properties of the constituent phases on the transformation toughening mechanism. Generally speaking, the continuum theories are only applicable to a composite with the same material properties as its constituents, which have to be equal to the properties of transformable materials.

In this project, a mean-field micromechanical approach is incorporated with the continuum model in order to develop a more realistic theory investigating the effect of microstructure and mismatch in thermo-mechanical

properties of constituent phases on the transformation toughening. Some useful and important information is obtained through the numerical examinations.

2.5.2 Design against fracture of FG TBCs

In the design of FG TBCs many researchers have been considering the reduction of thermal stresses. Most of them adopt the tensile strength of ceramics as a criterion of failure of FG TBCs. However, ceramics usually have low fracture toughness and behave as ideally brittle materials. The failure of such materials should be assessed and investigated using fracture toughness criterion. Some researchers have been investigating fracture behaviour of FG TBCs based on the linear elastic fracture mechanics [Konda and Erdogan1994; Chen and Erdogan1996; Jin and Batra 1996; Qian et al. 1997; Shaw 1998; Huang et al. 2002, 2003].

Meanwhile, many attempts have been made to improve the toughness of ceramics as already described. The new generation of ceramics includes multi-phase materials and ceramic composites that have vastly improved toughness. The mechanisms that lead to improved fracture resistance in modern ceramics and composites include micro-crack toughening, transformation toughening, ductile phase toughening, fiber bridging toughening and others. **However, to the best knowledge which is supported by a careful literature and patent search there have been no attempts to apply this mechanism to the toughening of FG TBCs. Design against fracture of FG TBCs using such a toughening mechanism has not been done yet.**

In this project, the transformation toughening, which is considered to be suitable mechanism of toughening of TBCs, is applied to the improvement of fracture properties of FG TBCs. A design against fracture of FG TBCs is performed based on the fracture mechanics and micromechanical considerations.

Chapter 3

Linear elastic fracture mechanics

3.1 Introduction

Linear elastic fracture mechanics estimate the stress field near the crack tip using the theory of elasticity based on the assumption that material is linear elastic. This relates the stress field to remote stresses applied to the cracked component, the crack size and shape as well as material properties of the cracked component. Most formulas are derived for either plane stresses or plane strains, associated with the three basic modes of loadings on a cracked body: opening, sliding, and tearing. Linear elastic fracture mechanics is valid only when the inelastic deformation is small compared to the size of the crack, which is called small-scale yielding.

Ceramics tend to be very brittle compared to metals. Traditional ceramics are monolithic and behave as ideally brittle materials and a propagating crack need only overcome the surface energy of materials because they do not yield. As described in Chapter 2, the new generation ceramics such as ceramic matrix composites have vastly improved toughness. Under certain conditions, two brittle solids can be combined to produce a material that is significantly tougher than either parent materials, for example, bridging toughening. For traditional and new generation ceramics, the theoretical investigation based on such a linear elastic fracture mechanics plays an important role.

In the following, the concept of linear elastic fracture mechanics is firstly stated. Then the complex variable method and definition of stress intensity factor representing a stress field in vicinity of a crack tip under Mode I loading are described. These concepts are directly related to the continuum model of transformation toughening described in Chapter 4. Lastly, singular integral equation method is described, which is accurate, useful and easy to handle and frequently applied to various crack problems. In the project, this method is used to investigate the influence of T (transverse)-stress on the short fibre-bridging toughening, which is described in Chapter 7.

3.2 Concept of linear elastic fracture mechanics

Linear elastic fracture mechanics theory is based on the following argument. Consider a crack in a reasonably brittle, isotropic solid. If the solid were ideally elastic, we would expect the asymptotic solution become accurate as well known. Away from the crack tip, the fields are influenced by the geometry of the solid and boundary conditions, and the asymptotic crack tip field would not be accurate. In practice, the asymptotic field will also not given an accurate representation of the stress fields very close to the crack tip either. The crack may not be perfectly sharp at its tip, and if it were, no solid could withstand the infinite stress predicted by the asymptotic linear elastic solution. Therefore it is anticipated that in practice the linear elastic solution will not be accurate very close to the crack tip either. The crack may not be perfectly sharp at its tip, and if it were, no solid could withstand the infinite stress predicted by the asymptotic linear elastic solution. Therefore, it is anticipated that in practice the linear elastic solution will not be accurate very close to the crack tip itself, where material nonlinearity and other effects play an important role. So the true stress and strain distributions will have 3 general regions as shown in Fig.3-1.

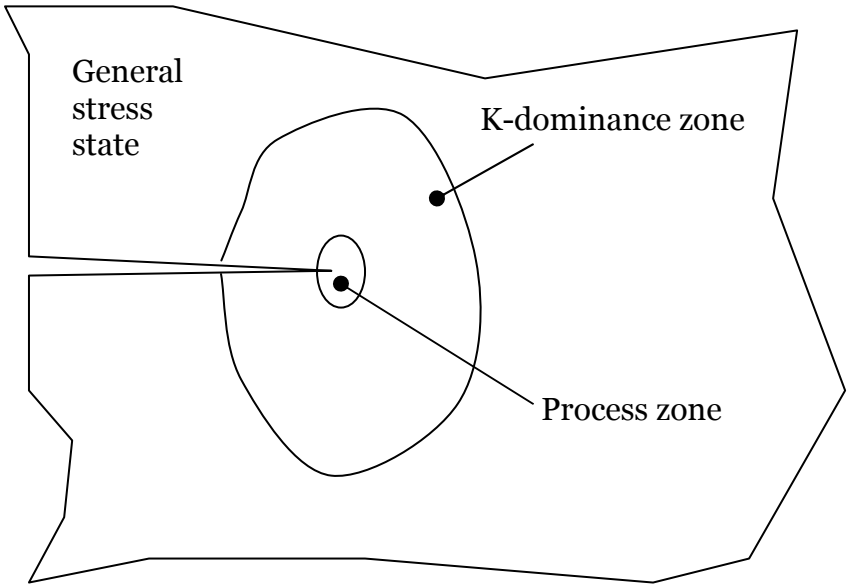

Figure 3-1: Schematic illustration of zones near crack tip.

(1) In the region immediately surrounding the crack tip, called the process zone (or cohesive zone), all of the nonlinear dissipative processes that ultimately allow a crack to move forward, are assumed to occur. Fracture mechanics avoids any sort of detailed description of this zone, and simply posits that it will consume some energy, G, per unit area of crack extension. The size of the process zone is material dependent, ranging from nano meters in glass to microns in brittle polymers. The typical size of the process zone can be estimated by using the radius at which an assumed linear elastic stress field surrounding the crack tip would equal the yield stress of the material.

The dissipative processes within the process zone determine the fracture energy, G, defined as the amount of energy required to form a unit area of fracture surface. In the simplest case, where no dissipative processes other than the direct breaking of bonds take place, C is a constant, depending on the bond energy. In the general case, G may well be a complicated function of both the crack velocity and history and differ by orders of magnitude from the surface energy defined as the amount of energy required to sever a unit area of atomic bonds. No general first principles description of the process zone exists, although numerous models have been proposed.

(2) A bit further from the crack tip, there will be a region where the linear elastic field asymptotic crack tip field might be expected to be accurate. This is known as the region of K dominance. In the vicinity of the tip, but outside of the process zone, the stress and strain fields adopt universal singular forms which solely depend on the symmetry of the externally applied loads. In two dimensions the singular fields surrounding the process zone are entirely described by three constants, stress intensity factors, K_{I}, K_{II} and K_{III}. The stress intensity factors incorporate all of the information regarding the loading of the material and are related to the energy flux into the process zone. The larger the overall size of the body in which the crack lives, the larger this region becomes.

(3) Far from the crack tip the stress field depends on the geometry of the solid and boundary conditions. Material failure (crack growth or fatigue) is a consequence of the stuff that goes on in the process zone. Linear elastic fracture mechanics postulates that one doesn't need to understand this stuff in detail, since the fields in the process zone are likely to be controlled mainly by the fields in the region of K dominance. The fields in this region depend only on the

stress intensity factors K_I, K_{II} and K_{III}. Therefore, the state in the process zone can be characterized for phenomenological purposes by the three stress intensity factors. If this is true, the conditions for crack growth, or the rate of crack growth, will be only a function of stress intensity factor.

The safety of a structure of component that containing a crack can be estimated with the materials characterized. Calculating the stress intensity factors for the crack in the structure and using phenomenological fracture or fatigue laws decide whether or not the crack will grow.

3.3 Stress intensity factor and fracture toughness

Stress intensity factor (SIF), K, is a parameter indicating the level of stress intensity near the tip of a crack caused by a remote load or residual stresses, which is useful for providing a failure criterion for brittle materials. There are three modes of fracture. Mode I fracture is the condition in which the crack plane is normal to the direction of largest tensile loading. This is the most commonly encountered mode and, therefore, for the remainder of the material we will consider K_I. Mode II is a sliding mode and mode III is a tearing mode. The stress intensity factor is a function of loading, crack size, and structural geometry. The expression of the stress intensity factor is given using the complex variable methods later.

Fracture toughness is a property which describes the ability of a material containing a pre-existing flaw to resist fracture. As the stress intensity factor reaches a critical value (K_c), unstable fracture occurs. This critical value of the stress intensity factor is known as the fracture toughness of the material. Fracture toughness is a very important material property since the occurrence of flaws is not completely avoidable in the fabrication, or service of a material/component. Since engineers can never be totally sure that a material is flaw free, it is common practice to assume that a flaw of some chosen size will be present in some number of components and use the linear elastic fracture mechanics approach to design critical components.

3.4 Complex variable method applied to a crack problem

The introduction of complex variables in the formulation of the two-dimensional elasticity problem offers significant advantages. In addition to algebraic compactness, the use of complex analytic functions ensures that the biharmonic are satisfied. In the adaptation of this approach to the crack problem, two formulations have been adopted. The classical Goursat-Kolosov approach, further developed by Muskhelishvili [1953], offers powerful tools, including conformal mapping, to solve a wide variety of singular problems. However, this approach is mathematically very demanding.

Fortunately, there is another complex-variable method, limited to straight crack problems only, that offers the advantage of algebraic compactness and simplicity without the disadvantages of the more arduous classical approach. This method, introduced by Westegaard in 1939, applies the semi-inverse method to the Airy stress function expressed in the complex domain. As originally formulated by Westergaard, this method could be applied only to infinite body problems with uniform (including zero) remote boundary conditions. These restrictions were known at the outset. Nonetheless, the method was widely used in the late 1950s and throughout the 1960s to solve a number of significant problems during the early development of fracture mechanics theory.

The method was modified by Sih [1966] and Eftis and Liebowitz [1972] to accommodate unequal remote biaxial loads, but otherwise the method still has restricted application. More recently, the Goursat-Kolousov representation of the Airy stress-function for planar crack problems was recast into Westergaard notation [Sanford 1979], and second analytic function was introduced into the analysis. This generalized Westergaard formulation remains both the completeness of Goursat-Kolosov approach and the algebraic simplicity of Westergaard's formulation. As a result, the method can now be applied to both infinite- and finite-body problems with the only restriction that the crack is constrained to lie along the y=0 plane. In the following, the generalized Westergaard method will be applied.

Here, an overview of the derivation of the mode I stress field equations is given. Now consider the specific problem of an infinite, biaxially loaded plate containing a crack. To solve this problem we can take a complex stress function of a type introduced by Westergaard mentioned above:

$$\Phi = \mathrm{Re}\bar{\bar{\phi}}(z) + y\,\mathrm{Im}\bar{\phi}(z) \tag{3.1}$$

In the equation, $\phi(z)$ is an analytic function of the complex variable z(x+iy), and $\bar{\phi}(z) = d\bar{\bar{\phi}}(z)/dz$ and $\phi(z) = \bar{\phi}(z)/dz$. It can be proved that the real (Re) and imaginary (Im) parts of such an analytic function fulfil the biharmonic equation, and that the products of these part with the variables x and y also do so. Thus analytic functions like that in the equation are used as stress functions. Using Caushy-Rieman equations,

$$\frac{\partial(\mathrm{Re}\,\phi(z))}{\partial x} = \frac{\partial(\mathrm{Im}\,\phi(z))}{\partial y} \tag{3.2}$$

and

$$\frac{\partial(\mathrm{Re}\,\phi(z))}{\partial y} = -\frac{\partial(\mathrm{Im}\,\phi(z))}{\partial x} \quad . \tag{3.3}$$

It is possible to find expressions for σ_x, σ_y and τ_{xy} by differentiating equation according to the rules of equation. This gives

$$\sigma_x = \mathrm{Re}\,\phi(z) - y\,\mathrm{Im}\,\phi'(z) \tag{3.4}$$

$$\sigma_y = \mathrm{Re}\,\phi(z) + y\,\mathrm{Im}\,\phi'(z) \tag{3.5}$$

$$\tau_{xy} = -y\,\mathrm{Re}\,\phi(z) \tag{3.6}$$

where $\phi'(z)$ is the first order derivative. Note that equations (3.4), (3.5) and (3.6) are general solution which give stresses for any $\phi(z)$. However, the correct

stresses for a particular problem will be obtained only by using a function $\phi(z)$ that fulfils a number of boundary conditions pertaining to that problem.

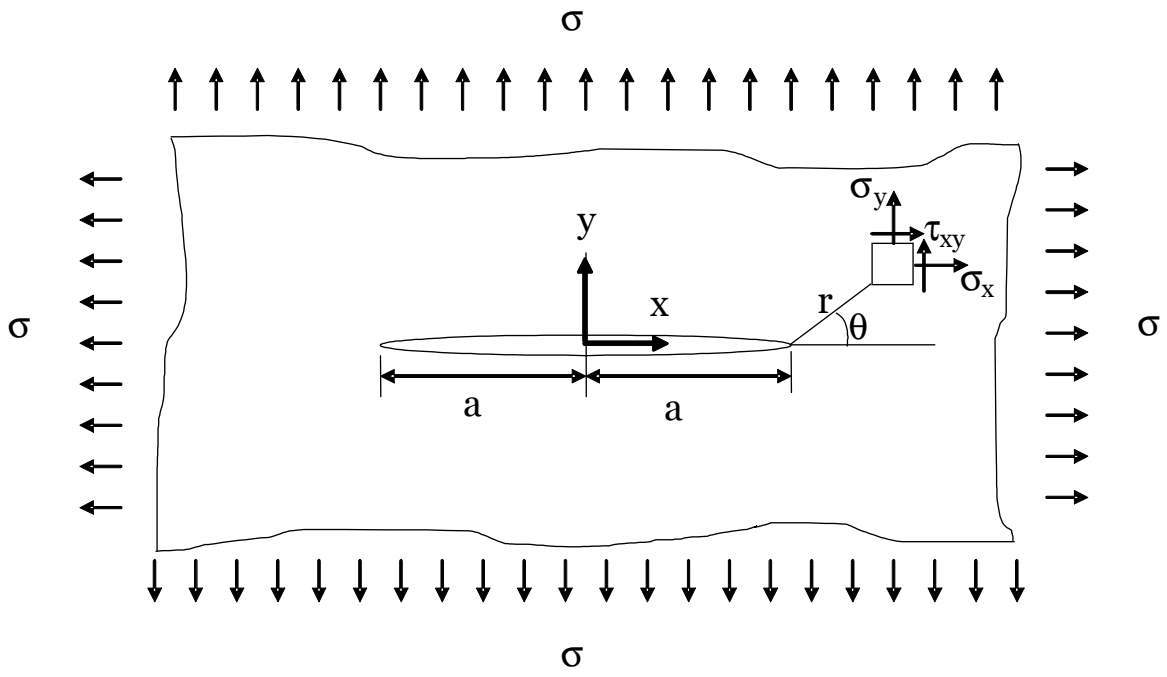

Figure3-2: Infinite plate containing a slit crack subjected to a biaxial loading.

For an infinite, biaxially loaded plate containing a crack as shown in Fig. 3-1 the boundary conditions are readily stated, namely

1) $\sigma_y = 0$ for $-a < x < +a$ and $y = 0$

2) $\sigma_y \to \sigma_0$ as $x \to \pm\infty$

3) $\sigma_y \to \infty$ (i.e. a singularity) at $x = 0$, since the crack is a stress raiser.

Now a function $\phi(z)$ that fulfils these boundary conditions must be chosen. One example is the function

$$\phi(z) = \frac{\sigma}{\sqrt{1 - a^2 / z^2}} . \qquad (3.7)$$

We know from equations (3.4), (3.5) and (3.6) that along the x-axis (i.e. y=0) $\sigma_y = \mathrm{Re}\,\phi(z)$, and it is seen from equation (3.7) that for $-a < x < +a$ $\mathrm{Re}\,\phi(z) = 0$ and hence $\sigma_y = 0$, as required by the first boundary conditions. Furthermore, for $z \to \infty$, i.e. for infinite thickness, equation (3.7) gives $\phi(z) = \sigma$, and for $x = a$ or $-a$ there is a singularity, so that the second and third boundary conditions are also fulfilled.

However, if the origin is translated to the crack tip by taking $\eta = x - a$, we obtain another suitable stress function which turns out to be easier to use.
This function is

$$\phi(\eta) = \frac{\sigma}{\sqrt{1 - a^2/(a+\eta)^2}} = \frac{\sigma(a+\eta)}{\sqrt{(a+\eta)^2 - a^2}} . \qquad (3.8)$$

A first order approximation for this equation, valid for $\eta << a$, is simply

$$\phi(\eta) = \frac{\sigma a}{\sqrt{2a\eta}} = \sigma\sqrt{\frac{a}{2\eta}} . \qquad (3.9)$$

Note that this approximation is the first term in a series expansion. Using equation (3.9) a change can easily be made to a polar coordinate representation (r, θ) with origin at the crack tip as shown in Fig. 3-1. Then $\eta = re^{i\theta}$ and

$$\phi(\eta) = \frac{\sigma\sqrt{a}}{\sqrt{2r}} \cdot e^{-\frac{1}{2}i\theta} \text{ or } \frac{\sigma\sqrt{\pi a}}{\sqrt{2\pi r}} \cdot e^{-\frac{1}{2}i\theta} . \qquad (3.10)$$

Equation (3.10) is only valid for $r << a$, owing to the approximation made to obtain equation (3.9). Having obtained equation (3.10) straightforward algebra

can be used to find $\mathrm{Re}\,\phi(\eta)$, $\mathrm{Re}\,\phi'(\eta)$ and $\mathrm{Im}\,\phi'(\eta)$. In turn these quantities can be substituted into equations (3.4), (3.5) and (3.6), resulting in

$$\sigma_x = \frac{\sigma\sqrt{\pi a}}{\sqrt{2\pi r}} \cdot \cos\frac{\theta}{2}\left(1 - \sin\frac{\theta}{2}\sin\frac{3\theta}{2}\right) \tag{3.11}$$

$$\sigma_y = \frac{\sigma\sqrt{\pi a}}{\sqrt{2\pi r}} \cdot \cos\frac{\theta}{2}\left(1 + \sin\frac{\theta}{2}\sin\frac{3\theta}{2}\right) \tag{3.12}$$

$$\tau_{xy} = \frac{\sigma\sqrt{\pi a}}{\sqrt{2\pi r}} \cdot \sin\frac{\theta}{2}\cos\frac{\theta}{2}\cos\frac{3\theta}{2}. \tag{3.13}$$

Equations (3.11), (3.12) and (3.13) show that all the stresses tend to infinity at $r = 0$ (the crack tip) and are products of the geometrical position $\frac{1}{\sqrt{2\pi r}} \cdot f(\theta)$ and a factor, $\sigma\sqrt{\pi a}$, which is a simple function of remote stress and crack length. Thus the factor, $\sigma\sqrt{\pi a}$, determines the magnitude of the elastic stresses in the crack tip field.

This factor, $\sigma\sqrt{\pi a}$, is called the mode I stress intensity factor:

$$K_I = \sigma\sqrt{\pi a}. \tag{3.14}$$

In practice, the far-field stress in the x direction does not have any effect on the crack tip stress field. Hence, the above expression (3.14) for K_I is also applicable when under uniaxial far-field stress in the y direction. This equation (3.14) is accompanied with the equations (3.11)-(3.13), which appears as an equation (4.1) in Capter4.

3.5 Hutchinson's solution for transformation spots in the vicinity of a semi-infinite crack

A solution was derived by Hutchinson [1974] for the stress and stress intensity factor induced by two symmetrically placed dilatation "spots" in the vicinity of a semi-infinite crack. Fig.3.3 shows the geometry of the problem. Plane strain and mode I behaviour were considered. The mean stress (at the

position of z) induce by dilatation spots with the area of dA and dilatation strain of θ, which are placed at $z_0 = x_0 + iy_0$ and $\tilde{z}_0 = x_0 - iy_0$, was derived as follows,

$$\sigma_m = \frac{E\theta}{18\pi}\frac{1+\nu}{1-\nu}\mathrm{Re}\left\{\frac{1}{\sqrt{zz_0}(\sqrt{z}+\sqrt{z_0})}+\frac{1}{\sqrt{z\bar{z}_0}(\sqrt{z}+\sqrt{\bar{z}_0})}\right\}dA \tag{3.15}$$

These dilatational spots also induce a change in the stress intensity factor, dK_{tip}, which can be given as,

$$dK_{tip} = \frac{E\theta}{6\sqrt{2\pi(1-\nu)}}\mathrm{Re}\left\{z_0^{-2/3}+\bar{z}_0^{-2/3}\right\}dA_0 \tag{3.16}$$

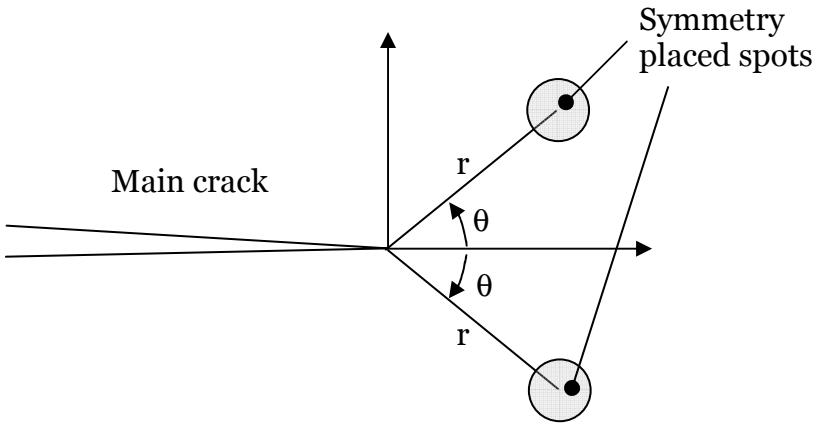

Figure 3-3: Geometry of the problem. Two transformation elements located with respect to the crack plane.

These two equations (3.15) and (3.16) are used in Chapter 4 for investigating the transformation toughening by ZrO_2 in "homogeneous" composites [Stump and Budiansky 1983]. Hutchinson [1974] also solved the more general case that the two symmetrically-placed spots have a transformation strain such as $(\varepsilon_{11}^T, \varepsilon_{22}^T, \varepsilon_{12}^T)$. In this case, the solution for a change in the stress intensity factor is given as,

$$dK_{tip} = (8\pi)^{-1/2}\frac{1}{(1-\nu_M^2)}Er^{-3/2}h_{\alpha\beta}(\theta)\varepsilon_{\alpha\beta}^T dA \tag{3.17}$$

where,

$$h_{11} = \frac{1}{4}\left(\cos\frac{3}{2}\theta + 3\cos\frac{7}{2}\theta\right) \tag{3.18}$$

$$h_{22} = \frac{1}{4}\left(7\cos\frac{3}{2}\theta - 3\cos\frac{7}{2}\theta\right) \tag{3.19}$$

$$h_{12} = h_{21} = \frac{3}{4}\left(\sin\frac{7}{2}\theta - \sin\frac{3}{2}\theta\right) \tag{3.20}$$

Hutchinson [1987] applied this solution to the analysis of micro-cracking toughening problems. The effect of profuse micro-cracking at the tip of a macroscopic crack was studied with emphasis on the reduction in stress intensity, or shielding, within the micro-crack region. Yang and Li [2003] also applied this solution to investigate the interaction between a main semi-infinite crack and micro-defects.

3.6 Stress intensity factor in an inhomogeneous body

In two-phase composites, when a crack occurs near an inhomogeneity, the shape of the inhomogeneity, the difference in the elastic property between the inhomogeneity and matrix material will cause the near-tip stress intensity factor to be greater or less than that in a homogeneous material. Due to the importance of the near crack-tip field for the fracture behaviour of the composites, the crack–inhomogeneity interaction studies have received considerable attention. The effect of the presence of inclusions on the stress states at the crack tip has been studied associated with various toughening effect as described in Chapter 1. Here we consider the interaction between cracks and inclusions. For analytical and numerical studies, the attention has been mostly focused on numerical analysis [Lipetzky and Schmauder 1994; Lipetzky and Knesl 1995; Papaioannou and Hilton 1974; Wang et al. 1998; Tamate 1968; Helsing 1999], such as finite element method (FEM) [Lipetzky and Schmauder 1994; Lipetzky and Knesl 1995; Papaioannou and Hilton 1974], boundary element method (BEM) [Papaioannou and Hilton 1974; Wang et al. 1998] and

singular integral equation method [Tamate 1968; Helsing 1999]. These numerical analyses provide some insight into better understanding of the interaction between crack and inhomogeneity. Yang and Li [2003] derived approximately analytical solutions for the lowest order solution to crack–inhomogeneity interaction. In the following, the singular integral equation methods to analyse the interaction between macro-crack and micro-defects are described, which was presented by Rubinstein [1986]. Problems are considered in terms of complex stress potentials for linear elasticity and formulated as a singular integral equation on the semi-infinite interval.

3.6.1 Approach based on singular integral equation method

The fracture toughness of engineering materials is influenced by the material microstructure. The existence of voids, inclusions, micro-cracks, etc., affects the possible propagation of macro-cracks. Here, a quantitative evaluation of the influence of these micro-structural properties on the stress intensity factor is described according to the work by Rubinstein [1986]. Based on Rubinstein's work, the elastic interaction of a macro-crack with particular micro-defects is discussed. The macro-crack is represented as a semi-infinite crack subjected to a remote stress field which is characterized by a remote stress intensity factor. The plane problem is considered here, and micro-defects are, therefore, represented as a cylindrical inclusion, hole and crack.

The formulation can be outlined as follows: The stress functions representing the interaction of a single dislocation with material defect are taken as influence functions in the formation of the total stress field. A statement of stress-free macro-crack surface leads to the formulation of the integral equation which defines the dislocation density distribution along the crack. The fundamental concept and procedure of this method is described in Appendix 1.

The standard formulation of linear plane elasticity in terms of complex potentials is employed [Muskhelishvili 1953].

$$\sigma_{11} + \sigma_{22} = 4\,\mathrm{Re}\,\phi(z) \tag{3.21}$$

$$\sigma_{22} - \sigma_{11} + 2i\sigma_{12} = 2(\bar{z}\phi''(z) + \psi'(z)) \tag{3.22}$$

$$u_1 + iu_2 = \frac{1+\upsilon}{E}(\kappa\phi(z) - z\overline{\phi'(z)} - \overline{\psi(z)}) \tag{3.23}$$

$$f(z) = -i(\phi(z) + z\overline{\phi'(z)} + \overline{\psi(z)}) \tag{3.24}$$

The function $\phi'(z)$ and $\psi'(z)$, which are analytic in the region, are determined as

$$\phi'(z) = \int_{-\infty}^{0}\left[\frac{\alpha b(t)}{2\pi i(z-t)} + \phi_k'(b,z,t)\right]dt + \phi_{0k}'(z) \tag{3.25}$$

$$\psi'(z) = \int_{-\infty}^{0}\left[-\frac{\alpha}{2\pi i}\left(\frac{\overline{b}(t)}{z-t} - \frac{tb(t)}{(z-t)^2}\right) + \psi_k'(b,z,t)\right]dt + \psi_{0k}'(z) \tag{3.26}$$

where $\alpha = E/4(1-\nu^2)$, $\kappa = 3-4\nu$ for the plane strain case and $\alpha = E/4$, $\kappa = (3-\nu)/(1+\nu)$ for the plane stress case, ν is the Poisson's ratio and E is Young's modulus. Function $\phi'_k(b,z,t)$ and $\psi'_k(b,z,t)$ represent the regular part, at z=t, of the interaction of the particular (k) defect with the dislocation of Burgers vector b(t) dt, positioned at z=t. Functions $\phi'_{0k}(z)$ and $\psi'_{0k}(z)$ represent the stress field created by transformation type inclusion. Then the integral equation, obtained from the condition $\sigma_{22} + i\sigma_{12} = 0$, becomes

$$\int_{-\infty}^{0}\left[\frac{\alpha\overline{b}(t)}{\pi i(t-x)} + b_R(t)K_1(x,t) + b_I(t)K_2(x,t)\right]dt = P(x)$$

$$-\infty < x \le 0 \tag{3.27}$$

Here

$$b(t) = b_R(t) + ib_I(t) \tag{3.28}$$

$$K_j(x,t) = \phi'_k(s_j,x,t) + \overline{\phi'_k(s_j,x,t)} + x\phi''_k(s_j,x,t) + \psi'_k(s_j,x,t) \tag{3.29}$$

$j = 1,2$, $s_1 = 1$, $s_2 = i$

$$P(x) = -\left[\phi'_{0k}(x) + \overline{\phi'_{0k}(x)} + x\phi''_{0k}(x) + \psi'_{0k}(x)\right] \tag{3.30}$$

Naturally, the stress functions satisfy the necessary conditions on the defect boundary. Next we look at the derivation of the interaction between dislocation and micro-defects such as circular inclusion and holes.

The solutions described here are known in the literature [Dundurs and Mura 1964; Dundurs 1968; Erdogan et al. 1974] in one form or another usually as long expressions for the stress tensor components. For convenience of the formulation, these results are given as stress potentials here. Practically, it is simpler to derive these potentials directly.

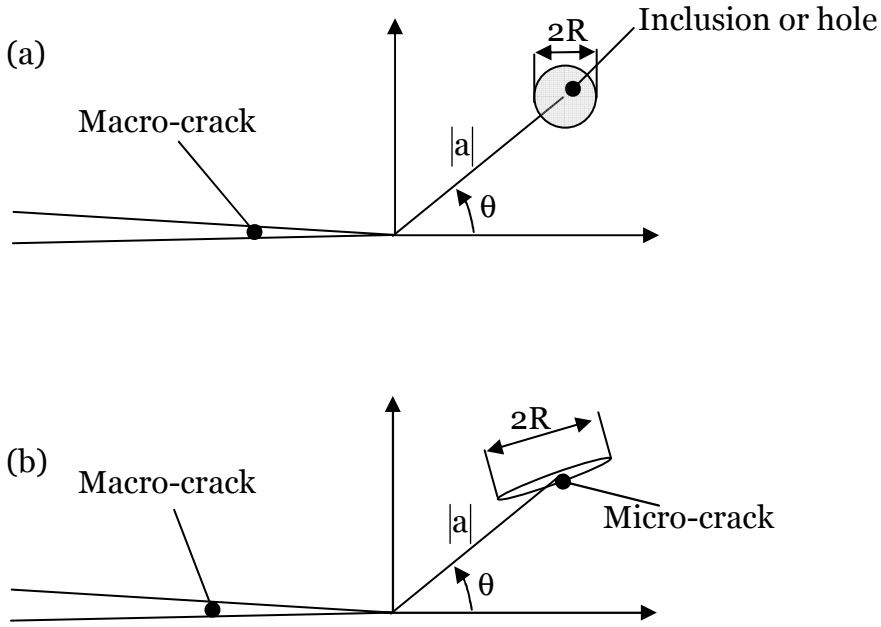

Figure 3-4: Geometry of the problem considered.
(a) Circular inclusion or hole, (b) Micro-crack

3.6.1.1 Circular inclusion

The stress field imposed by a dislocation positioned at point t is

$$\phi'_d(z) = \frac{A}{z-t},\ A = \frac{\alpha b}{2\pi i},\ \psi'_d(z) = \frac{\overline{A}}{z-t} + \frac{\bar{t}A}{(z-t)^2} \tag{3.31}$$

Consider a circular (radius R) inclusion located at the origin (Fig.3-4(a)). The inclusion can produce the stress field due to misfit, transformation, or different temperature expansion coefficients. This stress field does not depend on the dislocation and is determined by functions $\phi^{o}{}'_{01}(z)$ and $\psi^{o}{}'_{01}(z)$. An additional component of the stress field is the regular part of the dislocation-inclusion interaction, described by $\phi^{o}{}'_{1}(b,z,t)$ and $\psi^{o}{}'_{1}(b,z,t)$. The resulting (dislocation and regular part) stress field should satisfy the following condition

$$u_1 + iu_2 = C + iDz \text{ on } |z| = R,\ C, D = \text{const} \tag{3.32}$$

Functions $\phi^{o}{}'_{01}$, $\psi^{o}{}'_{01}$ and $\phi^{o}{}'_{1}$, $\psi^{o}{}'_{1}$ should be analytic for $|z| > R$, and vanish as $z \to \infty$. These functions should produce single valued displacement and a self-equilibrated stress fields. Take function in the form

$$\psi^{o}{}_{1} = \psi^{o}{}_{11} - \frac{R^2}{z}\phi^{o}{}'_{1}. \tag{3.33}$$

Then rewrite equation (3.32) as

$$\kappa\phi^{o}{}_{1}(z) - \overline{\psi^{o}{}_{11}(z)} = -\left[\kappa\phi_d - z\overline{\phi}'_d - \overline{\psi}_d\right] + CE/(1+\nu) + iDEz/(1+\nu),\ |z| = R \tag{3.34}$$

Substitute equation (3.31) in equation (3.34) and represent the right side as a combination of a constant, a boundary value of an analytic function for $|z| = R$ (use that on $|z| = R$, $\bar{z} = R^2/z$ and introduce $t^* = R^2/\bar{t}$. Thus equation (3.34) becomes

$$\kappa\phi^{o}{}_{1}(z) - \overline{\psi^{o}{}_{11}(z)} = -\left[\kappa\overline{A}\ln\frac{z - t^*}{z} + \overline{\left(\frac{A\bar{t}^*}{z}\right)}\right] + \frac{\overline{A}t^{*2}(t^* - t)}{R^2(z - t^*)} - A\ln\frac{z - t^*}{z} + \frac{\overline{A}t^*(t^* - t)}{R^2}$$
$$+ \kappa\overline{A}\ln\left(\frac{-R^2}{t^*}\right) - A\ln\left(\frac{-R^2}{t^*}\right) + CE/(1+\nu) + \frac{iDR^2E}{z(1+\nu)}$$

$$, |z| = R \tag{3.35}$$

Applying the principle of analytical continuation to functions in equation (3.28), one finds functions $\phi^o{}_1$ and $\psi^o{}_{11}$ that satisfy the above mentioned conditions

$$\phi^o{}_1 = -\frac{1}{\kappa}\left[\frac{\bar{A}t^{*2}(t^*-t)}{R^2(z-t^*)} - A\ln\frac{z-t^*}{z}\right] \tag{3.36}$$

$$\psi^o{}_{11} = \kappa\bar{A}\ln\frac{z-t^*}{z} + \frac{AR^2}{tz} + \frac{iDR^2E}{z(1+\nu)} \tag{3.37}$$

The branch cut of logarithmic function here is taken as a line without the circle $|z| < R$ connecting points $z = 0$ and $z = t^*$. The rigid displacement of the inclusion due to a dislocation stress field is determined by constants.

$$C = \frac{1+\nu}{E}\left[\bar{A}(t^*-t)/\bar{t} + \kappa A\ln(-t) - A\ln(-\bar{t})\right]. \tag{3.38}$$

$$D = (1+\nu)\,\mathrm{Im}(\kappa\bar{A}/\bar{t} - A/t)/E \tag{3.39}$$

D is found from the condition of zero resulting moment, that is $\mathrm{Re}\int\psi dz = 0$, integral taken around the inclusion. As an example of the stress field due to misfit of the inclusion, consider the case of homogeneous transformation. Then on the $z = Re^{i\theta}$

$$u_1 + iu_2 = \varepsilon z = \varepsilon R^2/\bar{z},\ \varepsilon = \mathrm{const} \tag{3.40}$$

Taking ψ_{01} in the form (equation (3.33)) and applying the same approach as above, the result is

$$\psi^o{}_{01}(z) = -\frac{\varepsilon R^2 E}{(1+\nu)z},\quad \phi^o{}_{01}(z) = 0 \tag{3.41}$$

The general case (centre of inclusion located at z=a) is obtained by the usual [Muskhelishvily 1975] transformation formulae (k=1 in this case)

$$\phi'_k(z,t) = \phi^{o\prime}{}_k(z-a, t-a) \tag{3.42}$$

$$\psi'_k(z,t) = \psi^{o\prime}{}_k(z-a, t-a) - \bar{a}\phi''_k(z,t) \tag{3.43}$$

3.6.1.2 Circular hole

Consider the circular hole instead of inclusion here (Fig. 3-4 (a)). Substituting in equations (3.35) and (3.36) $\kappa = -1$, one obtains the stress potential which satisfy the traction free boundary conditions $|z| = R$. Thus,

$$\phi^{o\prime}{}_2(b,z,t) = \frac{\alpha}{2\pi i}\left[b\left(\frac{1}{z} - \frac{1}{z-t^*}\right) + \frac{\bar{b}(t^*-t)t^*}{\bar{t}(z-t^*)^2}\right] \tag{3.44}$$

$$\psi^{o\prime}{}_2(b,z,t) = \frac{\alpha}{2\pi i}\left[b\left(\frac{1}{z} - \frac{1}{z-t^*}\right) + \frac{bR^2}{tz^2}\right] - \frac{R^2}{z}\phi^{o\prime\prime}{}_2 + \frac{R^2}{z^2}\phi^{o\prime}{}_2 \tag{3.45}$$

Relations (equation) (k=2) apply for the general case (centre of the hole at z=a)

3.6.1.3 Finite length crack

The solution of the interaction between the dislocation and finite crack is well known. Thus, for the case of crack located on the real axis between points $z_1 = -R$, $z_1 = R$ and dislocation at $z_1 = t_1$ stress functions are (Erdogan 1962; Lo 1978) (case of the single valued displacement):

$$\phi^{o\prime}{}_3(b,z,t) = -\left[AF(z,t) + AF(z,\bar{t}) + \bar{A}(t-\bar{t})\frac{\partial}{\partial \bar{t}}F(z,\bar{t})\right] + A/X(z) \tag{3.46}$$

$$\psi^{o\prime}{}_3(b,z,t) = \Phi^{o\prime}{}_3(-\bar{b},\bar{z},t) - \Phi^{o\prime}{}_3(b,z,t) - z\Phi^{o\prime\prime}{}_3(b,z,t) \tag{3.47}$$

here

$$F(z,t) = (1 - X(t))/X(z)/2(z-t) \tag{3.48}$$

$$X(z) = (z^2 - R^2)^{1/2} \tag{3.49}$$

For the general case of a crack with centre located at z=a and crack line with an inclination angle β with positive direction of x axis, Fig. 3-4 (b).

$$\phi'_3(b,z,t) = \phi^{o\prime}{}_3(b_1,z_1,t_1) \tag{3.50}$$

$$\phi''_3(b,z,t) = e^{-i\beta}\phi^{o\prime\prime}{}_3(b_1,z_1,t_1) \tag{3.51}$$

$$\psi'_3(b,z,t) = e^{-2i\beta}\psi^{o\prime}{}_3(b_1,z_1,t_1) - \bar{a}\phi''_3(b,z,t) \tag{3.52}$$

where

$$z_1 = (z-a)e^{-i\beta},\ t_1 = (t-a)e^{-i\beta} \text{ and } b_1 = be^{-i\beta} \tag{3.53}$$

3.6.1.4 Examination of singular integral equation

Equation (3.22) is a singular integral equation of the first kind of a semi-infinite interval. Generally, singular integral equations of the first kind have a family of solutions and in order to obtain a unique solution a supplementary condition has to be stated. From the physics of the problem and properties of Cauchy type of integrals, it is clear that $b(1) \to 0$ as $t \to -\infty$. Additionally, one observes that stress function

$$\phi'(z) \to K^{\infty}/2(2\pi z)^{1/2} \text{ as } z \to \infty \tag{3.54}$$

where K^{∞} is a conjugate of a remote stress intensity factor and it represents a remotely applied stress. Therefore,

$$b(t) \to -K^{\infty}/\alpha(2\pi t)^{1/2} \text{ as } t \to -\infty \tag{3.55}$$

and solution of equation (3.29) can be found only up to constant coefficient K^{∞} in expansion of b(t) by fractional powers (k/2) of (-1/t), as $t \to -\infty$. Functions ϕ'_k and ψ'_k are of the order $0(1/z)$ as $z \to \infty$ and, therefore, influence higher order terms of the expansion. The equation can be separated into nonhomogeneous equations (take K^{∞} real for simplicity)

$$\int_{-\infty}^{0}\left[\frac{\alpha}{\pi i}\frac{\overline{b_k(t)}}{(t-x)}+\mathrm{Re}\,b_k(t)K_1(x,t)+\mathrm{Im}\,b_k(t)K_2(x,t)\right]dt=-\int_{-\infty}^{0}(-t)^{-1/2}K_2(x,t)dt$$

$$-\infty<x\le 0 \qquad (3.56)$$

and

$$\int_{-\infty}^{0}\left[\frac{\alpha}{\pi i}\frac{\overline{b_{0k}}}{(t-x)}+\mathrm{Re}\,b_{0k}(t)K_1(x,t)+\mathrm{Im}\,b_{0k}(t)K_2(x,t)\right]dt=P(x) \qquad (3.57)$$

Transforming equation (3.56) and (3.57) on the finite interval [-1, 1] by substitution $t=R(u-1)/(u+1)$, one enforces condition (3.55) by seeking solutions in the form (m=k or m=0k accordingly)

$$b_m(t)=g_m(u)[(1+u)/(1-u)]^{1/2} \qquad (3.58)$$

with supplementary conditions

$$g_m(-1)=0,\ m=k \text{ or } m=0k \qquad (3.59)$$

Thus equations (3.56) and (3.57) become

$$\int_{-1}^{1}\left\{\frac{\alpha}{2\pi i}\frac{\overline{g_m(u)}}{(u-s)}+\left[\begin{matrix}\mathrm{Re}\,g_m(u)K_1(x(s),t(u))\\+\mathrm{Im}\,g_m(u)K_2(x(s),t(u))\end{matrix}\right]\frac{R}{(1+u)(1+s)}\right\}\frac{du}{\sqrt{1-u^2}}=F(s) \qquad (3.60)$$

with

$$F(s)=\int_{-1}^{1}(1-u^2)^{-1/2}K_2(x(s),t(u))\frac{Rdu}{(1+u)(1+s)} \tag{3.61}$$

for equation (3.48) (m=k) and

$F(s)=\frac{P(x(s))}{1+s}$, $m=0k$ for equation (3.51).

Then the stress intensity factor at the macro-crack tip (z=0) can be found as

$$K_I^o-iK_{II}^o=K^\infty(1-ig_k(1))-ig_{0k}(1)\alpha\sqrt{2\pi R} \tag{3.62}$$

The numerical scheme for solving equation (3.54) and the evaluation of K^o is based on Gaus-Chebyshev quadrature [Edogan and Gupta 1972] as given in Appendix 1.

3.6.1.5 Numerical examples by Rubinstein [1986]

Based on the above formulae (3.21)-(3.62), Rubinstein [1986] conducted some numerical examinations. Fig. 3-5 shows the relation between dimensionless stress intensity factor, $K^o(1-\nu)/\varepsilon E(R)^{1/2}$, and dimensionless distance, (a-R)/R. the inclusion is located on the crack line ahead of the crack. Solution of the integral equation is given for three values of κ=1.5, 2.0 and 2.5. This will be correspond to ν=0.37, 0.25 and 0.13 for plain strain and the last two correspond to ν=0.33 and 0.14 for plane stress. It can be seen that the effect of the size becomes important as the distance from the crack tip decreases. As the crack approaches the inclusion up to a distance of about 0.1R, the stress intensity increases and then its value drops, which indicates possible crack arrest.

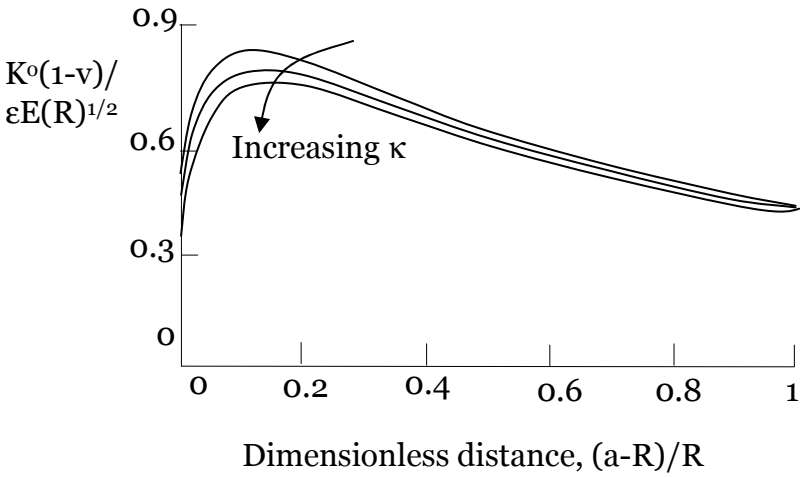

Figure 3-5: Variation of the stress intensity factor produced by dilational inclusion plotted against the distance from the crack tip to inclusion; θ=0. κ=1.5, 2.0 and 2.5 [Rubinstein 1986].

Fig. 3-6 shows the variation of stress intensity factor versus angular position of the inclusion. The inclusion is positioned at distance 1.2R from the crack tip under angle θ (Fig. 3-3(b)) and the resulting stress intensity factor is given as a ratio to the value corresponding to θ=0. We can see that the stress intensity factor for mode I, K_I, decreases with increasing the position angle. The stress intensity factor for mode II, K_{II}, decreases with increasing the position angle up to 60 deg., and it increases more than 60 deg. It can be seen that the influence of position angle on stress intensity factor for mode I and II is very strong and this result is very important for examining the transformation toughening. In the case of this distance (a=1.2R) between a main crack and an inclusion, the increase of the position angle can lead to the increase of shielding effect for mode I crack.

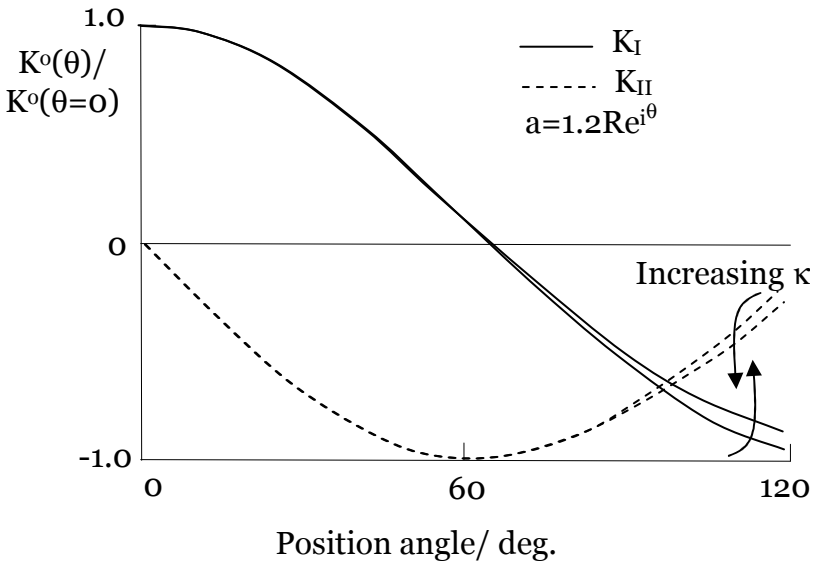

Figure 3-6: Variation of the stress intensity factor produced by dilational inclusion plotted against the position angle of inclusion; θ=0 [Rubinstein 1986]. κ is 1.5 and 2.5.

Fig. 3-7 shows the variation of the stress intensity factor (given as a ratio K^{o}/K^{∞}) versus the distance from the defect to the crack tip. The angle, β, of micro-crack is set at 0 deg. It can be seen from this figure that the hole creates the highest increase in the local stress intensity factor, and the rigid inclusion decreases it almost to zero. It was stated that all these lines join each other as the dimensionless distance increases to the value of 2.0. For the evaluation of the actual stress intensity factor in the case of a dilatational inclusion, the results in Fig.3-7 should be superimposed with the data in Fig. 3-5 with the specified value of a dilatation strain ε.

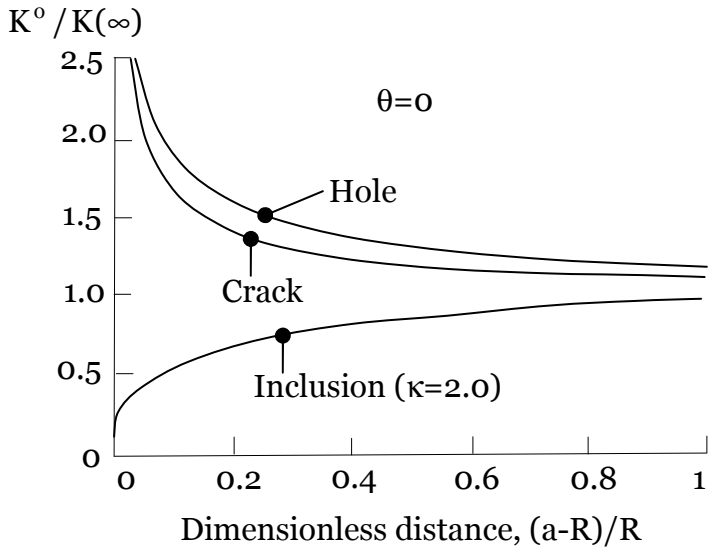

Figure 3-7: Variation of the local stress intensity factor produced by dilational inclusion plotted against the distance from the crack tip to the micro-defect [Rubinstein 1986].

Fig. 3-8 shows the variation of the local stress intensity factor due to the micro-defects plotted against the position angle. The defect is positioned at a constant distance (a=1.5R) but under a different angle with respect to the macro-crack line. The resulting stress intensity factor is given as a ratio of current value to the remote one. The stress intensity factors for mode I decrease with increasing the position angle in the case of hole and crack when the position angle is up to 130 deg., which means that the toughening effect increases. When the position angle is larger than 62 deg. for micro-crack or 75 deg. for hole, the propagation of cracks is arrested ($K^o(\theta)/K^o(\theta=0)<1$). The existence of an inclusion reduces the stress intensity factor for mode I when the position angle is up to 110 deg.

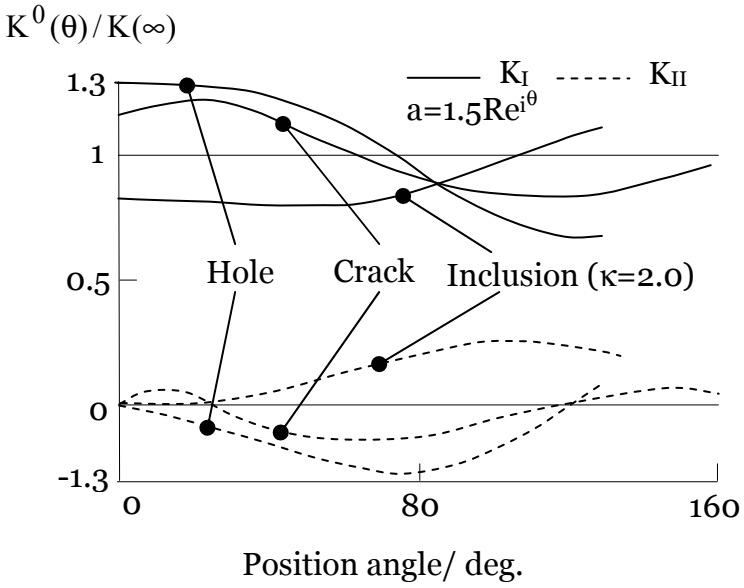

Figure 3-8: Variation of the local stress intensity factor produced by a dilational inclusion plotted against the position angle of the micro-defect [Rubinstein 1986].

3.6.2 Effect of inhomogeneity on stress intensity factor

Various toughening mechanisms such as transformation toughening, bridging toughening, micro-cacking toughening and others have been theoretically and experimentally studied by many researchers as described in Chapter2. Here, the effect of inhomogeneity on the stress intensity factor is discussed in terms of the interaction between one main crack and one micro-defect, which is the basic examinations for these toughening mechanisms. Most of the studies dealing with this issue use numerical techniques such as FEM and BEM or singular integral equation methods as described above.

The elastic problems on the interaction between dislocation and micro-defects such as an inclusions, a void, a micro-crack and others were studied by many researchers [Dundurs and Mura 1964; Dundurs 1968; Erdogan et al. 1974], which have been used for investigation of the effect of inhomogeneity on the crack tip stress fields through the singular integral equation method. Their

solutions assist in the understanding of the toughening due to microstructural inhomogeneities.

The typical characteristic of the interaction between a macro-crack and micro-defects is the short range of the defect influence on the stress intensity factor at the crack tip [Rubinstein 1986]. The effective distance is up to about 2 to 3 times the typical defect size. The position angle can influence significantly the acting stress intensity factor. Defects such as a micro-crack and void which are behind the critical angle actually reduce the stress intensity. The non-collinear cracks located near the tip of the macro-crack (small values of θ) produce a high rise of the local stresses intensity factor than the similar collinear case (at the same distance). The effect of dilation of the inclusion on the stress intensity factor is significantly large as shown in Figs. 3-5 and 3-6. From Fig. 3-6, with increase of the position angle of the dilational inclusion, the shielding effect for the mode I crack increase. As shown in the next chapter, for stress-induced transformation toughening in the composites, the hight of the wake zone of transformation has a significantly large influence on the crack-tip stress intensity factor.

3.7 Resistance curve (R-curve) behaviour

An increase in the resistance to crack growth (i.e. toughness) during crack extension has been termed Resistance curve (R-curve) behaviour. R-curve behaviour was originally noted for large-grained ceramics having thermal expansion anisotropy and the increasing resistance to crack extension with crack length was mainly attributed to mechanisms active in the crack wake that shielded the crack tip from the applied stress intensity [Knehans et al. 1983]. Various toughening mechanisms in ceramic and ceramic matrix composites contribute to R-curve behaviour. The literature on these toughening mechanisms has been already reviewed in Chapter 2, so the general concept of R-curve is described here.

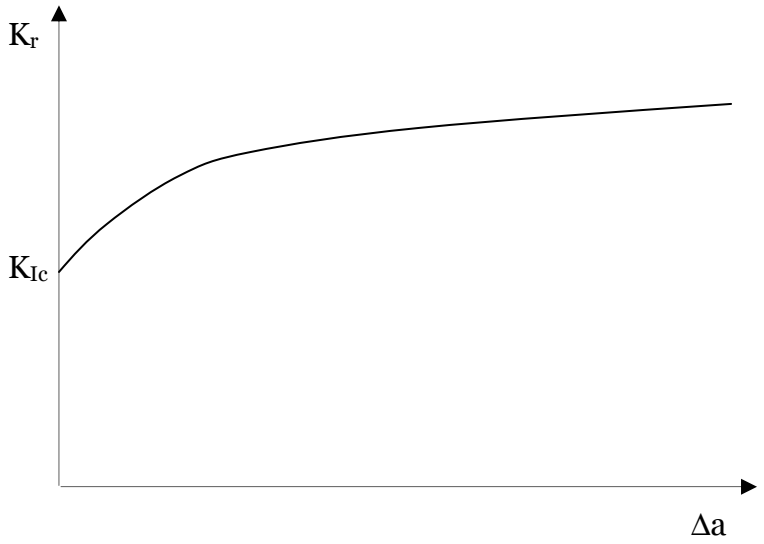

Figure 3-9: Schematic illustration of Resistance-curve (R-curve).

Fig. 3-9 shows the schematic illustration of typical R-curve behaviour. The fracture toughness, K_{Ic}, is the critical stress intensity factor required to initiate crack growth. The variation of fracture resistance with crack growth is denoted by $K_r(\Delta a)$. The resistance curve ($K_r - \Delta a$) is then used to predict the conditions necessary for unstable crack growth through the material. Consider a material containing a slit crack of length of 2*a*, subjected to a remote tensile stress σ. The stress intensity factor is $K_I = \sigma\sqrt{\pi a}$ as given in equation (3.14). Crack growth begins when $K_I = \sigma\sqrt{\pi a} = K_{Ic}$. Thereafter, there will be a period of stable crack growth, during which the applied stress increases. The stress satisfies the following equation:

$$K_I(a + \Delta a) = \sigma\sqrt{\pi(a + \Delta a)} = K_r(\Delta a). \qquad (3.63)$$

The stress will continue to increase as long as the increase in toughness with crack growth is sufficient to overcome the increase in stress intensity factor with crack growth. Catastrophic failure (unstable crack growth) will occur when continued crack growth is possible at constant or decreasing load. This requires

$$\left.\frac{\partial K_I}{\partial \Delta a}\right|_{\sigma} \geq \frac{dK_r}{d\Delta a}. \tag{3.64}$$

For the case of a slit crack, this gives

$$\sigma^2 = \frac{2}{\pi} K_r \frac{dK_r}{d\Delta a} \tag{3.65}$$

for the critical stress at unstable fracture. Accordingly it is important to examine the value of not only K_r but also $\frac{dK_r}{d\Delta a}$ in examining the R-curve behaviour.

3.8 Summary

Ceramics and their composites tend to be very brittle compared to metals. The linear elastic fracture mechanics contribute to the investigation of fracture behaviour of such materials. Some of the fundamental issues in the linear elastic fracture mechanics, which are relevant to the project, were discussed here.

First, the basic concept of linear elastic fracture mechanics was described. Complex variable method and stress intensity factor were described. Second, Hutchinson's solution for dilatation spot in the vicinity of a semi-infinite crack is briefly described. This solution is used in the next chapter. Third, the effect of the inhomogeneity on the stress intensity factor was discussed using the formulae and numerical results obtained by Rubinstein [1986], which were given through a singular integral equation method. The singular integral equation method was applied to the problem on the interaction between T (transverse)-stress and short–fibre bridging toughening in the current project as described in Chapter7. The influence of the elastic interactions between a semi-infinite macro-crack and micro-defects such as a circular inclusion, circular hole and arbitrarily oriented crack of finite size on the stress intensity factor was examined. Last, the basic concept of R-curves was stated for obtaining better understanding on the toughening behaviour of the composites in the following chapters. In this chapter, we summarized the basic results of the linier theory of elastic fracture mechanics required for the current project.

Chapter 4

Transformation toughening in composites

4.1 Introduction

The phenomenon of stress-induced transformation of partially stabilised ZrO_2 in zirconia-enriched composites was first reported by Garvie et al. [1975]. This mechanism for toughening brittle ceramics has received great attention in the last two decades [Kelly and Rose 2002; Basu et al. 2004]. Volume expanding due to the phase transformation (from tetragonal to monoclinic phases) can occur in the tensile stress field around a crack tip. For a crack growing under load, the stress-induced transformation results in a zone of higher monoclinic ZrO_2 concentration in the crack wake. The volume expansion induces a closing action in the crack wake and decreases the stress intensity experienced at the crack-tip.

This phase transformation toughening effect is the origin of high mechanical reliability of ZrO_2 materials. The toughness contribution from the transformation mechanism ($\approx$15MPam$^{1/2}$) exceeds that from micro-cracking ($\approx$2-6MPam$^{1/2}$) or deflection ($\approx$2-4MPam$^{1/2}$) mechanisms [Hannink 2000].

Many researchers have been investigating the transformation toughening of ZrO_2 in various composites such as ZrO_2-WC composites [Anné et al. 2005], mullite-ZrO_2 composites [Garrido et al. 2006] and $MoSi_2$-ZrO_2 composites [Suzuki et al. 1999]. In particular, ZrO_2-toughened Al_2O_3 (ZTA) composites have received increased attention as implant materials, structural materials, and cutting tools in metalworking and paper cutting, in which the transformation toughening mechanism works effectively [Bermejo et al 2007; Daguano et al. 2007; Cesari et al. 2006]. Fig. 4-1 shows the fracture toughness plotted against the volume fraction of ZrO_2 in ZTA composites, including experimental data obtained by Tuan et al. [2002]. From this figure, it is seen that about three-times the toughening effect (for 16 vol. % ZrO_2 composites) can be obtained due to this mechanism in comparison with monolithic Al_2O_3.

Budiansky and his colleagues [Budiansky et al. 1983; Amazigo and

Budiansky 1988; Stump and Budiansky 1989] theoretically investigated stress-induced transformation mechanisms based on continuum approaches. The model discussed in this chapter has been proposed by Stump and Budiansky [1989] for the transformation toughening mechanism in the composites with dispersed transformable particles. This theoretical model significantly enhanced the understanding of this toughening mechanism including the effect of transformation zone size [Rose 1986b]. However, the model is based on the assumption of an effectively homogenous composite material, where only macroscopic aspects of the material deformation are considered. As such, the continuum models ignore the mismatch effect in material properties of the constituent phases on the mechanism of transformation toughening and, generally speaking, are only applicable to a composite with constituent phases having the same material properties. In the current project, this model is linked with a micromechanical model to investigate the influence of the mismatch in thermo-material properties, which causes residual thermal stresses under temperature change conditions, and microstructure on the transformation toughening effect in ZrO_2-enriched composites.

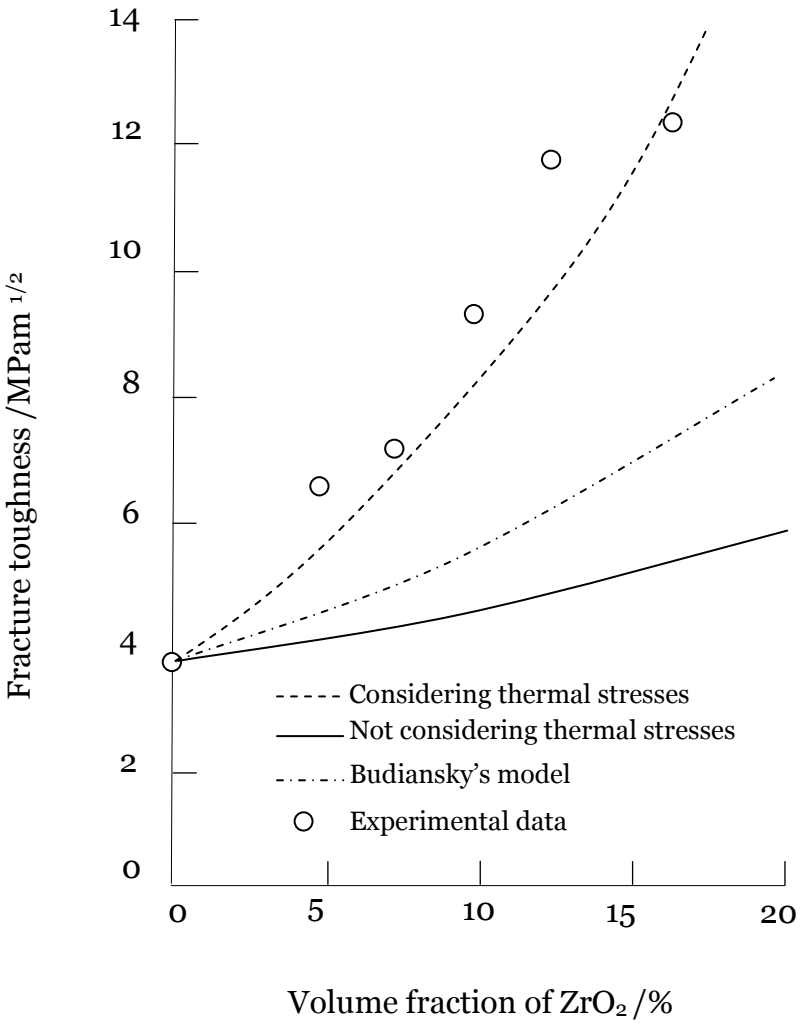

Figure 4-1: Fracture toughness plotted against the volume fraction of ZrO_2 in Al_2O_3/ZrO_2 composites. The experimental data was obtained by Tuan et al. [2002]. Simulation results are plotted based on the Budiansky's continuum model, micromechanical models considering thermal residual stresses and not considering thermal residual stresses for the steady-state crack. The detail description of the micromechanical model is provided in Chapter 5.

4.2 Continuum model

A brief description is given here on the continuum model of transformation toughening by Stump and Budiansky [1983]. Assume that a transformation zone surrounding the crack tip has undergone an irreversible transformation dilatation of strength $f^{(1)}\theta$ where $f^{(1)}$ is the zirconia particle volume fraction and θ is the unconstrained particle dilatation (Fig. 4-1). Since typical transformation zone sizes are of the order of 20 μm or less, the small-scale zone-size approximation can be invoked. The stress field in the vicinity of the crack tip, whose derivation was descried in Chapter 3, can be given as,

$$\sigma_{ik} = \frac{K_I}{\sqrt{2\pi r}} F_{ik}(\phi), \tag{4.1}$$

where K_I is the stress intensity factor at the crack tip, r is the distance from the crack tip, and $F_{ik}(\phi)$ is the well known trigonometric function.

The mean stress due to dilatation can be calculated using the Hutchinson's solution for two small circular spots of dilatation of area dA located at $z_o = x_o + iy_o$ and $\bar{z}_0 = x_0 - iy_0$ (Fig. 4-2) [Hutchinson 1974] as described in Chapter 3 (equations (3.15)):

$$\sigma_m = \frac{Ef^{(1)}\theta}{18\pi}\frac{1+\nu}{1-\nu}\mathrm{Re}\left\{\frac{1}{\sqrt{zz_0}(\sqrt{z}+\sqrt{z_0})} + \frac{1}{\sqrt{z\bar{z}_0}(\sqrt{z}+\sqrt{\bar{z}_0})}\right\}dA, \tag{4.2}$$

where E is Young's modulus and ν is Poisson's ratio.

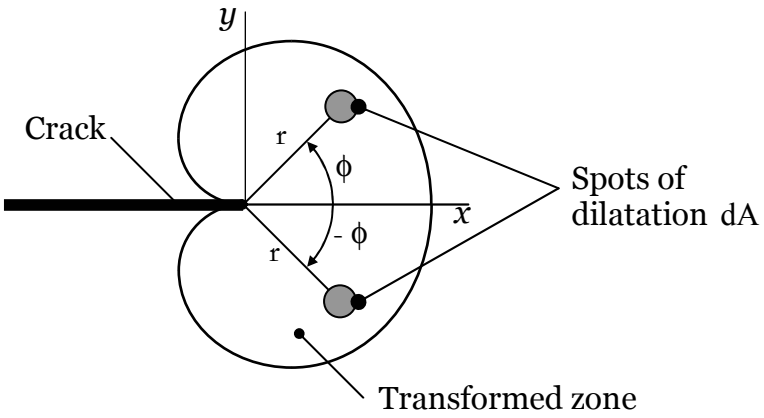

Figure 4-2: Symmetrically placed dilatant spots at a crack tip.

The equation for the zone boundary, $z = R(\phi)e^{i\phi}$, is then obtained by adding the near field mean stress of equation (4.1) to the zone contribution calculated by integrating equation (4.2) over the upper half of the transformed zone, and equating the sum to σ_m^c,

$$\sigma_m^c = \frac{K(1+\nu)}{3}\sqrt{\frac{\pi R}{2}}\cos(\phi/2) + \int_A F(z, z_0)dA, \qquad (4.3)$$

where σ_m^c is the critical value for mean stress corresponding to the phase transformation and F(z, z_o) is given by equation (4.2). The full transformation will be assumed to occur when mean stress attains a critical value σ_m^c. From equation (4.3), transformation zone is derived. Contrary to the micro-crack case [Kachanov et al. 1990], the contribution of the whole transformation zone is more significant. This is due to the non-singular nature of the stresses generated by the phase transformation of zirconia particles. Now we define the non-dimensional measure of the strength of the transformation, ω, which is given by

$$\omega = \frac{Ef^{(1)}\theta}{\sigma_m^c}\frac{1+\nu}{1-\nu}.. \tag{4.4}$$

Fig. 4-3 shows the initial transformed zones for various values of ω. Here, L is the characteristic length defined as follows:

$$L = \frac{2}{9\pi}\left[\frac{K_m(1+\nu)}{\sigma_m^c}\right]^2 \tag{4.5}$$

, which is the frontal intercept at $\phi = 0$ of the σ_m^c boundary for $\omega = 0$.

K_m is the critical intensity when crack growth occurs.

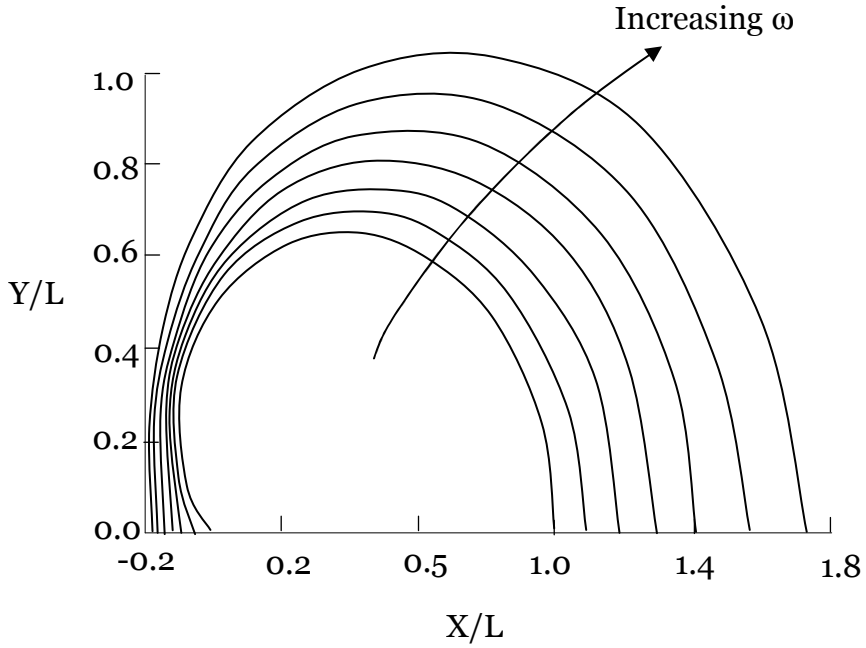

Figure 4-3: Initial transformation zones for various ω.
ω=0, 5, 10, 15, 20, 25 and 30.

Fig. 4-4 shows the initial zone-height shown in Fig.4-3, together with the zone-heights corresponding to steady-state crack growth calculated by Amazigo and Budiansky [1988]. For $\omega \approx 30$, the steady state zone height becomes infinite, and is called a "lock-up effect", which will be discussed later in this chapter.

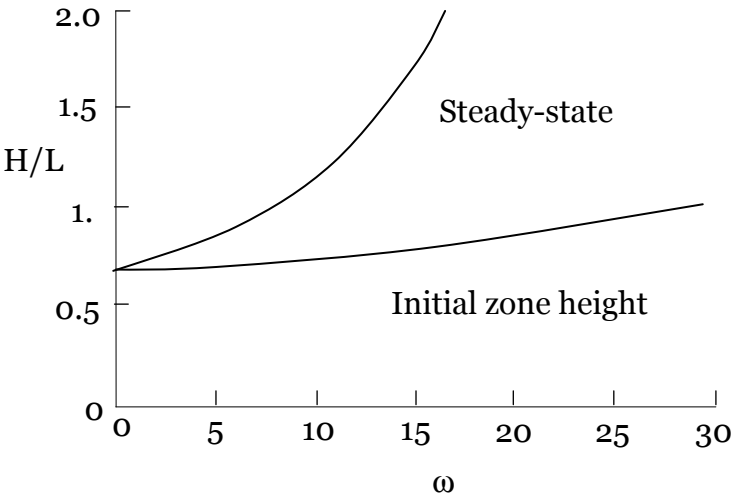

Figure 4-4: Steady-state and initial zone heights versus ω.

The stress intensity factor at the crack tip, K, is equal to the sum of the applied stress intensity factor K_{ap} and that induced by the presence of the transformed zone. Once the transformed zone is found, K as a function of K_{ap} can be obtained by integrating the change of the stress intensity factor ΔK due to the two small circular spots of dilatation as described in Chapter 3 (equation (3.16)):

$$\Delta K = \frac{Ef^{(1)}\theta}{6\sqrt{2\pi}(1-\nu)} \mathrm{Re}\left\{z_0^{-3/2} + \bar{z}_0^{-3/2}\right\} dA \qquad (4.6)$$

over the upper half of the transformed zone:

$$K = K_{ap} + \int_A \Delta K(z, z_0)\, dA\,. \qquad (4.7)$$

A similar procedure can be adapted to the growing crack case as well. The schematic illustration of the upper half of the instantaneous zone around a growing crack is shown in Fig.4-5. The boundary is modeled by three segments; active, passive and residual. The active segment AB is the portion of the

boundary where the mean stress has just reached σ_m^c. The mean stress on the remainder of the boundary is left behind with the first increment of crack growth. The intermediate passive portion BC is a growth dependent piece connecting the active and residual segments. The passive portion is comprised entirely of the end point B of previous active segments, several of which are shown in Fig. 4-5.

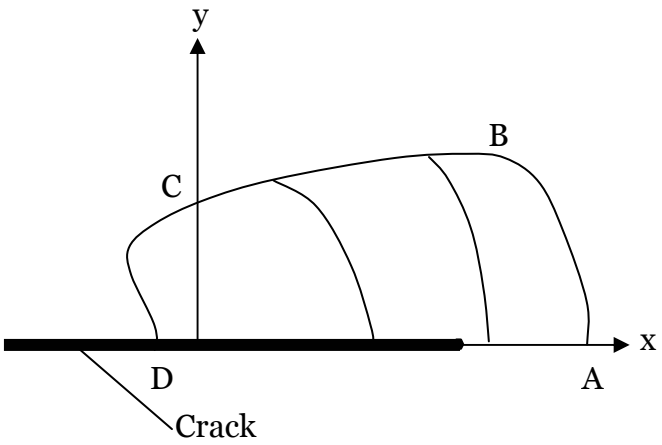

Figure 4-5: Transformation zone around a growing crack.

The solution of the growing crack problem involves adapting the three segment approach to a series of finite crack increments. In the limited continuous crack advance, the passive segment provides a smooth connection from the residual portion of the instantaneous active segment. However, for a series of finite crack increments, a piecewise linear approximation to the passive zone can be constructed by connecting the residual segment to the currently active segment with a series of straight lines running through the end points of previous active pieces. For infinitesimal crack increments, the approximate boundary should coincide with the actual passive segment. The analysis presented for the initial crack problem can be applied to the growing crack configuration with some slight modifications. The initial zone will be allowed to grow with an advancing crack tip under the dual requirements of satisfying the critical mean stress condition on the active zone boundary and maintaining the tip stress intensity at $K_{m,}$ which is the critical stress intensity factor. The growing zone shapes for ω=5 and 10 are shown in Fig.4-6. The dashed curves indicate the position of active segments for various amounts of crack extension; the innermost curve is the initial boundary.

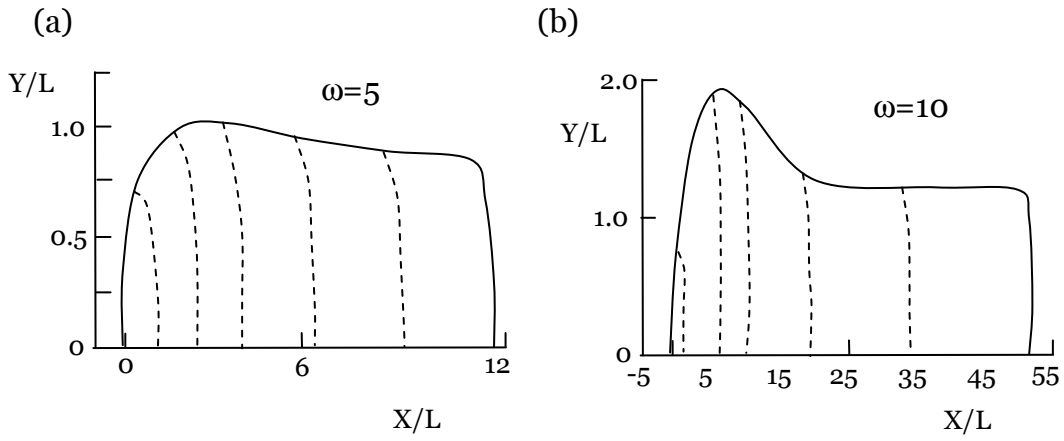

Figure 4-6: Growing zone for (a) ω=5 and (b) ω=10.

Next, the R-curves, which were described in Chapter 3, are focused on. The R (Resistance)-curves, plots of K_{ap}/K versus $\Delta a/L$, for w=5 and 10 along with their respective steady-state toughening asymptotes, as found by Amazigo and Budiansky [1988] are shown in Fig. 4-7. From Figs. 4-6 and 4-7, it is seen that the zone height and toughening K_{ap}/K both overshoot their steady state levels for finite amounts of crack advance before approaching them asymptotically. The R-curves of Fig. 4-7 are qualitatively consistent with some available experimental measurements. A number of investigators, including Swain [1983], and Swain and Hannink [1984], have reported R-curves which exhibit peaks in toughness.

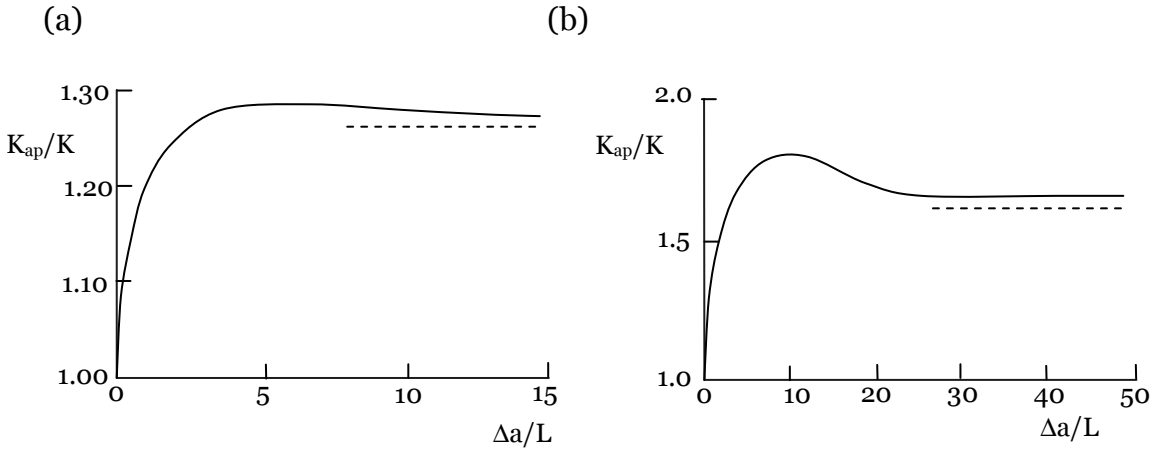

Figure 4-7: Resistance curves for (a) ω=5 and (b) ω=10.

By considering the initial slope of the R-curves, we can define an initial tearing resistance parameter $d(K_{ap}/K)/d(\Delta a/L)$, which represents the rate of toughening increase as the crack begins its initial growth. The relation between $d(K_{ap}/K)/d(\Delta a/L)$ and ω is shown in Fig. 4-8. A comparison can be made with the approximate results of Hutchinson [1986] who neglected the effect of transformation on the zone boundary in his study of initial tearing resistance. Fig. 4-9 shows a comparison of both sets of calculations for small ω.

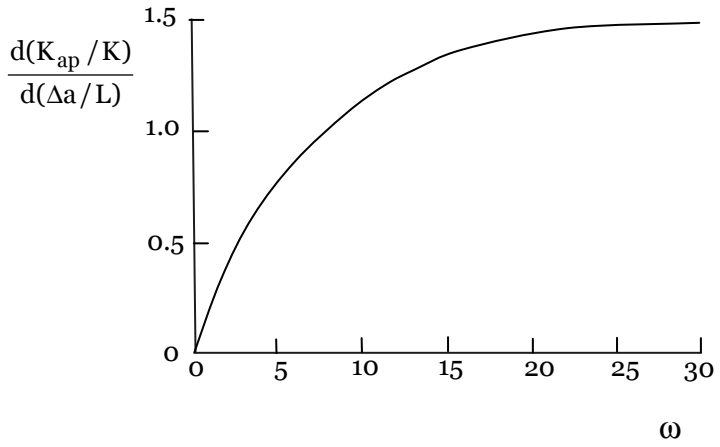

Figure 4-8: Initial crack growth resistance versus ω.

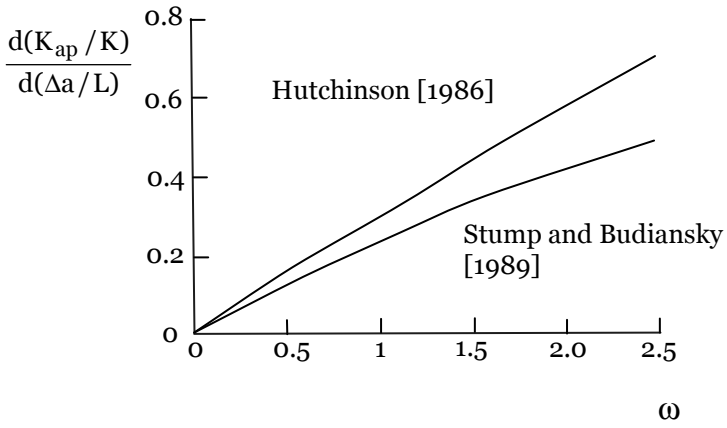

Figure 4-9: Comparison with Hutchinson's [1987] results for initial crack-growth resistance.

The final result of the calculation of the fracture toughening of the composite for stable and growing cracks is shown in Fig. 4-10.

The toughening effect increases with the increase of the strength ω of the transformation. The most notable features of Fig. 4-10 is the existence of the "lock-up" effect – i.e. infinite toughening of the composite – discovered by Rose [1986b]. It occurs at ω≈30 for steady state case and at ω≈20.2 for a growing crack.

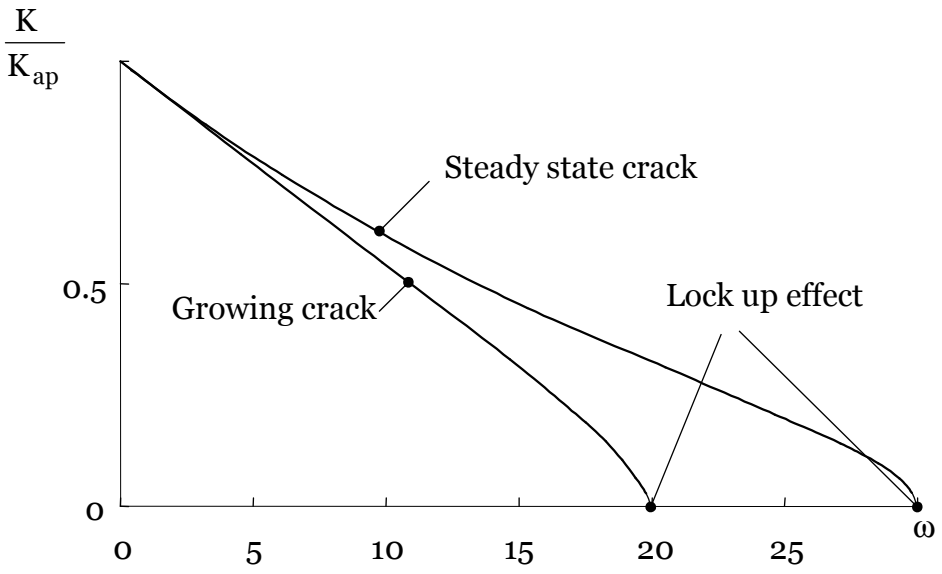

Figure 4-10: Fracture toughening versus the strength of transformation, ω.

This continuum model gave qualitative description of experimental data. However, due to ignorance of the effect of the mismatch in material properties of constituent phases on the strength of transformation toughening, the model can be applicable only to a composite with constituent phases having the same material properties. In practice, it is important to consider the effects of such a property mismatch in constituents. According to the work by Cesari et al. [2006], the residual stresses due to temperature change from the sintering temperature to the operating one exert a large influence on the toughening effect. The residual stresses can be generated during fabrication due to the mismatch in thermal expansion coefficients of constituent phases. In Fig. 4-1, the simulation results, obtained based on the Budiansky's continuum model, are

shown. The material properties data used for the calculation are given in Table A2-1 in Appendix 2. We can see that considerable difference exists between the simulation results and experimental data. It is considered that this difference is caused by not taking into account the effect of mismatch in thermo-mechanical properties of constituent phases. In order to take such effects into consideration, the micromechanical approaches are useful, one of which, the mean-field micromechanical approach, is described in the following chapter.

4.3 Summary

The study by Stump and Budiansky [1989] was a pioneering work formulating a continuum theory for transformation toughening in composite materials. Importantly, this theory reveals that the transformed zone has the remarkable property of allowing stable crack growth to occur in the composite materials and maximum toughening to occur for a finite amount of crack advance, which is called the "lock-up" effect. The toughening effects were given for both steady-state and growing cracks. As mentioned, this theory ignores the effect of the mismatch in material properties of constituent phases on the strength of transformation toughening and, generally speaking, is only applicable to a composite with constituent phases having the same material properties. In a real composite, however, the effect of the mismatch in material properties is very important and cannot be ignored. In the following chapter, a micromechanical approach is described and incorporated with this continuum theory for transformation toughening to investigate the effects of the mismatch in thermo-mechanical properties of the constituent phases, microstructures and residual thermal stresses on the transformation toughening in multi-phase composites.

Chapter 5

Micromechanical approach to transformation toughening

5.1 Introduction

Many studies have been devoted to predicting the effective thermo-mechanical properties of inhomogeneous materials [Markov 2000]. As mentioned in Chapter 2, the several different methods have been proposed such as mixture rules [Voigt 1928; Reuss 1929], variational approaches [Hashin and Shtrikman1963], numerical approaches [Paley and Aboudi 1992] and micromechanical theories [Hill 1965; Mori and Tanaka 1973; Norris 1985]. The micromechanical theories include a self-consistent model [Hill 1965], the Mori-Tanaka's concept [Mori and Tanaka 1973] and a differential scheme [Norris 1985].

A mean-field micromechanical approach such as Wakashima and Tsukamoto estimate [Wakashima and Tsukamoto 1991], which is based on Eshelby's equivalent inclusion methods and Mori-Tanaka's mean field concept, is used here. This estimate is effective to predict the overall thermo-mechanical properties of multi-phase composites. The prediction based on this estimate is within the Hashin-Shtrikman bounds [Hashin and Shtrikman 1963] for two phase composites and agreeable with some experimental data as shown later.

Based on Wakashima-Tsukamoto estimate the micromechanical formulation of thermo-mechanical properties for multi-phase composites with dispersed phases in the form of spherical particles is presented. Further, it is incorporated with the continuum model of transformation toughening by Stump and Budiansky [1989] to investigate the effect of the mismatch in thermo-mechanical properties of constituent phases, residual thermal stresses and microstructure on the transformation toughening mechanism in multi-phase composites. The influence of the addition of Ag or Ni into ZrO_2-enriched Al_2O_3 on the toughening effect is investigated, and the results are examined through comparison with some existing experimental data. As a case study,

ZrO_2-enriched SiC/Al composites, which are promising light-weight materials in automobile and aerospace industries, are investigated. Through these numerical investigations based on micromechanical considerations, the influence of the thermal residual stresses generated during fabrication process of the composites on the toughening effect is investigated.

5.2 Mean-field micromechanics

A composite consisting of N-types of inclusions uniformly and randomly dispersed in an isotropic continuum matrix is considered (Fig. 5-1). Let us introduce a representative volume element (RVE) of the general heterogeneous media. When the RVE is subjected to macro-stress $\overline{\sigma}_{ik}$ (corresponding to the traction vector: $t_i = \overline{\sigma}_{ik} n_k$), the volume average of the induced micro-stress, σ_{ik}^{ap}, over RVE is equal to the macro-stress, $\overline{\sigma}_{ik}$, such that,

$$\frac{1}{V^R} \int_{V^R} \sigma_{ik}^{ap} dV = \overline{\sigma}_{ik} \quad , \tag{5.1}$$

where V^R is the volume of RVE. The volume average of the internal stress, σ_{ik}^{in}, due to the presence of the eigenstrain, ε_{ij}^{*}, which is introduced by Mura [1987], is equal to zero, i.e.

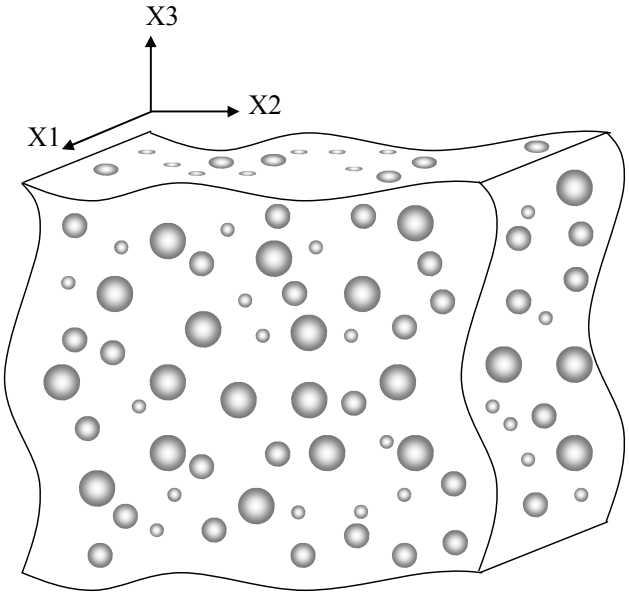

Figure 5-1: Schematic illustration of multi-phase composites with Cartesian coordinates.

$$\frac{1}{V^R}\int_{V^R}\sigma_{ik}^{in}dV = 0\ . \tag{5.2}$$

For the system under consideration, the potential energy, Φ, is defined as

$$\Phi = \frac{1}{2}\int_{V^R}(\sigma_{ik}^{ap}+\sigma_{ik}^{in})\cdot(\varepsilon_{ik}^{ap}+\varepsilon_{ik}^{in}-\varepsilon_{ik}^{*})dv - \int_{S^R}(\sigma_{ik}^{ap}n_k)\cdot(u_i^{ap}+u_i^{in})ds\ . \tag{5.3}$$

Here, S^R is the surface of the RVE and the repeated indexes assume the usual summation convention.

Equation (5.3) can be rewritten in terms of summations of piecewise uniform quantities as follows:

$$\begin{aligned}\Phi = &-\frac{1}{2}\overline{\sigma}_{ik}\sum_{r=0}^{N}f^{(r)}M_{iklm}^{(r)}\overline{\sigma}_{lm}^{ap(r)} - \frac{1}{2}\sum_{r=0}^{N}f^{(r)}\varepsilon_{ik}^{*(r)}\cdot\overline{\sigma}_{ik}^{in(r)}\\ &-\sum_{r=0}^{N}f^{(r)}\varepsilon_{ik}^{*(r)}\cdot\overline{\sigma}_{ik}^{ap(r)}\end{aligned}\ , \tag{5.4}$$

where the superscript (r) is the number to identify the constitutive phases and r runs from 0 to N; 0 denotes matrix and the numbers from 1 to N denotes the corresponding dispersed particle phase. $M^{(r)}_{iklm}$ is the elastic compliance tensor of r-th phase, and $\varepsilon^{*(r)}_{ik}$ is the eigenstrain in r-th phase. $\overline{\sigma}^{ap\ (r)}_{ik}$ and $\overline{\sigma}^{in\ (r)}_{ik}$ are the volumetric average of the micro-stresses in phase (r) due to external loading and internal factors such as thermal expansion, plastic deformations and etc, respectively. Hill [1963] reported that $\overline{\sigma}^{ap\ (r)}_{ik}$ is proportional to the applied macro-stress, $\overline{\sigma}_{ik}$. This can be written mathematically as,

$$\overline{\sigma}^{ap(r)}_{ik} = B^{(r)}_{iklm}\overline{\sigma}_{lm} \quad , \tag{5.5}$$

where $B^{(r)}_{iklm}$ is the stress concentration factor tensor. Equations (5.1) and (5.5) lead to the following relation:

$$\sum_{r=0}^{N} f^{(r)} B^{(r)}_{iklm} = I_{iklm} \tag{5.6}$$

where I_{iklm} is the fourth order identity tensor.

According to the mean-field micromechanical theory [Wakashima and Tsukamoto 1991] (see Appendix 3), which is based on Eshelby's equivalent inclusion method [Eshelby 1957; 1959; 1961] and Mori-Tanaka's mean-field approximation [Mori and Tanaka 1973], the following algebraic relations for $B^{(r)}_{iklm}$ can be derived:

$$B^{(r)}_{iklm} = C^{(r)}_{ikop}\left\{\sum_{s=0}^{N} f^{(s)} C^{(s)}_{oplm}\right\}^{-1} \tag{5.7}$$

where

$$C_{iklm}^{(r)} = \left\{ I_{iklm} + P_{ikop}^{(r)} \left(M_{oplm}^{(r)} - M_{oplm}^{(0)} \right) \right\}^{-1}, \tag{5.8}$$

$$P_{iklm}^{(r)} = L_{ikop}^{(0)} \left(I_{oplm} - S_{oplm}^{(r)} \right). \tag{5.9}$$

Here, $L_{ikop}^{(0)}$ is the elastic stiffness tensor of the matrix, and $S_{oplm}^{(r)}$ are the Eshelby's tensors for (r) phase. Further, the internal stress for each phase $\overline{\sigma}_{ik}^{in\,(r)}$ is also related to the eigenstrain, $\varepsilon_{ik}^{*(r)}$, and the stress concentration tensor, $B_{iklm}^{(r)}$, as

$$\overline{\sigma}_{ik}^{in\,(r)} = D_{iklm}^{(r)} \Delta\varepsilon_{lm}^{*(r)} - B_{ikop}^{(r)} \sum_{s=0}^{N} f^{(s)} D_{oplm}^{(s)} \Delta\varepsilon_{lm}^{*(s)} \tag{5.10}$$

with,

$$D_{oplm}^{(r)} = -C_{opik}^{(r)} P_{iklm}^{(r)}, \tag{5.11}$$

$$\Delta\varepsilon_{lm}^{*(r)} = \varepsilon_{lm}^{*(r)} - \varepsilon_{lm}^{*(0)}. \tag{5.12}$$

The macro strain $\overline{\varepsilon}_{ik}$ can also be related to macro stress $\overline{\sigma}_{ik}$ through the potential energy of the composite, Φ, as follows,

$$\overline{\varepsilon}_{ik} = -\frac{\partial \Phi}{\partial \overline{\sigma}_{ik}}. \tag{5.13}$$

Thus, from equations (5.4), (5.5), (5.10) and (5.13) the following constitutive relation of the composites can be written:

$$\overline{\varepsilon}_{ik} = \sum_{r=0}^{r} f^{(r)} M_{ikop}^{(r)} B_{oplm}^{(r)} \overline{\sigma}_{lm} + \sum_{r=0}^{r} f^{(r)} B_{iklm}^{(r)\,T} \varepsilon_{lm}^{*(r)}. \tag{5.14}$$

This method has been used in various applications. For example we are applying this method to biomechanical issues (see the publication list shown in Chapter 7). For two-phase composites, overall thermo-mechanical properties such as elastic constants and thermal expansion coefficients predicted by Wakashima-Tsukamoto estimate are within Hashin-Shtrikman bounds which are derived based on variational approach [Wakashima and Tsukamoto 1991]. Fig. 5-2 shows the relation between the ratio of Young's modulus of composites to matrix $E^c/E^{(0)}$and the volume fraction of inclusions for the composites consisting of glass sphere particles and polyester matrix. The calculation results based on Wakashima-Tsukamoto estimate described above are within Hashin-Shtrikman bounds and very close to experimental data obtained by Richard [1975] for the composites containing glass sphere particles with the diameter of 210-297μm. In this case, the results based on Wakashima-Tsukamoto estimate are exactly coincident with the lower bound of Hashin-Shtrikman ones. The material properties used in the calculation are $E^{(1)}/E^{(0)}$=40.8, $\upsilon^{(1)}$=0.21 and $\upsilon^{(0)}$=0.45.

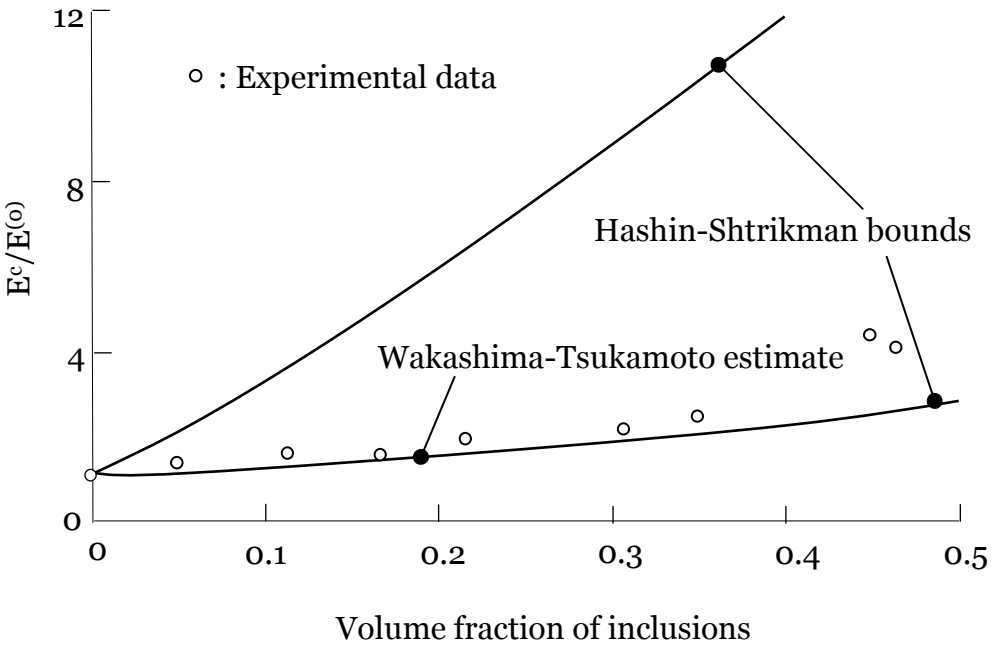

Figure 5-2: Young's modulus ratio ($E^c/E^{(0)}$) as a function of volume fraction of inclusions for glass particle-dispersed polyester composites. Experimental data was obtained by Richard [1975].

Fig. 5-3 shows the relation between the normalized thermal expansion coefficients of Ni/Al_2O_3 composites and volume fraction of Ni. The experimental data was obtained by Bruck and Rabin [1999]. The predictions by Voight model, Reuss model and Wakashima-Tsukamoto estimate are also shown. In the calculation by Wakashima-Tsukamoto estimate, Ni is assumed to be matrix for any volume fractions of Ni. The material properties used for the calculations are $E^{(Ni)}$=200GPa, $\nu^{(Ni)}$=0.3, α_{Ni}=14.3x10^{-6}°C^{-1}, $E^{(Al_2O_3)}$=380GPa, $\nu^{(Al_2O_3)}$=0.25, and $\alpha^{(Al_2O_3)}$=6.0x10^{-6}°C^{-1} [Bruck and Rabin 1999].

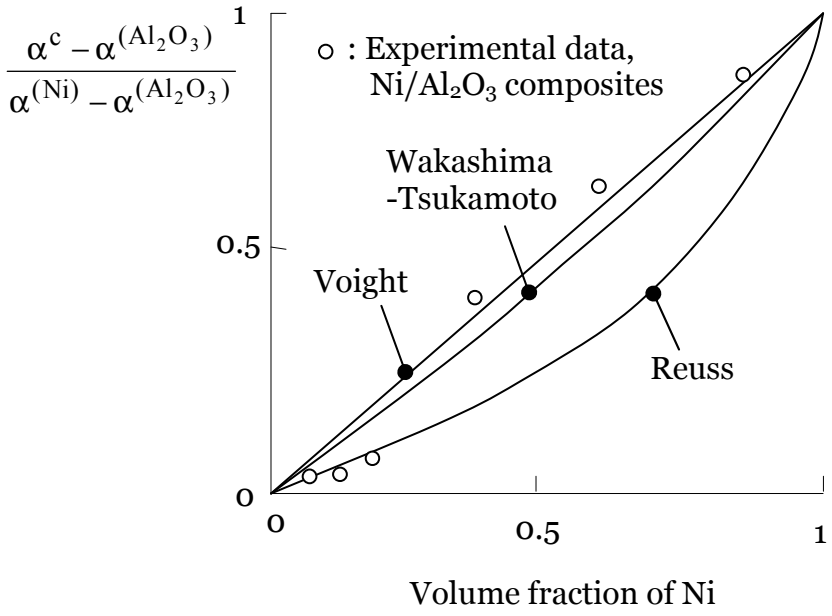

Figure 5-3: Normalized effective thermal expansion coefficient of $Ni\text{-}Al_2O_3$ composites as a function of volume fraction of Ni. The experimental data was obtained by Bruck and Rabin [1999]. In the calculation by Wakashima-Tsukamoto estimate, Ni is assumed to be matrix.

The results by Wakashima-Tsukamoto estimate are good agreeable with experimental data for the composites with a large volume fraction of Ni. This is because the matrix is assumed to be Ni in the calculation. Accordingly it is considered to be reasonable to use Wakashima-Tsukamoto estimate for predicting the effective thermo-mechanical properties of particle-dispersed composites.

5.3 Micromechanical modelling for transformation toughening

5.3.1 Micromechanical formulation

The effective elastic properties (bulk modulus and shear modulus) of the multi-phase composites with randomly distributed spherical particles can be derived by substituting the Eshelby's tensor for the spherical inclusions [Eshelby 1957]

$$S_{iklm} = \frac{1+\nu^{(0)}}{3(1-\nu^{(0)})}\delta_{ik}\delta_{lm} + \frac{8-10\nu^{(0)}}{15(1-\nu^{(0)})}(\delta_{il}\delta_{km} + \delta_{im}\delta_{kl} - \frac{2}{3}\delta_{ik}\delta_{lm}) \tag{5.15}$$

into equations (5.9), and from (5.7), (5.8), (5.9) and (5.14). In equation (5.15) $\nu^{(0)}$ is the Poisson's ratio of the matrix and δ_{ik} is the Kronecker delta. Finally, the effective bulk and shear modulus can be written as

$$k^c = \sum_{r=0}^{N} f^{(r)}\xi_{B0}^{(r)} \Bigg/ \sum_{r=0}^{N} \frac{f^{(r)}\xi_{B0}^{(r)}}{k^{(r)}}\ , \tag{5.16}$$

$$\mu^c = \sum_{r=0}^{N} f^{(r)}\eta_{B0}^{(r)} \Bigg/ \sum_{r=0}^{N} \frac{f^{(r)}\eta_{B0}^{(r)}}{\mu^{(r)}}, \tag{5.17}$$

respectively, with

$$\xi_{B0}^{(r)} = \frac{k^{(r)}}{k^{(0)}}\ \frac{3k^{(0)}+4\mu^{(0)}}{3k^{(r)}+4\mu^{(0)}} \tag{5.18}$$

$$\eta_{B0}^{(r)} = \frac{\mu^{(r)}}{\mu^{(0)}}\frac{\mu^{(0)}+\chi^{(0)}}{\mu^{(r)}+\chi^{(0)}} \tag{5.19}$$

and

$$\chi^{(0)} = \frac{\mu^{(0)}}{6}\frac{9k^{(0)} + 8\mu^{(0)}}{k^{(0)} + 2\mu^{(0)}} \tag{5.20}$$

In the above equations, $f^{(r)}$ is the volume fraction, $k^{(r)}$ the bulk modules, and $\mu^{(r)}$ the shear modulus of phase r. k^c and μ^c are the overall effective bulk modulus and shear modulus of the multi-phase composites.

Now, consider the unconstrained dilatational strain of the composite, Θ, corresponding to the unconstrained dilatational strain of the particles, $\theta^{(r)}$. The relation between Θ and $\theta^{(r)}$ is given as follows from the equations (5.7)-(5.9), (5.14) and (5.15);

$$\Theta\delta_{ik} = \sum_{r=1}^{n} f^{(r)} B_{iklm}^{(r)\,T} \delta_{lm} \theta^{(r)} \tag{5.21}$$

In the same way as the effective elastic constants were derived above, the relation between the dilatational strain component Θ of the composite and the dilatational strain of the unconstrained transformable particle $\theta^{(r)}$ can also be written as,

$$\Theta = \sum_{r=1}^{n} f^{(r)} \xi_B^{(r)} \theta^{(r)}\,, \tag{5.22}$$

where,

$$\xi_B^{(r)} = \xi_{B0}^{(r)} \Big/ \sum_{r=0}^{N} f^{(r)} \xi_{B0}^{(r)} \tag{5.23}$$

Further, in order to take into account the stress concentration effect on the stress transformation criterion, let us consider the mean stress in the particles of phase r. The mean stress in particles of phase r, $\sigma_m^{(r)}$, is given as follows:

$$\sigma_m^{(r)} = \frac{\overline{\sigma}_{ii}^{(r)}}{3} = \frac{B_{iikl}^{(r)}\overline{\sigma}_{kl} + \left(D_{iilm}^{(r)}\Delta\alpha_{lm}^{(r)} - B_{iiop}^{(r)}\sum_{s=0}^{N} f^{(s)} D_{oplm}^{(s)}\Delta\alpha_{lm}^{(s)} \right)\Delta T}{3}, \tag{5.24}$$

where

$$\Delta\alpha_{ik}^{(r)} = \alpha_{ik}^{(r)} - \alpha_{ik}^{(0)}. \tag{5.25}$$

Here, the internal stress caused by the mismatch in thermal expansion of each phase is considered. Here, $\alpha_{ik}^{(r)}$ is defined as $\alpha_{ik}^{(r)} = \alpha^{(r)}\delta_{ik}$. $\alpha^{(r)}$ is CTE of the phase r.

The following relations are also derived:

$$\sigma_m^{(r)} = \xi_B^{(r)}\overline{\sigma}_m + \Pi^{(r)}\Delta T \ , \tag{5.26}$$

with

$$\Pi^{(r)} = \xi_p\xi_{B0}^{(r)}\left(\sum_{s=0}^{N} f^{(s)}\xi_{B0}^{(s)}\Delta\alpha^{(s)} \Big/ \sum_{s=0}^{N} f^{(s)}\xi_{B0}^{(s)} - 3\Delta\alpha^{(r)} \right), \tag{5.27}$$

$$\xi_p = \frac{12k^{(0)}\mu^{(0)}}{3k^{(0)} + 4\mu^{(0)}}, \tag{5.28}$$

$$\Delta\alpha^{(r)} = \alpha^{(r)} - \alpha^{(0)}, \tag{5.29}$$

and

$$\Delta T = T - T_0 . \tag{5.30}$$

Here, T is the operational ambient temperature and T_o is the reference temperature at which no thermal stress exists in the materials. In equation (5.26) the first term is due to external loading and the second term is due to the internal stresses. $\xi_B^{(r)}$ is stress concentrate factor, which is shown in equation (5.23). $\Pi^{(r)}$ is the internal mean stresses introduced by unit temperature change. Consequently, using these equations, one can calculate the effective elastic constants, micro-stress in each phase and the unconstrained dilatation, Θ, of the composite due to dilatation $\theta^{(r)}$ of transformation and temperature rise of phase r.

5.3.2 Micromechanical expression for strength of transformation

Consider the toughening effect in a multi-phase composite enriched with spherical partially stabilized zirconia particles. The micro-mechanical model for multi-phase composites with spherical particles developed above can be directly incorporated with the continuum model [Stump and Budiansky 1989] described in Chapter 4 by replacing the corresponding material constants, dilatation and critical stress in equation (4.4) with those derived from the micromechanical model, equations (5.16), (5.17), (5.23) and (5.27). Such a substitution will not affect the fracture-toughening curve obtained with the continuum model and shown in Fig. 5-2. However the strength of the transformation will be modified as follows

$$\omega_m = \xi^2 \frac{1+\nu^c}{1-\nu^c} \frac{E^c f^{(t)} \theta}{\sigma_m^c - \Pi \Delta T}, \tag{5.31}$$

where ξ is the stress concentration factor, which corresponds to the transforming particles and can be calculated using equations (5.23) and (5.18), $f^{(t)}$ is the volume fraction of the transforming particles. Young's modulus E^c and Poisson's ratio ν^c are related to the bulk modulus k^c and shear modules μ^c (equations (5.16) and (5.17)), of the composite.

The strength of the transformation ω_m calculated from the developed micromechanical model equation (5.31) differs from that obtained from the continuum model equation (4.4). A factor ξ^2 is multiplied to the right side in equation (4.4), and σ_m^c in equation (4.4) is replaced by $\sigma_m^c - \Pi\Delta T$. ξ^2 represents the effect of the mismatch in the elastic properties of the constituent phases on the transformation toughening mechanism. This mismatch in the elastic properties results in two effects. The first one changes the unconstrained dilatation of the composite, and the second one influences the stress concentration around the transforming particles. Both effects lead to the appearance of the same factor, ξ, in the formula for the strength of the transformation parameter, ω_m, equation (5.31). They also act in the same direction together increasing or decreasing ω_m depending on the combination of material properties of the constituent phases of the composite. $\sigma_m^c - \Pi\Delta T$ in equation (5.31) is the critical mean stress in transformable particles (ZrO_2), considering the thermal residual mean stress, $\Pi\Delta T$, which is generated due to the temperature change, ΔT. Ceramic-metal composites are usually fabricated at high temperatures. Temperature change from the fabricating temperature to the ambient operating temperature causes thermal residual stresses in the composites due to the mismatch in thermal expansion coefficients of constituent phases. Such thermal stresses have a large influence on the toughening effect. The thermal stresses in the transforming particles can be large enough to trigger the phase transformation of these particles after the manufacturing process. The condition for toughening can be expressed as follows:

$$\sigma_m^c - \Pi\Delta T > 0 \qquad (5.32)$$

When the equation (5.32) is satisfied, toughening occurs, while when the equation (5.32) is satisfied, toughening does not occur. This equation (5.32) restricts the toughening zone, which is the range of volume fraction of constituent phases in which toughening is effective. The toughening zone is described later in this chapter through some numerical examinations.

5.3.3 Numerical examination for two-phase composites

Two-phase composites are investigated on the effect of mismatch in the elastic constants of constituent phases on toughening based on the derived micromechanical expression (5.31). The material properties of ZrO_2 particles used for the calculation are: Young's modulus of ZrO_2, $E^{(1)}$, is 200GPa, Poisson' s ratio of ZrO_2, $\nu^{(1)}$, is 0.3, thermal expansion coefficient of ZrO_2, $\alpha^{(1)}$ is 10.6 x $10^{-6}/^{o}C$, and the critical value of means stress, σ_m^c , is 500 MPa.

5.3.3.1 Effect of mismatch in elastic constants on the toughening effect

Fig. 5-4 shows the effect of elastic constants such as Young's modulus and Poisson's ratio of matrix on the toughening effect, K/K_{ap}, in two-phase composites. There is assumed to be no thermal stress in the composites. Here, K is the stress intensity factor at the crack tip, and K_{ap} is the applied stress intensity factor. There is not so much effect of Young's modulus of matrix on the tougheninig effect under no thermal stress conditions. Decreassing of the Poisson's ratio of matrix leads to the increase of the toiughening effects.

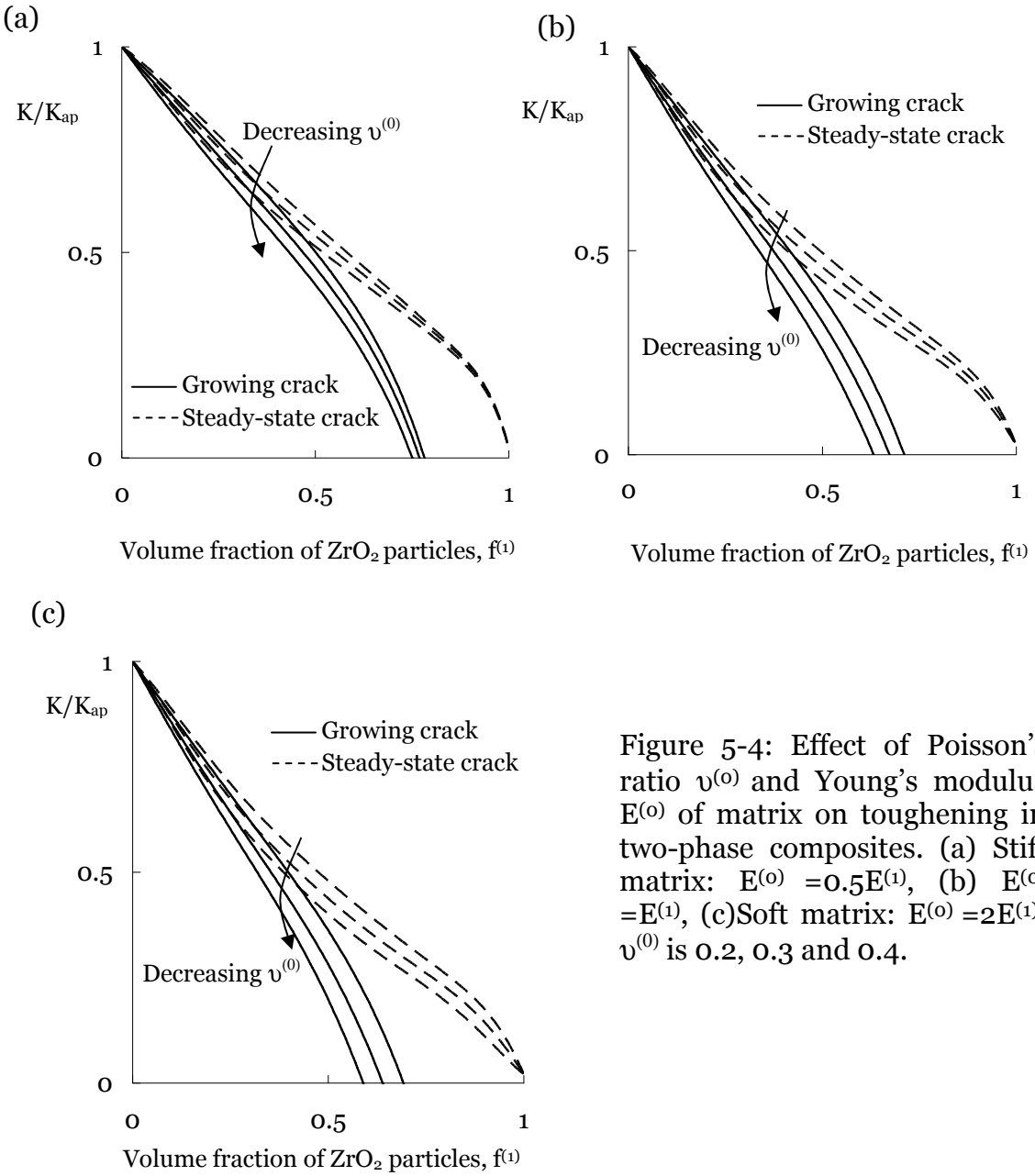

Figure 5-4: Effect of Poisson's ratio $\upsilon^{(o)}$ and Young's modulus $E^{(o)}$ of matrix on toughening in two-phase composites. (a) Stiff matrix: $E^{(o)} = 0.5E^{(1)}$, (b) $E^{(o)} = E^{(1)}$, (c)Soft matrix: $E^{(o)} = 2E^{(1)}$. $\upsilon^{(0)}$ is 0.2, 0.3 and 0.4.

5.3.3.2 Effect of mismatch in thermal expansion coefficients on the toughening effect

Fig. 5-5 shows the effect of mismatch in thermal expansion coefficients on the toughening effect in two-phase composites for varying elastic constants such

as Young's modulus and Poisson's ratio of matrix. The thermal expansion coefficient of matrix $\alpha^{(0)}$ is assumed to be smaller than that of ZrO_2, which is set at $0.5\alpha^{(1)}$. The temperature change, ΔT, is set at $-100^{o}C$, which is a relatively small value compared to the fabrication-operation temperature change but was chosen for the clear understanding of the effect of thermal stresses on toughening.

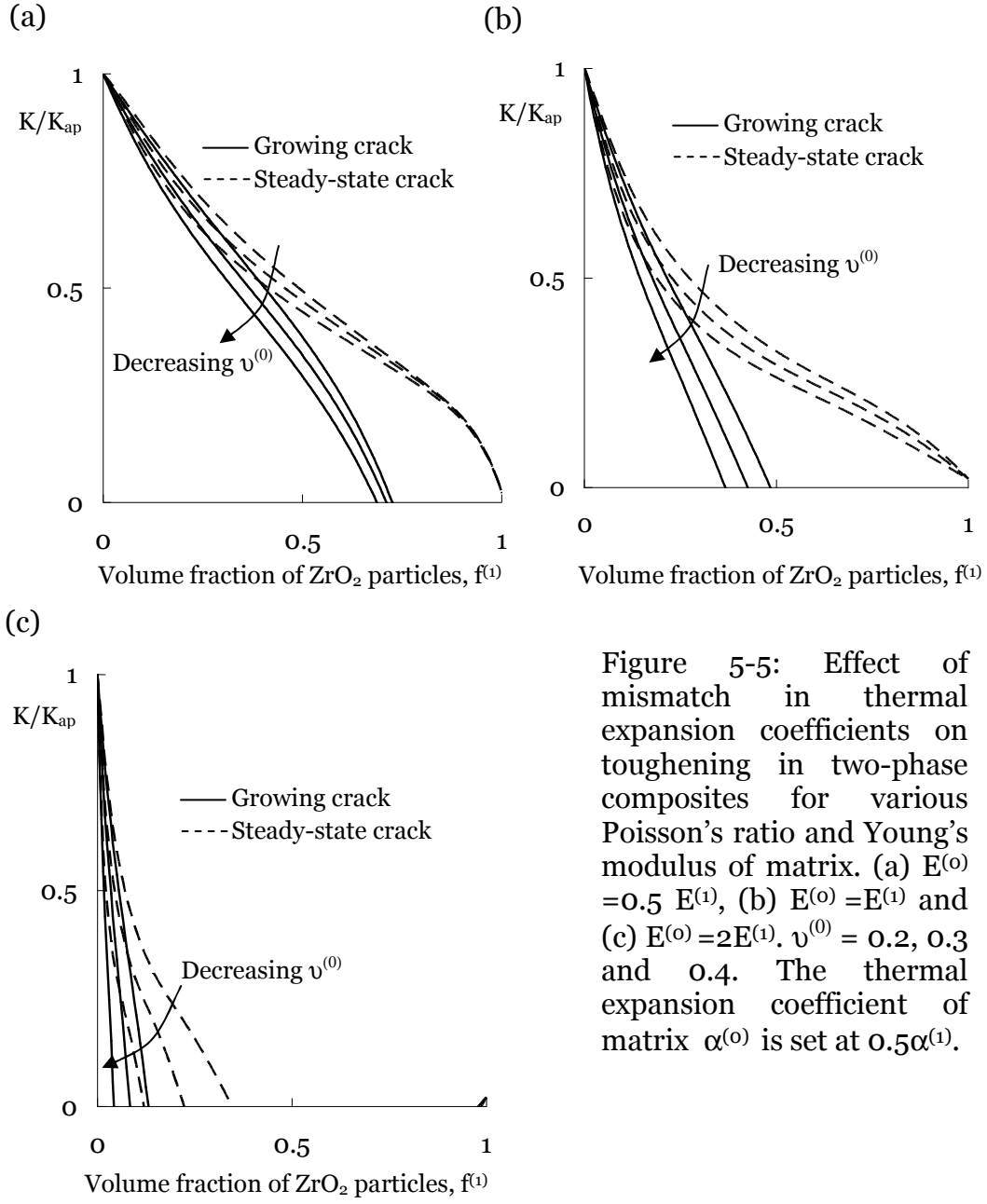

Figure 5-5: Effect of mismatch in thermal expansion coefficients on toughening in two-phase composites for various Poisson's ratio and Young's modulus of matrix. (a) $E^{(0)} = 0.5\ E^{(1)}$, (b) $E^{(0)} = E^{(1)}$ and (c) $E^{(0)} = 2E^{(1)}$. $\upsilon^{(0)}$ = 0.2, 0.3 and 0.4. The thermal expansion coefficient of matrix $\alpha^{(0)}$ is set at $0.5\alpha^{(1)}$.

As the Young's modulus of matrix increase, the effect of residual thermal stresses on toughening increases. When $E^{(0)} = 2E^{(1)}$ (shown in Fig.5-5 (c)), the toughening effect is largely affected by thermal stresses due to the temperature change compared to other cases such as $E^{(0)} = 0.5$ and $E^{(1)}$, even though compared to the case when there is no thermal stresses in the composites as shown in Fig.5-4 (c). Decreassing of the Poisson's ratio of matrix leads to increase of the toiughening effects.

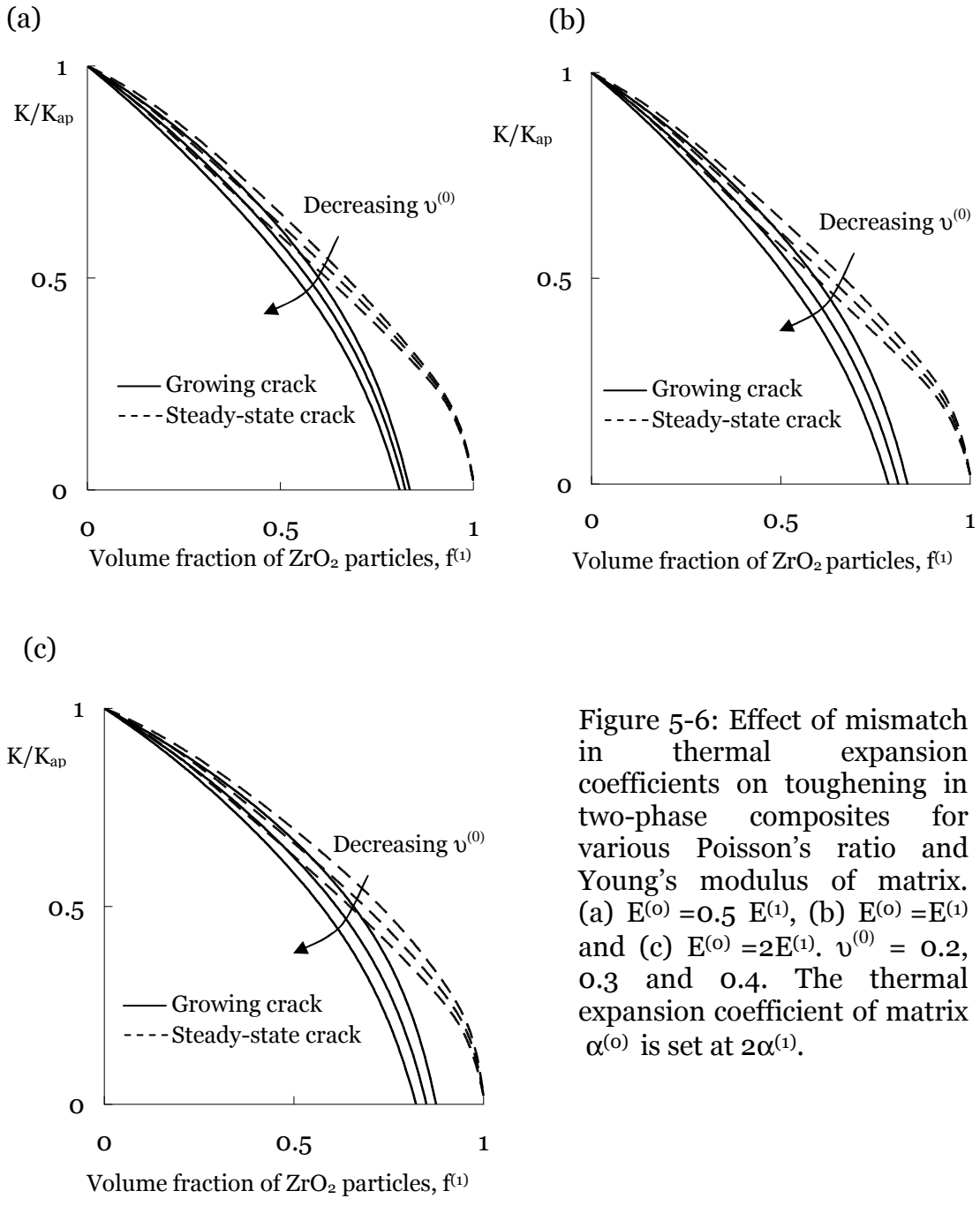

Figure 5-6: Effect of mismatch in thermal expansion coefficients on toughening in two-phase composites for various Poisson's ratio and Young's modulus of matrix. (a) $E^{(0)} = 0.5\ E^{(1)}$, (b) $E^{(0)} = E^{(1)}$ and (c) $E^{(0)} = 2E^{(1)}$. $\upsilon^{(0)} = 0.2$, 0.3 and 0.4. The thermal expansion coefficient of matrix $\alpha^{(0)}$ is set at $2\alpha^{(1)}$.

Fig. 5-6 shows the effect of mismatch in thermal expansion coefficients on the toughening effect in two-phase composites for the varying elastic constants such as Young's modulus and Poisson's ratio of matrix. The thermal expansion coefficient of matrix $\alpha^{(0)}$ is assumed to be smaller than that of ZrO_2, which is set at $2\alpha^{(1)}$. The temperature change, ΔT, is set at $-100^{o}C$. The influence of residual thermal stresses on the toughening effect is small compared to the case that $\alpha^{(0)}=0.5\alpha^{(1)}$. The influence of the Young's modulus of matrix on the toughening effect is also small under such thermal stress states with the conditions of $\alpha^{(0)}=2\alpha^{(1)}$ and $\Delta T<0$. Decreassing of the Poisson's ratio of matrix also leads to increase of the toiughening effect all the time. Accordingly, in two-phase composites, when $\alpha^{(0)}$ is smaller than $\alpha^{(1)}$, which is the thermal expansion coefficient of ZrO_2, the toughening effect is largely affected by the Young's modulus of matrix.

5.3.4 Numerical examination for three-phase composites

In this section, the toughening effect in three-phase composites is investigated in terms of the influences of mismatch in Young's modulus, Poisson's ratio and thermal expansion coefficients of constituent phases. The material properties of ZrO_2 used for the calculation are the same as those used in the previous section.

5.3.4.1 Effect of mismatch in elastic constants on the toughening effect

For three-phase composites, there are more number of combinations of variables such as Young's modulus, Poisson's ratio and thermal expansion coefficient of constituent phases, affecting the toughening effect, compared to the two-phase composites analysed above. Here we can chose some typical cases for the examination of the effect of mismatch in these thermo-mechanical properties of constituent phases on the toughening effect based on the derived micromechanical expression of equation (5.17).

It is assumed that the phase (0) corresponds to matrix, the phase (1) corresponds to ZrO_2 particles, and phase (2) corresponds to another kind of particles. The composites containing both transformable and non-transformable ZrO_2 particles can be considered to be a kind of two-phase composites, which is expressed by the composites with the same material properties except for the ability of the transformation of both kinds of ZrO_2 particles. The volume fraction of ZrO_2 is fixed at 0.3.

5.3.4.1.1 Effect of Young's modulus and Poison's ratio of matrix

Fig. 5-7 shows the effect of Young's modulus $E^{(0)}$ and Poisson's ratios $\upsilon^{(0)}$ of matrix on the toughening effect. In any cases, the smaller values of $\upsilon^{(0)}$ lead to higher toughening effect and lower values of K/K_{ap}.

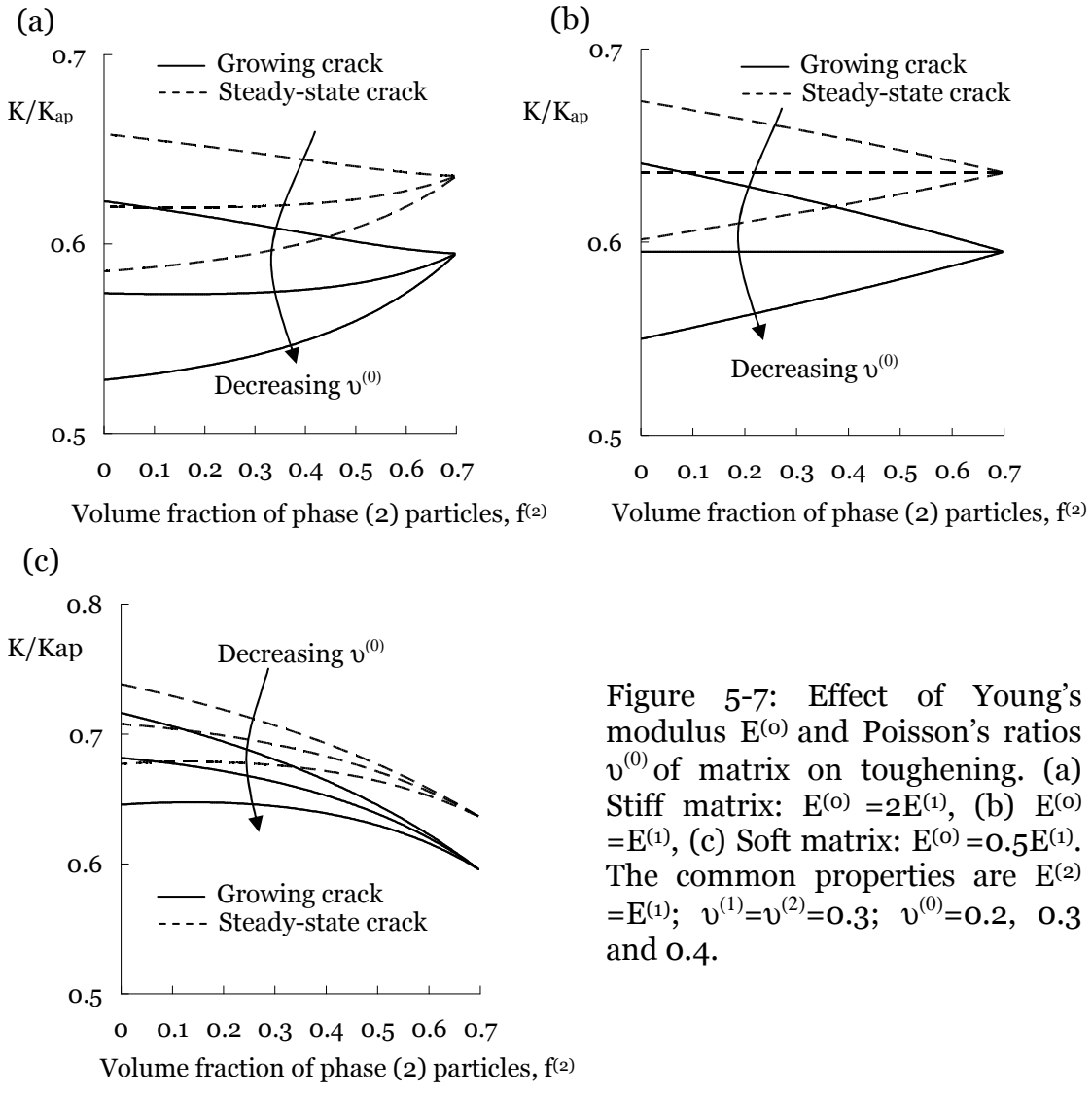

Figure 5-7: Effect of Young's modulus $E^{(0)}$ and Poisson's ratios $\upsilon^{(0)}$ of matrix on toughening. (a) Stiff matrix: $E^{(0)}=2E^{(1)}$, (b) $E^{(0)}=E^{(1)}$, (c) Soft matrix: $E^{(0)}=0.5E^{(1)}$. The common properties are $E^{(2)}=E^{(1)}$; $\upsilon^{(1)}=\upsilon^{(2)}=0.3$; $\upsilon^{(0)}=0.2$, 0.3 and 0.4.

When $E^{(0)} = 2E^{(1)}$ and $E^{(0)} = E^{(1)}$, in the only case of $\upsilon^{(0)}=0.4$, the toughening effect increases with increasing the volume fraction of phase(2) particles. When $E^{(0)} = 0.5E^{(1)}$, for any values of $\upsilon^{(0)}$, the toughening effect increases with increasing the volume fraction of phase(2) particles.

5.3.4.1.2 Effect of Young's modulus of particles and Poison's ratio of matrix

The effects of Young's modulus $E^{(2)}$ of phase (2) particles and Poisson's ratios $\upsilon^{(0)}$ of matrix on the toughening effect in the composites with stiff particles ($E^{(2)} = 2E^{(1)}$) and soft particles ($E^{(2)} = 0.5E^{(1)}$) are shown in Fig 5-7. For the composites with stiff particles ($E^{(2)} = 2E^{(1)}$), when $\upsilon^{(0)}=0.3$ and 0.4, the toughening effect increases with increasing the volume fraction of phase (2) particles.

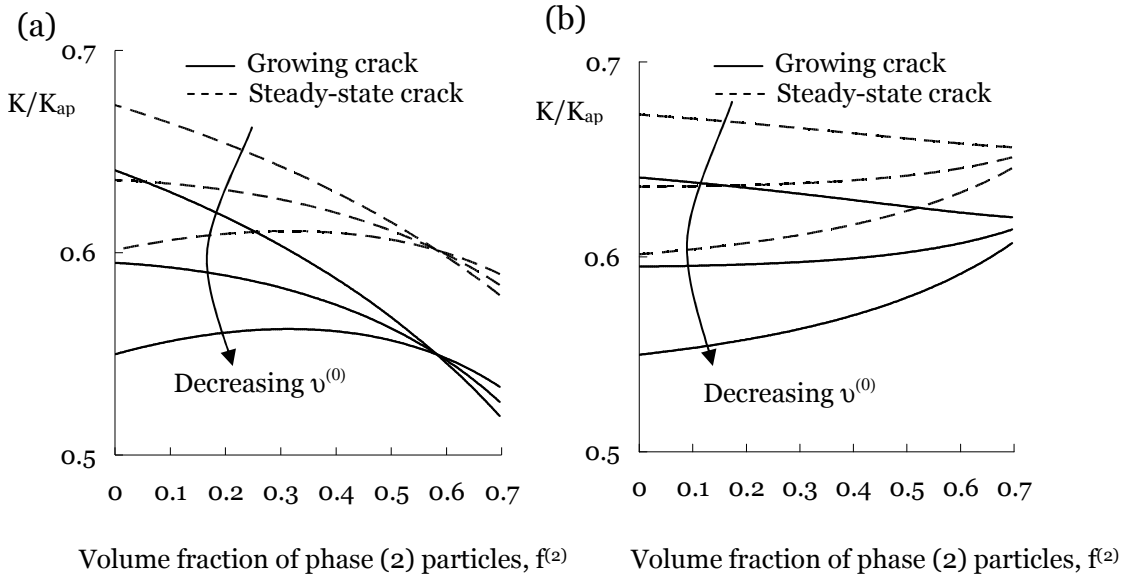

Figure 5-8: Effect of Young's modulus $E^{(2)}$ of phase (2) particles and Poisson's ratios $\upsilon^{(0)}$ of matrix on toughening. (a) Stiff particle: $E^{(2)} = 2E^{(1)}$, (b) Soft particle: $E^{(2)} = 0.5E^{(1)}$. The common properties are $E^{(0)} = E^{(1)}$; $\upsilon^{(1)}=\upsilon^{(2)}=0.3$; $\upsilon^{(0)}=0.2$, 0.3 and 0.4.

For the composites with $\upsilon^{(0)}$=0.2, in low volume fractions of phase (2), the toughing effect decreases with increasing the volume fraction of phase (2), while in high volume fractions of phase (2) the toughening effect increases with increasing the volume fraction of phase (2). At the volume fraction of around 0.6 of phase (2) particles, the toughening effects for $\upsilon^{(0)}$=0.2 and 0.4 become inversely related. For the composites with soft particles ($E^{(2)}$ =0.5$E^{(1)}$), the toughening effect increases with decreasing the Poisson's ration of matrix $\upsilon^{(0)}$.

5.3.4.1.3 Effect of Young's modulus and Poison's ratio of particles

Fig. 5-9 shows the effect of Young's modulus $E^{(2)}$ and Poisson's ratios $\upsilon^{(2)}$ of phase (2) particles on toughening in the composites with stiff particles ($E^{(2)}$ =2$E^{(1)}$) and soft particles ($E^{(2)}$ =0.5$E^{(1)}$). For the composites with stiff particles ($E^{(2)}$ =2$E^{(1)}$), the toughening effect almost increases with increasing the volume fraction of phase (2) particles in any cases.

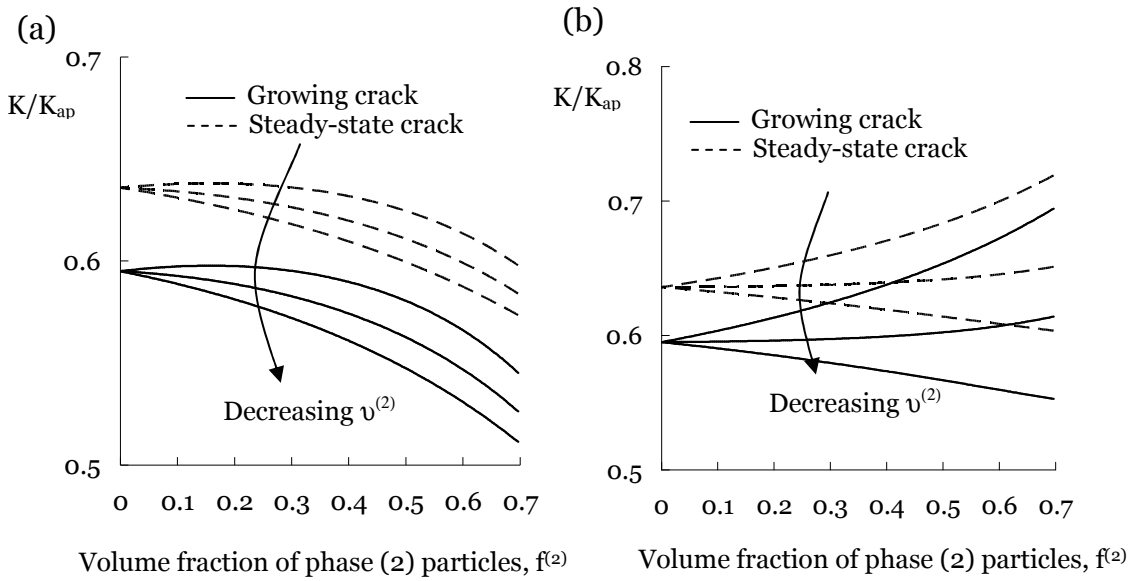

Figure 5-9: Effect of Young's modulus $E^{(2)}$ and Poisson's ratio $\upsilon^{(2)}$ of phase (2) particles on toughening. (a) Stiff particles: $E^{(2)}$ =2$E^{(1)}$, (b) Soft particles: $E^{(2)}$ =0.5$E^{(1)}$. The common properties are $E^{(0)}$ =$E^{(1)}$; $\upsilon^{(0)}$=$\upsilon^{(1)}$=0.3; $\upsilon^{(2)}$=0.2, 0.3 and 0.4.

Meanwhile, for the composites with soft particles ($E^{(2)}$ =0.5$E^{(1)}$), when $\upsilon^{(2)}$=0.4, the toughening effect decreases with increasing the volume fraction of phase (2), while when $\upsilon^{(2)}$=0.2, the toughening effect increases with increasing

the volume fraction of phase (2). Therefore, the phase (2) particles with low Young's modulus and high Poisson's ratios should be carefully added into ZrO_2-enriched composites. Here, in any cases, lower Poisson's ratios of phase (2) also bring higher toughening effects.

5.3.4.1.1 Effect of Young's modulus of matrix and Poison's ratio of particles

Fig. 5-10 shows the effects of Young's modulus $E^{(0)}$ of matrix and Poisson's ratio $\upsilon^{(2)}$ of Phase (2) particles on the toughening effect K/K_{ap} in the composites with stiff matrix ($E^{(0)}=2E^{(1)}$) and soft matrix ($E^{(0)}=0.5E^{(1)}$). For the composites with stiff matrix ($E^{(0)}=2E^{(1)}$), when $\upsilon^{(2)}=0.4$, the toughening effect decreases with increasing the volume fraction of phase (2), while when $\upsilon^{(2)}=0.2$, the toughening effect increases with increasing the volume fraction of phase (2).

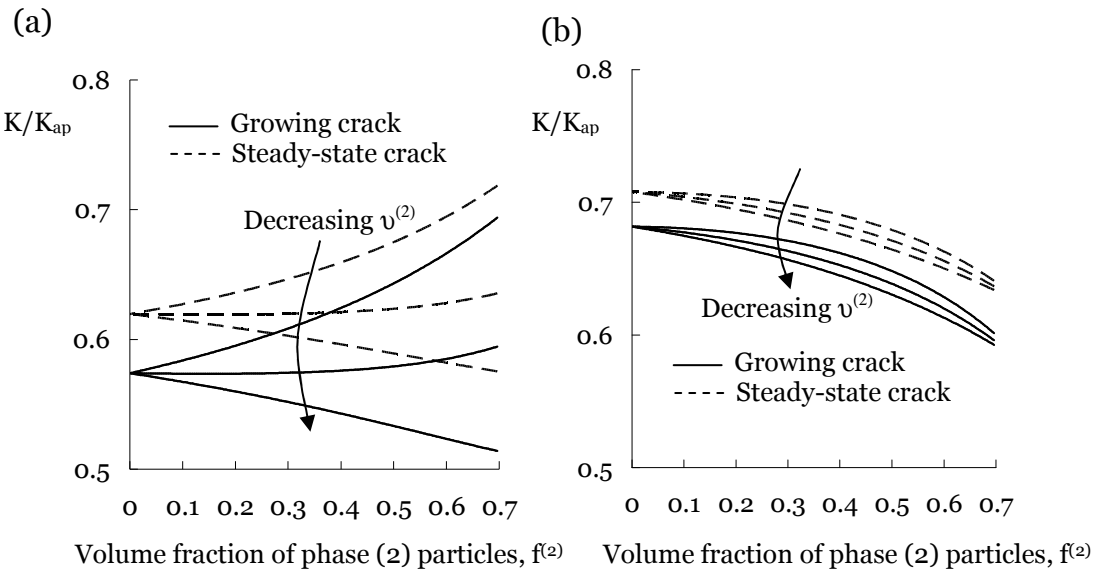

Figure 5-10: Effect of Young's modulus $E^{(0)}$ of matrix and Poisson's ratio $\upsilon^{(2)}$of phase(2) particles on toughening. (a) Stiff matrix: $E^{(0)}=2E^{(1)}$, (b) Soft matrix: $E^{(0)}=0.5E^{(1)}$. The common properties are $E^{(2)}=E^{(1)}$; $\upsilon^{(0)}=\upsilon^{(2)}=0.3$; $\upsilon^{(2)}=0.2$, 0.3 and 0.4.

Meanwhile, for the composites with soft matrix ($E^{(0)}=0.5E^{(1)}$), the toughening effect in the composites with any Poisson's ratios increases with increasing the volume fraction of phase (2) particles. In any cases, lower Poisson's ratios of phase (2) also bring higher toughening effects.

The tendency of the effect of mismatch in Young's modulus of constituents is summarized in Table 5-1. Both matrix and phase (2) particles with high Young's modulus and low Poisson's ratios, which are considered to be more likely ceramic properties rather than metal and alloy ones, leads to more increase of the transformation toughening under no thermal stress conditions. Decrease of Poisson's ratio of both constituents lead to increase of the toughening effect. Using these results, we can select the suitable ingredient materials for obtaining high toughening effects in multi-phase composites. In the following section, the effects of mismatch in thermal expansion coefficients are investigated.

Table 5-1: Diagram of effect of mismatch in Young's modulus of constituents in three-phase composites on the toughening effect. (The levels of the toughening effect are shown.)

Particle \ Matrix	Stiff	Similar	Soft
Stiff	Highest	High	Moderate
Similar	High	Moderate	Low
Soft	Moderate	Low	Lowest

5.3.4.2 Effect of mismatch in thermal expansion coefficients on the toughening effect

In this section, the effect of mismatch in thermal expansion coefficients on toughening effect toughening effect is investigated in three-phase composites for various Young's modulus and Poisson's ratio of constituent phases. Some typical results are shown.

5.3.4.2.1 Effect of Young's modulus of matrix and particles in case that the thermal expansion coefficient of matrix is higher than that of ZrO_2

The numerical examination for two-phase composites demonstrates that the mismatch in thermal expansion coefficients of constituent phases has a large

influence on the transformation toughening effect. Ceramic-metal composites are fabricated at high temperatures, and the difference between a fabricating temperature and an ambient operating temperature can cause the thermal residual stresses due to the mismatch in thermal expansion coefficients of constituent phases. Such thermal stresses are considered to largely influence the toughening effect [Orange et al. 1992].

The temperature change is assumed to be -1000°C from the view point of the fabricating temperature of the ZrO_2-enriuched composites [Shi et al. 1998]. Fig. 5-11 shows the effects of mismatch in thermal expansion coefficients of constituent phases on the toughening for various Young's modulus of matrix $E^{(0)}$ and phase (2) particles $E^{(2)}$. The thermal expansion coefficient of matrix is set at twice value of that of ZrO_2 ($\alpha^{(0)} = 2\alpha^{(1)}$). The mismatch in thermal expansion coefficients causes the thermal stresses under temperature change conditions. It is seen that the toughening effect increases with increasing the volume fraction of phase (2) particles. Lower Young's modulus $E^{(0)}$ of matrix and higher Young's modulus $E^{(2)}$ of phase (2) particles lead to the increase of the toughening.

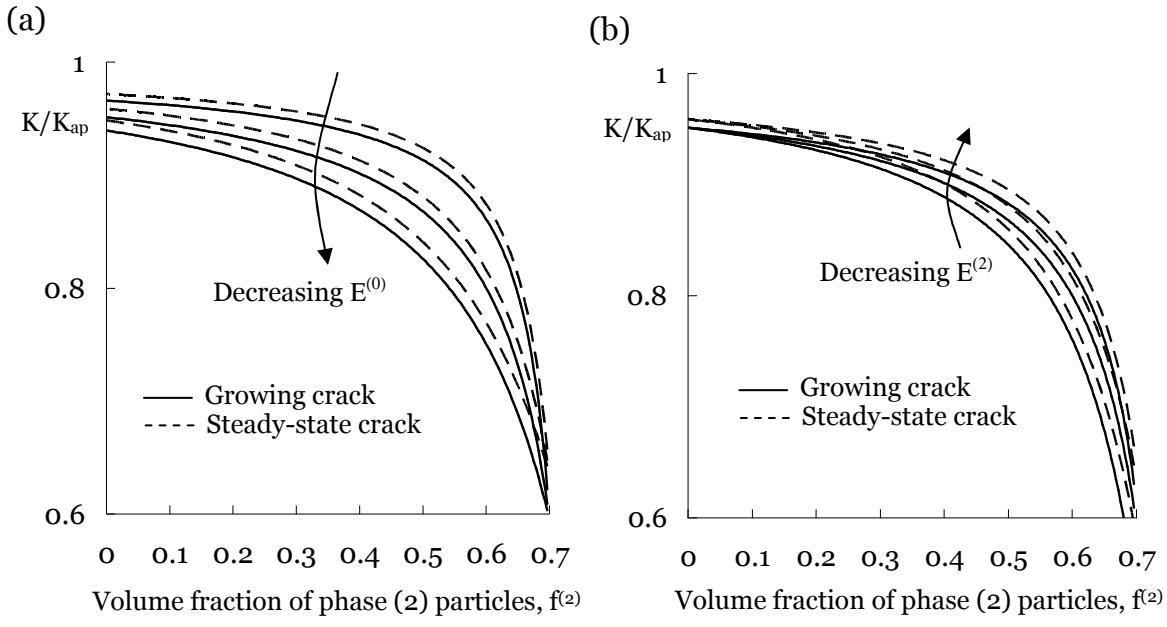

Figure 5-11: Effect of mismatch in thermal expansion coefficients on toughening for various Young's modulus of matrix and phase (2) particles. (a) $E^{(0)} = 2E^{(1)}$, $E^{(1)}$ and $0.5E^{(1)}$; $E^{(2)} = E^{(1)}$, (b) $E^{(2)} = 2E^{(1)}$, $E^{(1)}$ and $0.5E^{(1)}$, $E^{(0)} = E^{(1)}$. The common properties are $\alpha^{(0)} = 2\alpha^{(1)}$;$\alpha^{(2)} = \alpha^{(1)}$; $\upsilon^{(0)} = \upsilon^{(1)} = \upsilon^{(2)} = 0.3$.

5.3.4.2.2 Effect of Young's modulus of matrix and particles in case that the thermal expansion coefficient of additional particle is lower than that of ZrO_2

Fig. 5-12 shows the effects of mismatch in thermal expansion coefficients on the toughening effect for various Young's modulus of matrix and phase (2) particles. The composites contain matrix or phase (2) with low thermal expansion coefficients ($\alpha^{(0)}=0.5\alpha^{(1)}$ or $\alpha^{(2)}=0.5\alpha^{(1)}$). The investigation was made for three different values of Young's modulus of matrix and phase (2) particles. We can see the "lock-up" effect (see Fig. 4-5 in Chapter4), which corresponds to the intersection point of the horizontal axis and each toughening curve in both figures (Figs. 5-11(a) and (b)) say simply - infinite toughness. As the volume fraction of the phase with lower thermal expansion coefficients increases, the "lock-up" effect is more likely to occur. In addition, there is another important thing we should pay attention to besides this "lock-up" effect. Adding over the contents of constituent materials with low thermal expansion coefficients enough to introduce the "lock-up" effect can cause no toughening, which means that all the ZrO_2 particles in the composites can transform under given thermal conditions. For example, as shown in Fig 5-7 (b), no toughening effect is caused by adding more than 15 percent volume fraction of phase (2) particles. It is found that higher toughening effects are expected to appear by adding such materials with low thermal expansion coefficients into the composites, and more attention should be paid not to lose the whole toughening effects. There is a fine line between the maximum toughening and no toughening according to this analysis. Now we call a range of volume fractions of constituent phases, in which toughening is effective, the "toughening zone". This zone is restricted by the equation (5.32). As seen in Fig.5-12 (a), for the composites containing matrix with low thermal expansion coefficients ($\alpha^{(0)}=0.5\alpha^{(1)}$), higher Young's modulus of matrix leads to the increase of the toughening, and the toughening zone is reduced.

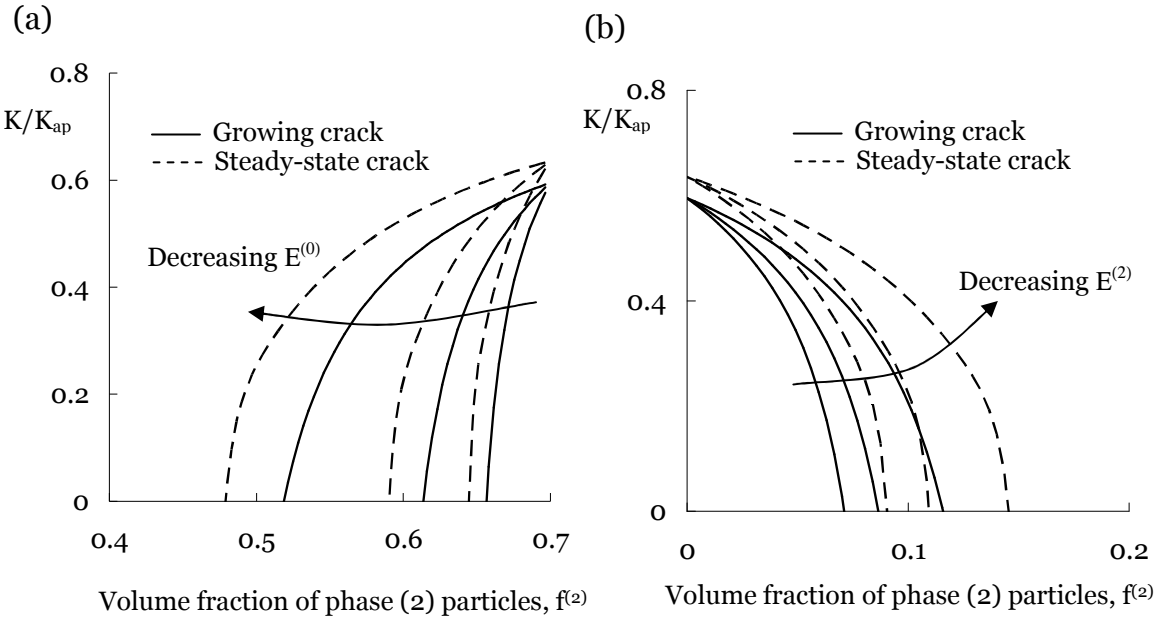

Figure 5-12: Effect of mismatch in thermal expansion coefficients on toughening for various Young's modulus of matrix and phase (2) particles. (a) $E^{(0)}=2E^{(1)}$, $E^{(1)}$ and $0.5E^{(1)}$; $E^{(2)}=E^{(1)}$; $\alpha^{(0)}=0.5\alpha^{(1)}$; $\alpha^{(2)}=\alpha^{(1)}$, (b) $E^{(2)}=2E^{(1)}$, $E^{(1)}$ and $0.5E^{(1)}$; $E^{(0)}=E^{(1)}$; $\alpha^{(2)}=0.5\alpha^{(1)}$; $\alpha^{(0)}=\alpha^{(1)}$. The common properties are $\upsilon^{(0)}=\upsilon^{(1)}=\upsilon^{(2)}=0.3$.

For the composites containing phase (2) particles with low thermal expansion coefficients ($\alpha^{(2)}=0.5\alpha^{(1)}$), higher Young's modulus of phase (2) particles leads to the increase of toughening effect, and the toughening zone also is reduced in comparison with phase (2) particles with the same thermal expansion coefficients as ZrO_2 ($\alpha^{(2)}=\alpha^{(1)}$).

5.3.4.2.3 Effect of Poisson's ratio of matrix and particles in case that the thermal expansion coefficient of matrix is higher than that of ZrO_2

The effect of mismatch in thermal expansion coefficients on the toughening effect for various Poisson's ratios of matrix and phase (2) particles is shown in Fig.5-13. The matrix has a high thermal expansion coefficients ($\alpha^{(0)}=2\alpha^{(1)}$). It can be seen that the toughening effect increases with increasing the

volume fraction of phase (2) particles. Lower Poisson's ratio $\upsilon^{(0)}$of matrix and phase (2) particles lead to the increase of the toughening.

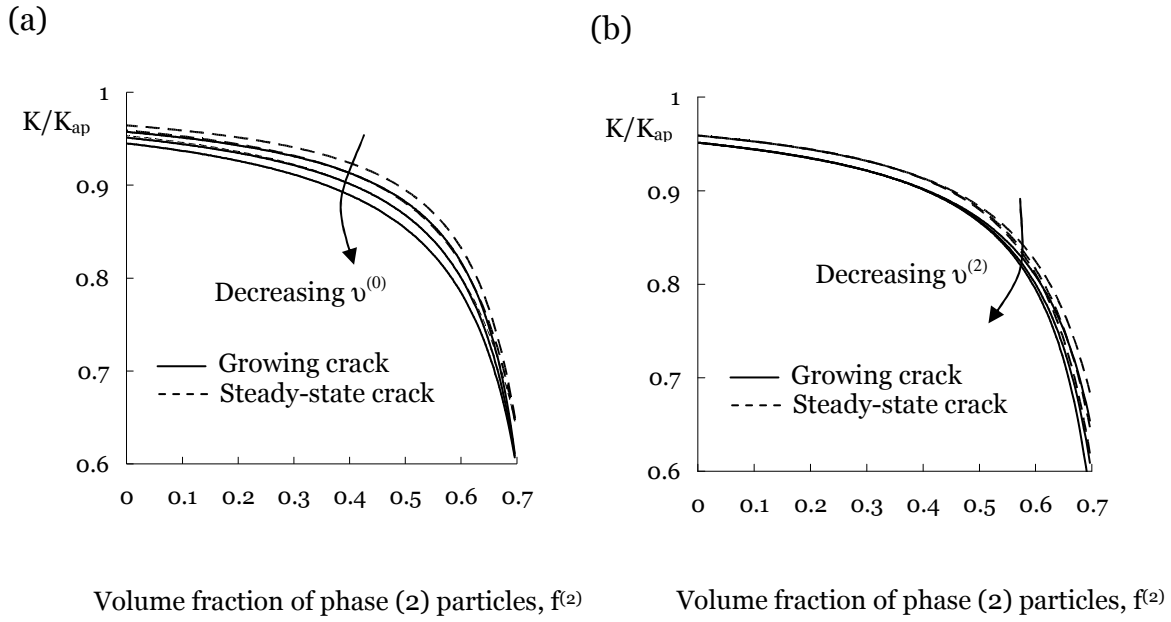

Figure 5-13: Effect of mismatch in thermal expansion coefficients on toughening for various Poisson's ratios of matrix and phase (2) particles. (a) $\upsilon^{(0)}=2\upsilon^{(1)}$, $\upsilon^{(1)}$and $0.5\upsilon^{(1)}$; $\upsilon^{(2)}=\upsilon^{(1)}$, (b) $\upsilon^{(2)}=2\upsilon^{(1)}$, $\upsilon^{(1)}$ and $0.5\upsilon^{(1)}$; $\upsilon^{(0)}=\upsilon^{(1)}$. The common properties are $\alpha^{(0)}=2\alpha^{(1)}$; $\alpha^{(2)}=\alpha^{(1)}$; $E^{(0)}=E^{(1)}=E^{(2)}$.

It is seen that the mismatch in Poisson's ratio have a small influence on the toughening effect compared with that of Young's modulus in the case of $\alpha^{(0)}=2\alpha^{(1)}$.

5.3.4.2.4 Effect of Poisson's ratio of matrix and particles in case that the thermal expansion coefficient of matrix or particles is lower than that of ZrO_2

Fig. 5-14 shows the effects of mismatch in the thermal expansion coefficients on the toughening for various Poisson's ratios of matrix and phase (2) particles in the composites containing matrix or phase (2) with low thermal expansion coefficients ($\alpha^{(0)}=0.5\alpha^{(1)}$ or $\alpha^{(2)}=0.5\alpha^{(1)}$). It can be also seen that the "lock-up" effects appear at the low volume fractions of the phases with low thermal expansion coefficient. For the composites containing matrix with low

thermal expansion coefficients ($\alpha^{(0)}=0.5\alpha^{(1)}$), higher Poisson's ratio of matrix leads to the increase of the toughening, and the toughening zone is reduced.

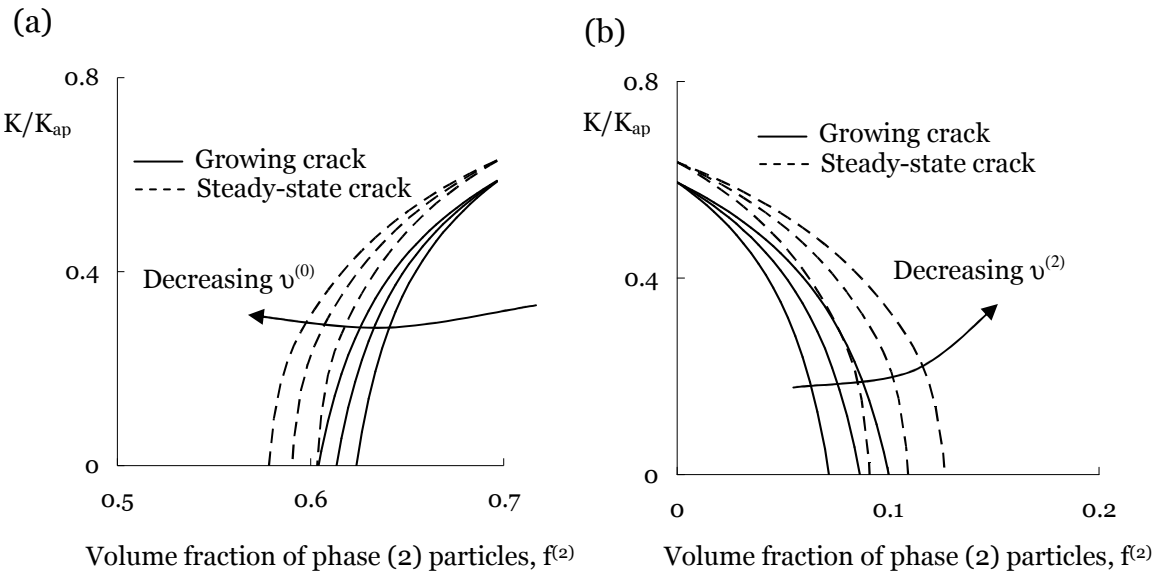

Figure 5-14: Effect of mismatch in thermal expansion coefficients on the toughening for various Poisson's ratios of matrix and phase (2) particles. (a) $\upsilon^{(0)}=2\upsilon^{(1)}$, $\upsilon^{(1)}$ and $0.5\upsilon^{(1)}$; $\upsilon^{(2)}=\upsilon^{(1)}$; $\alpha^{(0)}=0.5\alpha^{(1)}$; $\alpha^{(2)}=\alpha^{(1)}$, (b) $\upsilon^{(2)}=\upsilon^{(1)}$, $\upsilon^{(1)}$ and $0.5\upsilon^{(1)}$; $\upsilon^{(0)}=\upsilon^{(1)}$; $\alpha^{(2)}=0.5\alpha^{(1)}$; $\alpha^{(0)}=\alpha^{(1)}$. The common properties are $E^{(0)}=E^{(1)}=E^{(2)}$.

For the composites containing phase (2) particles with low thermal expansion coefficients ($\alpha^{(2)}=0.5\alpha^{(1)}$), higher Poisson's ratio of phase (2) particles leads to the increase of toughening, and the toughening zone is also reduced. The effects of the mismatch in thermal expansion coefficients of constituent phases, which introduce thermal stresses in the composites under temperature change conditions, on the toughening is extremely large as demonstrated above, and it is important to consider such effects in design of the composites toughened by transformation of ZrO_2.

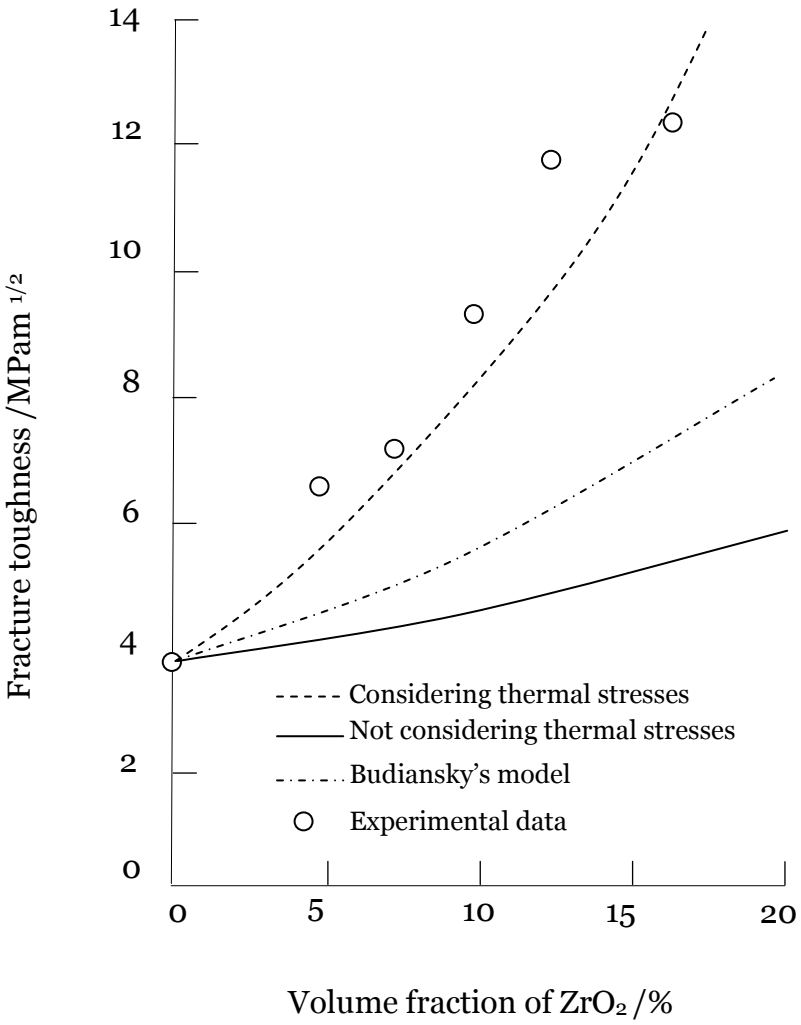

Figure 5-15: Fracture toughness plotted against the volume fraction of ZrO_2 in Al_2O_3-ZrO_2 composites. The experimental data was obtained by Tuan et al. [2002]. Simulation results based on the Budiansky's continuum model, micromechanical models considering thermal residual stresses and not considering thermal residual stresses for the steady-state crack are plotted.

Fig. 5-15 is the fracture toughness plotted against the volume fraction of ZrO_2 in Al_2O_3/ZrO_2 composites, which is the same as Fig. 4-1 in Chapter 4. The simulation results calculated based on the micromechanical developed model described above are shown. In this calculation, the temperature change is set at -200^{o}C. The simulation results based on the model not considering the effect of

thermal residual stresses in the composites are much lower than the experimental data even if they are compared to the results obtained from the Budiansky's original model. However, the results based on the developed model considering the effect of thermal residual stresses can represent the experimental data. It is important to investigate the effects of thermal residual stresses generated during the fabrication process due to mismatch in thermo-mechanical properties of constituent phases based on the micromechanical considerations for engineering the superior composites with higher fracture properties by using this transformation toughening.

5.3.4.3 Examination of ZrO_2-toughened Al_2O_3 composites with Ni or Ag particles based on the developed model

Next we investigate ZrO_2-toughened Al_2O_3 (ZTA) composites with another kind of particles. As seen in the above simulation, the existence of third phase particles (phase (2) particles) have a large influence on the transformation toughening effects, in particular, under thermal stress conditions, which is induced during the fabrication process. Here, we consider three-phase composites such as the ZTA with Ag or Ni particles. The effects of addition of third phase of Ag or Ni on the toughening are examined. Fig. 5-16 shows the effect of addition of Ag or Ni on the toughening effect for the composites not considering and considering thermal stresses due to the temperature change of -200^{o}C. In Al_2O_3-ZrO_2-Ag and Al_2O_3-ZrO_2-Ni composites, the volume fraction of Ag and Ni particles is set at the same value as that of ZrO_2 particles. The material data used for the calculation are given in Table A2-1 in Appendix 2.

When there is no temperature change, which means that no thermal residual stresses are generated in the composites, the toughening effects are the almost same in these three composites such as Al_2O_3-ZrO_2, Al_2O_3-ZrO_2-Ag and Al_2O_3-ZrO_2-Ni. In other words, the third (phase (2)) particles such as Ag and Ni have almost no influence on the toughing effect in these composites under no thermal stress conditions.

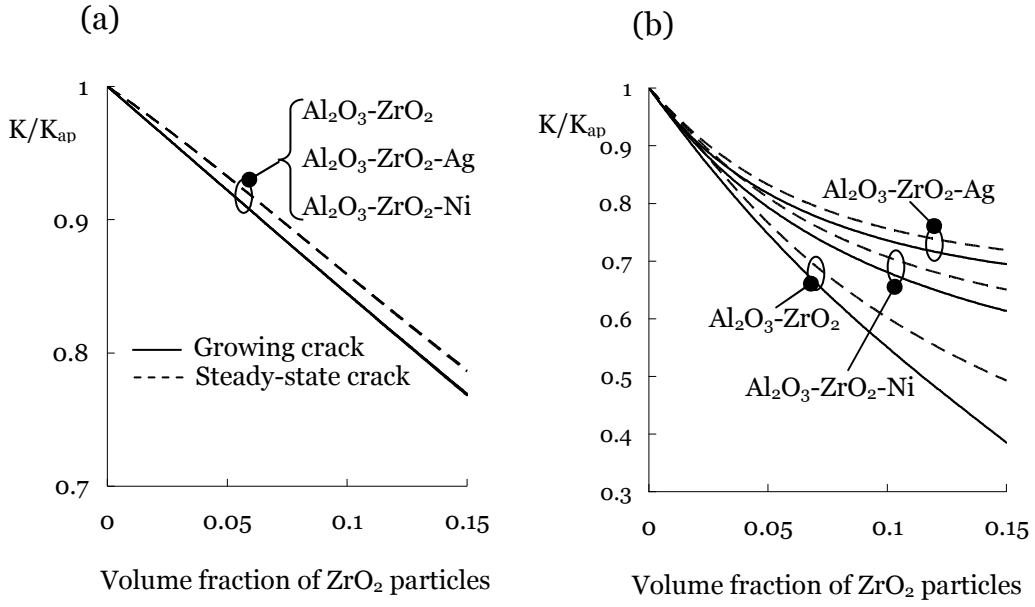

Figure 5-16: Effect of addition of Ag or Ni on toughening in the Al_2O_3-ZrO_2 composites (ZTA). (a) No thermal residual stresses and (b) thermal residual stresses exist.

However, such materials are usually subjected to a temperature change during the fabrication process, and the thermal residual stresses are generated in the materials. The effects of the thermal stresses on the toughening effect are shown in Fig. 5-16 (b). It can be seen that adding of both Ag and Ni particles decrease the toughening effect. In particular, adding of Ag particles causes a large amount of decrease of the toughening effect.

Fig. 5-17 shows an experimental result indicating the effect of adding Ag or Ni into the Al_2O_3-ZrO_2 composites on the toughening, which was obtained by Chen et al. [Chen and Tuan 2001; Chen et al. 2000]. Dashed line is the sum of the fracture toughness of Al_2O_3 and the increase of the fracture toughness by adding Ni or Ag, and ZrO_2 into Al_2O_3:

$$K_{Ic}^{sum} = K_{Ic}^{(Al_2O_3)} + \Delta K_{Ic}^{(Al_2O_3+Ni\,or\,Ag)} + \Delta K_{Ic}^{(Al_2O_3+ZrO_2)}. \qquad (6.18)$$

The second term $\Delta K_{Ic}^{(Al_2O_3+Ni\ or\ Ag)}$ in the right-hand side of the equation (6.18) is mainly attributed to the toughening by the soft metal bridging [Chen and Tuan 2001; Chen et al. 2000] (see Chapter 2).

From Fig. 5-16 (a), the fracture toughness of Al_2O_3-ZrO_2 composites can be seen to be largely enhanced by adding Ni particles. It was stated in their paper [Chen and Tuan 2001] that the toughening effect in the Al_2O_3-ZrO_2 composites with Ni particles is attributed to refined microstructures, and the presence of Ni particles increases the transformation ability of ZrO_2 inclusions due to the low elastic modulus of Ni. However, we consider this explanation is unclear. As seen in Fig.5-15, it can be considered that addition of Ni particles have almost no influence on the toughening effect in the composites in which no thermal stresses exist, while addition of Ni can reduce the toughening effect when the composites have thermal residual stresses generated during fabrication process. Therefore, the thermal stresses are considered to have a small negative effect on the strength of the toughening, and the high toughening effect by adding Ni can be considered to be induced by other factors such as the synergetic effects between soft metal bridging and transformation toughening mechanisms [Amazigo and Budiansky 1988], which indicates the increasing of the toughening effect due to the interaction of the both mechanisms such as soft metal-bridging and transformation toughening mechanisms.

From the experimental data shown in Fig. 5-16 (b), the effect of addition of Ag into the Al_2O_3-ZrO_2 composites on the toughening is considerably small compared to that of addition of Ni (Fig. 5-16 (a)). The increase of toughening effect by addition of Ag into such composites is almost the same as that by addition of Ag into monolithic Al_2O_3. This implies that the transformation toughening effect by ZrO_2 is considered to be reduced by addition of Ag. It was stated in their paper that the soft Ag inclusions act as cushion to absorb the transformation stresses induced by the phase transformation of nearby ZrO_2 particles. However, from Fig.5-15, this situation can be considered to attribute to not only low Young's modulus but also high thermal expansion coefficient of Ag. The thermal stresses generated during the fabrication process cause a large decrease of the transformation toughing effect by ZrO_2. Therefore, Al_2O_3-ZrO_2-Ag composites show lower fracture toughness than expected from that of Al_2O_3-ZrO_2 and Al_2O_3-Ag composites.

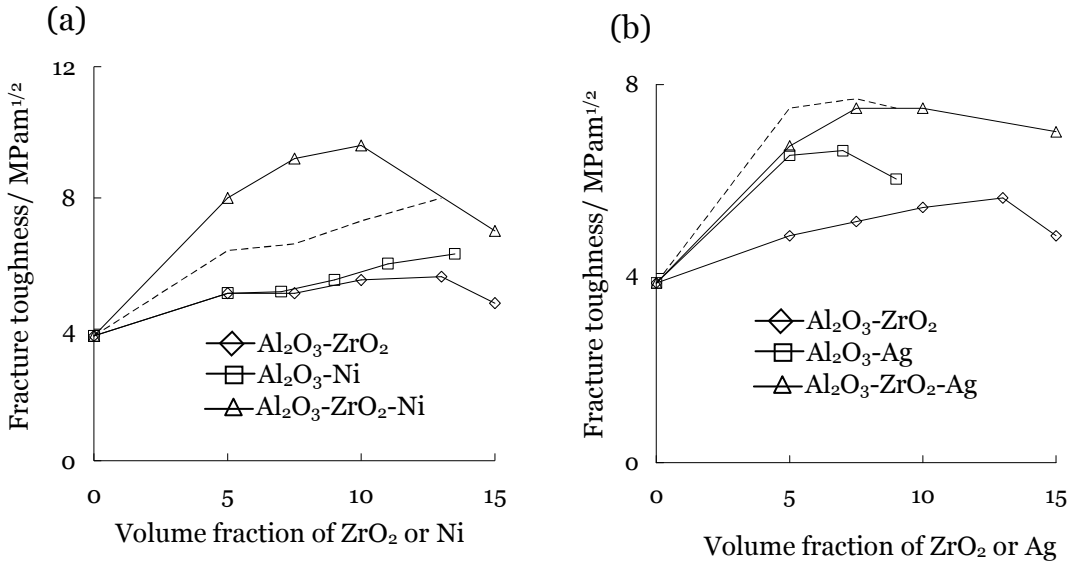

Figure 5-17: Effect of addition of Ag or Ni into the Al_2O_3 and Al_2O_3-ZrO_2 composites on toughening. (a) Adding Ni; (b) Adding Ag. Dashed line is the sum of the fracture toughness of Al_2O_3 and other toughening effects: $K_{Ic}^{sum} = K_{Ic}^{(Al_2O_3)} + \Delta K_{Ic}^{(Al_2O_3+Ni\,or\,Ag)} + \Delta K_{Ic}^{(Al_2O_3+ZrO_2)}$ [Chen and Tuan 2001; Chen et al. 2000].

In the following section, one of promising composites in aerospace and automobile industries, such as ZrO_2-enriched SiC/Al composites, are investigated in detail. Toughening effect and zone are investigated.

5.3.5 Case study - ZrO_2-enriched SiC/Al composites-

SiC/Al composites consists of high strength aluminum alloys reinforced with hard silicon carbide particles. Their low cost processing and blend of properties make them good candidates for many structural components demanding high stiffness, high strength, high resistance to wear and heat, and low weight. This translates into weight savings by producing lighter components capable of withstanding the required loads, which is of particular interest in the modern transportation industry (e.g., space frames and sheet panels). One of

the major concerns regarding the widespread applications of these composites is a relatively high brittleness in comparison with traditional materials [Ma et al. 2003; Agrawal and Sun 2004].

As described in Chapter 2, there are many mechanisms for toughening in ceramic and ceramic matrix composites such as micro-cracking, fibre-bridging, stress-induced transformation and others. Among these toughening mechanisms, the transformation toughening, which has recently received a large amount of attention in relation to toughening of brittle intermetallics, is now considered to be the best way of toughening SiC/Al composites. An application of the developed theory to ZrO_2-enriched SiC/Al composites will be considered.

In the beginning, the toughening zone of volume fractions of constituencies of ZrO_2-enriched SiC/Al composites, within which the toughening effect can be achieved, is considered. The thermal residual stresses in the transforming particles (ZrO_2) generated during the fabricating process can be large enough to trigger the phase transformation of these particles. The critical fractions of Al and SiC phases can be calculated from the equation (5.32) and shown in Fig.5-17. The material properties used for numerical calculations are shown in Table A2-1 in Appendix 2.

From Fig.5-18 it is seen that the microstructure of the composite has a large influence on the toughening zone, the zone where the toughening effect can be achieved by adding the transformable ZrO_2 particles, for example for SiC~matrix composites the toughening is not achievable at all when the volume fraction of SiC is above 52 percent. Much less constraints on volume fractions of SiC and Al take place for Al~matrix composites.

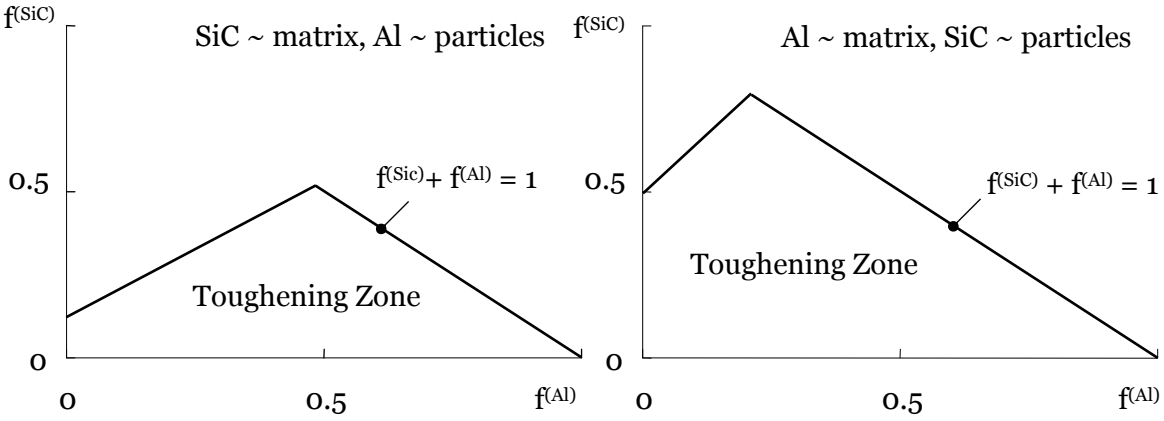

Figure 5-18: Volume fractions of composite constituents for which the toughening effect can be reached by adding ZrO_2 particles
(The difference between sintering and ambient temperatures ΔT=-600°C).

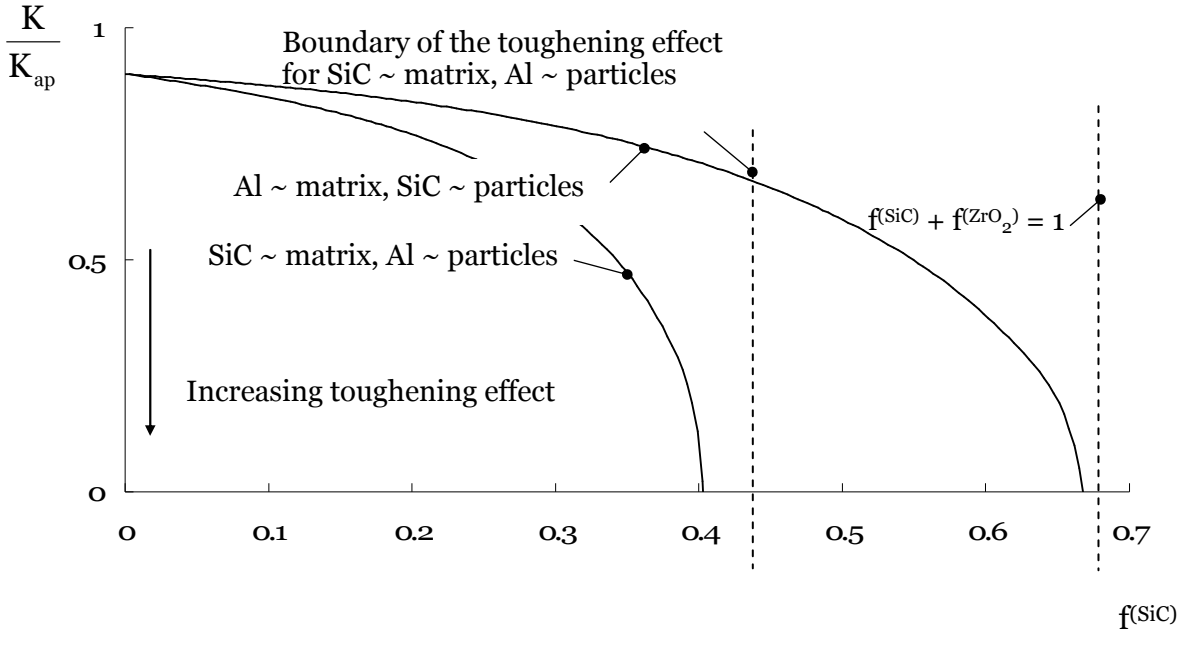

Figure 5-19: Toughening effect for a steady state crack by adding ZrO_2 particles to SiC/Al composites when the difference between the operating and sintering temperatures ΔT=-300°C. The volume fraction of ZrO_2 particles is set at 30%.

The toughening effect of adding 30 percent of ZrO_2 particles to SiC/Al composites is calculated by substituting the corresponding values of material properties into equations (5.2), (5.3), (5.8), (5.12) and (5.17) and shown in Fig.5-19. It can be observed that a rather small toughening effect is achieved at volume fractions of SiC less than 20 percent. Much higher toughening effect can be reached for SiC~matrix composites when the volume fraction of SiC is above 30 percent and for Al~matrix composites when it is above 60 percent. However, the increase of the volume fraction of SiC in the first case (SiC~matrix) increases the risk of the phase transformation during the manufacturing or can restrict significantly the level of the external loading which can be applied to a defect-free structure without triggering the phase transformation in zirconia particles. In the second case (Al~matrix), the significant toughening effect can be achieved when the volume fraction of SiC is above 60 percent. It means that the volume fraction of the matrix should be less than 10 percent, which makes it practically impossible to achieve such microstructure using known manufacturing techniques.

This simple analysis demonstrates that the SiC~matrix and Al~ZrO_2 particle composites are most suitable for enhancing the fracture toughness using the transformation toughening mechanism of zirconia. However, to properly engineer such composites it is necessary to consider the expected operating conditions including the thermal conditions to prevent the phase transformation during normal operation in a defect-free structure.

5.4 Summary

The mean-field micromechanical approach was described for predicting the effective thermo-mechanical properties of multi-phase composites. The approach considered here, which was formulated by Wakashima and Tsukamoto [1991], is based on the Eshelby's equivalent inclusion methods and Mori-Tanaka's mean-field concept. Wakashima-Tsukamoto estimate was verified through comparison with Hashin and Shtrikman bounds and some experimental data.

A micromechanical formulation was carried out to investigate the toughening mechanism by the transformation of partially stabilized ZrO_2 particles in multi-phase composites. The theoretical results obtained based on the developed model demonstrate a very strong influence of the material properties of the constituent phases, thermal stresses as well as microstructure on the transformation toughening effect. For two-phase composites, when Young's modulus of matrix is higher and thermal expansion coefficient of matrix is lower than those of ZrO_2, the thermal stresses generated during the fabrication process cause a large increase of toughening. For three-phase composites, both matrix and additional particles with higher Young's modulus and lower Poisson's ratios, which is considered to be ceramics rather than metals and alloys in practical, leads to increase of the transformation toughening effect under no thermal stress conditions. The effect of thermal stresses on toughening in three-phase composites is also large in the same way as two-phase composites. A large attention has to be paid to the toughening zone in design of such composites not to lose the whole toughening effect. The numerical results for ZrO_2/Al_2O_3 composites with Ni or Ag particles obtained based on the developed model considering thermal residual stresses gave the better understanding of the existing experimental data.

As a case study, the transformation toughening in ZrO_2-enriched SiC/Al, which has a significant potential for application to aerospace and automotive structures, was investigated based on the developed model. From the examination of the toughening zone, much less constraints on volume fractions of SiC and Al take place for Al~matrix composites. A high level of the fracture toughening can be reached by adding ZrO_2 particles to such composites when the microstructure is SiC~matrix and Al~ZrO_2 particles.

Chapter 6

Design against fracture of FG TBCs

6.1 Introduction

FG TBCs are macroscopically and microscopically heterogeneous. Macroscopic heterogeneity means the gradation of material properties through the thicknesses of TBC, and microscopic heterogeneity is due to the fact that the composite materials are composed of several constituents, for TBCs they are usually metal and ceramics. To properly develop mathematical models of such macro- and micro- heterogeneous systems a formulation of the constitutive equations from the standpoints of these two different scales is required.

Many methods for design and analysis of FG TBCs have been investigated as described in Chapter 2. However, there have not been so many studies which consider the existence of cracks in FG TBCs and propose design methods based on the consideration of fracture mechanics. Ceramic coatings are usually very brittle and this consideration is necessary to investigate and adequately address during design and fabrication.

In this chapter, the developed micromechanical theory for the study of the transformation toughening is incorporated with the classical lamination theory (CLT). The methodology of design against fracture of FG TBCs is described. A new parameter, which is the crack tip stress intensity factor K divided by $\sqrt{\pi a}$, is introduced for assessing the fracture behaviour and toughening effect in the FG TBCs. The design against fracture in the FG TBCs under an unsteady-state heat flow (thermal shock) and various mechanical boundary conditions is carried out by minimizing the values of this new fracture parameter at the ceramic surface and ceramic-rich FG layers. As a case study, Ni-ZrO_2 FG TBCs, which attract a great deal of attention as superior TBCs in automobile and aerospace industries, are investigated The simulation results are examined through comparison with the existing theoretical and experimental studies.

6.2 Modelling of FG TBCs

6.2.1 Unsteady heat-flow analysis

The theoretical approach to be used here is based on the earlier work by the author [Tsukamoto 2003]. The illustration of a model of a FG TBC is shown in Fig.6-1.

The unidirectional heat flow is assumed to be made in the thickness direction (z-direction). The temperature distribution $\theta(z,t)$ can be determined by solving the following equation:

$$c(z)\rho(z)\frac{\partial\theta(z,t)}{\partial t}=\frac{\partial}{\partial z}\lambda(z)\frac{\partial\theta(z,t)}{\partial z} \tag{6.1}$$

where, $c(z)$ is the specific heat, $\rho(z)$ the mass density and $\lambda(z)$ the thermal conductivity of two phase composite materials, which can be derived based on micromechanical consideration (see Appendix 4).

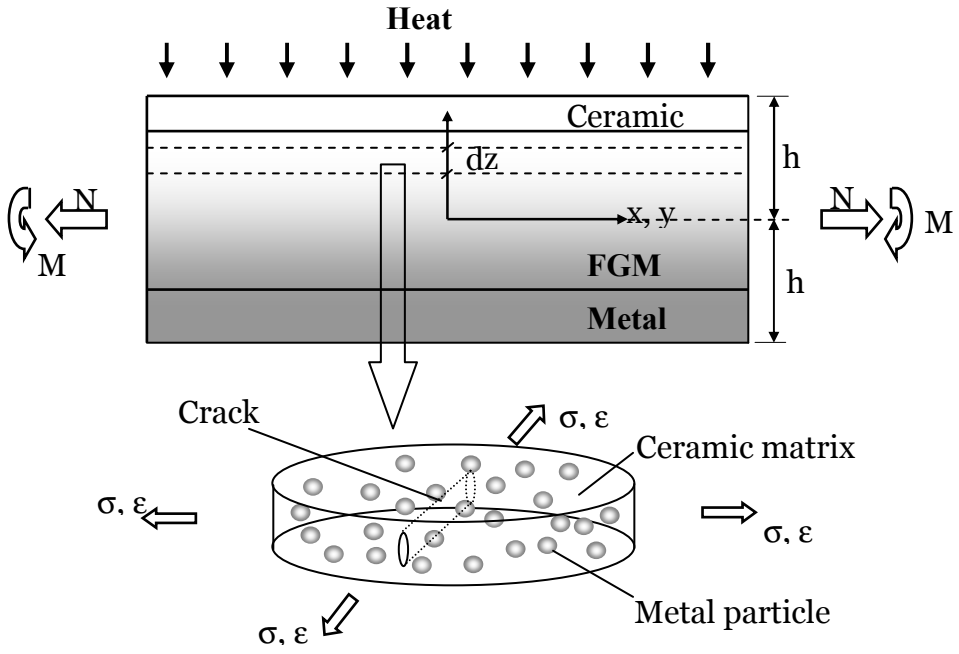

Figure 6-1: Schematic illustration of a functionally graded thermal barrier coating subjected to thermo-mechanical loadings and its building block composed of spherical particle-dispersed composites containing a small crack.

6.2.2 Classical Lamination Theory (CLT)

The classical lamination theory (CLT) with a piece-wise constant approximation is used here [Wakashima and Tsukamoto 1990; Wakashima, Tsukamoto and Ishizuka 1992; Erdogan and Wu 1996]. Macroscopically homogeneous composites with spherical particles are considered for a building block of the FG plate as illustrated in Fig.6-1. Each building block (layer) is subjected to a balanced bi-axial plane stresses due to the symmetry of the problem.

Let σ be an in-plane stress in a layer, which is caused by the bi-axial loading. Under plane-stress conditions the constitutive equations can be written as

$$\dot{\sigma}(z,t) = \left\{S^{e}(z)\right\}^{-1}\left\{\dot{\varepsilon}(z,t) - \alpha(z)\dot{\theta}(z,t)\right\} \tag{6.2}$$

$\dot{\sigma}(z,t)$ is the in-plane stress rate, $S^{e}(z)$ the overall plane-stress elastic compliance, $\alpha(z)$ the overall in-plane thermal expansion coefficient the micromechanical descriptions for these properties are given in Appendix 4.

Consider a FG plate consisting of thin layers with thickness dz located at position z in the coordinates as shown in Fig.6-1. The in-plane stress rate is satisfied with the following relation:

$$\dot{\sigma}(z,t) \equiv \dot{\sigma}_{x}(z,t) = \dot{\sigma}_{y}(z,t) \ . \tag{6.3}$$

All the other macro-stress rate components are zero. The corresponding in-plane strain rate is expressed as

$$\dot{\varepsilon}(z,t) \equiv \dot{\varepsilon}_{x}(z,t) = \dot{\varepsilon}_{y}(z,t) \tag{6.4}$$

The out-of-plane strain rate component is not zero. The in-plane strain rate component $\dot{\varepsilon}(z,t)$ can be related to the mid-plane strain rate $\dot{\varepsilon}^{0}(t)$ and the curvature rate $\dot{\kappa}(t)$ according to the strain compatibility condition as,

$$\dot{\varepsilon}(z,t) = \dot{\varepsilon}^0(t) + z\dot{\kappa}(t) \tag{6.5}$$

The in-plane force rate $\dot{N}$ and bending moment rate $\dot{M}$ (per unit edge length of the FGM plate) are expressed through the macro-stress rate $\dot{\sigma}(z,t)$ as follows

$$\dot{N}(t) = \int_{-h}^{h} \dot{\sigma}(z,t)dz \tag{6.6}$$

$$\dot{M}(t) = \int_{-h}^{h} \dot{\sigma}(z,t)zdz \tag{6.7}$$

Here, the thickness of FGM plate is set at 2h. Using equations (6.2) - (6.7), the following expression for macroscopic constitutive relation of the FGM can be derived:

$$\begin{bmatrix} \dot{\varepsilon}^0(t) \\ \dot{\kappa}(t) \end{bmatrix} = \begin{bmatrix} A_{11} & A_{12} \\ A_{21} & A_{22} \end{bmatrix}^{-1} \left\{ \begin{bmatrix} \dot{N}(t) \\ \dot{M}(t) \end{bmatrix} + \begin{bmatrix} \dot{B}_1(t) \\ \dot{B}_2(t) \end{bmatrix} \right\} \tag{6.8}$$

with

$$\begin{bmatrix} A_{11} & A_{12} \\ A_{21} & A_{22} \end{bmatrix} = \int_{-h}^{h} \begin{bmatrix} 1 & z \\ z & z^2 \end{bmatrix} \left\{ S^e(z) \right\}^{-1} dz \tag{6.9}$$

$$\begin{bmatrix} \dot{B}_1(t) \\ \dot{B}_2(t) \end{bmatrix} = \int_{-h}^{h} \begin{bmatrix} 1 \\ z \end{bmatrix} \left\{ S^e(z) \right\}^{-1} \left\{ \alpha(z)\dot{\theta}(z,t) \right\} dz \tag{6.10}$$

where A_{11}, A_{12} and A_{22} are known functions of the elastic and plastic constants. A_{11} is the in-plane stiffness, A_{22} is the bending stiffness and $A_{12} = A_{21}$ is the coupling stiffness. $\dot{B}_1(t)$ and $\dot{B}_2(t)$ are the in-plane force rate and bending-moment rate, respectively, due to the difference of coefficient of thermal expansion of each layer.

The formulated theory on transformation toughening of multi-phase composites is directly incorporated into the CLT based on the assumption that cracks are small compared to thickness of each layer so that the effect of the

existence of interfaces between layers on the stress states of crack tips can be neglected.

6.2.3 Compositional gradation patterns

We model a FG TBC with a step-wised gradation of the volume fraction as shown in Fig.6-2.

For a parametric description of the compositional gradation in a FG layer, we introduce the following expression [Wakashima, Ishizuka and Tsukamoto 1992]:

$$f_m(i) = 1 - f_c(i) = (i-1)^n / (P-1)^n \tag{6.11}$$

where, $f_m(i)$ and $f_c(i)$ are the volume fractions of metal and ceramic phases in the i-th sub-layer, respectively. The sub-layers, which have the same thickness, compose a FG layer. P is the total number of sub-layers in a FG layer. The exponent n is the parameter characterizing the compositional gradation. In the following calculation, P is set at 10. For the gradation parameter n, n= 1 means the linear compositional gradation, n > 1 means the ceramic-rich gradation and n < 1 means the metal-rich gradation.

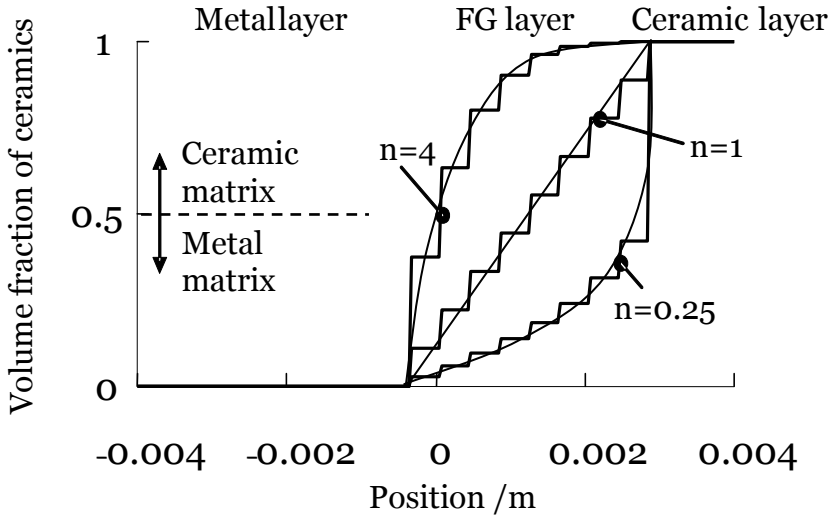

Figure 6-2: Compositional gradation patterns in FG TBCs.

6.2.4 Overall heat-transfer coefficient and average density

We examine the effect of gradation pattern parameter n on the overall heat-transfer coefficient and average density of the FG TBCs with a certain thickness. Both parameters are important in design of FG TBCs from the viewpoints of the thermal efficiency of TBCs. The overall heat-transfer coefficient is expressed as follows,

$$k_{FGM} = \frac{1}{2h}\left(\frac{1}{P}\sum_{i=1}^{P}\frac{1}{\lambda_i}\right)^{-1}. \tag{6.12}$$

Here, the overall heat-transfer coefficient, k_{FGM}, can be related to the heat flux, q, and the difference of the temperatures between the ceramic and metal sides, Tc and Tm such that

$$q = k_{FGM}(T_c - T_m). \tag{6.13}$$

The average density of FG TBCs is given as,

$$\rho_{FGM} = \frac{1}{P}\sum_{i=1}^{P}\left[f_m(i)\cdot\rho_m + f_c(i)\cdot\rho_c\right]. \tag{6.14}$$

6.2.5 A new parameter for assessing fracture and toughening properties

A new parameter is introduced to assess the fracture properties of FG TBCs. Fig. 6-3 shows the schematic illustration of FG TBCs with small cracks surrounded by phase transformation zone. As mentioned in 6.2.2, it is assumed that there is no effect of interfaces between layers on the stress states near crack tips, which means that existing cracks are extremely small compared to the thickness of a layer. Applied stress intensity factor in each layer is expressed as follows (see Chapter 3 for the definition of the stress intensity factor),

$$K_{ap} = \sigma\sqrt{\pi a}\ . \tag{6.15}$$

In the case of composites toughened by transformable particles, the stress intensity factor K at the crack tip is given by

$$K = \lambda K_{ap} \tag{6.16}$$

where λ is the parameter of toughening effect as already mentioned. From equations (6.15) and (6.16), we can obtain the following relation:

$$K/\sqrt{\pi a} = \lambda\sigma\ (=\ \beta). \tag{6.17}$$

From equation (6.17), we introduce a new parameter, β, which is called the "effective stress intensity factor," for investigating the fracture properties of FG TBCs.

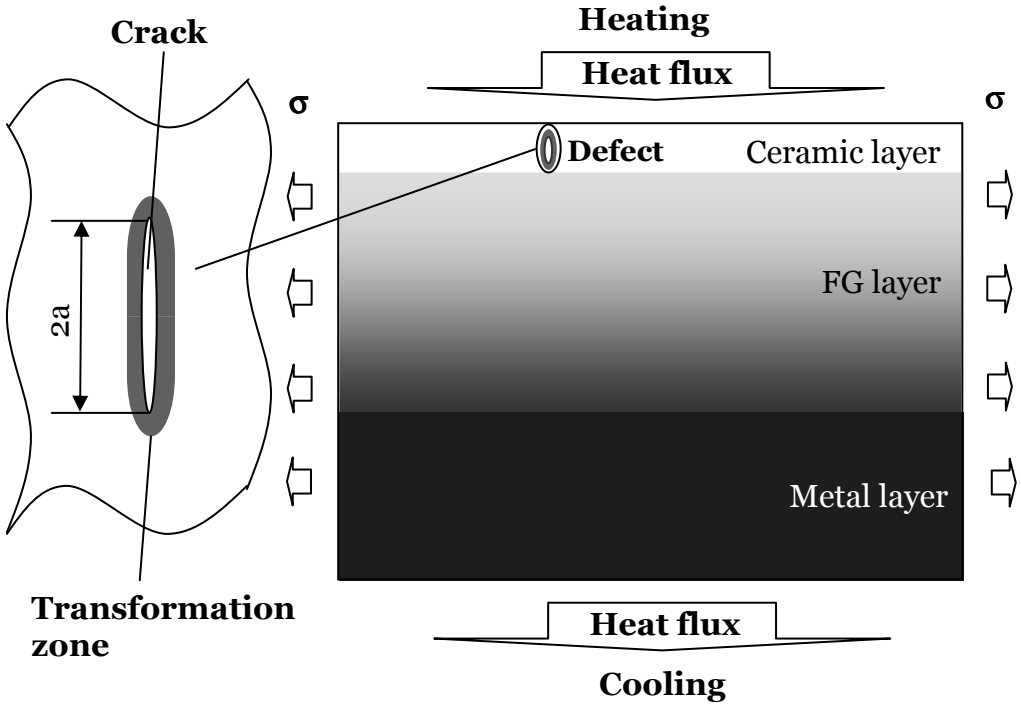

Figure 6-3: Schematic illustration of a FG TBC with a crack surrounded by the transformation zone.

6.2.6 Methodology of design against fracture of FG TBCs

The Methodology of design against fracture of FG TBCs used in the project follows the procedure shown in Fig. 6-4. The fracture properties are investigated under given thermo-mechanical boundary conditions for various compositional gradations using a new fracture parameter, β . By selecting the compositional gradation parameter, n, FG TBCs with improved fracture properties toughened by transformation of ZrO_2 can be designed based on the fracture-mechanics consideration. For reference, the thermal shielding properties such as overall heat-tranfer coefficients and average densities are calculated for various compositional gradation patterns.

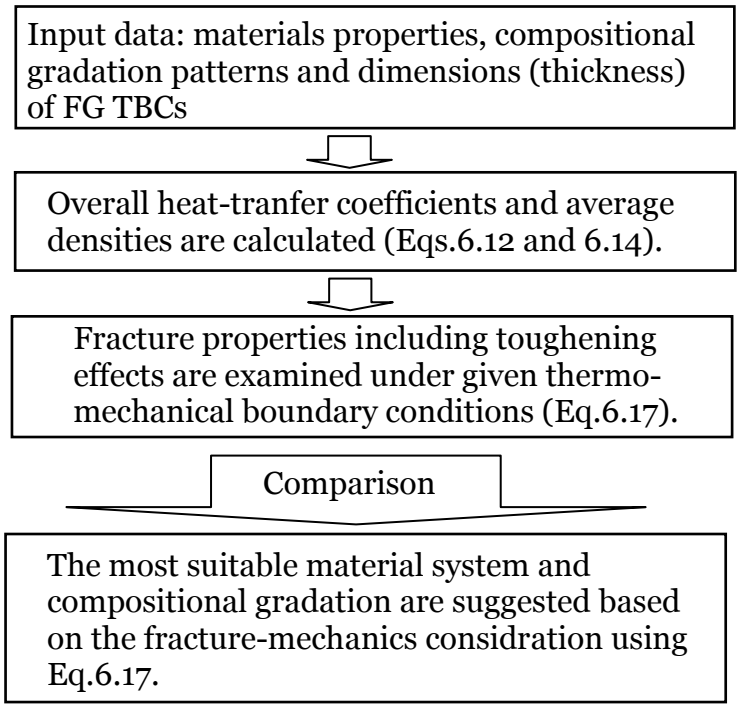

Figure 6-4: Flow chart for design against fracture of FG TBCs. The effective stress intensity factor, β, is introduced. For variable parameters, material properties and compositional gradations are considered.

6.3 Case study –Ni-ZrO_2 FG TBCs-

6.3.1 Input data and thermo-mechanical boundary conditions

We consider a Ni-ZrO_2 FG TBC system, which currently attracts a great deal of attention as an effective thermal shielding in aerospace and automobile applications [Polanco et al.2006; Li et al. 2003; Polat et al. 2002]. The material properties of both Ni and ZrO_2 phases used for the calculations are given in Table A2-1 in Appendix 2. It is assumed that partially stabilized ZrO_2, which can undergo stress-induced transformation with the critical mean stress of 700 MPa, accounts for 50% out of whole ZrO_2 contents. The composites making up the FG TBCs are considered to be three-phase composites consisting of Ni, "transformable" and "non-transformable" ZrO_2. No difference is considered in material properties expect for the ability of the transformation between these two kinds of ZrO_2. The dimensions of the FG TBCs are given as follows: the thickness of a ceramic (ZrO_2) coating layer is 0.8mm, the thickness of a FG layer is 4 mm, and the thickness of a metal (Ni) substrate layer is 3.2mm.

The thermal shock temperature profile is used here as a thermal boundary condition shown as follows: The initial temperature distribution is uniform over the whole TBC with 300K and the initial stresses in the TBC are assumed to be zero. Then, the temperature of the ceramic surface suddenly rises to 1600K, which is subsequently held for 20 sec., while the temperature of metal surface is kept at 300K. Then, the temperature of ceramic surface is suddenly cooled down to 300K, which is held for 20sec. Fig. 6-5 shows the temperature transient at the ceramic surface of the FG TBCs. Such a thermal loading resistance are investigated by many researchers [Jin 2004; Jin and Luo 2006; Wang et al. 2004].

For the mechanical boundary conditions, we consider three cases: for Case 1, any deformation in the TBC is unconstrained i.e. $\dot{N}(t) = \dot{M}(t) = 0$; for Case 2, the TBC is constrained in the out-of-plane deformation, i.e. $\dot{\varepsilon}^0(t) \neq 0$ and $\dot{\kappa}(t) = 0$; for Case 3, the TBC is fully constrained in both the in-plane and out-of-plane deformations i.e. $\dot{\varepsilon}^0(t) = 0$ and $\dot{\kappa}(t) = 0$. Cases 1 and 2 correspond to a high temperature-resistant panel structure, which is relatively thin and

Case 3 corresponds to a thermal barrier structure laid on a rigid and thick substrate.

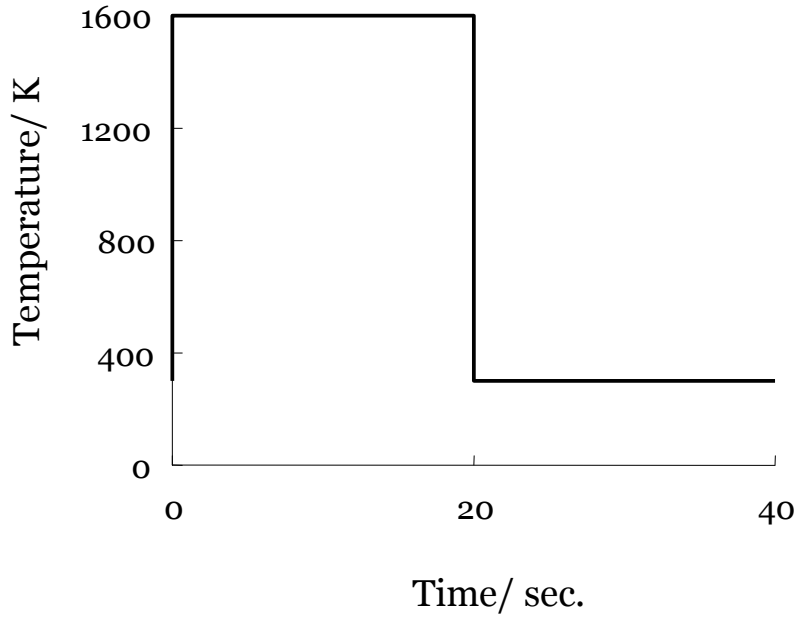

Figure 6-5: Temperature transient on the ceramic surfaces of FG TBCs.

6.3.2. Effect of compositional gradation patterns on overall heat-transfer coefficient and average density

Fig.6-6 shows the overall heat-transfer coefficients and average densities of FG layers with the thickness of 4 mm as a function of the compositional gradation parameter n. It can be seen that with increase of n, which corresponds to increase of the volume fraction of ceramics, both characteristics such as the overall heat-transfer coefficients and average densities decrease. It can be said that the lager value of n (or higher volume fraction of ceramics in FG layers) leads to better thermal-shielding and light- weight properties of TBCs. Here, for n over 4, it is seen that both characteristics are almost constant.

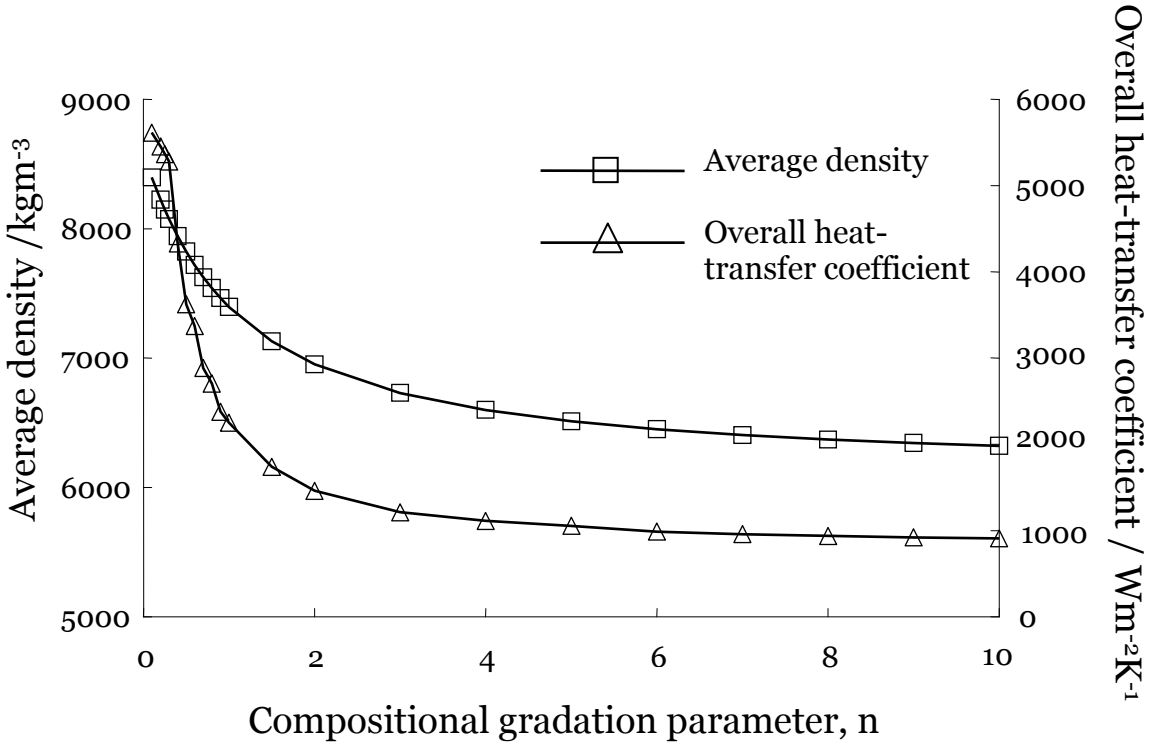

Figure 6-6: Overall heat-transfer coefficient and average density for FG layers as a function of gradation parameter, n.

6.3.3. Design against fracture of FG TBCs

Fig.6-7 shows the toughening effect, λ, in Ni-ZrO_2 FG TBCs with three different compositional gradation patterns (n=0.25, 1 and 4) subjected to no temperature change. The toughening effect, λ, in Ni-ZrO_2 systems is not so much affected by the temperature change because their thermal expansion coefficients are similar to each other (see the discussion in 6.3.4). The value of λ increases as the content of the ceramic of ZrO_2 increases.

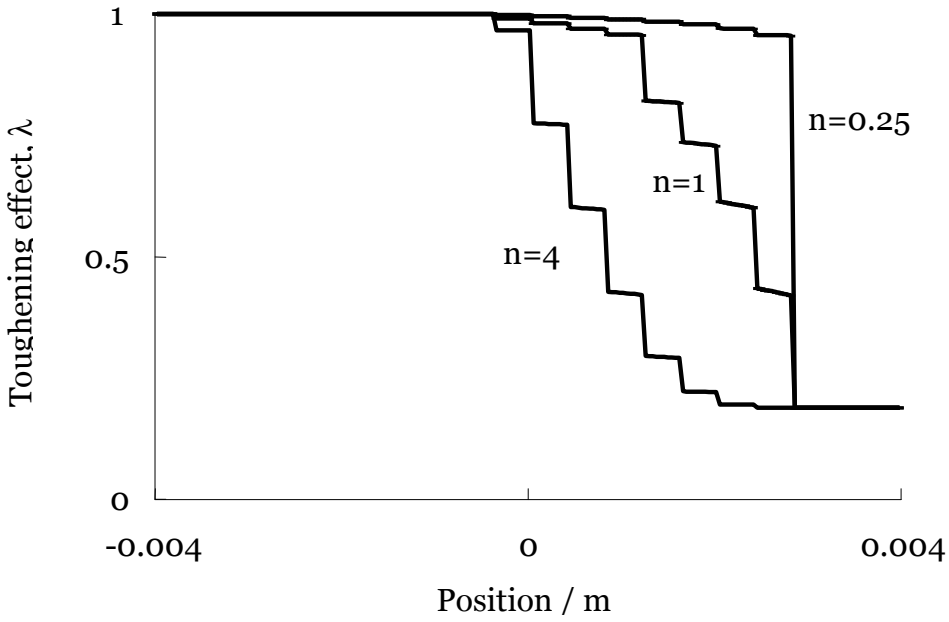

Figure 6-7: Toughening effect, λ, in a FG TBC with n=0.25, 1 and 4 under no temperature change conditions, which is plotted against the position.

Fig. 6-8 shows a simulation result indicating the distribution of the new parameter, that is the effective intensity factor, $\beta = K/\sqrt{\pi a}$, at 20 and 20.1 sec. for FG TBCs with n=1 under the mechanical boundary condition of Case1. It is seen that there are two points where the values of the effective intensity factor, β, reach maximum. The first one is in the ceramic surface layer. Under the thermal shock loading, when cooling starts after 20 sec., the ceramic surface layer is

shrunken, which causes a large in-plane tensile stress in the ceramic surface layer. It was also reported by Han et al. [2007], Kokini et al. [2002] and Kawasaki and Watanabe [1997] that some cracks were introduced on the ceramic surface coating in FG TBCs just after cooling starts on the ceramic surface under thermal shock conditions. It is reasonable to consider that such tensile stresses lead to the initiation and propagation of these cracks in the ceramic surface layer. The second maximum is in the FG layer. The purpose of gradation of composition in FG structures is basically to reduce thermal stresses and improve fracture properties at the interface between ceramic coating and metal substrate. It is expected that some level of tensile stresses can also be generated in the FG layer over the whole stages of heating, isothermal and cooling.

In the following, we pay an attention to these two peak values of the effective intensity factor, β, and select such a gradation which minimizes the values of the maximum β. Although the simulations are made for FG TBCs under typical mechanical boundary conditions of Case1 (No mechanical constraint), Case2 (In-plane deformation constraint) and Case3 (In- and Out-of-plane deformation constraint), the results for Case 3 is omitted because in Case3 the stress states over the FG TBCs are always negative, which means that the values of the effective stress intensity factor, β, are always negative, so it is considered that no crack generation and propagation in the FG TBCs occur in Case3. However, the present analysis does not take into account the important effect by inelastic deformations which can affect the integrity of TBC. In practical situation the inelastic deformations such as plastic and creep deformations possibly occur, which may produce different stress states in FG TBCs leading to the critical conditions of failure of FG TBCs even if in Case3. The details of the effect of the inelastic deformations on thermal stress states in FG TBCs were investigated by Tsukamoto [2003]. Now we focus on the thermo-elastic deformations, and the simulations were conducted for two cases of mechanical boundary conditions such as Case1 and Case 2.

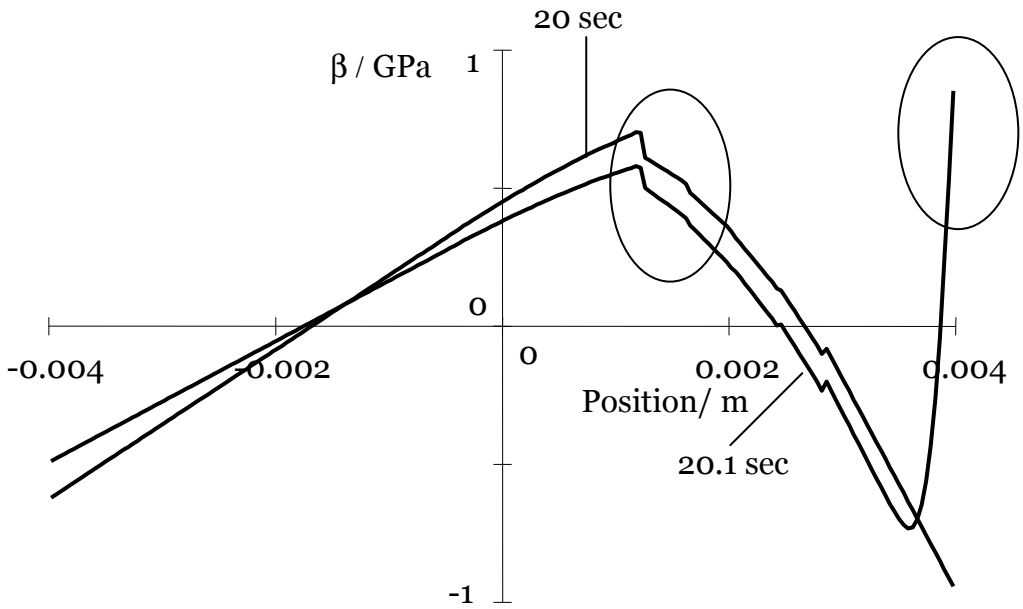

Figure 6-8: Distribution of β for a steady-state crack in a FG TBC with n=1 at 20 sec. and 20.1 sec. under the mechanical boundary condition of Case 1. (20.1 sec. is just after start of cooling of a ceramic surface.) The high value of β can be seen in a FG layer at 20 and 20.1 sec. and in a ceramic surface layer at 20.1 sec.

Fig. 6-9 shows the transients of the maximum effective stress intensity factor, β, in ceramic surface layers for steady-state and growing cracks from the start of sudden cooling under the mechanical boundary condition of Case 1. The values of maximum β in ceramic surface layers gradually decrease from the start of cooling. For both steady-state and growing crack propagations, the value of β for the gradation pattern of n=0.25 is the lowest among these three different compositional gradation patterns all the time. The values of maximum β in the ceramic surface layers for steady-state cracks are always higher than those for growing cracks for any gradation patterns, which is expected from Fig. 4-10 because the value of strength of transformation, ω, in equation (5.31) is large in ceramic layers.

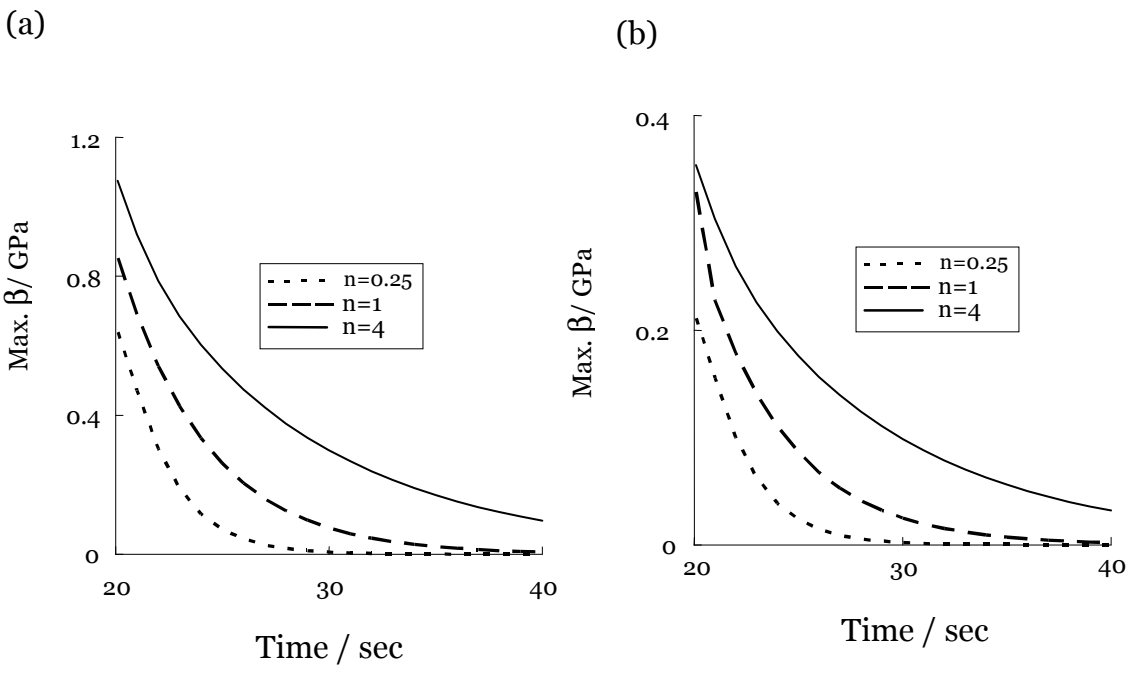

Figure 6-9: Transient of β in a ceramic surface layer from the start of sudden cooling-down under the mechanical boundary condition of Case1: (a) for a steady-state crack and (b) for a growing crack.

Fig. 6-10 shows the transients of the maximum effective stress intensity factor, β, in FG layers for steady-state and growing cracks under the mechanical condition of Case1. The volume fraction of ZrO_2 at the position that the values of maximum β is generated, is also shown for steady-state and growing cracks. This volume fraction is limited to more than 0.5 (for ceramic matrix) because the brittle fracture is considered to be more dominant in the ceramic-matrix composites rather than metal-matrix composites [Zhu et al. 1996]. In the FG TBCs with n=0.25, the highest value of maximum β are generated at the beginning of heating, and in the FG TBCs with other two compositional gradations, the highest values of maximum β are generated at the end of isothermal stage at the upper temperature of 1600K. Consequently, the value of maximum β in FG layers for n=0.25 is the lowest among these three compositional gradation patterns. There is almost no difference in maximum β between steady-state cracks and growing cracks, which is expected from Fig. 4-10 because the value of strength of transformation, ω, in equation (5.31) is not so large in FG layers.

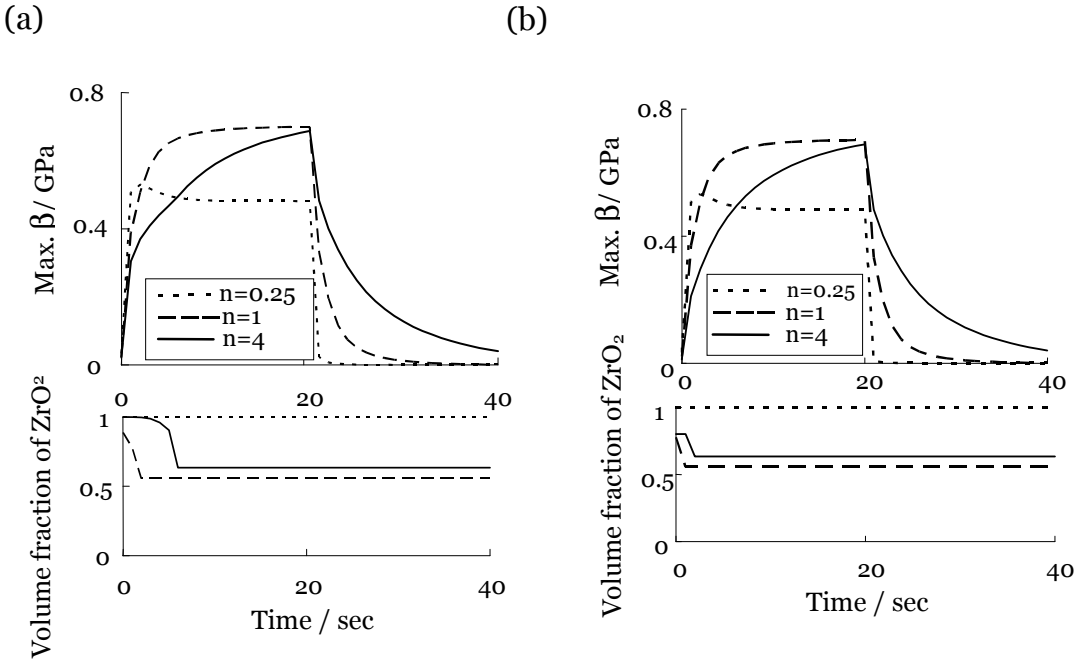

Figure 6-10: Transient of maximum β in a FG layer and the volume fractions of ZrO_2 that maximum β generates (more than 0.5): (a) for a steady-state crack and (b) for a growing crack.

Fig.6-11 shows the transients of the maximum effective stress intensity factor, β, in ceramic surface layers for steady-state and growing cracks from the start of sudden cooling under the mechanical boundary condition of Case 2. The tendency is the same as that of Case 1. The values of maximum β gradually decrease from the start of cooling. For both steady-state and growing crack propagations, the value of maximum β for n=0.25 is also lowest among three different compositional gradation patterns. The maximum values of β for steady-state cracks are higher than those for growing cracks. The absolute values of β for Case2 are smaller than those for Case1 shown in Fig. 6-9.

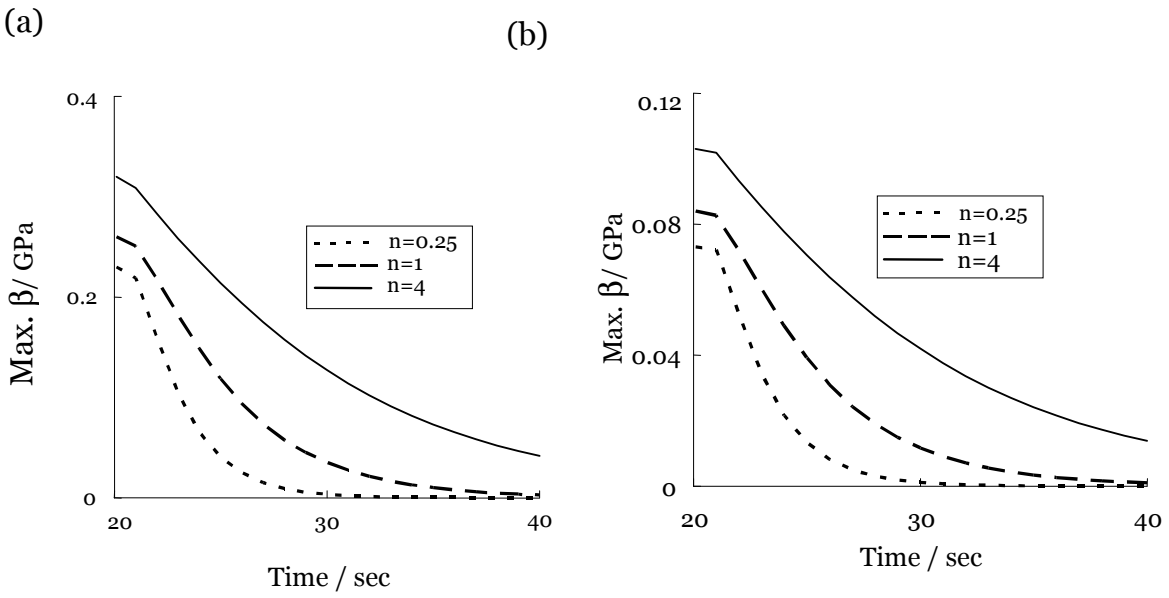

Figure 6-11: Transient of maximum β in a ceramic surface layer of FG TBCs under the mechanical condition of Case2: (a) for a steady-state crack and (b) for a growing crack.

Fig. 6-12 shows the transients of the maximum effective stress intensity factor, β, in the FG layers for steady-state and growing cracks under the mechanical condition of Case 2. The volume fractions of ZrO_2 at the position

that the maximum values of β are generated are also shown for steady-state and growing cracks, which are limited to more than 0.5. The tendency is also similar to that of Case 1 except for n=0.25 (the metal-rich gradation). The value of maximum β in the FG TBCs with n=0.25 is considerably lower. In the FG TBCs with n=0.25, the value of maximum β are high just after start of heating, and in the FG TBCs with other two compositional gradations, the values of maximum β are high at the end of isothermal stage at the upper temperature of 1600K. It is obviously seen that the value of maximum β for n=0.25 is the lowest among these three compositional gradation patterns. There is also almost no difference in the values of maximum β between steady-state and growing cracks.

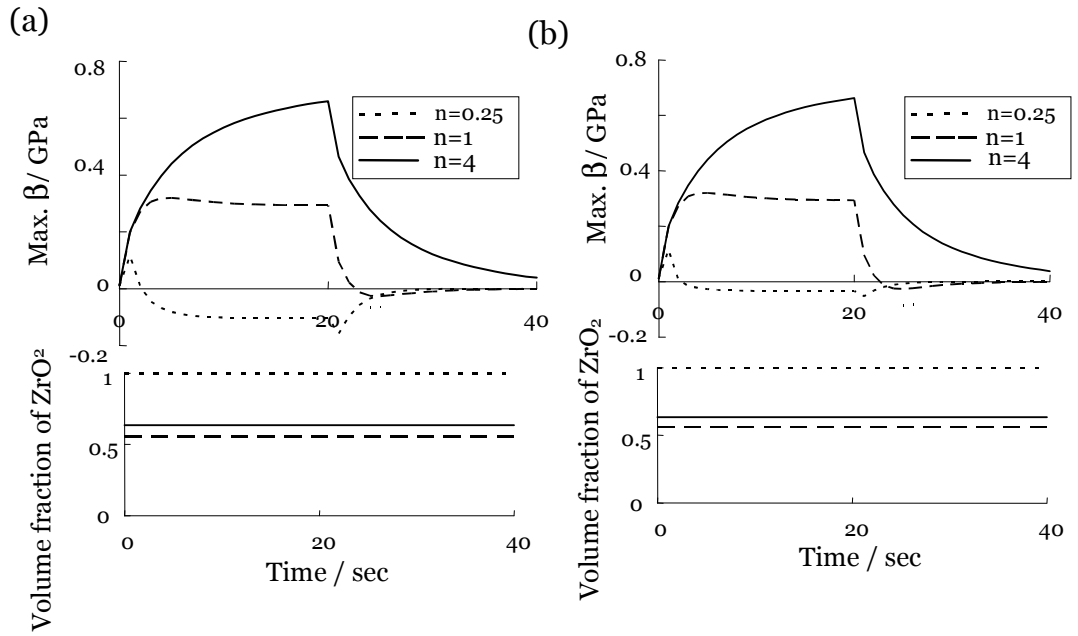

Figure 6-12: Transient of maximum β and volume fraction of ZrO_2 that the maximum β is generated (more than 0.5) in a FG layer under the mechanical condition of Case2: (a) for steady-state crack and (b) for growing crack.

Fig.6-13 shows the maximum effective stress intensity factor, β, in ceramic surface layers for steady-state and growing cracks under the mechanical boundary conditions of Case 1 and Case2 as a function of the compositional gradation parameter n. It is seen that under both mechanical boundary conditions, with decreasing values of n, the values of maximum β decrease. Therefore, in order to prevent the fracture of ceramic surface of FG TBCs, which is expected to occur just after the start of cooling under thermal shock loading conditions, the metal-rich gradations, which correspond to smaller values of n, are better than ceramic-rich gradations. In Case3, the values of maximum β in the ceramic surface layer are always negative.

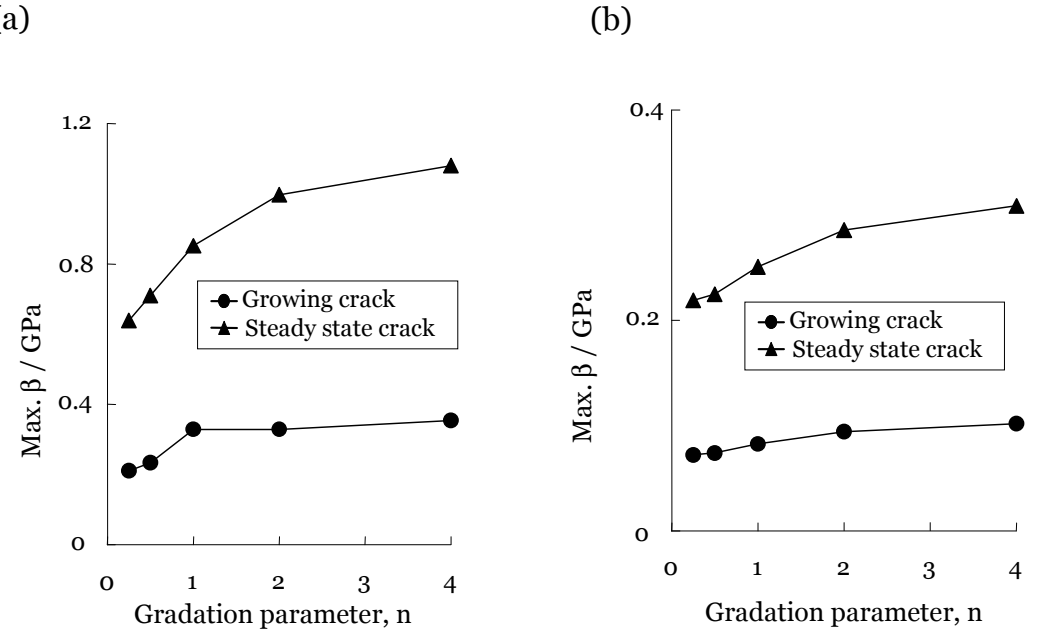

Figure 6-13: Maximum β for steady state and growing cracks in ceramic surface layers plotted against the compositional gradation parameter n: (a) Case 1; (b) Case2. In Case3, the values of β in ceramic surface layers are always negative.

The maximum effective stress intensity factor, β, in FG layers for steady-state and growing cracks is plotted against the compositional gradation parameter n for the mechanical boundary conditions of Case 1 and Case2 in Fig. 6-14. It can be seen that with decreasing the value of n, the fracture properties become better for both mechanical boundary conditions. In particular, the smallest value of maximum β takes place for n=0.25 among the investigated gradation patterns. In order to prevent the fracture in the FG layers, which is expected to occur during the isothermal stage at the upper temperature of 1600K, the metal-rich gradations, which correspond to smaller values of n, are more suitable than the ceramic-rich gradations. As mentioned, the values of maximum βin FG layers are always negative in Case3.

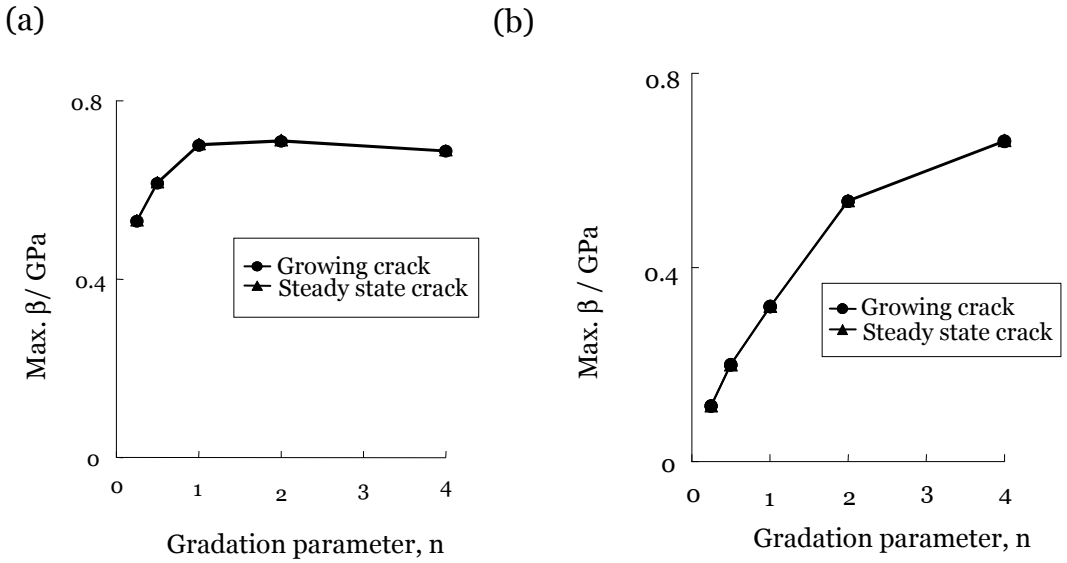

Figure 6-14: Maximum β for steady-state and growing cracks in FG layers plotted against the compositional gradation parameter n: (a) Case 1; (b) Case2. In Case3, the values of β in FG layers are always negative.

From the obtained results, it is followed that the metal-rich gradation is better than ceramic-rich gradation. Meanwhile, from the viewpoint of thermal shielding effects and light-weight, ceramic-rich gradation is better as seen in Fig. 6-6. In practice design process, it is better to consider not only fracture properties but also such thermal shielding and light-weight properties.

There are various thermo-mechanical boundary conditions in practice. Recommended compositional gradation patterns strongly depend on these boundary conditions. The results shown here were obtained for the FG TBCs under a typical boundary condition. It is necessary to perform such calculation for design against fracture of FG TBCs to the practical boundary conditions.

Now, let us consider the practical design procedure for FG TBCs toughened by transformation of ZrO_2. According to the experimental data obtained by Zhu et al. [1996; 1997], the fracture toughness (K_{Ic}) of ZrO_2-Ni composites with the volume fraction of ZrO_2 of more than 0.6 is around $4\text{MPa}\sqrt{\text{m}}$ (see Fig. 6-15). If we assume that the initial length of existing cracks which can lead to the failure of the FG TBCs, is 0.1 mm, the critical value of $\beta_C = K_{Ic} / \sqrt{\pi a}$ is about 0.226 GPa.

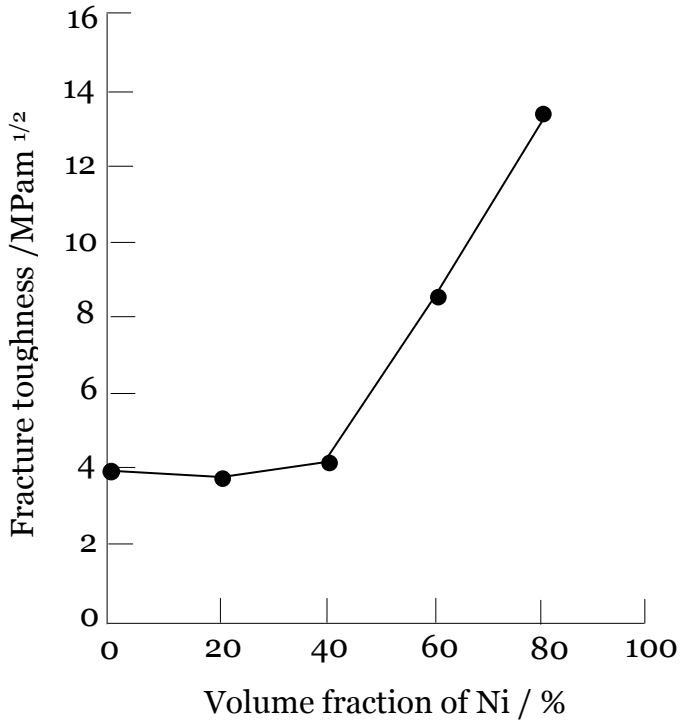

Figure 6-15: Fracture toughness plotted against volume fraction of Ni in ZrO_2-Ni FG TBCs [Zhu et al. 1996; 1997].

First, the maximum effective stress intensity factor, β, in ceramic surface layers are examined. As seen in Fig. 6.13 (a), for Case1, the value of maximum β in ceramic surface layers is more than 0.226 GPa for any given gradation patterns, so it is better to chose more metal-rich gradation patterns to reduce the value of maximum β as much as possible. For Case 2 shown in Fig. 6.13 (b), the value of maximum β in ceramic surface layers for growing cracks is less than 0.226 GPa for any given gradation patterns. At the beginning of the rapid cooling during the thermal shock loading, the maximum β for the growing crack should be more used in assessment of fracture of such FG TBCs compared to that for the steady-state crack. From this consideration, we possibly choose ceramic-rich gradation patterns to achieve better thermal-shielding and light-weight properties.

Second, the maximum effective stress intensity factor, β, in the FG layers are examined. From Fig. 6-14 (a), for Case 1, the value of maximum β is more than 0.226 GPa for any gradation patterns, so it is better to chose more metal-rich gradation pattern for arresting the crack growth in the FG layers as much as possible. For Case 2 shown in Fig. 6-14 (b), in the case of only n=0.25, the value of maximum β is less than 0.226 GPa, so it is also better to chose more metal-rich gradation patterns such as n=0.25 for preventing the fracture in the FG layers.

The design of FG TBCs toughened by transformation of ZrO_2 can be performed this way. According to which objective functions are weighed in design of FG TBCs, the suitable design procedure will be selected and conducted to practical situations.

The significant features of the developed methodology of design against fracture of FG TBCs are summarised as follows:

(1) Because the theory was formulated based on the micromechanical approach, it can be properly taken into account the influence of the inhomogeneity of the materials such as mismatch in thermo-mechanical properties of constituents, contents of constituent phases and microstructures on fracture and toughening properties of FG TBCs.

(2) The developed micromechanical theory for the transformation toughening can investigate the influence of mismatch in thermo-mechanical properties of constituent phases on the toughening effect in multi-phase composites. According to careful review of literature on theoretical study on the transformation toughening, there are few studies investigating this problem.
(3) The developed theory for the transformation toughening was effectively incorporated with the CLT to investigate the fracture and toughening properties of FG TBCs. To the best knowledge which is supported by careful review of literature on design and analysis of FG TBCs, the transformation toughening mechanisms in FG TBCs have not been studied. The design against the fracture of FG TBCs considering the transformation toughening based on the micromechanical approach is extremely new.
(4) A new parameter, β, which is termed an "effective stress intensity factor" in the current project, was introduced for assessing the fracture risk of TBC and level of toughening. Some researchers [Wang et al. 2004, Cho and Ha 2002a, Cho 2006, Tsukamoto et al. 2006] adopted the maximum local tensile stresses for failure criterion of FG TBCs. However, it is considered that successful application of these materials depends on more understanding of their fracture mechanics since their fracture is the most important key failure mode of FG TBCs, which is described in the following discussion section.

6.3.4 Discussion

The validity of the numerical result obtained based on the developed model is examined through the review of theoretical and experimental literature. Firstly, the results obtained based on the maximum effective stress intensity factor criterion in the current project are compared with the results based on the maximum thermal stress criterion. Secondly, the results obtained here are examined through comparison with the results in the literature in which the crack problems in FG TBCs are theoretically investigated using the singular integral equation techniques. Lastly, the results obtained here are examined using some existing experimental data.

Cho and Ha [2002b] conducted an optimization by minimizing thermal stresses in Ni–Al_2O_3 functionally graded materials as described in Chapter 2.

Thermo-mechanical boundary conditions used in their work are different from those used here, so it is difficult to compare the data directly. Tsukamoto et al. [2006] carried out the design of FG TBCs by minimizing the tensile micro-stresses in ceramic phases based on the micromechanical approach, in which the toughening effects were not taken into account. Thermo-mechanical boundary conditions are almost the same as those used in this study [Tsukamoto et al. 2006]. Fig. 6-16 shows the maximum tensile micro-stresses in ceramic phase as a function of compositional gradation patterns. For Case 2, the metal-rich composition is better, which is the same tendency as seen in the results obtained here. Meanwhile, for Case 1, the compositional gradation pattern of n=0.25 can not be suitable. The results of the design based on the "maximum local tensile stress criterion" are different from those obtained here based on the "maximum stress intensity factor criterion". It can be more reasonable, however, to use the "maximum stress intensity factor criterion" for assessing the fracture of such brittle materials as ceramic and FG coatings from the following examination with existing theoretical and experimental work on the failure behaviour of FG TBCs.

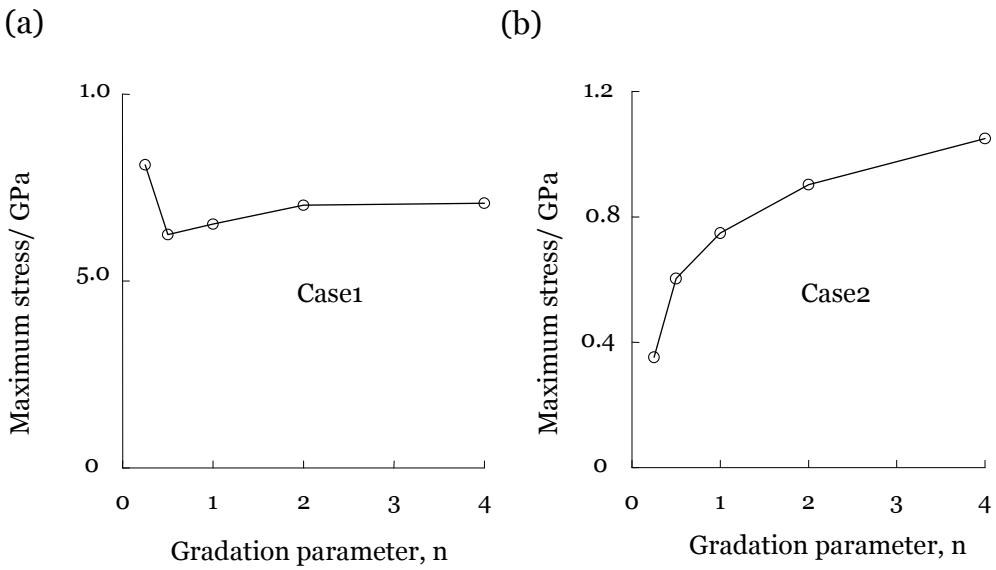

Figure 6-16: Maximum tensile micro-stresses in ceramic phases as a function of compositional gradation patterns, n, for (a) Case 1 and (b) Case 2 [Tsukamoto et al. 2006].

There are several theoretical and experimental studies investigating thermo-mechanical behaviour of FG TBCs subjected to a thermal shock loading, which can result in very high stresses in the materials. It has been reported by some researchers [Jin 2004; Jin and Luo 2006; Wang et al. 2004; Han et al. 2006; Kokini et al. 2002] that cracks initiating and propagating in the surface coating have a large influence on the failure of the FG TBCs under such conditions.

For the theoretical studies, Jin et al. [Jin 2004; Jin and Luo 2006] have been investigating the effect of thermal property gradients on the edge cracking in a functionally graded coating (FGM coating) bonded to a homogeneous substrate subjected to a thermal shock. Here, the work by Jin and Luo [2006] is briefly described. They presented a thermo-fracture mechanics model to study the residual strength behaviour of thermally shocked FG TBCs. The mechanical constraint is assumed free. In their study, it was considered that the thermal shock damage mainly results from the extension of a pre-existing edge crack initially located at the thermally shocked surface of an FG TBC specimen. They adopt a singular integral equation approach to solve a thermal fracture problem of the edge cracked FG TBC strip (See Chapter 3 and Appendix 1). The integral equation has the form:

$$\int_{-1}^{1}\left[\frac{1}{s-r}+K(r,s)\right]\frac{B_y(s,\tau)}{\sqrt{1-s}}ds=-\frac{2\pi(1-\nu^2)}{E}\sigma_{yy}^{T}(r,\tau),\quad |r|\le 1 \tag{6.17}$$

where $K(r,s)$ is a known kernel, $r=2x/a-1$, a the current crack length, τ the non-dimensional time, B_y a continuous function related to the dislocation density along the crack surface.

Once the solution of the integral equation (6.17) is obtained, the stress intensity factor at the edge crack tip can be calculated. The “residual strength”, which is a parameter of the strength of the FG strip after the thermal shock loading, and the “thermal shock threshold”, which a critical temperature change during a thermal shock loading at which the crack propagation can occur, were expressed based on the thermal stress intensity factor. Two FG TBC systems, i.e., Al_2O_3/Si_3N_4 and TiC/SiC FG TBC strips were investigated.

In their study a compositional gradation parameter, p, is defined as follows,

$$f^{(0)} = \left(\frac{x}{b}\right)^{p}, \tag{6.18}$$

where $f^{(0)}$ is the volume fraction of the substrate materials, b is the thickness of FG strips, and x is the position in the thickness direction ($0 \le x \le b$). The smaller p corresponds to the substrate material-rich compositional gradation pattern.

Fig. 6-17 shows the thermal shock residual strength of an Al_2O_3/ Si_3N_4 and TiC/SiC FG strip plotted against the thermal shock , ΔT. The thermal shock thresholds, ΔT_c, are also shown. The material properties they used in the calculation are given in Table A2-1 in Appendix 2. It can been seen in Fig. 6-17 that the smaller p, which means more substrate material-rich compositional gradation, induces the larger thermal shock residual strength and thermal shock threshold, ΔT_c, in both material systems of the FG strips such as Al_2O_3/Si_3N_4 and TiC/SiC.

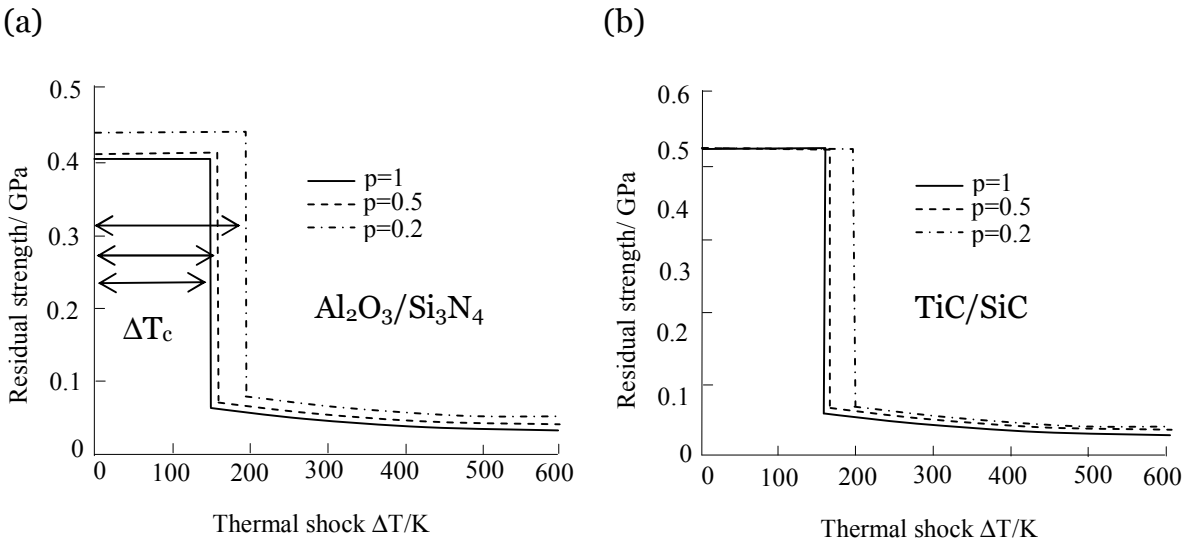

Figure 6-17: Residual strength of (a) Al_2O_3/Si_3N_4 and (b) TiC/SiC . The thickness, b, of FG TBC strip is 5 mm, and the ratio of crack length to thickness, a_o/b, is 0.005 [Jin and Luo 2006].

In their study the following mixture rule was used for the fracture toughness of the composites at any position (x) in FG strips [Jin and Luo 2006]:

$$(K_{Ic}(x))^2 = f^{(0)}(x)(K_{Ic}^{(0)})^2 + f^{(1)}(x)(K_{Ic}^{(1)})^2 \tag{6.19}$$

where $K_{Ic}(x)$, $K_{Ic}^{(0)}$ and $K_{Ic}^{(1)}$ are the fracture toughness for the composites at any position (x), phase (0) (substrate materials) and phase (1) (coating materials), respectively. If we assume a certain mixture rule for predicting the effective fracture toughness of the composites and assume an initial crack length in the current project, the "thermal shock threshold" and "residual strength" can be also obtained in the same way as their study. In the work by Jin [2004], the thermal stress intensity factor was used for investigation of the effect of the gradation patterns, and the similar tendency was obtained. To the best of the knowledge and information in the existing literature and patents, there seems to be no theoretical study on design of FG TBCs toughened by transformation of ZrO_2, so we can not directly compare the developed model and its calculation results with those in the other works at the moment. Accordingly, we can state that to some extent the results obtained based on the "maximum effective stress intensity factor criterion" in the current project seems to be reasonable from this examination even though Jin's analysis dealt with the different material system and did not consider any toughening effects.

Furthermore, the similar analyses were conducted by some researches. Wang et al. [2004], which were introduced in Chapter2, calculated transient temperature fields and associated thermal stresses in FG TBCs by a finite element/finite difference method. Thermal shock fracture of a FGM plate was analysed when the plate is suddenly exposed to an environmental medium of a different temperature. The thermal shock resistance of the FG TBCs was analysed using both "maximum local tensile stress criteria" and "maximum stress intensity factor criteria". They obtained the result that an FGM with high metal (substrate) contents exhibits significant resistance to crack growth in TiC/Ni FG TBCs based on "maximum stress intensity factor criteria". This tendency is the same as the results obtained in the current project.

The work by Han et al. [2006] supports our results in terms of the location cracks initiate and the effect of gradation on the fracture resistance under thermal shock conditions. They considered that the multiple cracking is a common phenomenon for a medium subjected to a sudden temperature change, which will be seen in the following review of experimental studies. They carried out a multiple surface cracking analysis using a finite element method (FEM). They found that the thermal shock strength of the FG TBCs can be improved considerably by increasing the metal content in the FG TBCs.

Some researchers [Kokini et al. 2002; Han et al. 2007; Hamatani et al. 2003] conducted experimental works to investigate the thermal shock fracture resistance of FG TBCs. In the following, the fracture behaviour of FG TBCs is discussed based on these experimental data.

The works by Kokini et al. [2002] and Han et al. [2007] identified that vertical cracks are possibly generated in the ceramic surface layers in FG TBCs as considered in the current project. Kokini et al. [2002] conducted an experimental study to investigate the thermal fracture behaviour of plasma-sprayed yttria stabilized zirconia-NiCoCrAlY bond coat alloy FG TBCs when subjected to a thermal shock loading. They investigated one, three, six and nine layer TBCs. Their results showed that the compositional gradation affects the surface and interface cracking. Fig.6-18 shows the schematic illustration of FG TBCs with surface and horizontal cracks. In particular, multiple surface cracks form with compositional gradation. The increased gradation prevents the initiation of horizontal cracks, which was attributed to the combined effect of a more gradual thermo-mechanical property transition and presence of multiple surface cracks. This result indicates that the horizontal cracks were more hardly generated with the compositional gradation in the FG TBCs more smoothly.

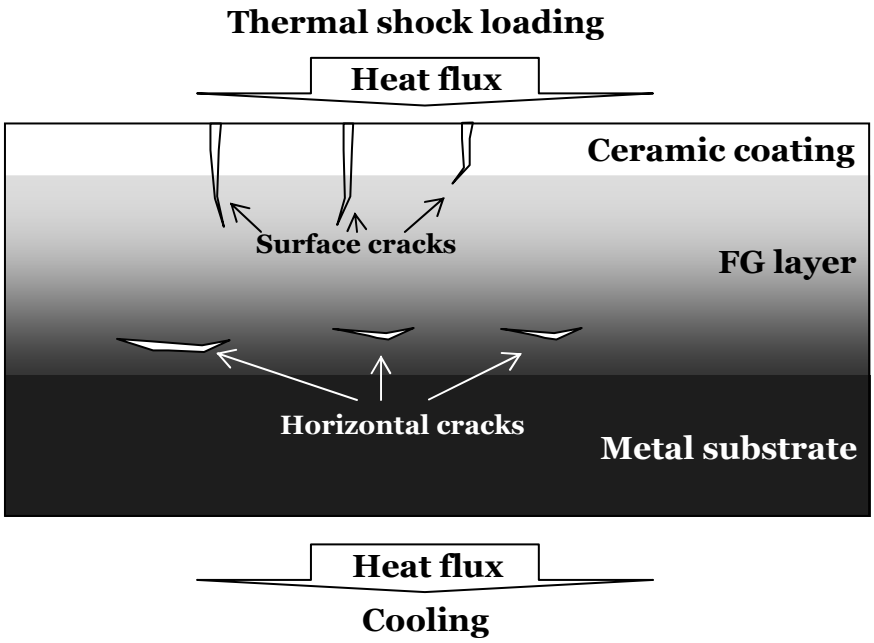

Figure 6-18: Schematic illustration of FG TBCs with surface and horizontal cracks under thermal shock conditions.

In addition, the influence of gradation of the composition on thermal shock behaviour of CeO_2–Y_2O_3–ZrO_2 graded thermal barrier coatings was investigated by Han et al. [2007]. They evaluated the thermal shock resistance of three kinds of TBCs such as 2-layer, 5-layer and graded-layer (FG TBCs) structured ZrO_2 TBC systems. Their result showed that the thermal shock resistance of FG TBCs was superior compared to two other types of TBCs as the surface of FG TBCs presents only little visible cracks but the 5 layer structured TBCs appear obviously delaminated at the layer interfaces. According to their results, the assumption in the current project that the fracture toughness of a ceramic surface and FG layers largely affect the fracture behaviour of FG TBCs seems to be reasonable.

Hamatani et al. [2003] investigated the effects of the compositional gradation profile and coating density in FG TBCs on the thermal shock resistance. The FG TBCs consisted of ZrO_2-8wt.%Y_2O_3 (YSZ) top coating, YSZ-Ni-20 wt. %Cr (NiCr) FGM coating, NiCr under coating and copper substrate.

The ZrO_2-8wt%Y_2O_3 (YSZ) is a perfectly stabilized ZrO_2, so stress-induced transformation toughening can not be expected.

The composition profile analysed by electron probe micro analyser is shown in Fig. 6-19. Type A corresponds to the metal-rich gradation pattern, and Type C corresponds to the ceramic-rich pattern. Type B almost corresponds to the linear gradation pattern.

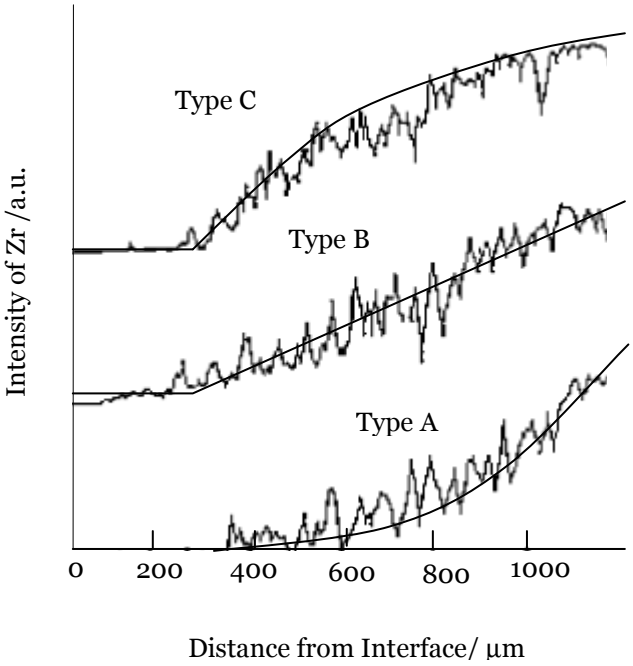

Figure 6-19:
The composition profile in FG TBCs. The intensity of Zr corresponds to YSZ contents [Hamatani et al. 2003].

A comparison is made on the thermal shock resistance for the composition profile and YSZ coating density in Fig. 6-20. Most attention is paid to the effect of compositional gradation. The values in bracket indicate the surface maximum temperature. The profile with a Type A demonstrated the highest thermal shock resistance, with crack forming thermal cycle in excess of 30. Two reasons were stated for this result in their paper. One was that, in the case of Type C, the higher thermal stress was loaded on YSZ coating due to the higher YSZ content. Another one is that because the lower surface temperature

in the case of Type A yielded the higher strength of YSZ coating during the test, the higher strength contributed to the higher thermal shock resistance. This result that FGMs with a metal-rich gradation pattern have a better fracture resistance is the same tendency as that predicted in the current project. It can be considered that the result obtained in the current project should be reasonable.

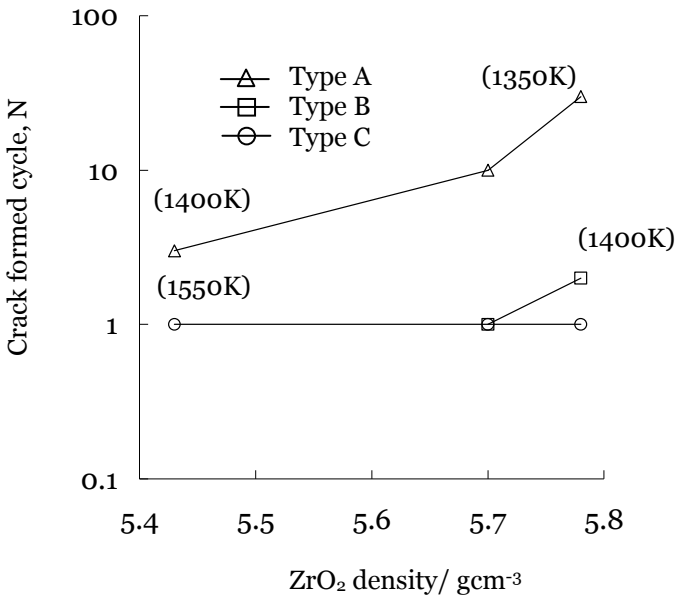

Figure 6-20: Thermal shock resistance plotted against YSZ coating density for the FG TBCs with three different compositional gradations [Hamatani et al. 2003].

The fracture resistance for FG TBCs with three kinds of compositional gradations under various surface temperatures is plotted against the NiCr density in Fig. 6-21. Here, FGMs with the Type A gradation (metal-rich gradation pattern) also shows higher thermal fracture resistance than those with the Type C gradation (ceramic-rich gradation pattern) for any NiCr densities.

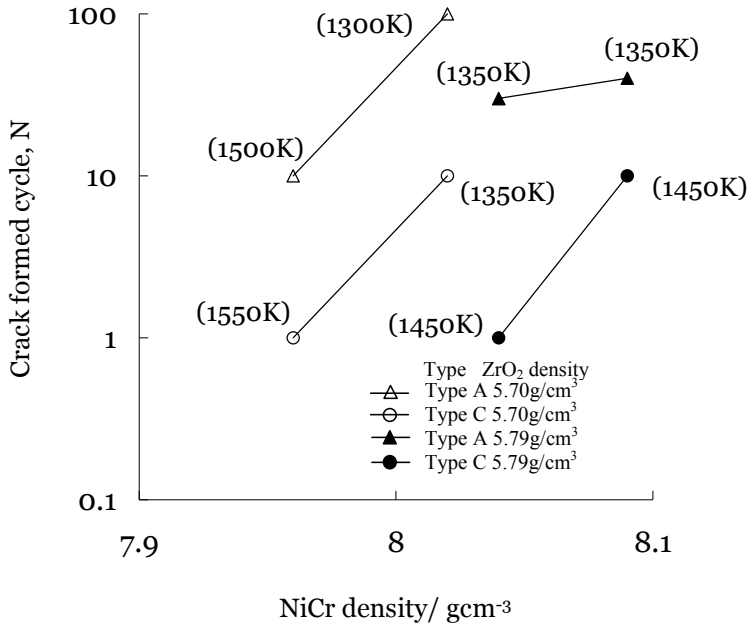

Figure 6-21: Crack formed cycle, N, plotted against NiCr density [Hamatani et al. 2003].

Through discussion on the thermal-shock fracture resistance of FG TBCs with the existing theoretical and experimental studies, the validity of the developed model was examined and verified to some extent. However, there is no study to investigate the transformation toughening in FG TBCs, so the direct comparison of the results obtained in the current project with existing data seems to be impossible. Systematic experimental works to investigate this toughening in FG TBCs are desired, which will be able to confirm the effectiveness of the developed model for design of this new type of high fracture-resistant FG TBCs.

Now we make a discussion on toughening in macroscopic homogeneous composites with various contents of constituents as seen in 5.3.4. The ZrO_2-Ni system is attractive as macroscopic homogeneous composites because nickel and zirconia are relatively inexpensive, chemically stable and immiscible with each other over a wide range of temperatures. They are promising candidates for high added-value functional applications in temperature and flow sensors, thermal protectors for supersonic propulsion systems and others. For

comparison, we also look at a zirconia/ alumina system, which is also attractive not only homogeneous composites but also FG TBCs. Widjaja et al. [2003] investigated zirconia/ alumina FG TBCs. They concluded that the incorporation of Al_2O_3 interlayer between a zirconia top-coating and NiCoCrAlY bond-coat results in manageable residual stresses. Here we examined the effect of the temperature change on the toughening effect in both macroscopic homogeneous ZrO_2-Ni composites and ZrO_2-Al_2O_3 composites with various contents of constituents (the volume fraction of ZrO_2 is more than 0.5, and the transformable ZrO_2 particles account for a half of whole ZrO_2). Fig. 6-22 shows the relation between the toughening effect, λ, (for a steady-sate crack) and the volume fraction of Ni in ZrO_2-Ni composites subjected to various temperature changes. It is seen that the toughening effect is not so affected by the temperature change in these composites with any contents of constituents. As already stated, this is because the thermo-mechanical properties, such as elastic constants and thermal expansion coefficients, of Ni and ZrO_2 are similar.

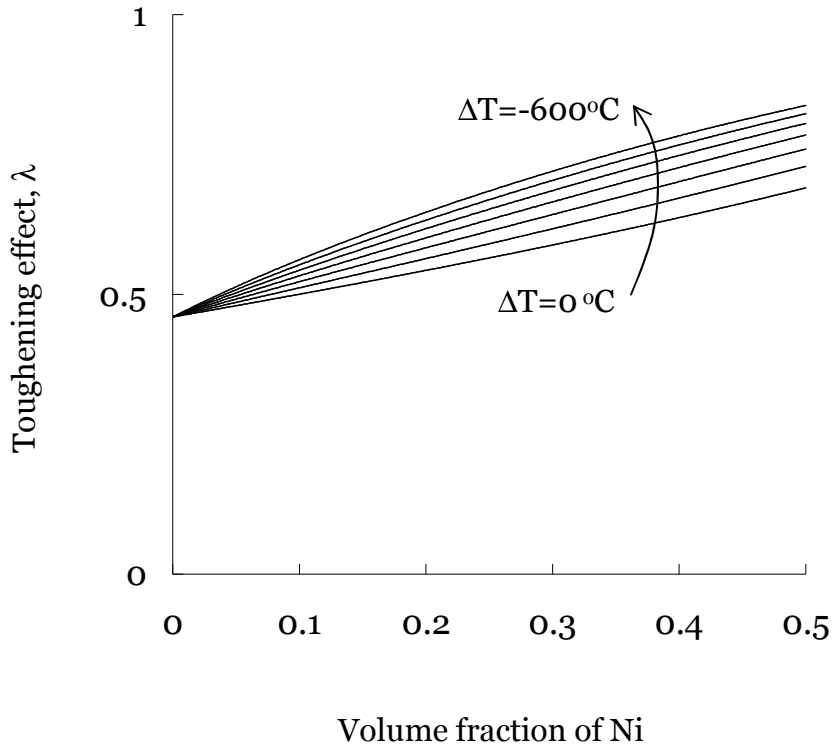

Figure 6-22: Toughening effect, λ, plotted against volume fraction of Ni in ZrO_2-Ni composites. ΔT=0, -100, -200, -300, -400, -500 and -600°C.

Fig. 6-23 shows the relation between the toughening effect, λ, (for a steady-sate crack) and the volume fraction of Al_2O_3 in ZrO_2-Al_2O_3 composites subjected to various temperature changes. In contrast to ZrO_2-Ni composites, it is seen that the toughening effect is largely affected by the temperature change in these composites with any contents of constituents. When the temperature change is higher than -300°C, the toughening effect decreases with increasing the volume fraction of Al_2O_3. Meanwhile when the temperature change is lower than -400°C, the toughening effect increases with increasing the volume fraction of Al_2O_3. It has been reported by some researchers [Miyazaki et al. 2006; Cesari et al. 2006] that the high fracture toughness can be achieved in ZrO_2-Al_2O_3 composites with volume fraction of Al_2O_3 of around 0.5 although both ceramics of ZrO_2 and Al_2O_3 have low fracture toughness. This tendency can not be explained without considering the influence of thermal stresses caused by the temperature change on the toughening effect.

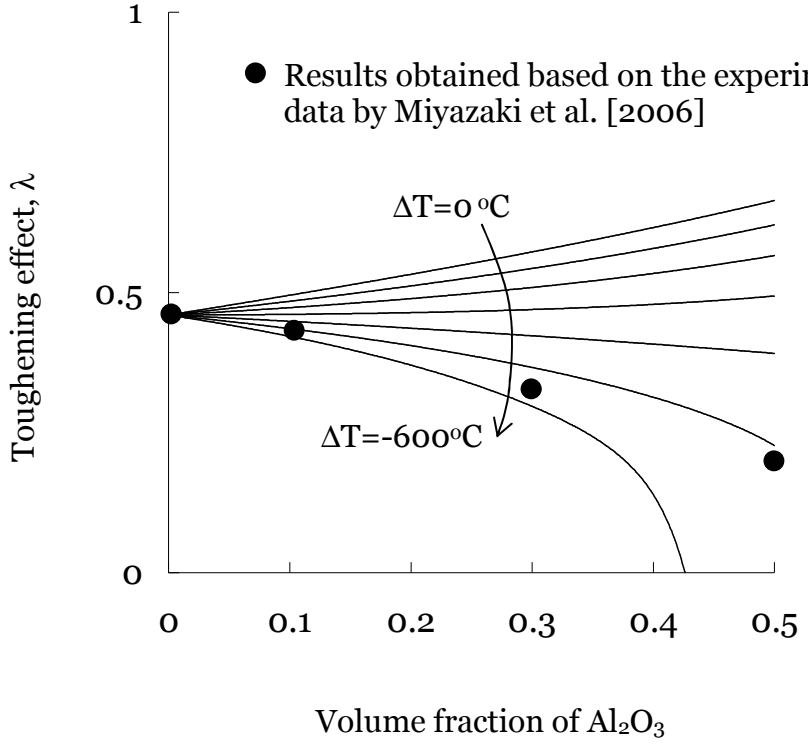

Figure 6-23: Toughening effect, λ, plotted against volume fraction of Al_2O_3 in ZrO_2-Al_2O_3 composites. ΔT=0, -100, -200, -300, -400, -500 and -600°C.

Fig. 6-24 shows the experimental data on the relation between the fracture toughness and the volume fraction of Al_2O_3 in ZrO_2-Al_2O_3 composites, which is obtained by Miyazaki et al. [2006]. It is seen that the fracture toughness reaches its peak value around the volume fraction of Al_2O_3 of 0.5. The toughing effect, λ, is calculated based on these experimental data, which is also shown in Fig. 6-23. As seen in these figures, it is important to consider the effect of the temperature change on toughening to understand the fracture properties of ZrO_2-Al_2O_3 composites. Accordingly, it can be stated that more attention should be paid to the toughening effect in design of ZrO_2-Al_2O_3 FG TBCs compared to ZrO_2-Ni FG TBCs when these are subjected to various temperature conditions.

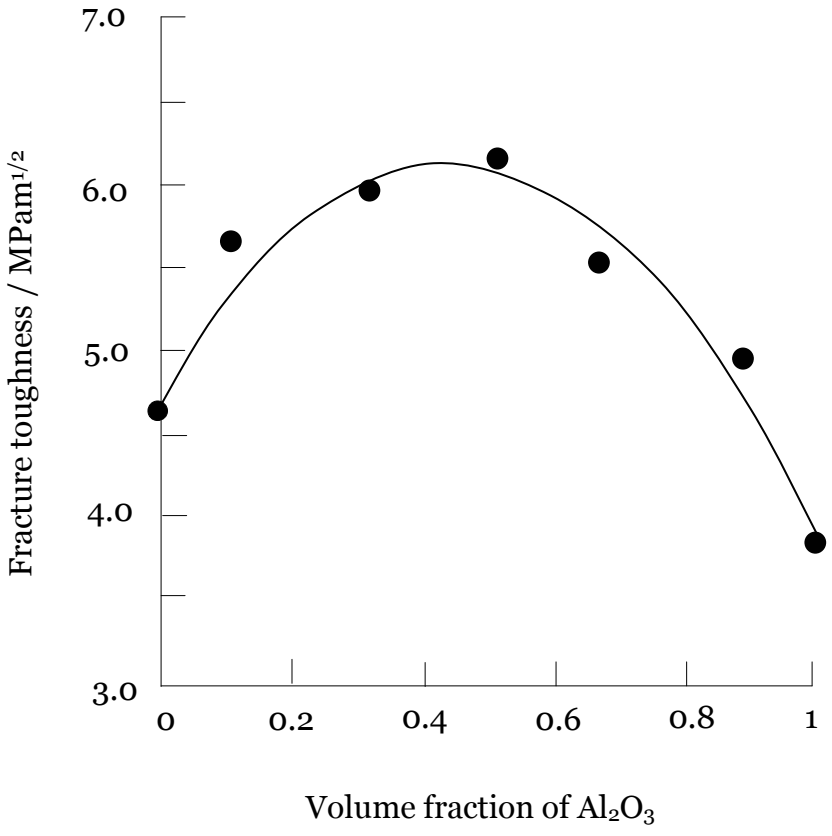

Figure 6-24: Dependence of fracture toughness of ZrO_2-Al_2O_3 composites on volume fraction of Al_2O_3 [Miyazaki et al. 2006].

6.4 Summary

The micromechanical theory for investigation on the transformation toughening in multi-phase composites, developed in Chapter 5, was incorporated into the classical lamination theory (CLT). A new parameter relevant to the stress intensity factors at crack tips, which is termed a effective stress intensity factor, was introduced for assessing the fracture toughness and toughening effects in FG TBCs, and using this parameter a methodology of design against fracture in FG TBCs was developed based on fracture-mechanics considerations.

According to this methodology, Ni-ZrO_2 FG TBCs, which attract a great deal of attention for their superior thermo-mechanical properties in automobile and aerospace industries, were investigated. The design against fracture of Ni-ZrO_2 FG TBCs subjected to various different mechanical loadings and an unsteady heat-flow such as a thermal shock loading was carried out by minimizing the new fracture parameter such as the effective stress intensity factor in ceramic surface layers as well as FG layers. It was shown that the metal-rich compositional gradation is suitable within the considered compositional gradation patterns under all the mechanical boundary conditions. It is necessary to compare such an effective stress intensity factor with empirically-obtained fracture toughness data of the composites in the practical design procedure of FG TBCs. Through discussion on failure of FG TBCs subjected to thermal shock loadings using some the existing theoretical and experimental works, the validity of the results obtained in the present project were examined.

Chapter 7

Conclusions

7.1 Conclusions

In the present project, a new concept of FG TBCs toughened by phase transformation of ZrO_2 was proposed. A new design and analytical method for such FG TBCs was developed based on micromechanics and fracture mechanics approaches.

Transformation toughening by ZrO_2 in multi-phase composites was analysed based on the new micromechanical model. This model is based on a mean-field micromechanical approach by Wakashima and Tsukamoto [1991] and a continuum model by Stump and Budiansky [1989]. This new micromechanical model was used to investigate the effect of mismatch in material properties of constituents, microstructure as well as residual thermal stresses on the toughening effect in multi-phase composites. The composites usually include residual thermal stresses generated during the fabrication processes. As a case study, the effect of these factors on toughening was investigated with ZrO_2-enriched SiC/Al composites. The new results included the finding that not only "lock-up" effect but also "toughening zone" appear in the compositions subjected to a certain temperature change. In the design of such composites, much attention should be paid to both the toughening effect and toughening zone.

Further, the developed micromechanical theory for the transformation toughening mechanisms was incorporated into the classical lamination theory (CLT) for investigation of fracture and toughening behaviour of FG TBCs. Based on the developed theory, Ni-ZrO_2 FG TBCs were investigated. A new parameter relevant to the stress intensity factor at crack tips, which was termed the effective stress intensity factor in the current project, was introduced for assessing the fracture properties and toughening effects in FG TBCs. Using this parameter, a methodology of design against fracture of FG TBCs was proposed. A design of Ni-ZrO_2 FG TBCs was implicated, which are subjected to various

mechanical loadings and an unsteady heat flow such as a thermal shock loading. The gradation patterns which minimize the new parameter such as the effective stress intensity factor in ceramic surface as well as FG layers were obtained.

Major outcomes of the project are described as follows:

(1) The current project theoretically investigated a new concept of FG TBCs toughened by phase transformation of ZrO_2. The methodology for design of FG TBCs with superior fracture properties was provided on the basis of micromechanics and fracture-mechanics considerations through the modelling of the transformation toughening mechanism in multi-phase composites and the incorporation of the developed model into the CLT. The design against fracture of the toughened FG TBCs can provide essential knowledge for material selections, compositional gradations and dimensions in the FG TBCs, which can be used in aerospace and automobile components exposed to super high temperature and temperature gradients.

(2) A new theoretical model for transformation toughening in multi-phase composites was developed based on a combination of micromechanics and fracture mechanics approaches. This model revealed important findings that the transformed zone has a remarkable property of allowing stable crack growth to occur in the composite materials and the infinite toughening, which is called a "lock-up" effect, occurs for a finite amount of crack advance under thermal residual stress conditions.

(3) According to the developed model, the effect of thermal residual stresses due to the mismatch in thermal expansion coefficients of constituent phases on toughening was found to be very strong. For two-phase composites, the toughening effect in the composites containing the matrix with higher Young's modulus and lower thermal expansion coefficient than those of ZrO_2 is largely affected by thermal residual stresses generated during the fabrication process. For three-phase composites, when both the matrix and additional particles have higher Young's modulus and lower Poisson's ratios compared to those of ZrO_2, considered to be more likely properties of typical ceramics rather than metals and alloys, the high transformation toughening effect can be achieved under no thermal residual stress conditions. When the thermal residual stresses are

induced during their fabrication processes in ZrO_2-enriched composites, addition of the third ingredient materials with low thermal expansion coefficients into the composites can not only increase the toughening effect but also reduce the toughening zone. Through the simulation for ZrO_2/ Al_2O_3 three-phase composites, a better understanding was obtained of the influence of thermal residual stresses on the toughening effect.

(4) From the numerical examination on ZrO_2-enriched SiC/ Al composites, the transformation toughening effect in such composites was found to be largely affected by mismatch in thermo-mechanical properties of constituent phases. Both toughening zone and toughening effect are strongly dependent on the states of thermal residual stresses in ZrO_2 particles, which can be generated during the fabrication process.

(5) A methodology of design of FG TBCs toughened by phase transformation of ZrO_2 was investigated by incorporating the developed micromechanics-based model for transformation toughening in multi-phase composites into the classical lamination theory (CLT). A new parameter such as an effective stress intensity factor was introduced for investigating the fracture behaviour and toughening effect in FG TBCs. The design against fracture of Ni-ZrO_2 FG TBCs subjected to a thermal shock loading under various mechanical boundary conditions was implemented by minimizing the effective stress intensity factors in ceramic surface as well as FG layers. The practical recommendations for Ni-ZrO_2 FG TBCs were suggested.

(6) The simulation results obtained, based on the developed model for design against fracture of FG TBCs, were examined using existing theoretical and experimental data in the literature. Within the compositional gradation patterns investigated in the project, the substrate material-rich compositional gradation (metal-rich gradation in the ceramic-metal FG TBCs) was considered to be the most suitable in FG TBCs subjected to thermal shock loadings based on fracture-mechanics consideration. This tendency was theoretically and experimentally confirmed with results available in the open literature.

7.2 Additional work

(1) Bridging toughening is one of the effective toughening mechanisms in ceramic and ceramic matrix composites. Recently synergetic effect between bridging toughening by short fibres and transformation toughening by ZrO_2 particles was studied experimentally by some investigators, while theoretical study on this issue has not been done. Amagigo and Budiansky [1988] formulated theory on synergetic effect between bridging toughening by soft metal particles and transformation toughening by ZrO_2 particles. These two synergetic effects are completely different in their mechanisms and the synergetic effect caused by short fibres can be expected to be much higher than that by soft metal particles. It is very important and useful to analyse this mechanism theoretically. The effect of T-stress on the short-fibre bridging toughening is also investigated. Now formulation of theory is being performed using a continuously distributed dislocation technique shown in Chapter 2.

(2) The failure of composites, bi-materials and coated materials, are associated with the cracks occurring near the interface between bonded dissimilar materials. Cracks in the interface between two materials with different thermo-mechanical properties are of considerable practical interest. Geometric singularities for perfect bond constitute a fairly well explored area in linear elasticity. Williams [1952] first showed the stress singularities in the sharp corner of a thin plate under extension or bending with various boundary conditions along the intersecting edges. Stress singularity and non-singularity fields are now theoretically investigated for the interface crack of bi-materials with both materials undergoing time-dependent inelastic deformations.

(3) Currently, adhesively retained resin-base restorations based on polymeric resins often reinforced with inorganic particles or short cut fibres are being employed to a large extent in contemporary restorative dentistry. The adhesive resins are considered as alternatives to traditional metal- and ceramics-based dental restorations because of their ability to bond the restoration to tooth structure, better aesthetics, avoidance of mercury, reduced fracture susceptibility, as well as the potential for a more conservative cavity

preparation with less reliance on mechanical retention. The resins, however, have disadvantages stemming from the polymerisation contraction and the mismatch in mechanical properties with tooth structure. The shrinkage stresses that develop during cure of an adhesive restoration can lead to the initiation and development of interfacial defects. For such problems, it is possible to reduce the volumetric shrinkage by adding suitable inorganic particles to the resin, while such composition also results in an increase in stiffness, which is normally associated with higher polymerisation stresses to be more deleterious. An understanding of these opposing effects is critical to ensure optimal performance in selection of the restorative material. The current study investigates the design procedure of the resin-base composite restorations. A mean-field micromechanics-based approach described in Chapter5 is applied to giving a practical guidance to the material selection process. The suitable shape and concentration of filler particles are proposed to design optimal resin-base composites to prevent interface debonding and fracture due to their shrinkage and thermal stresses under temperature change conditions. The results have been made in shape of a paper submitted to the international journal of Dental Materials as shown in the publication list.

7.3 Publication list

5 first-author papers have been submitted to refereed journals.

（In them 3 papers have been already accepted.）

3 first-author proceeding papers have been submitted to international conferences. (All papers have been already accepted and presented.)

Now some other papers are in progress.

[Journals]

Tsukamoto H. and Kotousov A. 2007, Micromechanical approach to transformation toughening in zirconia-enriched multi-phase composites. *Journal of Mechanics of Materials and Solids*, 2, 5, 937-950.

Tsukamoto H. and Kotousov A., 2007, Micromechanical study on high-temperature behaviour of ZrO_2 particle-dispersed Ni composites. *Key Engineering Materials*, 340-341, 95-100.

Tsukamoto H. and Kotousov A., 2006, Transformation toughening in zirconia-enriched composites: Micromechanical modelling. *International Journal of Fracture*, 139, 161-168.

Tsukamoto H. and Kotousov A. On effectiveness of transformation toughening mechanism in multi-phase composites enriched with zirconia particles. Micromechanical approach. *Composite structures,* submitted.

Tsukamoto H. and Kotousov A. Design of functionally graded thermal barrier coatings. *Composites Part B*, submitted.

Codrington J., Nguyen P., Ho S., Kotousov A. and Tsukamoto H., Experimental Apparatus for Super High Temperature Testing of Thermo-mechanical Properties, *Experimental Mechanics*, submitted.

[International Conferences]

Tsukamoto H., Kotousov A., Ho, S.-Y. and Codrington J., 2006, Analysis and design of functionally graded thermal coating, *Proceedings of International Conference on Structural Integrity and Failure, SIF2006*, 25-32.

Tsukamoto H., Kotousov A. and Codrington J., 2006, Micromechanical study on high temperature behaviour of ZrO_2 particle-dispersed Ni composites. *International Conference on Structural Integrity and Failure*, SIF2006, 427-433.

Tsukamoto H. and Kotousov A., 2006, Micromechanical Modelling of Transformation Toughening Mechanism in Zirconia-Enriched Multi-Phase Composites. *Deformation & fracture of Materials 2006, 722-725.*

Codrington J., Nguyen P., Ho S.-Y., Kotousov A. and Tsukamoto H., 2006, Experimental apparatus for high temperature testing of thermo-mechanical properties. *International Conference on Structural Integrity and Failure*, SIF2006, 148-153.

Blazewicz A., Kotousov A. and Tsukamoto H., 2006, Generalization of the distribured dislocation techniques on problems with semi-infinite. *International Conference on Structural Integrity and Failure*, SIF2006, 210-214.

Bibliography

Abd-Alla A.M., Abd-Alla A.N., Zeidan N.A. (2000) Thermal stresses in a nonhomogeneous orthotropic elastic multi-layered cylinder, J. Thermal Stresses, 23, 413–428.

Agrawal P., Gonlon K., Bowman K.J., Sun C.T., Cichocki F.R., Trumble K.P. (2003) Thermal residual stresses in co-continuous composites, Acta Mater., 51, 4, 1143–1156.

Agrawal P., Sun C.T. (2004) Fracture in metal–ceramic composites, Comp Sci Tech, 64 (9), 1167-1178.

Alex R., Schovanec L. (1996) An anti-plane crack in a nonhomogeneous viscoelastic body. Eng Fract Mech., 55, 727–735.

Amazigo J.C., Budiansky B. (1988) Interaction of particulate and transformation toughening, Journal of the Mechanics and Physics of Solids, 36, 5, 581-595.

Amazigo J.C., Budiansky B. (1988) Steady-state crack growth in supercritically transforming nmaterials, Int. J. Solids. Structures, 24, 751-755.

Anderson T.L. (2005) Fracture mechanics; fundamentals and application, CRC press.

Anné G., Put S., Vanmeensel K., Jiang D., Vleugels J., and Biest O.V. (2005) Hard, tough and strong ZrO_2–WC composites from nanosized powders. Journal of the European Ceramic Society, 25, 1, 55-63.

Arai Y., Kobayashi H., Tamura M. (1990) Analysis on residual stress and deformation of functionally gradient material and its optimum design. Proc. of the First Int. Symp. FGM, Sendai.

Asakawa A., Noda N., Tohgo K., Tsuji T. (1994) Constitutional equations of thermal stresses of particle-reinforced composite. JSME Ser A, 60 (575), 1632–1637.

Ashby M. F., Blunt F. J., Bannister M. (1989) Flow characteristics of highly constrained metal wires. Acta Metallurgica, 37 (7), 1847-1857.

Atkinson C., Chen C.Y. (1996) The influence of layer thickness on the stress intensity factor of a crack lying in an elastic (viscoelastic) layer embedded in a different elastic (viscoelastic) medium (mode III analysis). Int J Eng Sci., 34, 639–658.

Atkinson C., Chen C.Y. (1997) The influence of layer thickness on the stress intensity factor of a crack lying in an (visco) elastic layer embedded in a different (visco)elastic medium (plane strain, mode I analysis). Proc Royal Soc London: A, 453, 1445–1471.

Baldacim S.A., Santos C., Silva O.M.M., Silva C.R.M. (2003) Mechanical properties evaluation of hot-pressed Si3N4–SiCw composites, International Journal of Refractory Metals & Hard Materials, 21, 233–239.

Basu B., Vleugels J., Biest O.V. (2004) Toughness tailoring of yttria-doped zirconia ceramics, Mater Sci Eng A, 380 (1-2), 215-221.

Basu B., Vleugels J., Biest O.V.D. (2004) ZrO_2-Al_2O_3 composites with tailored toughness, J Alloy Compd, 372, 278-284.

Becher P.F., Wei G.C. (1984) Toughening behaviour in SiC-whisker reinforced alumina. J. Am. Ceram. Soc., 67 (12), 267–269.

Becher P.F., Tiegs T.N., Ogle J.C., Warwick W.H. (1986) Toughening of ceramic by whisker reinforcement. In Fracture Mechanics of Ceramics (Vol 7), ed. R. C. Bradt, A. G.

Bermejo R., Torres Y., Baudín C., Sánchez-Herencia A.J., Pascual J., Anglada M., Llanes L. (2007) Threshold strength evaluation on an Al_2O_3–ZrO_2 multilayered system. Journal of the European Ceramic Society, 27, 2-3, 2007, 1443-1448.

Broberg K.B. (1999) Cracks and Fracture. London: Academic Press.

Broberg K. B. (2005) International Journal of Fracture, 131, 1-14.

Broek D. (1982) Elementary engineering fracture mechanics, Martinus Nijhoff Publishers, Boston, USA.

Bruck H.A., Rabin B.H. (1999) An evaluation of rule-of-mixtures predictions of thermal expansion in powder processed Ni-Al_2O_3 composites, J. Am. Cer. Soc., 82, 2927-2930.

Budiansky B. (1965) On the elastic moduli of some heterogeneous materials, J. Mech. Phys. Solids, 13 (4), 223–227.

Budiansky B., Hutchinson J.W, Evans A.G. (1986) Matrix fracture in fiber reinforced ceramics, J. Mech. Phys. Solids, 34, 167-189.

Budiansky B., Hutchinson J.W., Lambropoulos J.C. (1983) Continuum theory of dilatant transformation toughening in ceramics, Int J Solids Struct, 19 (4), 337-355.

Cai H., Bao G. (1998) Crack Bridging in functionally graded coatings, Int. J. Solids Structures, 35, 7-8, 701-717.

Casellas D., Cumbrera F.L., Sánchez-Bajo F., Forsling W., Llanes L., Anglada M. (2001) On the transformation toughening of Y–ZrO_2 ceramics with mixed Y–TZP/PSZ microstructures, J Eur Ceram Soc, 21 (6), 765-777.

Cesari F., Esposito L., Furgiuele F.M., Maletta C., Tucci A. (2006) Fracture toughness of alumina–zirconia composites. Ceramics International, 32, 3, 249-255.

Charalambides P. G., McMeeking R. M. (1987) Finite element method simulation of crack propagation in a brittle microcracking solid. Mechanics of Materials, 6 (1), 71-87.

Chen R. Z., Chiu Y. T., Tuan W.H. (2000) Toughening alumina with both nickel and zirconia inclusions. Journal of the European Ceramic Society, 20 (12), 1901-1906.

Chen Y.F., Erdogan F. (1996) The interface crack problem for a nonhomogeneous coating bonded to a homogeneous substrate Journal of the Mechanics and Physics of Solids, 44, 5, 771-787 .

Chen B., Tong L. (2005) Thermomechanically coupled sensitivity analysis and design optimization of functionally graded materials, Comput. Methods Appl. Mech. Engrg., 194, 1891–1911.

Chen R.Z., Tuan W.H. (2001) Toughening alumina with silver and zirconia inclusions, Journal of the European ceramic Society; 21, 2887-2893.

Chi S-H., Chung Y-L. (2003) Cracking in coating–substrate composites with multi-layered and FGM coatings, Engineering Fracture Mechanics, 70, 10, 1227-1243.

Chiang Y.C., Wang A.S.D., Chou T.W. (1993) On matrix cracking in fiber reinforced ceramics, J. Mech. Phys. Solids, 42, 1137-1154.

Cho J.R., Ha D.Y. (2001) Averaging and finite-element discretization approaches in the numerical analysis of functionally graded materials, Materials Science and Engineering A302, 196, 187–196.

Cho J.R., Ha D.Y. (2002a) Volume fraction optimization for minimizing thermal stress in Ni–Al_2O_3 functionally graded materials, Mater. Sci. Engrg. A, 334, 147–155.

Cho J.R., Ha D.Y. (2002b) Optimal tailoring of 2D volume fraction distributions for heat resisting functionally graded material using FDM, Comput. Methods Appl. Mech. Engrg. 191, 3195–3211.

Cho J.R., Choi J.H. (2004) A yield-criteria tailoring of the volume fraction in metal-ceramic functionally graded material. Eur J Mech A/Sol, 23, 271–281.

Cho J.R., Shin S.W. (2004) Material composition optimization for heat-resisting FGMs by artificial neural network Composites Part A: Applied Science and Manufacturing, 35 (5), 585-594.

Christensen R. M. (1969) Viscoelastic properties of heterogeneous media. Journal of the Mechanics and Physics of Solids, 17 (1), 23-41.

Chudnovsky A., Shaofu W. (1992) Evaluation of energy release rate in the crack-microcrack interaction problem. International Journal of Solids and Structures, 29 (14-15), 1699-1709.

Chudnovsky A., Wu S. (1991) Elastic interaction of a crack with a random array of microcracks, Int. J. Fracture, 49, 123-140.

Christensen R.M. (1971) Theory of Viscoelasticity. New York: Academic Press.

Claussen N. (1976) Fracture toughness of Al_2O_3 with an unstabilized ZrO_2 dispersed phase, J. Am. Ceram. Soc., 59, 49-51.

Daguano J.K.M.F., Santos C., Souza R.C., Balestra R.M., Strecker K., Elias C.N. (2007) Properties of ZrO_2–Al_2O_3 composite as a function of isothermal holding time. International Journal of Refractory Metals and Hard Materials, 25, 5-6, 374-379.

Dundurs J. (1968) Elastic interaction of dislocations with inhomogeneities, in Mathematical Theory of Dislocations, American Society of Mechanical Engineers, New York, 70-115.

Dundurs J., Mura T., (1964) Interaction between an edge dislocation and a circular inclusion, J. Mech Phys. Solids, 12, 177-189.

Eftis J., Liebowitz H(1972) On the modified Westergaard equations for certain plane crack problems, Int. J. Fract. Mech., 8,383-392.

Elperin T., Rudin G. (2002) Thermal stresses in functionally graded materials caused by a laser thermal shock, Heat Mass Transfer, 38 (7–8), 625–630.

Erdogan F. (1995) Fracture mechanics of functionally graded materials. Compos Eng., 5, 753–770.

Erdogan F., Gupta G.D., Ratwani M. (1974) Interaction between a circular inclusion and arbitraly oriented crack, ASME J. Appl. Mechanics, 1007-1013.

Erdogan F., Wu B.H., (1993). Analysis of FGM specimens of fracture toughness testing, Ceramic Trans., 34, 39-46.

Erdogan F., Wu B.H. (1996) Crack Problems in FGM Layers under Thermal Stresses, Journal of Thermal Stresses, 19, 31, 237-265.

Erdogan F., Gupta G.D. (1972) Quarterly of Applied Mathematics, 525-534.

Eshelby J.D. (1957) The determination of the elastic field on an ellipsoidal inclusion, and related problems, Proc. R. Soc. London, A241, 376-396.

Eshelby J.D. (1959) The elastic field outside an ellipsoidal inclusion. Proc. R. Soc. London, A252, 561-569.

Eshelby J.D. (1961) Elastic inclusions and inhomogeneities, Prog. Solid Mech, 2, 89-140.

Eso O., Fang Z., Griffo A. (2005) Liquid phase sintering of functionally graded WC–Co composites, International Journal of Refractory Metals and Hard Materials, 23, 4-6, 233-241.

Evans A.G., Heuer A.H. (1980) Transformation toughening in ceramics martensitic transformations in crack-tip fields. Journal of the American Ceramic Society, 63, 244-248.

Evans A.G., Faber K.T. (1984) Crack-growth resistance of microcracking brittle materials. J. Am. Ceram. Soc., 6, 255–260.

Evans A.G., Fu Y. (1985) Some effects of microcracking on the mechanical properties of brittle solids II. Microcrack toughening, Acta Metallurgica, 8, 1525-1531.

Evans, D. P. H. Hasselmanand F. F. Lange. Plenum Press, New York, 61–73.

Faber K.T., Evans A.G. (1983) Crack deflection processes - II. Experiment, Acta Metallurgica, 4, 577-584.

Finot M., Suresh S. (1996). Small and large deformation of thick and thin film multi-layers: effects of layer geometry, plasticity and compositional gradients, J. Mech. Phys. Solids, 44 (5), 683–721.

Finot M., Suresh S., Bull C., Sampath S. (1996) Curvature changes during thermal cycling of a compositionally graded Ni–Al_2O_3 multi-layered material, Mater. Sci. Engrg., A 205, 59–71.

Fuchiyama T., Noda N, Tsuji T, Obata Y. Analysis of thermal stress and stress intensity factor of functionally gradient materials. In: Holt JB, Koizumi M, Hirai T, Munir ZA, editors. Ceramic transactions, Functionally graded materials, vol. 34. The American Ceramic Society, 1993. p. 425–430.

Fukui Y., Yamanaka N. (1993) The stresses and strains in a thick-walled tube for functionally graded material under uniform thermal loading, JSME Series A 36, 156-162.

Gao Y.C., Mai Y.W., Cottrell B. (1998) Fracture of fibre-reinforced materials. ZAMP, 39, 550-572.

Garnier V., Fantozzi G., Nguyen D., Dubois J. and Thollet G. (2005)_Influence of SiC whisker morphology and nature of SiC/Al_2O_3 interface on thermomechanical properties of SiC reinforced Al_2O_3 composites, Journal of the European Ceramic Society, 25, 15, 3485-3493.

Garrido L.B., Aglietti E.F., Martorello L., Camerucci M.A., Cavalieri A.L. (2006) Hardness and fracture toughness of mullite–zirconia composites obtained by slip casting. Materials Science and Engineering: A, 419, 1-2, 15, 290-296.

Garvie R.C., Hannink R.H., Pascoe R.T. (1975) Ceramic steel. Nature, 258, 704-730.

Giannakopoulos A.E, Suresh S., Finot M., Olsson M. (1995) Elastoplastic analysis of thermal cycling: layered materials with compositional gradients**.** Acta Metallurgica et Materialia, 43 (4), 1335-1354.

Gong S.X., Horii H. (1989) General solution to the problem of microcracks near the tip of a main crack. J. Mech. Phys. Solids, 37, 27-46.

Gong S.X., Meguid S.A. (1991) A general solution to the antiplane problem of an arbitrarily located elliptical hole near the tip of a main crack. Int. J. Solids Structures, 28, 249-263.

Gong S.X., Meguid S.A. (1992) Microdefect interacting with a main crack: a general treatment. Int. J. Mech. Sci., 34, 933-945.

Gong S.X., Meguid S.A. (1993) Interacting circular inhomogeneities in plane elastostatics, Acta Mech., 99, 49-60.

Gong S.X., Meguid S.A. (1991) On the effect of the release of residual stresses due to near-tip microcracking. Int. J. Fracture, 52, 257-274.

Grujicic M., Zhang Y. (1998) Determination of effective elastic properties of functionally graded materials using Voronoi cell finite element method. Materials Science and Engineering A, 251 (1-2), 64-76

Gu Y.W., Khor K.A., Fu Y.Q., Wang Y. (1997) Functionally graded ZrO_2-NiCrAlY coatings prepared by plasma spraying using pre-mixed, spheroidized powders, Surface and Coatings Technology, 96, 2-3, 305-312.

Gu W.H., Faber K.T., Steinbrech R.W. (1992) Microcracking and R-curve behavior in SiC-TiB_2 composites, Acta metall. mater. 40, 11, 3121-3128.

Guo L.-C., Wu L. Z., Ma L. Z. (2004) The interface crack problem under a concentrated load for a functionally graded coating–substrate composite system. Composite Structures, 63 (3-4), 397-406.

Guo L-C., Wu L-Z., Zeng T., Cao D-H. (2005) The transient response of a coating–substrate structure with a crack in the functionally graded interfacial layer, Composite Structures, 70, 109–119.

Gupta T.K, Lange F.F., Bechtold J.H. (1978) Effect of stress-induced phase transformation on the properties of polycrystalline zirconia containing metastable tetragonal phase. J. Mater. Sci., 13, 1464-1470.

Hamatani H., Shimoda N., Kitaguchi S. (2003) Effect of the composition profile and density of LPPS sprayed functionally graded coating on the thermal shock resistance. Science and Technology of Advanced Materials, 4 (2), 197-203.

Han L.X., Suresh S. (1989) High-temperature failure of an alumina-silicon carbide composite under cyclic loads: mechanisms of fatigue crack tip damage, J. Am. Ceram. Soc., 72, 1233-1238.

Han J.C., Wang B.L. (2006) Thermal shock resistance enhancement of functionally graded materials by multiple cracking. Acta Materialia, 54, 4, 963-973.

Han Z., Xu B., Wang H., Zhou S. (2007) A comparison of thermal shock behavior between currently plasma spray and supersonic plasma spray CeO_2–Y_2O_3–ZrO_2 graded thermal barrier coatings. Surface and Coatings Technology, 201, 9-11, 5253-5256.

Hannink R.H.J, Kelly P.M, Muddle B.C. (2000) Transformation toughening in zirconia-containing ceramics. J Am Ceram Soc, 83(3), 461–87.

Hashin Z. (1983) Analysis of composite-materials – A survey. J. Appl. Mech. –TRANS. ASME 50 (3), 481-505.

Hashin Z., Shtrikman S. (1963) A variational approach to the theory of the elastic behaviour of multiphase materials, J. Mech. Phys. Solids, 11, 127-140.

Helsing J. (1999) Stress intensity factors for a crack in front of an inclusion. Engineering of Fracture and Mechanics, 64, 245–253.

Herrmann J.M., Schovanec L. (1990) Quasi-static mode III fracture in a nonhomogeneous viscoelastic body, Acta Mechanica, 85, 235–249.

Herrmann J.M., Schovanec L. (1994) Dynamic steady-state mode III fracture in a nonhomogeneous viscoelastic body, Acta Mechanica, 106, 41–54.

Heian E.M., Gibeling J.C., Munir Z.A. (2004) Synthesis and characterization of Nb5Si3/Nb functionally graded composites, Materials Science and Engineering A368, 168–174

Hill R. (1963) Elastic properties of reinforced solids: some theoretical principles. J Mech Phys Solids, 11, 357-372.

Hill R. (1965) A self-consistent mechanics of composite materials, J. Mech. Phys. Solids, 13 (4), 213–222.

Hirano T., Teraki J. (1993) Computational approach to the design of functionally graded energy conversion materials. In: Nishijima, S., Onodera, H. (Eds.), Modelling and Simulation for Materials Design, 303-308.

Hoagland R.G., Hahn G.T., Rosenfield A.R. (1973) Influence of microstructure on fracture propagation in rock, Rock Mech., 5, 77-106.

Homeny J., Vaughn W.L., Ferber M.K. (1987) Processing and mechanical properties of SiC-whisker-Al_2O_3-matrix composites. Am. Ceram. Soc. Bull., 66(2), 333–338.

Hori M., Nemat-Nasser S. (1987) Interacting micro-cracks near the tip in the process zone of a macro-crack, J. Mech. Phys. Solids, 35, 601-629.

Huang G.Y., Wang Y.S. (2002) Fracture analysis of functionally graded coatings: antiplane deformation, Dietmar G.,Eur.J. Mech. A/Solids 21 (3), 391 -400.

Huang G.Y., Wang Y.S., Gross D. (2003) Fracture analysis of functionally graded coatings: plane deformation, Eur.J. Mech. A/Solids., 22, 4, 535-544.

Huang G.Y., Wang Y.S., Yu S.W. (2004) Fracture analysis of a functionally graded interfacial zone under plane deformation, Int. J. Solids Struct.,41, 731-743.

Huang J.H., Fadel G.M., Blouin V.Y., Grujicic M. (2002) Bi-objective optimization design of functionally gradient materials, Mater. 657–666.

Hu X.Z., Wittmann F.H. (1992) Fracture energy and fracture process zone, Mater. Struct. 25, 319-326.

Hutchinson J.W. (1974) On steady state quasi-static crack growth. Harvard University Report, Division of Applied Sciences, DEAP S-8, April.

Hutchinson J.W. (1987) Initial crack growth tearing resistance in transformation toughed ceramics, Advanced Materials for Severe Service Applications (Edited by Iida K.), 77-90.

Hutchinson J.W. (1987) Crack tip shielding by micro-cracking in brittle solids. Acta metall, 35, 7, 1605-1619.

Hutchinson J.W., Jensen H.N. (1990) Model of fibre debonding and pull-out in brittle composites with friction. Mechanics of Materials, 9,139-163.

Hvizdoš P., Jonsson D., Anglada M., Anné G., Biest O.V.D. (2007) Mechanical properties and thermal shock behaviour of an alumina/zirconia functionally graded material prepared by electrophoretic deposition, J. European Ceram. Soc., 27, 2-3, 1365-1371.

Ito S., Nishii J., Takahashi Y., Nakamura R., Fujii T. (2001) Transport phenomena in some solids under hipping pressure, Solid State Ionics, 141-142, 301-306.

Jiang X., Chen Y., Sun X.-W., Huang L.-P. (1999) Mechanical property improvement and microstructure observation of SiCw–AlN composites. J. European Ceramic Society, 19, (11), 2033-2038.

Jin Z.H. (2004) Effect of thermal property gradients on the edge cracking in a functionally graded coating. Surface and Coatings Technology, 179, 2-3, 23, 210-214.

Jin Z.H., Batra R.C. (1996) Some basic fracture mechanics concepts in functionally graded materials. J Mech Phys Solids, 44, 1221–1235.

Jin Z.-H., Luo W.J. (2006) Thermal shock residual strength of functionally graded ceramics. Materials Science and Engineering: A, 435-436, 71-77.

Jin Z.H., Noda N. (1994) Crack-tip singular fields in nonhomogeneous materials. ASME J Appl Mech, 61, 738–740.

Jin Z.H., Paulino J.H. (2002) Dodds R.H., Finite element investigation of quasi-static crack growth in functionally graded materials using a novel cohesive zone fracture model, ASME J. Appl. Mech., 69, 370–379.

Jin Z.H., Paulino G.H. (2002) Engineering Fracture Mechanics 69, 1769–1790-1789.

Kachanov M. (1987) Elastic solids with many cracks: a simple method of analysis, Int. J. Solids Structures, 23, 23-43.

Kachanov M., Montagut E.L.E., Laures J.P. (1990). Mechanics of crack-microcrack interactions. Mechanics of Materials, 10, 59-71.

Kato H.T., Iwai M., Muramatsu Y., Kinoshita K., Yoda S. (2000) Single crystal growth of compositionally graded $In_XGa_{1-X}As$, Materials Science and Engineering B, 75, 2-3, 143-148.

Kawasaki A., Watanabe R. (1997) Evaluation of thermomechanical performance for thermal barrier type of sintered functionally graded materials Composites Part B, 28B, 29-35.

Kelly P.M., Rose L.R.F. (2002) The martensitic transformation in ceramics — its role in transformation toughening, Progress in Materials Science, 47, 5, pp. 463-557.

Knehans R., Steinbrech R., Schaarwächter W. (1983) Quantitative correlation of acoustic emission to the brittle fracture of porous sintered glass. Materials Science and Engineering, 61(1), 17-22.

Kessler H., Kleebe H.-J., Cannon R.W., Pompe W. (1992) Influence of internal stresses on crystallization of intergranular phases in ceramics, Acta Metallurgica et Materialia, 40, 9, 2233-2245.

Kieback B., Neubrand A., Riedel H. (2003) Processing techniques for functionally graded materials, Materials Science and Engineering A, 362 (1-2), 81-106.

Kim J.K., Mai Y.W. (1998) Engineered interfaces in fibre-reinforced composites. Oxford: Elsevier, 1998.

Kim J.H., Paulino G.H. (2003) An accurate scheme for mixed-mode fracture analysis of functionally graded materials using the interaction integral and micromechanics models, Int. J. Numer. Meth. Eng., 58 (10), 1457–1497.

Knechtel M., Prielipp H., Müllejans H., Claussen N., Rödel J. (1994) Mechanical properties of Al/Al_2O_3 and Cu/Al_2O_3 composites with interpenetrating networks, Scripta Metallurgica et Materialia, 31, 8, 1085-1090.

Kokini K., DeJonge J., Rangaraj S., Beardsley B. (2002) Thermal shock of functionally graded thermal barrier coatings with similar thermal resistance, Surface and Coatings Technology, 154, 223–231.

Koizumi M. (1997) FGM activities in Japan, Composites Part B: Engineering, 28 (1-2), 1-4.

Konda N., Erdogan F. (1994) The mixed mode crack problem in a nonhomogeneous elastic medium Eng. Fract. Mech., 47, 4, 533-545.

Kotoul M., Vrbka J. (2003) Crack bridging and trapping mechanisms used to toughen brittle matrix composite, Theoretical and Applied Fracture Mechanics, 40, 23–44.

Lambros J., Santare M.H., Li H., Sapna III G.H. (1999) A novel technique for the fabrication of laboratory scale model functionally graded materials. Exp Mech., 39, 184–190.

Lange F.F. (1982) Transformation toughening, part 4, fabrication, fracture toughness and strength of Al_2O_3-ZrO_2 composites, J Mater Sci, 17, 247-254.

Lee C.S., Zhang X.F., Thomas G. (2001) Novel joining of dissimilar ceramics in the Si_3N_4–Al_2O_3 system using polytypoid functional gradients, Acta Materialia, 49, 18, 3775-3780.

Li C.Y., Weng G.J. (2001) Mech.Mater., 33, 325-333.

Li M., Soboyejo W.O. (1999) Synergistic toughening of a hybrid NiAl composite reinforced with partially stabilized zirconia and molybdenum particles, Materials Science and Engineering A, 271, 1-2, 491-495.

Li Z., Bradt R. (1989) Micromechanical stresses in SiC-reinforced Al_2O_3 composites. J. Am. Ceram. Soc., 72(1), 70–77.

Li A., Zhen Y., Yin Q., Ma L., Yin Y. (2006) Microstructure and properties of (SiC, TiB2)/B4C composites by reaction hot pressing, Ceramics International, 32, 849–856.

Liebfried G. (1951) Verteilung von Versetzungen im statischen Gleichgewicht. Zeitschrift fur Physik, 130, 214-226.

Limarga A.M., Widjaja S., Yip T.H. (2005) Mechanical properties and oxidation resistance of plasma-sprayed multilayered Al_2O_3/ZrO_2 thermal barrier coatings Surface and Coatings Technology, 197 (1), 93-102.

Lipetzky P., Knesl Z. (1995). Crack-Particle Interaction in Two-Phase Composites, Part II: Crack Deflection. International Journal of Fracture, 73, 81–92.

Lipetzky P., Schmauder S. (1994) Crack-Particle Interaction in Two-Phase Composites, Part I: Particle Shape Effects. International Journal of Fracture, 65, 345–358.

Lipton R. (2002) Design of functionally graded composite structures in the presence of stress constraints. Int J Sol Struct, 39, 2575–2586.

Larsson C., Odén M. (2004) Hardness profile measurements in functionally graded WC–Co composites, Materials Science and Engineering A 382, 141–149.

Ma T., Yamaura H., Koss D.A., Voigt R.C. (2003) Dry sliding wear behavior of cast SiC-reinforced Al MMCs, Mater Sci Eng A, 360 (1-2), 116-125.

Markov K.Z. (2000) Elementary Micromechanics of Heterogeneous Media, Chapter 1 in the collection: Heterogeneous Media: Modelling and Simulation, edited by Konstantin Z. Markov and Luigi Preziosi, Birkhauser Boston, 1-162.

Markworth A.J., Ramesh K.S., Parks Jr. W.P. (1995) Review modeling studies applied to functionally graded materials, J. Mater. Sci. 30, 2183–2193.

Markworth A.J., Saunders J. (1995) A model of structure optimization for a functionally graded material, Mater. Lett., 22, 103– 107.

Martena M., Botto D., Fino P., Sabbadini S., Gola M.M. and Badini C. (2006) Modelling of TBC system failure: Stress distribution as a function of TGO thickness and thermal expansion mismatch, Engineering Failure Analysis, 13, 3, 409-426.

Marur P.R., Tippur H.V. (2000) Dynamic response of bimaterial and graded interface cracks under impact loading. Int. J. Fract., 103, 95–109.

McCartney L.N. (1987) Mechanics of matrix cracking in brittle-matrix fiber reinforced composites, Pro. R. Soc. London A409, 329-350.

McMeeking R.M., Evans A.G. (1982) Mechanics of transformation toughening in brittle materials, J. Am. Ceram. Soc. 1982, 65, 242-246.

Meguid S.A. (1996) Mechanics and mechanisms of toughening of advanced ceramics, J. Mater. Process. Tech., 56, 1-4, 978-989.

Miyazaki H., Yoshizawa Y., Hirao K. (2006) Effect of the volume ratio of zirconia and alumina on the mechanical properties of fibrous zirconia/alumina bi-phase composites prepared by co-extrusion, Journal of the European Ceramic Society, 26, 3539–3546.

Mori T., Tanaka K. (1973) Average stress in matrix and average elastic energy of materials with misfitting inclusions, Acta Metall, 21, 571-574.

Muskhelishvili N.I. (1953) Some basic problems of the mathematical theory of elasticity: Groningen, Netherlands, P. Noordhoof.

Mura T. (1987) Micromechanics of defects in solids. second, revised edition. Dordrecht, The Netherlands, Martinus Nijhoff Publishers.

Mura T. (1963) Continuous distribution of moving dislocations. Philos. Mag., 89, 843–857.

Muskhelishvili S.G. (1953) Some basic problems of the mathematical theory of elasticity. P. Noordhoff, Groningen, the Netherlands.

Nadeau J.C., Ferrari M. (1999) Microstructural optimization of a functionally graded transversely isotropic layer. Mechanics of Materials, 31, 10, 637-651.

Noda N.A., Ohzono R., Chen M.C. (2003) Analysis of an elliptical crack parallel to a bimaterial interface under tension, Mech. Mater., 11, 1059–1076.

Noda N. (1999) Thermal stresses in functionally graded materials, J. Therm. Stress., 22, 477–512.

Noda N., Nakai S., Tsuji T. (1998) Thermal stresses in functionally graded material of particle-reinforced composite. JSME Ser A, 41(2), 178–84.

Norris A.N. (1985) A differential scheme for the effective moduli of composites. Mechanics of Materials, 4 (1), 1-16.

Obata Y., Noda N. (1993) Transient thermal stresses in a plate of functionally gradient material. Am. Cer. Soc., Ceram. Trans. 34 (1993) 403-410.

Obata Y., Noda N. (1994) Steady thermal stresses in a hollow circular cylinder and a hollow sphere of a functionally graded material. J. Thermal Stresses, 17, 471-487.

Orange G., Fantozzi G., Homerin P., Thevenot F., Leriche A., Cambier F. (1992) Preparation and characterization of a dispersion toughened ceramic for thermomechanical uses (ZTA). Part II: Thermomechanical characterization. Effect of microstructure and temperature on toughening mechanisms. Journal of the European Ceramic Society, 9 (3), 177-185.

Oritz M. (1987) Continuum theory of crack shielding in ceramic. J. App.Mech., 54, 54–58.

Ortiz M., Giannakopoulos A.E. (1989) Maximal crack tip shielding by microcracking. J. appl. Mech., 56, 279-283.

Ozturk M., Erdogan F. (1995) An axisymmetric crack in bonded materials with a nonhomogeneous interfacial zone under torsion, ASME J. Appl. Mech., 62, 116–125.

Ozturk M., Erdogan F. (1996) Axisymmetric crack problem in bonded materials with a graded interfacial region, Int. J. Solids Struct., 33, 193–219.

Pace N.G., Saunders G.A., Stimengen Z., Thorp J.S. (1969) J. Mater. Sci., 4, 1106-l 110.

Paley M., Aboudi J. (1992) Micromechanical analysis of composites by the generalized cells model. Mechanics of Materials, 14, 2, 127-139.

Papaioannou S.G., Hilton P.D. (1974) A finite element method for calculation stress intensity factors and its application to composites. Engineering of Fracture and Mechanics, 6, 807–823.

Parameswaran V., Shukla A. (1998) Dynamic fracture of functionally gradient material having discrete property variation. J Mater Sci., 33, 3303–3311.

Paulino G.H., Jin Z.H. (2001) Correspondence principle in viscoelastic functionally graded materials, ASME J Appl Mech, 68, 129–32.

Paulino G.H., Jin Z.H. (2001) Viscoelastic functionally graded materials subjected to antiplane shear fracture. ASME J. Appl. Mech., 68, 284–93.

Paulino G.H., Jin Z.H. (2001) A crack in a viscoelastic functionally graded material layer embedded between two dissimilar homogeneous viscoelastic layers––antiplane shear analysis. Int. J. Fract., 111, 283–303.

Predecki P., Abuhasan A., Barrett C.S. (1988) Residual stress determination in Al2O3/SiC (whisker) composites by X-ray diffraction. Adv. X-ray Anal., 31, 231–243.

Prielipp H., Knechtel M., Claussen N., Streiffer S.K., Müllejans H., Rühle M., Rödel J. (1995) Strength and fracture toughness of aluminum/alumina composites with interpenetrating networks, Mater. Sci. Eng.A, 197, 1, 19-30.

Qian G., Nakamura T., Berndt C.C., Leigh S.H. (1997) Tensile toughening test and high temperature fracture analysis of thermal barrier coatings, Acta Mater., 45 (4), 1767-1784.

Ravichandran K.S. (1994) J. Am. Ceram. Soc. 77 (5) 1178.

Reddy J.N., Chin, K. (1998) Thermomechanical behavior of functionally graded cylinders and plates. Journal of Thermal Stresses, 21(3), 593-626.

Reiter T., Dvorak G.J. (1998) Micromechanical models for graded composite materials: II. Thermomechanical loading. J. Mech. Phys. Solids, 46 (9), 1655–1673.

Reuss A. (1929) Berechnung der Fliessgrenze von Mischkristallen auf Grund der Plastizita¨tsbedingung fu¨ r Einkristalle, Z. Angew. Math. Mech., 9, 49– 58.

Richard T. (1975) The mechanical behavior of a solid micro-sphere filled composite. J. Compos. Mater., 9, 108-113.

Rose L.R.F. (1986a) Effective fracture toughness of microcracked materials, J. Am. Ceram. Soc. 69, 212-214.

Rose L.R.F. (1986b) The size of the transformed zone during steady-state cracking in transformation-toughened materials, J Mech Phys Solids, 34, 609-616.

Rubinstein A.A. (1986). Macrocrack-microdefect interaction. J. Appl. Mech., 53, 505-510.

Ruhle M., Evans A.G., McMeeking R.M., Charalambides P.G., Hutchinson J.W. (1987) Microcrack toughening in alumina/zirconia, Acta Metall., 35, 2701-2710.

Ruhle M., Claussen N., Heuer A.H. (1986) Transformation and microcrack toughening as complementary processes in ZrO_2-toughened Al_2O_3, J. Am. Ceram. Soc., 69, 605-697.

Sami E.B., Erdogan F., Hatira F.B. (2003) Mater. Sci. Forum 423/425, 601- 606.

Sanford R.J. (1979) A critical re-examination of the Westergaard method for solving opening-mode crack problems. Mechanics Research Communications, 6(5), 289-294.

Sanford R.J. (2003) Principles of Fracture Mechanics, Prentice Hall/Pearson Education, Inc.

Sbaizero O., Roitti S., Pezzotti G. (2003) R-curve behavior of alumina toughened with molybdenum and zirconia particles. Mater. Sci. Eng. A, 359 (1-2), 297-302.

Schovanec L., Walton J.R. (1987) The quasi-static propagation of a plane strain crack in a power-law inhomogeneous linearly viscoelastic body. Acta Mechanica, 67, 61–77.

Schovanec L., Walton J.R. (1987) The energy release rate for a quasi-static mode I crack in a nonhomogeneous linearly viscoelastic body. Eng. Fract. Mech, 28, 445–454.

Shabana Y.M., Noda N. (2001) Thermo-elasto-plastic stresses in functionally graded materials subjected to thermal loading taking residual stresses of the fabrication process into consideration, Composites Part B, 32, 2, 2001, 111-121.

Shaw L.L. (1998) Thermal residual stresses in plates and coatings composed of multi-layered and functionally graded materials , Composites Part B, 29 (3), 199-210.

Shaw, L.L. (1998) The crack driving force of functionally graded materials, J. Mater. Sci. Lett., 17, 65–67.

Shi S.L., Pan W. (2007) Toughening of Ti_3SiC_2 with 3Y-TZP addition by spark plasma sintering. Materials Science and Engineering: A, 447 (1-2), 303-306.

Shum D.K.M., Hutchinson J.W. (1990) On toughening by microcracks, Mech. Mater., 9, 83-91.

Sigl L.S. (1996) Microcrack toughening in Brittle materials containing weak and strong interfaces, Acta mater., 44, 9, 3599-3609.

Sigl L.S., Mataga P.A., Dalgleish B.J., McMeeking R.M., Evans A.G. (1988) On the toughness of brittle materials reinforced with a ductile phase. Acta Metallurgica, 36 (4), 945-953.

Sih G.C. (1966) On the Westergaad method of crack analysis, Int. J. Fract. Mech, 2, 628-631.

Simha N.K., Fischer F.D., Kolednik O., Chen C.R. (2003) Inhomogeneity effects on the crack driving force in elastic and elastic–plastic materials, J. Mech. Phys. Solids, 51, 209–240.

Simmons G., Wang H. (1971) Single Crystal Elastic Constants and Calculated Aggregate Properties. A Handbook, second ed., MIT Press, Cambridge, MA.

Sladek J., Sladek V., Zhang C. (2005) An advanced numerical method for computing elastodynamic fracture parameters in functionally graded materials, Computational Materials Science, 32, 3-4, 532-543

Song G.M., Zhou Y., Sun Y. (1999) Modeling of fiber toughening in fiber-reinforced ceramic composites, Ceramics International 25, 257-260.

Stump M.D., Budiansky B. (1989) Crack-growth resistance in transformation-toughened ceramics, Int. J. Solids Struct., 25 (6), 635-646.

Suzuki Y., Morgan P.E.D., Niihara K. (1999) The improvement in mechanical properties of $MoSi_2$ through in situ crystallization of grain boundary silica glass by the additions of refractory oxides. Materials Science and Engineering A, 261, 1-2, 15, 188-195.

Swain M.V. (1983) R-curve behaviour of magnesia-partially-stabilized zirconia and its significance for thermal shock. In Fracture Mechanics of Ceramics (Edited by Gradt R.C. et al.) 6, 355-370, Plenum New York.

Swain M.V., Hannink R.H.J. (1984) R-curve behaviour of zirconia ceramics. In Advances in Ceramics (Edited by Claussen N., Herver A.), American Ceramics Society, 12, 255-239.

Tamate O. (1968) The effect of a circular inclusion on the stresses around a line crack in a sheet under tension. International Journal of Fracture 4, 257–266.

Tanigawa Y., Akai T., Kawamura R., Oka N. (1996) J. Thermal Stresses, 19, 77.

Tanigawa, Y. (1995) Some basic thermoelastic problems for nonhomogeneous structural materials. Appl. Mech. Rev. 48, 287-300.

Tanigawa Y. (1995) Some basic thermoelastic problems for nonhomogeneous structural materials, Appl. Mech. Rev., 48 (6), 287–300.

Taya M., Lee J.K., Mori T. (1997) Dislocation punching from interfaces in functionally-graded materials. Acta Materialia, 45 (6), 2349-2356.

Thouless M.D. (1988) Evans A.G., Effects of pull-out on mechanical properties of ceramic-matrix composites, Acta Metall., 36, 517-522.

Tsukamoto H. (2003) Analytical method of inelastic thermal stresses in a functionally graded material plate by a combination of micro- and macro-mechanical approaches. Composites Part B, 34 (6), 561-568.

Tsukamoto H., Kotousov A., Ho S.-Y., Codrington J. (2006) Analysis and design of functionally graded thermal coating. Proceedings of International Conference on Structural Integrity and Failure, SIF2006, 25-32.

Tuan W.H. (2000) Toughening alumina with nickel aluminide inclusions. Journal of the European Ceramic Society, 20, 7, June 2000, 895-899.

Tuan W.H., Chen R.Z., Wang T.C., Cheng C.H., Kuo P.S. (2002) Mechanical properties of Al_2O_3/ ZrO_2 composites. J. European Ceramic Society, 22, 16, 2827-2833.

Vashishth D., Behiri J.C., Bonfield W. (1997) Crack growth resistance in cortical bone: Concept of microcrack toughening. J. Biomechanics, 30 (8), 763-769.

Voigt W. (1928) Lehrbuch der Kristallphysik, Teubner, Leipzig, Germany.

Wakashima K., Tsukamoto H. (1990) Micromechanical approach to the thermomechanics of ceramic-metal gradient materials. Proc. of the 1st Int. Symp. on Functionally Gradient Materials, FGM Forum, pp.19-26.

Wakashima K., Tsukamoto H., Ishizuka T. (1992) Numerical approach to the elastic-plastic analysis of thermal stresses in a ceramic-metal bi-material plate with graded microstructure; Modelling of plastic deformation its engineering applications, Proc. of the 13th Risϕ Int. Symp. on Metall. Mater. Sci., Risϕ National Laboratory, 503-510.

Wakashima K., Tsukamoto H. (1991) Mean-field micromechanics model and its application to the analysis of thermomechanical behaviour of composite materials. Mater. Sci. Eng. A, 146, 291-316.

Wakashima K., Tsukamoto H. (1992) Micromechanical Approach toward thermomechanical tailoring of metal matrix composites, ISIJ International, 32, 883-892.

Wang, C., Libardi, N. and Baldo, J.B. (1998). Analysis of Crack Extension Paths and Toughening in a Two Phase Brittle Particulate Composites by the Boundary Element Method. International Journal of Fracture. 94, 177–188.

Wang B.L, Mai Y-W., Zhang X-H. (2004) Thermal shock resistance of functionally graded materials, Acta Materialia, 52, 4961–4972.

Wang X.Y., Zou Z.Z., Wang D. (1997) On the penny-shaped crack in a nonhomogeneous interlayer of adjoining two different elastic materials, Int. J. Solids Struct.34 (30) 3911-3921.

Wang Y.S., Huang G.Y., Gross D. (2003) Fracture analysis of functionally graded coatings: plane deformation , European Journal of Mechanics - A/Solids, 22, 4, 2003, 535-544.

Watanabe Y., Eryu H. and Matsuura K. (2001) Evaluation of three-dimensional orientation of Al_3Ti platelet in Al-based functionally graded materials fabricated by a centrifugal casting technique, Acta mater., 49, 775–783.

Wei G.C., Becher P.F. (1985) Development of SiC-whisker-reinforced ceramic, Am. Ceram. Soc. Bull., 64(2), 298–304.

Weissenbek E., Pettermann H.E., Suresh S. (1997) Elasto-plastic deformation of compositionally graded metal–ceramic composites, Acta Mater., 45 (8), 3401–3417.

Widjaja S., Limarga A.M., Yip T.H. (2003) Modeling of residual stresses in a plasma-sprayed zirconia/alumina functionally graded-thermal barrier coating, Thin Solid Films, 434 (1-2), 216-227.

Wittmann F.H., Slowik V., Alvaredo A.M. (1994) Probabilistic aspects of fracture energy of concrete, Mater. Struct., 27, 499-504.

Williams M.L. (1952) Stress singularities resulting from various boundary conditions in angular corners of plates in extension. J Appl Mech, 19, 526–528.

Williams M.L. (1952) Surface stress singularities resulting from various boundary conditions in angular corners of plates under bending. Proceedings of the first US national congress of applied mechanics, New York, ASME, 325–329.

Yang L., Li Z. (2003) The lowest order solution of the crack-inhomogeneity interaction for mode I crack. Mechanics Research Communications, 30, 143-149.

Yang Y.Y. (2000) Time-dependent stress analysis in functionally graded materials. Int J Solids Struct., 37, 7593–7608.

Yang Y.Y. (1998a) Stress analysis in a joint with a functionally graded material under a thermal loading by using the Mellin transform method, Int. J. Solids Struct., 35, 1261-1287.

Yang Z.M., Zhou Z.G., Zhang L.M. (2003) Characteristics of residual stress in Mo–Ti functionally graded material with a continuous change of composition, Materials Science and Engineering A, 358, 1-2, 214-218.

Yue Z.Q., Xiao H.T. (2002) Generalized Kelvin solution based boundary element method for crack problems in multilayered solids, Engng. Anal. Bound. Elem., 26, 691–705.

Yue Z.Q., Xiao H.T., Tham L.G. (2003) Boundary element analysis of crack problems in functionally graded materials, Int. J. Solids Struct. 40, 3273–3291.

Zeng D., Katsube N., Soboyejo W.O. (2004) Discrete modelling of transformation toughening in heterogeneous materials. Mechanics of Materials, 36, 1057-1071.

Zhou Y.C., Hashida T. (2002) Thermal fatigue failure induced by delamination in thermal barrier Coating, International Journal of Fatigue, 24, 407–417.

Zhu J.C., Lee S.Y., Yin Z.D., Lai Z.H. (1996, 1997) Mechanical Performance of ZrO–Ni Functionally Graded Material by Powder Metallurgy. Functionally Graded Material, 203-208.

Appendices

Appendix 1 Singular integral equation method

A1.1 Fundamental concept

This method is based on the concept that a crack can be represented by a continuous distribution of dislocations. The basic mathematical apparatus for discrete dislocations was established by Liebfried [1951] in early 1950's, although the target was physical dislocation with discrete Burgers vector and discrete position. The concept of distributed dislocation arrays with continuos Burgers vectors is based on the pioneering work of Eshelby in the late 1950's, and developed by many researchers [Erdogan and Gupta 1972; Mura 1963]. The technique is quite efficient, and may be applied to model cracks in two and three dimensions and used to determine very accurately the stress intensity factor as well as the T-stress, with about the same accuracy [Broberg 2005].

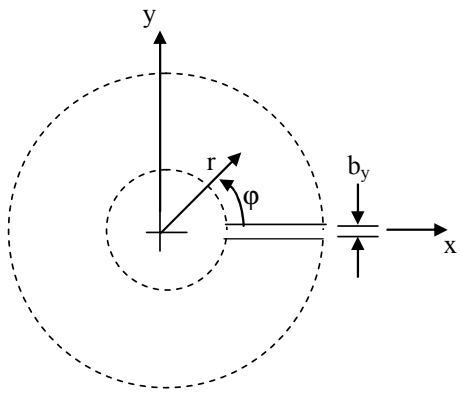

Figure A1-1:
Displacement jump due to an edge dislocation.

The basic idea is to use the superposition principle for the uncracked body, together with an unknown distribution of dislocation placed along the crack, chosen so that the crack faces become traction-free. As a preparation of the formulation, we first consider the displacements and stresses obtained from the complex potentials

$$\Phi(z) = A \ln z, \quad \Psi(z) = \overline{A} \ln z \tag{A1.1}$$

where A here is specifically replaced by the real parameter $A = -\mu b_y / \pi(\kappa+1)$:

$$\begin{Bmatrix} u \\ v \end{Bmatrix} = \frac{-b_y}{2\pi(\kappa+1)} \begin{Bmatrix} (\kappa-1)\ln r - \cos 2\varphi \\ (\kappa+1)\varphi - \sin 2\varphi \end{Bmatrix} \tag{A1.2}$$

$$\begin{Bmatrix} \sigma_x \\ \sigma_y \\ \sigma_z \end{Bmatrix} = \frac{-b_y \mu}{\pi(\kappa+1)r} \begin{Bmatrix} \cos\varphi + \cos 3\varphi \\ 3\cos\varphi - \cos 3\varphi \\ -\sin\varphi + \sin 3\varphi \end{Bmatrix} \quad . \tag{A1.3}$$

While the displacement u does not experience any change along a full circle enclosing the origin from $\varphi = 0$ to $\varphi = 2\pi$, the displacement v exhibits a displacement jump (discontinuity) of the magnitude $v(0) - v(2\pi) = v^+ - v^- = b_y$. Thus, the potentials describe an edge dislocation with a displacement jump in y-direction. This dislocation is accompanied with stresses $\sigma_x = \sigma_y = -2\mu b_y / \pi(\kappa+1)x$ and $\tau_{xy} = 0$ acting along the x-axis. If a general displacement jump b_y in y-direction and b_x in x-direction is described, the constant A in equation (A1.1) must be replaced by $A = -\mu(b_y - ib_x)/\pi(\kappa+1)$.

As a specific problem, we again consider in the following the already investigated crack under constant crack-face loading σ (pressure) as shown in Fig. A1-2 (a). The crack now is represented as a continuous distribution of dislocations which are located in the interval $-a \le t \le +a$ on the x-axis as shown in Fig. A1-2 (b). After renaming $b_y \to db_y = B_y(\xi)d\xi$, $x \to x - \xi$, $z \to z - \xi$, we obtain from equations (A1.2) and (A1.3) for the stress σ_y along the x-axis and for the potential $\phi'(z)$ the representations

$$\sigma_y(x,0) = -\frac{2\mu}{\pi(\kappa+1)} \int_{-a}^{+a} \frac{B_y(\xi)d\xi}{x-\xi} \tag{A1.4}$$

$$\Phi'(z) = -\frac{\mu}{\pi(\kappa+1)} \int_{-a}^{+a} \frac{B_y(\xi)d\xi}{z-\xi} \quad . \tag{A1.5}$$

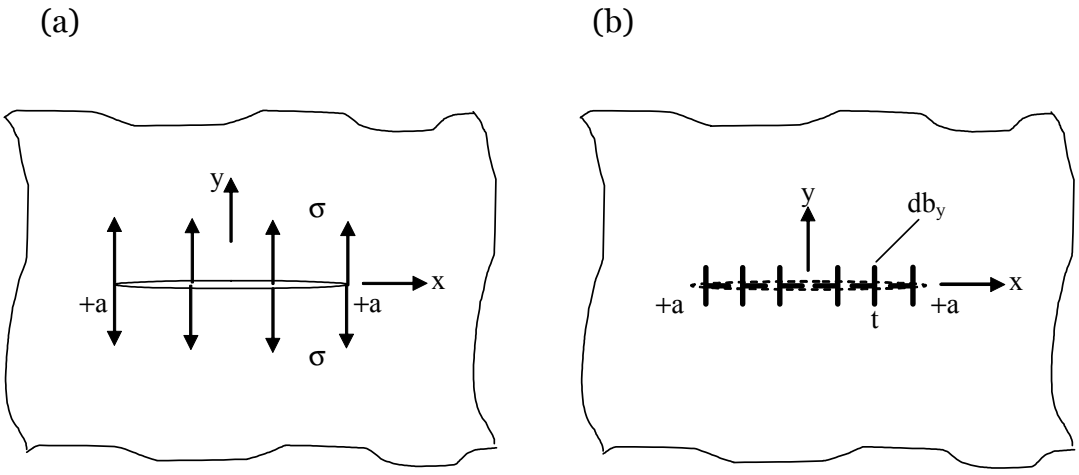

Figure A1-2: Crack represented as distribution of dislocations (a) A crack under constant crack-face loading, σ, (b) A continuous distribution of dislocations.

In this case, the left-hand side of equation (A1.4), i.e. the stress σ_y along the crack, is known: $\sigma_y = \sigma$. Accordingly equation (A1.5) is a singular integral equation for the unknown distribution B_y. Its solution is given by

$$B_y(x) = \frac{\sigma(\kappa+1)}{2\mu}\frac{x}{\sqrt{a^2 - x^2}} \tag{A1.6}$$

Knowing $B_y(x)$ the problem is practically solved because the potentials Φ and Ψ can be found from $B_y(x)$ by integration. For example, from equation (A1.5) we obtain

$$\Phi'(z) = -\frac{\sigma}{2\pi}\int_{-a}^{+a}\frac{x\,dx}{(z-x)\sqrt{a^2 - x^2}} = \frac{\sigma}{2}\left[\frac{z}{\sqrt{z^2 - a^2}} - 1\right] \tag{A1.7}$$

from which the stress intensity factor can be determined.
If only the stress intensity factor is of interest, this quantity can be directly determined from $B_y(x)$. Along the crack $B_y = db_y/dx = d(v^+ - v^-)/dx$ is valid. Combining this with the crack-tip field formulas (A1.1), the following relation for the right crack tip yields:

$$K_I = \lim_{x \to a} \frac{2G}{\kappa + 1} \sqrt{2\pi} \sqrt{a - x} B_y(x) \ . \qquad \text{(A1.8)}$$

When introducing the distribution, we have earlier derived the known result, $K_I = \sigma\sqrt{\pi a}$.

The integral equation formulation is applicable not only for straight cracks. It can easily be extended to curved cracks, bounded domains, and arbitrary loadings. In addition it can be used as a starting point for numerical method, tailored specifically for the solution of crack problems.

A1.2 Approach to general crack problems

For simplicity, only straight semi-infinite cracks and mode I are considered here, although the general procedure may be extended to also cove curved cracks and other modes.

Assume that a crack is located along $-\infty < x < 1,\ y = 0$ in a linearly elastic plate subjected to mode I tractions along its boundary $\sigma_y(x)$. In many cases, the problem can be reduced to the following singular equation with the Cauchy kernel (from equation (A1.4)):

$$-\frac{\kappa + 1}{2\mu} \sigma_y(x) = \frac{1}{\pi} \int_{-\infty}^{+1} B_y(\xi) \left\langle \frac{1}{x - \xi} + K(x, \xi) \right\rangle d\xi \qquad -\infty < x < 1, \qquad \text{(A1.9)}$$

where $\kappa = \dfrac{1 - 2\nu}{2(1 - \nu)}$ for plane stress and $\kappa = (1 - \nu)/2$ for plane stress conditions, respectively, μ is the shear modulus, $B_y(\xi)$ is the dislocation density to be

determined from the solution of equation (A1.9) and K(x, ξ) is non-singular kernel representing the effect of the particular geometry of the problem.

The dislocation density is connected with the opening of the crack by the following relationship

$$B_y(\xi) = -\frac{dg(\xi)}{d\xi}. \tag{A1.10}$$

Let us introduce, for example, the following substitution into the integral (A1.9)

$$x = \frac{2u}{u+1} \text{ and } \xi = \frac{2\eta}{\eta+1}. \tag{A1.11}$$

Then, the integral (A1.9) becomes

$$-\frac{\kappa+1}{2\mu}\frac{\sigma_y(u)}{1+u} = \frac{1}{\pi}\int_{-1}^{+1}\frac{\overline{B}_y(\eta)}{1+\eta}\left\langle\frac{1}{u-\eta}+\frac{2\overline{K}(u,\eta)}{(1+u)(1+\eta)}\right\rangle d\eta. \tag{A1.12}$$

Assume that the transformed kernel $\overline{K}(u, \eta)$ and the tractions at the crack faces σ(u) are such that the all necessary conditions for the associated problem with a finite crack length located along -1 < x < 1, y = 0 are satisfied. Then, through the use of function-theoretic methods [Erdogan and Gupta 1972; Muskhelishvili 1953] the behavior of the function $\overline{B}_y(\eta)/(\eta+1)$ at $\eta = \pm 1$ for practically important cases can be the following:

$$\frac{\overline{B}_y(\eta)}{1+\eta} \sim (1+\eta)^{1/2}(1-\eta)^{-1/2} \tag{A1.13}$$

or

$$\frac{\overline{B}_y(\eta)}{1+\eta} \sim (1+\eta)^{-1/2}(1-\eta)^{-1/2}. \tag{A1.14}$$

The first singular behaviour (A1.13) corresponds to the case when the dislocation density $B(\xi) \sim |\xi|^{-3/2}$ at $\xi \to -\infty$, and the second case (A1.14) when B(ξ)

$\sim |\xi|^{-1/2}$ at $\xi \to -\infty$. Physically, the first case means that the faces of a semi-infinite crack are gradually closing together on infinity and the second case corresponds to a gradual increase of the crack opening $g(\xi)$ as $\sim \sqrt{|\xi|}$ at $\xi \to -\infty$. In general, it can be associated with a stress intensity factor applied on infinity. Now we develop a numerical procedure to solve the singular equation (A1.12) for these two different cases.

A1.3 Numerical Procedure

In the first case (closing crack faces on infinity) we represent $\overline{B}_y(\eta)/(\eta+1)$ as

$$\frac{\overline{B}_y(\eta)}{1+\eta} = \phi(\eta)(1+\eta)^{1/2}(1-\eta)^{-1/2}, \qquad \text{(A1.15)}$$

where $\phi(\eta)$ is a non-singular function.

Then, we define the set of N integration and N-1 collocation points by

$$s_i = \cos\left(\pi\frac{2i-1}{2N+1}\right) \qquad i = 1...N, \qquad \text{(A1.16)}$$

$$t_k = \cos\left(\pi\frac{2k}{2N+1}\right) \qquad k = 1...N-1, \qquad \text{(A1.17)}$$

respectively.

Using the Gauss-Chebyshev quadrature formulae the singular integral equation (A1.13) can now be reduced to a set of N-1 algebraic equations having the form

$$-\frac{\kappa+1}{2\mu}\sigma(t_k) = \frac{2}{2N+1}\sum_{i=1}^{N}\phi(s_i)\left\langle\frac{(1+t_k)(1+s_i)}{t_k-s_i} + 2\overline{K}(t_k,s_i)\right\rangle \qquad k = 1...N-1. \qquad \text{(A1.18)}$$

The condition of the closing faces on infinity, may be discredited, giving

$$\frac{2\pi}{2N+1}\sum_{i=1}^{N}\phi(s_i)=0\,. \qquad \text{(A1.19)}$$

The last equation (A1.19) together with N-1 equations given by (A1.18) provide a system of N algebraic equations in the N unknowns $\phi(s_i)$, i = 1,2,...N. It is a straightforward task to programme the system of equations and to use a computer library routine to invert the resulting N× N matrix.

The stress intensity factor can be found from the crack tip crack opening displacement near the tip of a crack as

$$K=\frac{2\mu}{\kappa+1}\sqrt{2\pi r}\,\frac{\partial g(r)}{\partial r}\,. \qquad \text{(A1.20)}$$

Finally, through an asymptotic analysis, the stress intensity factor can be written in the form

$$K=\frac{2\mu}{\kappa+1}2\sqrt{2\pi}\phi(1)\,. \qquad \text{(A1.21)}$$

In the second case (stress intensity factor K_o applied on infinity) we represent the function $\overline{B}_y(\eta)/(\eta+1)$ in the form

$$\frac{\overline{B}_y(\eta)}{1+\eta}=\phi(\eta)(1+\eta)^{-1/2}(1-\eta)^{-1/2}\,. \qquad \text{(A1.22)}$$

Similar to the previous case we introduce the set of N integration and N-1 collocation points by

$$s_i = \cos\left(\pi\frac{2i-1}{2N}\right) \qquad i = 1...N, \qquad \text{(A1.23)}$$

$$t_k = \cos\left(\pi\frac{k}{N}\right) \qquad k = 1...N-1, \qquad \text{(A1.24)}$$

respectively.

The integral equation (A1.13) can now be reduced to a set of N-1 algebraic equations having the form

$$-\frac{\kappa+1}{2\mu}\sigma(t_k)=\frac{1}{N}\sum_{i=1}^{N}\phi(s_i)\left\langle\frac{(1+t_k)}{t_k-s_i}+\frac{2\overline{K}(t_k,s_i)}{1+s_i}\right\rangle \qquad k = 1...N-1. \qquad \text{(A1.25)}$$

The condition of a stress intensity factor applied on infinity can be rewritten in the following form

$$\phi_N=\frac{K_0}{\sqrt{2\pi}}. \qquad \text{(A1.26)}$$

Similar to the previous case, equations (A1.25) and (A1.26) provide a system of N algebraic equations in the N unknowns $\phi(s_i)$, i = 1,2,...N and the solution of these equations is a straightforward task.

The stress intensity in this case can be found as

$$K=\frac{2\mu}{\kappa+1}\sqrt{2\pi}\,K_0\,\phi(1). \qquad \text{(A1.27)}$$

A1.4 Examples

A1.4.1 Semi-infinite crack loaded by a constant step pressure function

Assume that a crack is located along $-\infty < x < 1$, $y = 0$ in a linearly elastic plate is subjected to pressure p_0 applied to the crack faces in the interval $0 < x < 1$. Obviously this problem relates to the first case (closing faces on infinity) and, consequently, its solution can be obtained using equation (A1.8)-(A1.21). An analytical solution to this problem is also well known and can be expressed as,

$$K=2\sqrt{\frac{2}{\pi}}\,p_0\approx 1.596\,p_0. \qquad \text{(A1.28)}$$

Table A1-1 shows the calculated stress intensity factor together with the error for various numbers of integration points. From this example it is clear seen that the method has a good convergence and very accurate when sufficient number of integration points used. It seems a practical number of integration points ensuring a reasonable accuracy is around 70 which corresponds to that found in the study by Broberg [2005].

Table A1-1: Stress intensity factor and error for various numbers of integration points N.

N	5	10	20	50	100	200	500	1000
K/p_0	1.35	1.71	1.656	1.620	1.608	1.602	1.598	1.597
ε, %	15.4	7.1	3.8	1.5	0.8	0.4	0.1	0.06

A1.4.2 Semi-infinite crack near a circular hole loaded by a stress intensity factor K_o applied on infinity

The geometry of problem is shown in Fig. A1-3. From dimensionless considerations it follows that the stress intensity factor can be written as

$$K = K_o\, Y(c/r), \qquad \text{(A1.29)}$$

where Y is a geometry correction function. The result of calculation of the geometry correction function Y = Y(c/r) based on N = 200 collocation points given below in Table A1-2.

It is clear seen from the obtained solutions that the presence of a small hole in the vicinity of a large crack do not significantly effect the stress intensity factor until the distance between the hole and crack tip becomes less than the radius of the hole. This result supports the suggestion that there is no great benefit from the crack arresting properties of holes in the case of an unstiffened sheet [Broek 1982].

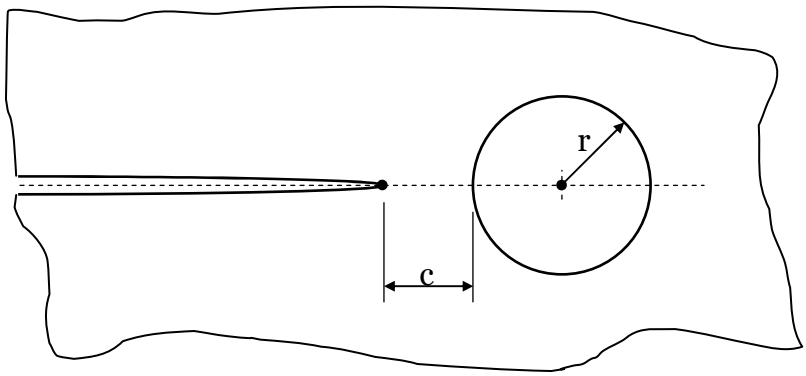

Figure A1-3: Geometry of the problem on a semi-infinite crack near a circular hole.

Table A1-2: Stress intensity magnification function Y for problem A.1.4.2.

c/r	0.001	0.005	0.01	0.05	0.1	0.5	1	5
Y	7.65	4.44	3.58	2.26	1.89	1.29	1.14	1.01

A1.4.3 Semi-infinite crack near a circular hole loaded by pressure

Consider a problem with the same geometry as the previous problem (Fig. A1-3). Let an internal pressure p acts on the edge of the hole. The stress intensity factor in this case can be represented as

$$K = Y(c/r)\, p\sqrt{\pi r}\,, \qquad \text{(A1.30)}$$

where the stress intensity magnification function Y = Y(c/r) is found using equations (A1.15)-(A1.21) and given in Table A1-3. At c/r > 1 a very good approximation to the problem can be obtained based on the well known formula

for a semi-infinite crack subjected to tractions $\sigma_y(x)$ acting normal to the faces ignoring the hole:

$$K = \sqrt{\frac{2}{\pi}} \int_{-\infty}^{0} \frac{\sigma_y(\omega)}{\sqrt{\omega}} d\omega, \qquad \text{(A1.31)}$$

which suggest that the presence of the hole is significant if the distance between the tip of the crack and the edge of the hole less than the radius of the hole.

Table A1-3. Stress intensity magnification function Y for problem A.1.4.3.

c/r	0.001	0.005	0.01	0.05	0.1	0.5	1	5
Y	3.79	2.19	1.75	1.06	0.85	0.42	0.26	0.05

Appendix 2 Input data of material properties

The material properties used for the calculations are shown below.

Table A2-1: Material properties of Al_2O_3, ZrO_2, , SiC, Ag, Ni and Al.

	Al_2O_3[1]	ZrO_2 [2]	SiC [3]	Ag [4]	Ni [4]	Al [4]
Young's Modulus/ GPa	380	200	430	100	207	70
Poisson's Ratio	0.25	0.3	0.17	0.36	0.31	0.3
CTE $10^{-6}/^{0}C$	8.4	10.6	4.3	19.0	13.3	24
Thermal conductivity / $Wm^{-1}K^{-1}$		3.0			89.9	
Specific heat / $Jkg^{-1}K^{-1}$		443			3000	
Density / kgm^{-3}		8890			5990	

The critical value for mean stress corresponding to the phase transformation of ZrO_2 particles [5]: σ_m^c =500MPa

1. Teng X., Liu H., Huang C. (2007) Effect of Al_2O_3 particle size on the mechanical properties of alumina-based ceramicsMaterials Science and Engineering, 452-453, 15, 545-551.
2. Pace N.G., Saunders G.A., Stimengen Z., Thorp J.S. (1969) The elastic constants and interatomic binding in yttria stabilised zirconia. J. Mater. Sci., 4, 1106-1110.
3. Jackson K.M. (2005)Fracture strength, elastic modulus and Poisson's ratio of polycrystalline thin film silicon carbide found by microsample tensile testing. Sensor Actuat A-Phys, 125 (1), 34-40.
4. Simmons G., Wang H. (1971) Single Crystal Elastic Constants and Calculated Aggregate Properties. A Handbook, second ed., MIT Press, Cambridge, MA.
5. Zeng D., Katsube N., Soboyejo W.O. (2004) Discrete modelling of transformation toughening in heterogeneous materials. Mech. Mater., 36, 1057-1071.

Table A2-2: Material properties of Al_2O_3, Si_3N_4, TiC and SiC [Jin and Luo 2006].

	Al_2O_3	Si_3N_4	TiC	SiC
Young's modulus (GPa)	320	320	450	450
Poisson's ratio	0.25	0.25	0.2	0.2
CTE ($\times 10^{-6}$ K^{-1})	8.0	3.0	7.0	4.0
Thermal conductivity (W/m K)	20	35	20	60
Mass density (g/cm3)	3.8	3.2	4.9	3.2
Specific heat (J/g K)	0.9	0.7	0.7	1.0
Fracture toughness ($MPam^{1/2}$)	4	5	5	5

Appendix 3
Micromechanical derivation

The mean-field micromechanical approach formulated by Wakashima and Tsukamoto [1991], which stems from Eshelby's equivalent inclusion method [Eshelby 1957; 1959; 1961] and Mori-Tanaka's mean-field approximation [Mori and Tanaka 1973] is described briefly for obtaining the micromechanical expressions (5.7)-(5.12). Based on Eshelby's equivalent inclusion concept, we can replace the micro-inhomogeneous material by the homogeneous comparison material (HCM) with the equivalent inclusions and the fictitious eigenstrain distribution to represent the disturbance of stress field in the micro-inhomogeneous material. The HCM has exactly the same micro-geometry as the multi-phase composite. For the micro-inhomogeneous material the Hooke's law can be written as

$$\bar{\varepsilon}_{ik}^{ap\ (r)} = M_{iklm}^{(r)} \bar{\sigma}_{lm}^{ap\ (r)}, \tag{A3.1}$$

while for the homogeneous comparison material (HCM),

$$\bar{\varepsilon}_{ik}^{ap\ (r)} = M_{iklm}^{(r)} \bar{\sigma}_{lm}^{ap\ (r)} + \varepsilon_{ik}^{**(r)} \tag{A3.2}$$

where, $\varepsilon_{ik}^{**(r)}$ is a uniform "fictitious" eigenstrain, defined in the equivalent inclusions corresponding to the r-th phase. From equations (A3.1) and (A3.2) it follows

$$\varepsilon_{ik}^{**(r)} = (M_{iklm}^{(r)} - M_{iklm}^{(0)}) \bar{\sigma}_{lm}^{ap\,(r)}, \tag{A3.3}$$

were,

$$\varepsilon_{ik}^{**(r)} = 0\,. \tag{A3.4}$$

According to the Eshelby's solution [Eshelby 1957], the following relation is derived

$$\overline{\sigma}_{ik}^{ap\,(r)} - \overline{\sigma}_{ik} = -P_{iklm}^{(r)} \varepsilon_{lm}^{**(r)}, \tag{A3.5}$$

where

$$P_{iklm}^{(r)} = L_{ikop}^{(0)} (I_{oplm} - S_{oplm}^{(r)}). \tag{A3.6}$$

$S_{oplm}^{(r)}$ denotes the Eshelby's tensor, whose components are dimensionless and dependent on the axial ratios of the elliptical inclusions and Poisson's ratio of the matrix which is assumed to be isotropic. This scheme is only applicable to the case when the discrete phases are dilute. To overcome this limitation, the Mori-Tanaka concept will be used. The equation (A3.5) is replaced by the following equation:

$$\overline{\sigma}_{ik}^{ap\,(r)} - \overline{\sigma}_{ik}^{ap\,(0)} = -P_{iklm}^{(r)} \varepsilon_{lm}^{**(r)}. \tag{A3.7}$$

From equations (A3.3) and (A3.7), the following relation can be derived

$$\overline{\sigma}_{ik}^{ap\,(r)} = C_{iklm}^{(r)} \overline{\sigma}_{lm}^{ap\,(0)}, \tag{A3.8}$$

where

$$C_{iklm}^{(r)} = \left\{ I_{iklm} + P_{ikop}^{(r)} (M_{oplm}^{(r)} - M_{oplm}^{(0)}) \right\}^{-1}. \tag{A3.9}$$

By considering equation (5.1), the sum of the micro-stress can be written as

$$\overline{\sigma}_{ik} = \sum_{r=0}^{N} f^{(r)} \overline{\sigma}_{ik}^{ap\,(r)} . \qquad (A3.10)$$

Therefore, the stress concentration factor $B_{ijkl}^{(r)}$ is calculated as follows

$$B_{iklm}^{(r)} = C_{ikop}^{(r)} \overline{C}_{oplm}^{-1} . \qquad (A3.11)$$

where

$$\overline{C}_{iklm} = \sum_{r=0}^{N} f^{(r)} C_{iklm}^{(r)} \quad . \qquad (A3.12)$$

Next, the internal stress in the micro-inhomogeneous material will be considered. For the internal strain in the micro-inhomogeneous material

$$\overline{\varepsilon}_{ik}^{in\,(r)} = M_{iklm}^{(r)} \overline{\sigma}_{lm}^{in\,(r)} + \varepsilon_{ik}^{*(r)} . \qquad (A3.13)$$

In accordance with the last equation (A2.13), in the equivalent homogeneous material

$$\overline{\varepsilon}_{ik}^{in\,(r)} = M_{iklm}^{(0)} \overline{\sigma}_{lm}^{in\,(r)} + \varepsilon_{ik}^{*(r)} + \varepsilon_{ik}^{**(r)} , \qquad (A3.14)$$

here, $\varepsilon_{ik}^{**(r)}$ is the fictitious eigenstrain, which is found from (A3.13) and (A3.14), as follows

$$\varepsilon_{ik}^{**(r)} = (M_{iklm}^{(r)} - M_{iklm}^{(0)}) \overline{\sigma}_{lm}^{in\,(r)} . \qquad (A3.15)$$

Using the Mori-Tanaka concept [1973], the following equation can be written

$$\overline{\sigma}_{ik}^{in\,(r)} - \overline{\sigma}_{ik}^{in\,(0)} = -P_{iklm}^{(r)} (\Delta\varepsilon_{lm}^{*(r)} + \varepsilon_{lm}^{**(r)}) , \qquad (A3.16)$$

where $\Delta\varepsilon_{kl}^{*(r)}$ is defined by equation (5.12). From equations (A3.15) and (A3.16), it follows

$$\overline{\sigma}_{ik}^{in\,(r)} = B^{0\,(r)}_{iklm}(\overline{\sigma}_{lm}^{in\,(0)} - P^{(r)}_{lmop}\Delta\varepsilon^{*(r)}_{op}) . \tag{A3.17}$$

Since, the sum of the internal stress must be equal to zero,

$$\sum_{r=0}^{N} f^{(r)}\overline{\sigma}_{ik}^{in\,(r)} = 0 , \tag{A3.18}$$

therefore,

$$\overline{\sigma}_{ik}^{in\,(0)} = \overline{C}^{-1}_{iklm}\sum_{r=0}^{N} f^{(r)}C^{(r)}_{lmop}P^{(r)}_{opvw}\Delta\varepsilon^{*(r)}_{vw} \ . \tag{A3.19}$$

By comparing equation (A3.19) with equation (5.10), $D^{(r)}_{ijkl}$ is obtained as given in equation (5.11),

$$D^{(r)}_{ijkl} = -C^{(r)}_{ikop}P^{(r)}_{oplm} \ . \tag{A3.20}$$

Appendix 4
Micromechanical expression for effective properties of two-phase composites with spherical particles

Based on the micromechanical consideration [Tsukamoto 2003], the effective specific heat c(z) , the mass density ρ(z) , the effective thermal conductivity λ(z) , the effective thermal expansion coefficient α(z) , the effective bulk modulus $\kappa(z)$, the effective shear modulus $\mu(z)$ and the overall plane-stress elastic compliance $S^e(z)$ for two-phase composites with spherical particles are expressed as follows:

$$c(z) \cong f_m(z)c_m + f_c(z)c_c \tag{A4.1}$$

$$\rho(z) = f_m(z)\rho_m + f_c(z)\rho_c \tag{A4.2}$$

$$\lambda(z) = f_m(z)\lambda_m + f_c(z)\lambda_c + f_m(z)f_c(z)\frac{\lambda_m - \lambda_c}{\frac{3}{(\lambda_c/\lambda_m)} + f_m(z)} \tag{A4.3}$$

$$\alpha(z) = f_m(z)\alpha_m + f_c(z)\alpha_z + f_m(z)f_c(z)\frac{(\alpha_m - \alpha_c)(\kappa_m - \kappa_c)}{f_m(z)\kappa_m + f_c(z)\kappa_c + \frac{3\kappa_m\kappa_c}{4\mu_m}} \tag{A4.4}$$

$$\kappa(z) = f_m(z)\kappa_m + f_c(z)\kappa_c + f_m(z)f_c(z)\frac{(\kappa_m - \kappa_c)\left(\frac{1}{\kappa_m} - \frac{1}{\kappa_c}\right)}{\frac{f_m(z)}{\kappa_m} + \frac{f_c(z)}{\kappa_c} + \frac{4\mu_m}{3\kappa_m\kappa_c}} \tag{A4.5}$$

$$\mu(z) = f_m(z)\mu_m + f_c(z)\mu_c + f_m(z)f_c(z)\frac{(\mu_m - \mu_c)\left(\frac{1}{\mu_m} - \frac{1}{\mu_c}\right)}{\frac{f_m(z)}{\mu_m} + \frac{f_c(z)}{\mu_c} + \frac{9\kappa_m + 8\mu_m}{6\mu_m(\kappa_m + 2\mu_m)}} \tag{A4.6}$$

$$S^e(z) = \frac{2}{9\kappa(z)} + \frac{1}{6\mu(z)}\,. \tag{A4.7}$$